

An Analysis of Pre-Flashover Fire Experiments with Field Modelling Comparisons



Christian Nielsen

Fire Engineering Research Report 2000/10

March 2000

ISSN 1173-5996



An Analysis of Pre-Flashover Fire Experiments with Field Modelling Comparisons

By

Christian Nielsen

Supervised by

Dr Charles Fleischmann

Fire Engineering Research Report

March 2000

This report was presented as a project report as part of the M.E (Fire) degree at the
University of Canterbury

School of Engineering
University of Canterbury
Private Bag 4800
Christchurch, New Zealand

Phone 643 364-2250

Fax 643 364-2758

Abstract

Firstly, this report investigates the behaviour of pre-flashover fires conducted in a two-compartment structure. Secondly, it looks at preliminary field modelling results of the pre-flashover fires using the SMARTFIRE program.

A two-compartment structure was built so that pre-flashover fire experiments could be conducted. Each room in the compartment measured 2.4 m wide, 3.6 m long, and 2.4 m high. A doorway, with dimensions 2.0 m high and 0.8 m wide separated the rooms. All fires were placed in one room (the fire room) where seven fire experiments were conducted consisting of four differently sized fires. Six of the fires, 55 kW, 110 kW, and 160 kW in size were located in the centre of the fire room. The seventh fire was located in the corner of the fire room and was 110 kW in size. Thermocouple trees were located along the centre-line of the compartment so that vertical temperature profiles could be measured; floor and ceiling thermocouples accompanied the thermocouple trees. In addition, gas sampling points measuring O₂ and CO₂ concentrations were positioned evenly throughout the compartment.

Temperature profiles in the fire room revealed constant cool lower layer and hot upper layer temperatures with a sharp temperature gradient between the two layers. Temperatures in the upper layer for the centrally located fires reached 130°C for the 55 kW fire, 200°C for the 110 kW fire, and 250°C for the 160 kW fire. Temperature profiles in the upper layer for the corner fire were not constant with height but showed a temperature gradient, where the temperature reached 335°C near the ceiling. Temperature profiles in the room next to fire room (the adjacent room) showed constant temperature profiles that were close to the ambient temperature in the lower layer. The upper layer temperature profiles displayed temperature gradients that continued up to the ceiling. Temperatures in the upper layer for the centrally located fires in the adjacent room reached 110°C for the 55 kW fire, 160°C for the 110 kW fire, 200°C for the 160 kW fire, and 225°C for the corner fire.

Preliminary simulations of the four different fire experiments were conducted using the SMARTFIRE field modelling program. Each fire size simulated twice – one with

and one without the six-flux radiation sub-model. A qualitative analysis revealed temperatures in the lower layer of the fire room were under predicted. Temperature gradients were predicted for the upper layer temperature profiles for the centrally located fires, rather than the constant upper layer temperature profiles that were seen experimentally. Overall, simulations predicted closer temperature profiles to the experimental results when the six-flux radiation sub-model was incorporated.

Acknowledgements

I would like to acknowledge the following people all of whom assisted me throughout the course of this project:

- Dr Charley Fleischmann, my supervisor.
- Associate Professor Andrew Buchanan; thank you for allowing me (a non-engineering student) to participate in the M.E.F.E course.
- The New Zealand Fire Service, for their financial assistance.
- Dr Tony Enright, for encouraging me to 'Faculty Jump' from Chemistry to Engineering.
- Carol Caldwell, for the work experience you provided during the year and for introducing me to a sensible and practical approach to fire engineering.
- Dr Hamish McLennan, my future employer with Holmes Fire and Safety Limited.
- Peter Coursey, civil computer lab technician, for your prompt help with installing the SMARTFIRE program.
- Simon Weaver, my classmate and project partner.
- Most of all my Mother, and sister, Carla, for all the encouragement and support you have both given me throughout my university years.

Table of Contents

Abstract	iii
Acknowledgements	v
List of Figures	xii
List of Tables	xvi
1 Introduction	1
1.1 Overview	1
1.2 Experiments	1
1.3 Zone and Field Models	2
1.4 Grounds for the Research	3
1.5 Goals of the Research	3
1.6 Outline of this Report	4
1.7 Limitations of this Report	4
2 Experimental Set-up	6
2.1 General Description	6
2.2 Metal Frame	7
2.3 Insulation	7
2.3.1 Gib [®] Fyreline	7
2.3.2 Intermediate Service Board	8
2.4 Fire Set-up	9
2.4.1 Gas Burner	9
2.4.2 Spark and Pilot Flame	10
2.4.3 Gas Supply	11
2.5 Fume Hood and Chimney	11
3 Instrumentation	12
3.1 General Description	12

3.2	<i>Thermocouples</i>	12
3.2.1	Field Trees	13
3.2.2	Zone Trees	14
3.2.3	Floor and Ceiling Surface Thermocouples	15
3.2.4	Corner Thermocouples	16
3.2.5	Aspirated Thermocouples	17
3.3	<i>Gas Analysis</i>	18
3.4	<i>Bi-directional Probes</i>	20
3.5	<i>Data Acquisition</i>	21
3.6	<i>Mass Flow Meter</i>	22
3.7	<i>Visual Record</i>	22
4	Observations	23
5	Experimental Results and Discussion	28
5.1	<i>Aims</i>	28
5.2	<i>Data Presentation and Analysis</i>	28
5.2.1	Field Trees:	28
5.2.2	Corner Thermocouples	29
5.2.3	Surface Thermocouples:	29
5.2.4	Gas Analysis	30
5.3	<i>Method</i>	30
5.3.1	General Method for the Field Trees, Corner Thermocouples and Surface Thermocouples	30
5.3.2	Method for Field Trees	31
5.3.3	Corner Thermocouples	31
5.3.4	Surface Temperature Profiles	32
5.3.5	Gas Analysis	32
5.4	<i>Results</i>	33
5.4.1	Field Trees	33
5.4.2	Corner Thermocouples	52
5.4.3	Surface Temperatures	60

5.4.4	Gas Analysis	63
5.5	<i>Discussion</i>	65
5.5.1	General Behaviour for Field Trees	65
5.5.2	Fire Room Field Trees	66
5.5.3	The Adjacent Room Field Trees	71
5.5.4	Doorway Field Tree	74
5.5.5	Corner Thermocouples	76
5.5.6	Surface Temperatures	78
5.5.7	Gas Analysis	80
5.6	<i>Overall Discussion</i>	82
5.7	<i>Limitations and Assumptions</i>	83
6	SMARTFIRE Introduction and Overview	85
6.1	<i>Introduction</i>	85
6.2	<i>Overview of the SMARTFIRE System</i>	86
6.2.1	Front End User Interface	87
6.3	<i>Knowledge Based System (KBS)</i>	88
6.3.1	Overview of Mesh Generation by KBS	88
6.3.2	Knowledge Acquisition	89
7	SMARTFIRE Simulation Methodology and Parameters	93
7.1	<i>Introduction</i>	93
7.2	<i>Computer Hardware and Software</i>	93
7.3	<i>SMARTFIRE Variables</i>	93
7.3.1	Fire Properties	93
7.3.2	Surface Material	94
7.3.3	Temperature	94
7.3.4	Grid Generation	94
7.3.5	Convergence Limits and Radiation Issues	95
7.3.6	Running the Simulation	95
7.3.7	Data Exploration and Exporting	95

8	SMARTFIRE Results and Discussion	96
8.1	<i>Results</i>	97
8.1.1	55 kW Fire	97
8.1.2	110 kW Fire	101
8.1.3	160 kW Fire	105
8.1.4	110 kW Corner Fire	109
8.2	<i>Grid Statistics for the Fire Simulations</i>	113
8.3	<i>Computer Simulation Times</i>	113
8.4	<i>Discussion</i>	113
8.4.1	Fire Simulation Visual Profiles	113
8.4.2	Grid Statistics for the Fire Simulations	115
8.4.3	Computer Simulation Time	115
9	Comparisons	117
9.1	<i>Aim</i>	117
9.2	<i>Method</i>	117
9.3	<i>Results</i>	118
9.3.1	55 kW Fire Comparisons	118
9.3.2	110 kW Fire Comparisons	123
9.3.3	160 kW Fire Comparisons	128
9.3.4	110 kW Corner Fire Comparisons	133
9.4	<i>Discussion</i>	138
9.4.1	Discussion Structure	138
9.4.2	Comparisons for the 55 kW Fire	138
9.4.3	Comparisons for the 110 kW Fire	140
9.4.4	Comparisons for the 160 kW Fire	142
9.4.5	Comparisons for the 110 kW Corner Fire	144
9.5	<i>Overall Discussion</i>	146
10	Conclusions	148
10.1	<i>Conclusions from the Pre-flashover Fire Experiments</i>	148

10.2	<i>Conclusions from the SMARTFIRE Simulations</i>	150
10.3	<i>Conclusions from the Comparisons</i>	150
10.4	<i>Further Research</i>	151
11	Nomenclature	152
12	References	153
	Appendix 1: Tabulated Experimental Field Tree Temperatures	156
	Appendix 2: Tabulated Surface Temperatures	184
	Appendix 3: Reproducibility	185
	Appendix 4: Gas Analysis – Background Theory	193

List of Figures

Figure 2.1 Illustration of the Final Layout of Two-Compartment Structure	8
Figure 2.2 The Intermediate Service Board	8
Figure 2.3 Gas Burner.	9
Figure 3.1 Field Tree Positions.	13
Figure 3.2 Field Thermocouple Trees in the Fire Room.	14
Figure 3.3 Zone Tree in the Adjacent Room	15
Figure 3.4 Corner Thermocouple Locations	16
Figure 3.5 Corner Thermocouple Positions.	16
Figure 3.6 Corner Thermocouples	17
Figure 3.7 Aspirated Thermocouples	18
Figure 3.8 Bi-directional Probes	20
Figure 4.1 55 kW Fire Photo	24
Figure 4.2 110 kW Fire Photo	25
Figure 4.3 160 kW Fire Photo	26
Figure 4.4 110 kW Corner Fire Photo	27
Figure 5.1 Temperature Profile for Tree 1 (All Fires)	33
Figure 5.2 Temperature Profiles for Tree 2 (All Fires)	34
Figure 5.3 Temperature Profiles for Tree 3 (55 kW, 110 kW, and 160 kW fires)	34
Figure 5.4 Temperature Profiles for Tree 4 (All Fires)	35
Figure 5.5 Temperature Profiles for Tree 5 (Doorway, All Fires)	35
Figure 5.6 Temperature Profiles for Tree 6 (All Fires)	36
Figure 5.7 Temperature Profiles for Tree 7 (All Fires)	36
Figure 5.8 Temperature Profiles for Tree 8 (All Fires)	37
Figure 5.9 Temperature Profiles for Tree 9 (All Fires)	37
Figure 5.10 Temperature Variations For Tree 1 (All Fires)	38
Figure 5.11 Temperature Variations for Tree 2 (All Fires)	39
Figure 5.12 Temperature Variations for Tree 3 (55 kW, 110 kW, 160 kW fires)	40
Figure 5.13 Temperature Variations for Tree 4 (All Fires)	41
Figure 5.14 Temperature Variations for Tree 5 (Doorway, All Fires)	42
Figure 5.15 Temperature Variations for Tree 6 (All Fires)	43
Figure 5.16 Temperature Variations for Tree 7 (All Fires)	44
Figure 5.17 Temperature Variations for Tree 8 (All Fires)	45

Figure 5.18	Temperature Variations for Tree 9 (All Fires)	46
Figure 5.19	Temperature Profiles for Fire Room, 55 kW Fire	47
Figure 5.20	Temperature Profiles for the Adjacent Room, 55 kW Fire	48
Figure 5.21	Temperature Profiles for the Fire Room, 110 kW Fire	49
Figure 5.22	Temperature Profiles for the Adjacent Room, 110 kW Fire	49
Figure 5.23	Temperature Profiles for the Fire Room, 160 kW Fire	50
Figure 5.24	Temperature Profiles for the Adjacent Room, 160 kW Fire	50
Figure 5.25	Temperature Profiles for the Fire Room, 110 kW Corner Fire	51
Figure 5.26	Temperature Profiles for the Adjacent Room, 110 kW Corner Fire	51
Figure 5.27	Floor Temperatures throughout Two-Compartment Structure	60
Figure 5.28	Ceiling Temperatures throughout Two-Compartment Structure	61
Figure 5.29	Temperature Difference between 300 mm TC and Floor TC	61
Figure 5.30	Temperature Difference between 2375 mm TC and Ceiling TC	62
Figure 6.1	SMARTFIRE Block Diagram	87
Figure 6.2	Example of Efficient Cell Distribution	89
Figure 6.3	SMARTFIRE CBR Cycle	90
Figure 6.4	Adjacency Aspect Ratio Examples	91
Figure 8.1	Visual Contour Profile for the Two-compartment Structure (55 kW Fire without Six-flux Radiation Sub-model)	97
Figure 8.2	Visual Contour Profile for the Two-compartment Structure (55 kW Fire with Six-flux Radiation Sub-model)	98
Figure 8.3	Visual Contour Profile for the Fire Room (55 kW Fire without Six-flux Radiation Sub-model)	99
Figure 8.4	Visual Contour Profile for the Fire Room (55 kW Fire with Six-flux Radiation Sub-model)	99
Figure 8.5	Visual Contour Profile for the Adjacent Room (55 kW Fire without Six- flux Radiation Sub-model)	100
Figure 8.6	Visual Contour Profile for the Adjacent Room (55 kW Fire with Six-flux Radiation Sub-model)	100
Figure 8.7	Visual Contour Profile for the Two-compartment Structure (110 kW Fire without Six-flux Radiation Sub-model)	101
Figure 8.8	Visual Contour Profile for the Two-compartment Structure (110 kW Fire with Six-flux Radiation Sub-model)	102

Figure 8.9 Visual Contour Profile for the Fire Room (110 kW Fire without Six-flux Radiation Sub-model)	103
Figure 8.10 Visual Contour Profile for the Fire Room (110 kW Fire with Six-flux Radiation Sub-model)	103
Figure 8.11 Visual Contour Profile for the Adjacent Room (110 kW Fire without Six-flux Radiation Sub-model)	104
Figure 8.12 Visual Contour Profile for the Adjacent Room (110 kW Fire with Six-flux Radiation Sub-model)	104
Figure 8.13 Visual Contour Profile for the Two-compartment Structure (160 kW Fire without Six-flux Radiation Sub-model)	105
Figure 8.14 Visual Contour Profile for the Two-compartment Structure (160 kW with Six-flux Radiation Sub-model)	106
Figure 8.15 Visual Contour Profile for the Fire Room (160 kW Fire without Six-flux Radiation Sub-model)	107
Figure 8.16 Visual Contour Profile for the Fire Room (160 kW Fire with Six-flux Radiation Sub-model)	107
Figure 8.17 Visual Contour Profile for the Adjacent Room (160 kW Fire without Six-flux Radiation Sub-model)	108
Figure 8.18 Visual Contour Profile for the Adjacent Room (160 kW Fire with Six-flux Radiation Sub-model)	108
Figure 8.19 Visual Contour Profile for the Two-compartment Structure (110 kW Corner Fire without Six-flux Radiation Sub-model)	109
Figure 8.20 Visual Contour Profile for the Two-compartment Structure (110 kW Corner Fire with Six-flux Radiation Sub-model)	110
Figure 8.21 Visual Contour Profile for the Fire Room (110 kW Corner Fire without Six-flux Radiation Sub-model)	111
Figure 8.22 Visual Contour Profile for the Fire Room (110 kW Corner Fire with Six-flux Radiation Sub-model)	111
Figure 8.23 Visual Contour Profile for the Adjacent Room (110 kW Corner Fire without Six-flux Radiation Sub-model)	112
Figure 8.24 Visual Contour Profile for the Adjacent Room (110 kW Corner Fire with Six-flux Radiation Sub-model)	112
Figure 9.1 Comparisons for Tree 1 (55 kW Fire)	118
Figure 9.2 Comparisons for Tree 2 (55 kW Fire)	119

Figure 9.3 Comparisons for Tree 3 (55 kW Fire)	119
Figure 9.4 Comparisons for Tree 4 (55 kW Fire)	120
Figure 9.5 Comparisons for Tree 5 (Doorway, 55 kW Fire)	120
Figure 9.6 Comparisons for Tree 6 (55 kW Fire)	121
Figure 9.7 Comparisons for Tree 7 (55 kW Fire)	121
Figure 9.8 Comparisons for Tree 8 (55 kW Fire)	122
Figure 9.9 Comparisons for Tree 9 (55 kW Fire)	122
Figure 9.10 Comparisons for Tree 1 (110 kW Fire)	123
Figure 9.11 Comparisons for Tree 2 (110 kW Fire)	123
Figure 9.12 Comparisons for Tree 3 (110 kW Fire)	124
Figure 9.13 Comparisons for Tree 4 (110 kW Fire)	124
Figure 9.14 Comparisons for Tree 5 (Doorway, 110 kW Fire)	125
Figure 9.15 Comparisons for Tree 6 (110 kW Fire)	125
Figure 9.16 Comparisons for Tree 7 (110 kW Fire)	126
Figure 9.17 Comparisons for Tree 8 (110 kW Fire)	126
Figure 9.18 Comparisons for Tree 9 (110 kW Fire)	127
Figure 9.19 Comparisons for Tree 1 (160 kW Fire)	128
Figure 9.20 Comparisons for Tree 2 (160 kW Fire)	128
Figure 9.21 Comparisons for Tree 3 (160 kW Fire)	129
Figure 9.22 Comparisons for Tree 4 (160 kW Fire)	129
Figure 9.23 Comparisons for Tree 5 (Doorway, 160 kW Fire)	130
Figure 9.24 Comparisons for Tree 6 (160 kW Fire)	130
Figure 9.25 Comparisons for Tree 7 (160 kW Fire)	131
Figure 9.26 Comparisons for Tree 8 (160 kW Fire)	131
Figure 9.27 Comparisons for Tree 9 (160 kW Fire)	132
Figure 9.28 Comparisons for Tree 1 (110 kW Corner Fire)	133
Figure 9.29 Comparisons for Tree 2 (110 kW Corner Fire)	133
Figure 9.30 Comparisons for Tree 3 (110 kW Corner Fire)	134
Figure 9.31 Comparisons for Tree 4 (110 kW Corner Fire)	134
Figure 9.32 Comparisons for Tree 5 (Doorway, 110 kW Corner Fire)	135
Figure 9.33 Comparisons for Tree 6 (110 kW Corner Fire)	135
Figure 9.34 Comparisons for Tree 7 (110 kW Corner Fire)	136
Figure 9.35 Comparisons for Tree 8 (110 kW Corner Fire)	136
Figure 9.36 Comparisons for Tree 9 (110 kW Corner Fire)	137

List of Tables

Table 2.1 Compartment Dimensions.....	7
Table 3.1 Thermocouple Locations on Field Trees.....	14
Table 3.3 Aspirated Thermocouple Positions	18
Table 3.4 Gas Sampling Point Locations.....	19
Table 5.1 Fire Room Rear Corner Temperatures (°C) for the 55 kW Fire	52
Table 5.2 Fire Room Rear Corner Temperature Standard Deviations (°C) for the 55 kW Fire.....	52
Table 5.3 Fire Room Front Corner Temperatures (°C) for the 55 kW Fire	52
Table 5.4 Fire Room Front Corner Temperature Standard Deviations (°C) for the 55 kW Fire.....	53
Table 5.5 Adjacent Room Corner Temperatures (°C) for the 55 kW Fire	53
Table 5.6 Adjacent Room Corner Temperature Standard Deviations (°C) for the 55 kW Fire.....	53
Table 5.7 Fire Room Rear Corner Temperatures (°C) for the 110 kW Fire	54
Table 5.8 Fire Room Rear Corner Temperature Standard Deviations (°C) for the 110 kW Fire.....	54
Table 5.9 Fire Room Front Corner Temperatures (°C) for the 110 kW Fire	54
Table 5.10 Fire Room Front Corner Temperature Standard Deviations (°C) for the 110 kW Fire.....	55
Table 5.11 Adjacent Room Corner Temperatures (°C) for the 110 kW Fire	55
Table 5.12 Adjacent Room Corner Temperature Standard Deviations (°C) for the 110 kW Fire.....	55
Table 5.13 Fire Room Rear Corner Temperatures (°C) for the 160 kW Fire	56
Table 5.14 Fire Room Rear Corner Temperature Standard Deviations (°C) for the 160 kW Fire.....	56
Table 5.15 Fire Room Front Corner Temperatures (°C) for the 160 kW Fire	56
Table 5.16 Fire Room Front Corner Temperature Standard Deviations (°C) for the 160 kW Fire.....	57
Table 5.17 Adjacent Room Corner Temperatures (°C) for the 160 kW Fire	57
Table 5.18 Adjacent Room Corner Temperature Standard Deviations (°C) for the 160 kW Fire.....	57
Table 5.19 Fire Room Rear Corner Thermocouple Temperatures (°C) for the 110 kW Corner Fire	58
Table 5.20 Fire Room Rear Corner Temperature Standard Deviations (°C) for the 110 kW Corner Fire.....	58
Table 5.21 Fire Room Front Corner Temperatures (°C) for the 110 kW Corner Fire	58
Table 5.22 Fire Room Front Corner Temperature Standard Deviations (°C) for the 110 kW Corner Fire.....	59
Table 5.23 Adjacent Room Corner Temperatures (°C) for the 110 kW Corner Fire	59
Table 5.24 Adjacent Room Corner Temperature Standard Deviations (°C) for the 110 kW Corner Fire.....	59
Table 5.25 O ₂ Consumption and CO ₂ Production Profiles for Tree 2 (% vol)	63
Table 5.26 O ₂ Consumption and CO ₂ Production Profiles for Tree 4 (% vol)	63
Table 5.27 O ₂ Consumption and CO ₂ Production Profiles for Tree 7 (% vol)	64
Table 5.28 O ₂ Consumption and CO ₂ Production Profiles for the Doorway (% vol)	64
Table 7.1 Fire Dimensions for Simulations	94

Table 7.2 Ambient Temperatures for Simulations	94
Table 8.1 Grid Statistics for Each Simulation.....	113
Table 8.2 Computer Simulation Times for the Four Fires	113
Table A.1 Run 1 Temperatures for Field Trees 1, 2, and 3.....	156
Table A.2 Run 1 Temperatures for Field Trees 4, 6, and 7.....	157
Table A.3 Run 1 Temperatures for Field Trees 8 and 9.....	158
Table A.4 Run 1 Temperatures for Field Tree 5 (Doorway)	159
Table A.5 Run 2 Temperatures for Field Trees 1, 2, and 3.....	160
Table A.6 Run 2 Temperatures for Field Trees 4, 6, and 7.....	161
Table A.7 Run 2 Temperatures for Field Trees 8 and 9.....	162
Table A.8 Run 2 Temperatures for Field Tree 5 (Doorway)	163
Table A.9 Run 3 Temperatures for Field Trees 1, 2, and 3.....	164
Table A.10 Run 3 Temperatures for Field Trees 4, 6, and 7.....	165
Table A.11 Run 3 Temperatures for Field Trees 8 and 9.....	166
Table A.12 Run 3 Temperatures for Field Tree 5 (Doorway)	167
Table A.13 Run 4 Temperatures for Field Trees 1, 2, and 3.....	168
Table A.14 Run 4 Temperatures for Field Trees 4, 6, and 7.....	169
Table A.15 Run 4 Temperatures for Field Trees 8 and 9.....	170
Table A.16 Run 4 Temperatures for Field Tree 5 (Doorway)	171
Table A.17 Run 5 Temperatures for Field Trees 1, 2, and 3.....	172
Table A.18 Run 5 Temperatures for Field Trees 4, 6, and 7.....	173
Table A.19 Run 5 Temperatures for Field Trees 8 and 9.....	174
Table A.20 Run 5 Temperatures for Field Tree 5 (Doorway)	175
Table A.21 Run 6 Temperatures for Field Trees 1, 2, and 3.....	176
Table A.22 Run 6 Temperatures for Field Trees 4, 6, and 7.....	177
Table A.23 Run 6 Temperatures for Field Trees 8 and 9.....	178
Table A.24 Run 6 Temperatures for Field Tree 5 (Doorway)	179
Table A.25 Run 7 Temperatures for Field Trees 1, 2, and 3.....	180
Table A.26 Run 7 Temperatures for Field Trees 4, 6, and 7.....	181
Table A.27 Run 7 Temperatures for Field Trees 8 and 9.....	182
Table A.28 Run 7 Temperatures for Field Tree 5 (Doorway)	183
Table A.29 Tabulated Floor Temperatures	184
Table A.30 Tabulated Ceiling Temperatures	184
Table A.31 Conditions for Each Run	185
Table A.32 Results for Tree 1 Comparisons	187
Table A.33 Results for Tree 2 Comparisons	187
Table A.34 Results for Tree 3 Comparisons	188
Table A.35 Results for Tree 4 Comparisons	188
Table A.36 Results for Tree 5 (Doorway) Comparisons	189
Table A.37 Results for Tree 6 Comparisons	189
Table A.38 Results for Tree 7 Comparisons	190
Table A.39 Results for Tree 8 Comparisons	190
Table A.40 Results for Tree 9 Comparisons	191

1 Introduction

1.1 Overview

In 1992, the performance-based building code (BIA, 1992) was introduced in New Zealand. This has allowed fire engineers to employ innovative design, with the aim of more efficient use of space, building materials, and a more cost effective design, provided that performance and safety requirements can be demonstrated (Buchanan, 1999). Commonly, the design process for this involves fire engineers using computer models that simulate fires in enclosures such as buildings, yet fire experiments used to verify the accuracy of fire computer models are significantly more simplistic than the scenarios that computer models are applied to.

1.2 Experiments

Fire experiments were conducted at McLeans Island to validate zone and field modelling programs (discussed under the next subheading). These experiments were conducted to provide a more comprehensive set of data than the Steckler et al. (1982) experiments commonly used to validate zone and field modelling simulations. The experiments were conducted in a two-compartment structure; each compartment measured 2.4 m wide, 3.6 m long and 2.4 m high. A doorway, with dimensions 2.0 m high and 0.8 m wide, separated the rooms. All fires were placed in one room (hereon referred to as the fire room). The room next to the fire room and separated by the doorway (hereon referred to as the adjacent room), opened out to the atmosphere and had no soffit or doorway. Four different fire experiments were conducted in the two-compartment structure; all were fixed sizes and used LPG (liquid petroleum gas) as the fuel source. Three fires were located in the centre of the fire compartment and were sized at 55 kW (two runs), 110 kW (one run), and 160 kW (three runs), with another 110 kW fire (one run) positioned in the corner of the fire room. Nine thermocouple trees (hereon referred to as field trees) were positioned evenly along the centre-line of the room, with an additional thermocouple tree located in the corner of each room. Thermocouples were positioned on the ceiling and floor of the compartment in line with the field trees so that surface temperatures could be measured. Aspirated thermocouples were also positioned throughout the two

compartments to correct for radiation effects. Bi-directional probes were placed in the doorway between the fire and adjacent rooms. Gas sampling lines, 16 in all, were positioned along the centre of the room.

1.3 Zone and Field Models

Two types of computer models, zone and field, are used to simulate fires in enclosures. Zone models divide the volume to be simulated into uniform hot upper, and cold lower, layers, solving the conservation equations of mass, energy and species for each zone, and use empirical correlations to describe characteristics such as entrainment into the fire plume. The advantages of zone models are: - they are easy to run, require little computational time, and are relatively inexpensive. Disadvantages associated with zone models are scenarios where the limitations of the empirical correlations are breached, such as irregular geometries, or fires which have restricted entrainment areas; results of zone models are then likely to be imprecise.

Field models on the other hand divide the volume to be simulated into a three-dimensional grid of tiny cells. The field model then calculates changes in each cube by using fundamental equations of fluid dynamics. They consist generally of a set of three-dimensional, time dependant, non-linear partial differential equations, referred to as the Navier-Stokes equations (Stroup, 1995). These equations express conservation of mass, momentum, and energy. This process of solving the fundamental fluid dynamics with computers is commonly referred to as Computational Fluid Dynamics (CFD). The field model calculates the physical conditions of each cell, which results from changes in adjacent cells. The advantages of field models are that they rely minimally on empirical correlations, so are capable of simulating scenarios without the limitations associated with empirical correlations. The disadvantages are that they are difficult to use as they require a good understanding of the specialist knowledge associated with fluid dynamics (of which most fire engineers know little), need considerably more computer power than zone models, and are relatively expensive.

1.4 Grounds for the Research

With the rapid advancement of computer processing power, reducing computational times of field models to practical levels, the option is becoming viable for fire engineers to use field models to simulate fires to determine the performance and safety levels in buildings, in the event of a fire. It is commonly assumed that field models produce far more accurate results than zone models. However, field models have not been subjected to extensive validation procedures. The most commonly used experimental data used to validate field models is the Steckler et al. (1982) room fire experiments. This involved a series of 45 experiments conducted in a compartment measuring 2.8 m × 2.8 m in plane and 2.18 m in height. The walls were 0.1 m thick and all were covered with light weight ceramic fibre board. The series of experiments consisted of a gas burner fuelled by methane being placed systematically in eight different floor locations with a variety of single compartment openings ranging from small windows to wide doors. Fires were fixed in size for the duration of each experiment, producing strengths of 31.6, 62.9, 105.3 and 158 kW. Steady state was assumed to be reached in 30 minutes. Instrumentation included bi-directional probes and bare wire thermocouples being placed in a vertical plane located midway between the inner and outer edges of the doorjamb. Also, a stack of aspirated thermocouples were placed in the front corner of the room to measure the gas temperature profiles.

Clearly, the validation of field models needs to extend well beyond this simplified scenario, yet there is insufficient data available for more complex geometries and scenarios that field models can be validated with. This research aims to provide data in greater detail and for more complex scenarios to validate field models.

1.5 Goals of the Research

Data collected from the four fire experiments conducted at McLeans Island during the period of 26 November to 1 December, provides an extensive insight into pre-flashover compartmentalized fires. Hence, the major portion of this report will deal with the results obtained from these experiments. Characteristics to be analysed for the fire room, adjacent room, and the doorway include temperature profiles,

temperature variations, corner temperatures, surface temperatures, and concentrations for O₂ and CO₂.

Following the analysis of the four fire experiments, simulations using the SMARTFIRE fire field modelling program developed by the University of Greenwich Fire Safety Engineering Group will be conducted and compared with the experimental results. Two simulations will be run for each fire, one with and one without the six-flux radiation model. Validation with experimental data will only include temperatures measured by the field trees.

1.6 Outline of this Report

Following this introduction, chapter 2 specifies the experimental set-up, and chapter 3 specifies instrumentation used, for the experiments. Observations from the experiments are described in the next in chapter 4. The results and discussion for the experiments are discussed extensively in chapter 5.

The next chapters (6, 7, and 8) relate to the SMARTFIRE field modelling program. Chapter 6 provides an overview of SMARTFIRE; chapter 7 outlines the details of how simulations were run for each experiment; chapter 8 gives the results computed by the SMARTFIRE simulations.

Finally, in chapter 9, comparisons are made between experimental temperature profiles and SMARTFIRE simulations, with an overall conclusion closing the report in chapter 10.

1.7 Limitations of this Report

The limitations of the fire experiments carried out at McLeans Island are as follows:

- Thermocouples were uncorrected for the effects of radiation. Twenty aspirated thermocouples were placed throughout the compartment, however, it was discovered that insufficient quantities of air could be drawn through the steel

pipes housing the thermocouples, rendering temperatures measured by the aspirated thermocouples unusable for radiation correction.

- No experiment is repeated with exactly the same conditions. Appendix 3 gives a fuller account of this and determines how accurately each experiment is likely to be repeated.

The limitations of the SMARTFIRE simulations carried out are as follows:

- It has been assumed that the KBS system used by SMARTFIRE assigns the appropriate number of cells to the problems and distributes the cells appropriately. No runs have been done with higher cell resolutions.
- All surfaces of the compartment were modelled as gypsum plaster. The interior surface of the two-compartment structure was insulated with Intermediate Service Board, with Gib[®] Fyrelite underneath. The option to select two surfaces for the compartments was not available with the SMARTFIRE program, so gypsum plaster was used as a surface for the two-compartment structure.
- The arrival of the SMARTFIRE program for the use in this project was late. Because of this, simulations were run by selecting recommended default settings. Thus, **SMARTFIRE simulations and results must be viewed as PRELIMINARY RESULTS ONLY.**

2 Experimental Set-up

The purpose of this chapter is to describe the configuration of the two compartment experimental set-up used to conduct the fire experiments at McLeans Island for the period 26 November to 1 December 1999. First, a general description is given, followed by specific details on how the two-compartment structure was built.

2.1 General Description

A two-compartment building was constructed to conduct pre-flashover experiments. Starting from steel sections, the frame was built which then allowed Gib[®] Fyreline and Intermediate Service Board to be placed in the interior of the compartment.

The two compartments were separated by a doorway, which had been constructed from steel studs that were welded to the steel frame. This doorway was then insulated with Gib[®] Fyreline and Intermediate Service Board, along with the interior of the compartments.

An illustration of the final layout of the two-compartment structure is shown in Figure 2.1 with interior dimensions specified in Table 2.1.

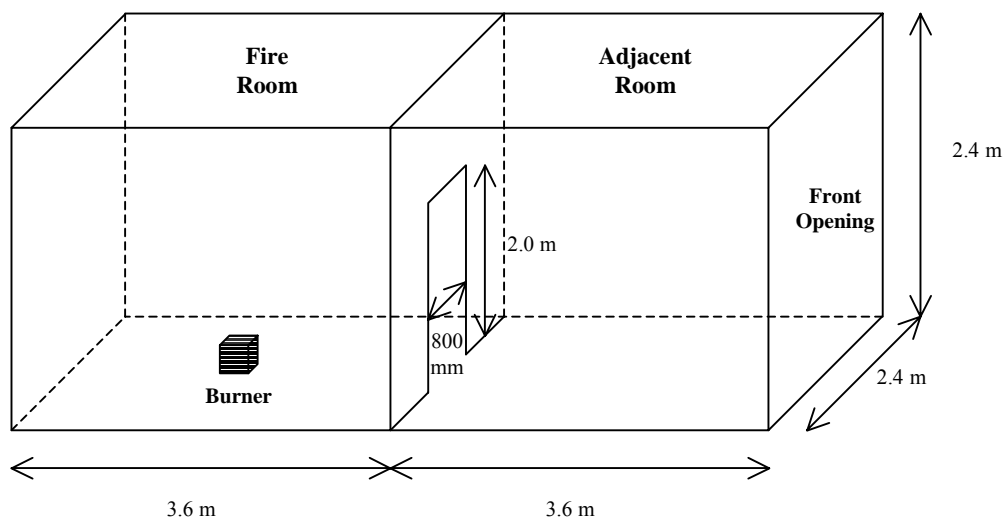


Figure 2.1 Illustration of the Final Layout for the Two-Compartment Structure.

Table 2.1 Compartment Dimensions

Dimensions	Fire Room	Doorway	Adjacent Room
<i>Height (m)</i>	2.4	2.0	2.4
<i>Length (m)</i>	3.6	0.1	3.6
<i>Width (m)</i>	2.4	0.8	2.4

2.2 Metal Frame

Construction of the two-compartment structure began with a metal frame that was slightly larger than the final interior dimensions. This allowed space for the installation of insulating materials on the inside of the container, so that the final interior dimensions would be met.

The frame was first constructed in two separate sections, and then welded together to form the frame for the two-compartment structure. This formed the starting point for the construction of the two-compartment structure. The frame was elevated 0.5 m to allow access underneath the structure so various instruments could be installed later.

Wooden joists 140 mm × 40 mm were attached to the steel frame at spacings of 600 mm to the horizontal section of the steel frame to provide the foundation for a floor and ceiling.

2.3 Insulation

Once the compartment frame was constructed, the interior was insulated with Gib[®] Fyreline and Intermediate Service Board to minimize heat transfer and damage to the structure and attached instrumentation.

2.3.1 Gib[®] Fyreline

Steel studs spaced at 600 mm were attached to the steel framework of the steel structure to allow 12.5 mm Gib[®] Fyreline to be fixed to the interior of the compartments. The Gib[®] Fyreline sheets were fixed to the steel studs at 600 mm

vertical and horizontal centres. The 12.5 mm Gib[®] Fyreline provides 60 minutes of post-flashover fire protection.

Generous amounts of Gib[®] 4 Plus was used to seal all joints between Gib[®] Fyreline plasterboards to ensure minimum leakage within the compartment.

2.3.2 Intermediate Service Board

Upon exposure to temperatures over 100°C (which fire gases exceed considerably), the Gib[®] Fyreline can dehydrate, altering the thermal properties of the Gib[®] Fyreline. This undesirable effect would lead to changing thermal properties of the Gib[®] Fyreline with each experiment. To prevent the dehydration of the Gib[®] Fyreline from the effects of the fire experiments, Intermediate Service Board (0.6 m × 1.2 m) was fitted to the interior of the compartment, over the Gib[®] Fyreline (see Figure 2.2 below).



Figure 2.2 The Intermediate Service Board used to line the Interior of the two-compartment structure.

The Intermediate Service Board is made of glass fibres which have good insulating properties. All Insulation Service Boards were tightly fitted throughout the interior of the compartment to ensure minimal thermal leakage to the Gib[®] Fyreline, and provided uniform thermal insulation properties for all surfaces of the compartment.

2.4 Fire Set-up

2.4.1 Gas Burner

A square gas burner 300 mm wide, elevated 300 mm above the surface of the compartment floor, was placed in the centre of the fire room to provide the fire (see Figure 2.3 below).



Figure 2.3 Gas Burner.

Note: Pilot flame pipe and electrodes to the left of the burner.

A square gas burner is desirable for this experiment as when field models are used to simulate fires, the volume of the compartment is meshed into square and rectangular volumes (see Section 1.3 Zone and Field Models). Therefore a square burner is likely to be modelled more accurately than a circular burner, particularly when a fire is placed in the corner of a room, since a square burner can sit flush in the corner whereas a circular burner cannot.

The combustible gas flowing out of the burner must flow out at low Froude numbers (< 1) for these experiments, as real fires are mostly buoyancy driven flames. Low Froude numbers represent buoyancy driven flames (McCaffery, 1995). Buoyancy driven flames are found in most circumstances where combustion takes place, such as upholstered furniture, wooden cribs, wardrobes with clothing, pool fires etc. A fire at

the end of a pipe that is expelling combustible gases rapidly is not a buoyancy driven flame, but a momentum driven flame (McCaffery 1995).

The Froude number is a dimensionless number and is determined using the following expression:

$$Fr = \frac{V^2}{g2r} \quad (2.1)$$

Where: V is the gas velocity (ms^{-1}),
 r is the radius of the orifice (m), and
 g is the gravitational constant (9.8 ms^{-1}).

To ensure that the LPG from the LPG supply (see Section 2.4.3 for details of the gas supply) is a buoyancy driven flame and not a momentum driven flame, the LPG was dispersed over a much wider area than the diameter of the pipe from the LPG supply that supplies the burner. By feeding the LPG line into the bottom of the burner and dispersing it through a gravel bed of a much larger area, a diffusion flame was established.

2.4.2 Spark and Pilot Flame

A pilot flame was set up to ensure ignition of the burner. The tip of the pilot flame pipe was positioned approximately 150 mm from the fire, at a height of approximately 400 mm. LPG from the main gas source was fed to the pilot flame pipe through the floor.

To ignite the pilot flame, two electrodes were placed approximately 50 mm in front of the pilot flame pipe. The electrodes had a separation of 5 – 10 mm and were attached to high voltage wire through the floor of the compartment. To supply the voltage to the electrodes, a 15 000 volt transformer was attached to the high voltage wires. This set-up consistently produced a spark across the pilot flame. Figure 2.3 shows the pilot flame pipe and electrodes to the left of the burner.

2.4.3 Gas Supply

LPG was used to supply the burner and pilot flame for all experiments. Four 45 kg LPG cylinders were stored outside the building and placed on a load cell, enabling the mass loss rate of LPG to be measured during experiments. For all experiments, all the gas cylinders were connected to a single gas line feeding the burner, ensuring consistent gas flow. Gas flow to the burner was controlled by a mass flow meter (see Section 3.6 Mass Flow Meter).

2.5 Fume Hood and Chimney

To prevent the shed from filling up with hot gases that the two-compartment structure was located in, a fume hood and chimney was built and placed directly over the opening of the adjacent compartment where the fires gases exited, exhausting the fire's gases outside.

3 Instrumentation

The purpose of this chapter is to describe the instrumentation used to measure properties such as temperature profiles, gas species concentrations, and velocities of gas currents generated by the compartmented fires.

3.1 General Description

After the construction of the compartment (the steel frame, Gib[®] Fyreline, and Intermediate Service Board) was complete, instrumentation was put in place to measure properties of the fires. The physical properties measured were:

- Vertical temperature profiles throughout the compartment,
- Surface temperatures throughout the compartment,
- O₂, and CO₂ concentrations at various locations in the compartment, and
- Velocity profiles through the central doorway and exterior opening.

All of these properties are commonly predicted using computer zone or field models (Cox, 1994) to give an approximation of the behaviour of compartmented fires. Thus, instrumentation that measures these properties was placed extensively throughout the compartment.

3.2 Thermocouples

To measure vertical temperature profiles throughout the compartment, thermocouple trees were placed evenly throughout the compartment. Nine were positioned evenly through the centre of the compartment, with the aim of validating any field model applied to the scenario. Two more were placed on the sidewalls (one in each room), with the intention of validating zone model simulations of the same experiments. Surface temperatures were measured using black steel plates with thermocouples attached to the underside (i.e. the thermocouples were not exposed to the atmosphere in the compartment), on the floor and ceiling of both compartments, in line with the thermocouple trees that are positioned to validate field model data. To correct for radiation on thermocouples, 20 aspirated thermocouples were placed in various

positions throughout the compartment enabling exposed thermocouples to be corrected for radiation.

3.2.1 Field Trees

To enable the validation of vertical temperature profiles for field models such as SMARTFIRE, thermocouple trees were placed evenly throughout the compartment. Spacing for the nine thermocouple trees is illustrated in Figure 3.1 below.

Fire Room					Adjacent Room			
Tree 1	Tree 2	Tree 3	Tree 4	Tree 5	Tree 6	Tree 7	Tree 8	Tree 9
+	+	+	+	+	+	+	+	+
150 mm	900 mm	1800 mm	2700 mm	3600 mm	4500 mm	5400 mm	6300 mm	7200 mm

Figure 3.1 Field Tree Positions (Crosses indicate field trees).

The thermocouple trees were positioned 100 mm off the centre of the compartment, with the end 100 mm bent at a 90° angle so that the tip of the thermocouple was positioned along the centre of the room.

Thermocouples used on the trees were type K bare bead 24 gauge with low temperature glass insulation (K24lt), and type K bare bead 24 gauge with high temperature glass insulation (K24ht). Each thermocouple tree held 14 thermocouples (tied in place with wire). Each tree had identical thermocouple spacing, with the exception of the thermocouple tree in the central doorway of the compartment. This had 13 thermocouples spaced evenly at 150 mm, starting at 1900 mm from the floor. Type K24ht were used for the top nine thermocouples for each tree (which were fed into the compartment through the ceiling), as this region undoubtedly reaches high temperatures. The remaining five thermocouples below were of type K24lt (fed through the floor). Spacing for the thermocouples (abbreviated as TC) are listed in Tables 3.1 and 3.2 for the field trees and doorway field tree, respectively. A picture of the upper portion of a thermocouple tree can be seen in Figure 3.2.

Table 3.1 Thermocouple Locations on Field Trees

TC Height (mm)	2375	2350	2300	2250	2200	2150	2100
<i>TC Type</i>	K24ht	K24ht	K24ht	K24ht	K24ht	K24ht	K24ht
TC Height (mm)	1850	1600	1350	1100	900	600	300
<i>TC Type</i>	K24ht	K24ht	K24lt	K24lt	K24lt	K24lt	K24lt

Table 3.2 Thermocouple Locations on Field Trees in the Doorway

TC Height (mm)	1900	1750	1600	1450	1300	1150	1000
<i>TC Type</i>	K24ht	K24ht	K24ht	K24ht	K24ht	K24ht	K24ht
TC Height (mm)	850	700	550	400	250	100	
<i>TC Type</i>	K24ht	K24ht	K24lt	K24lt	K24lt	K24lt	



Figure 3.2 Field Thermocouple Trees in the Fire Room.

Note how the thermocouples are bent 90°. This is so they are positioned along the centre-line of the room.

Type K24ht and K24lt thermocouples measured temperature as a voltage, which was sent to a computer and converted to a temperature (see Section 3.5 Data Acquisition).

3.2.2 Zone Trees

To verify zone fire modelling for the experiments conducted, two separate trees were fixed to each room wall in the compartment. Each tree was located 150 mm from the rear wall of each room. The trees each had 15 thermocouples; type K24lt thermocouple wire was used for each tree. The thermocouples were spaced evenly at 150 mm (this allows the determination of the interface height by various methods

(Weaver, 2000) which can then be compared to zone model data) with each thermocouple insulated with stainless steel piping that was mounted to the wall through the exterior of the compartment. Figure 3.3 shows the configuration of the zone thermocouple tree in the adjacent room.



Figure 3.3 Zone Tree in the Adjacent Room

3.2.3 Floor and Ceiling Surface Thermocouples

To measure the surface temperature of the compartment, modified type K24lt thermocouples were positioned on the floor and ceiling of the compartment in line with the field trees. Thin steel plates (approximately 1 mm thick and 100 mm square) were first spray-painted black creating an absorptivity of approximately 1. The thermocouples were then glued on in the centre of the plates with high temperature cement. Four holes on the outer edges of the plates were drilled, and the thermocouple plates were fixed into line on the floor and ceiling with the field trees. Figure 3.2 illustrates a surface thermocouple. Note: Due to experimental difficulties, some thermocouples were absent - one floor thermocouple in line with tree 3, and two ceiling thermocouples - one at tree 5 and one at tree 9.

3.2.4 Corner Thermocouples

To measure temperature profiles in the corner (along the centre-line of the compartment) of each room, thermocouples (type K24ht) were positioned in the corners, as shown in Figure 3.4. Thermocouples were positioned in a similar way to the field trees, where they were aligned along the ceiling 100 mm off the centre-line of the compartment, with the end 100 mm bent at a 90° angle so the tip of the thermocouple was positioned along the centre-line of the room. Each corner contained 15 evenly spaced thermocouples. Figure 3.5 shows the spacing for the corner thermocouples. Figure 3.6 shows a picture of the corner thermocouples located near the back wall of the fire compartment.

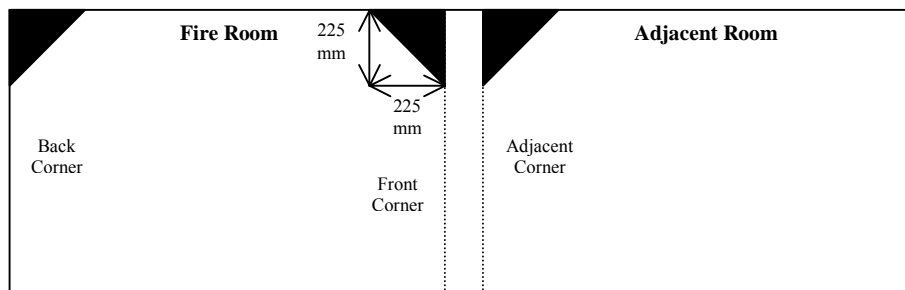


Figure 3.4 Corner Thermocouple Locations

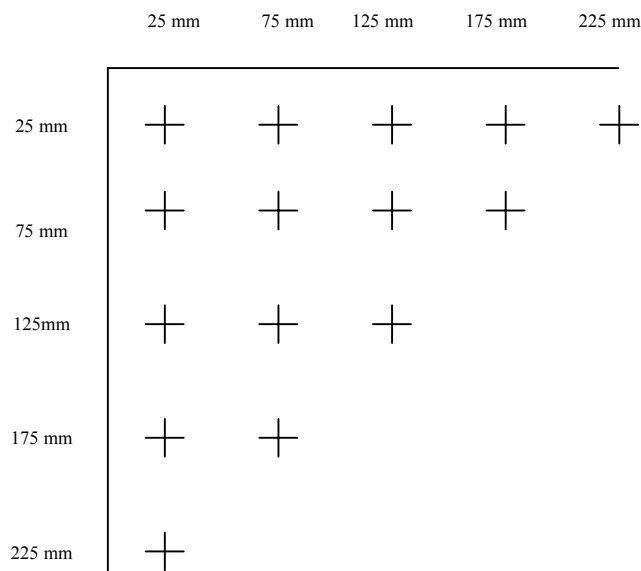


Figure 3.5 Corner Thermocouple Positions. Each cross represents a thermocouple position.



Figure 3.6 Corner Thermocouples

3.2.5 Aspirated Thermocouples

Radiation can be emitted and absorbed by thermocouples (Blevins, 1999). If the thermocouple's temperature is high it will radiate heat, lowering its temperature. If a thermocouple is cool but near the fire (for instance, near the floor by the fire) it will absorb radiation, increasing its temperature. Both of these affect the thermocouple's ability to measure the surrounding air temperature accurately. To overcome this, 20 aspirated thermocouples were positioned throughout the compartment. The aspirated thermocouples were type K24lt thermocouples but insulated with $\frac{1}{4}$ inch steel tubing. Air is drawn through the steel tubing from a pump. Since the steel pipe conceals the thermocouples, radiation from the fire does not increase its temperature, and emission of radiation by the thermocouple does not reduce its temperature as the constant airflow ensures a very low temperature gradient between the thermocouple and the air.

The aspirated thermocouples were used to correct the thermocouples on the field trees for the effects of radiation. The positions of the 20 aspirated thermocouples are listed in Table 3.3. Each was held in place by a steel brace. Figure 3.7 shows aspirated thermocouples with bracings.

Table 3.3 Aspirated Thermocouple Positions

Location	Height (mm)
<i>Tree 2</i>	300, 600, 2100, 2250
<i>Tree 4</i>	300, 600, 2100, 2250
<i>Tree 5</i>	300, 600, 1600, 1900
<i>Tree 7</i>	300, 600, 2100, 2250
<i>Tree 9</i>	300, 600, 2100, 2250



Figure 3.7 Aspirated Thermocouples and Gas Sample Lines

Note: Unfortunately the aspirated thermocouples were not able to be used to correct for the effects of radiation on the bare thermocouples as it was discovered that the pump was drawing insufficient air through the aspirated thermocouple lines.

3.3 Gas Analysis

To measure O₂, CO₂, and CO concentrations, 16 gas sampling points were positioned at various locations along the centre-line in the two-compartment structure. Table 3.4 lists the sample point locations.

Table 3.4 Gas Sampling Point Locations

Position	Sampling Point (Height from Floor, mm)
<i>Tree 2</i>	300, 600, 1950, 2250
<i>Tree 4</i>	300, 600, 1950, 2250
<i>Tree 5</i>	400, 700, 1600, 1900
<i>Tree 7</i>	300, 600, 1950, 2250

The gas analysing equipment (referred to as gas analyser throughout the rest of this report) used to determine the concentrations of O₂, CO₂, and CO consisted of a Servomex 540A paramagnetic oxygen analyser for O₂ and a Siemens ULTRAMAT 6.0 NDIR gas analyser (dual-cell, dual beam with a flowing reference gas) for CO₂ and CO. Note: The CO concentration for these experiments was below the limitations of the gas analyser, therefore no analysis of CO concentrations for the experiments is given.

A valve, that could be opened or closed manually, was attached to each sampling line. This allowed each sample point location to be sampled by the gas analyser for a set time (for these experiments each sample line was sampled for three minutes).

3.4 Bi-directional Probes

Velocity profiles through the doorway and on the ceiling of the compartment were measured using bi-directional probes, as shown in Figure 3.8.



Figure 3.8 Bi-directional Probes Located in the Doorway

The 7 bi-directional probes in the doorway were spaced at intervals of 300 mm starting at 100 mm off the floor. The bi-directional probes were then connected to a differential pressure transducer that measured the pressure difference across the bi-directional probe head as a voltage. A computer then recorded this voltage.

By measuring the pressure drop across the bi-directional probe, the velocity can be determined (Emmons, 1995). This is done using the following expression:

$$V = 0.93 \sqrt{\frac{2\Delta p}{\rho}} \quad (3.1)$$

Where: V is the velocity (ms^{-1}),
 Δp is the pressure drop across the bi-directional probe (N/m^2), and
 ρ is the density of the air (kg/m^3).

Air density is determined using the ideal gas law:

$$\rho = \frac{Mp}{RT} \quad (3.2)$$

Where: M is the molecular mass of the air in the compartment (kg/mol),
 p is the pressure in the compartment (N/m^2),
 R is the universal gas constant (8134 J/kg.mol.K), and
 T is the temperature in Kelvin (K).

The air in the compartment contains combustion products. Since the exact composition of the combustion gasses is not known and 10% of the air or less is used for combustion, the composition is assumed to be ambient air. The molecular weight of air is 28.95 mol/kg at 25°C. Using the ideal gas law the density can be determined:

$$\rho = \frac{352.8 \text{ (kg)}}{T \text{ m}^3} \quad (3.3)$$

Therefore, the temperature is required at each bi-directional probe location to determine the density of air. Each bi-directional probes position was in line with type K24lt and type K24ht thermocouples, enabling the temperature at each bi-directional probe to be measured. Note: Unfortunately the bi-directional probe data was unable to be analysed as preliminary results suggested the bi-directional probes contained blockages.

3.5 Data Acquisition

Two computers were used to monitor and record data collected by thermocouples, bi-directional probes and gas analyser. A 90 MHz Pentium Pro was used to record temperatures for the zone trees and gas concentrations and a 450 MHz Pentium III

was used to record temperatures measured by the field, corner and surface thermocouples. All measurements were recorded every 5.2 – 5.3 seconds by both computers and saved as CSV files, which were on average a size of one Mbyte.

3.6 *Mass Flow Meter*

The mass flow rate of LPG to the burner must be controlled to produce consistent and reproducible fire sizes. To control the mass flow rate of LPG to the burner, a High Flow Mass Controller and Meter Model 5853E was installed between the burner and LPG cylinders. The High Flow Mass Controller and Meter Model 5853E controlled mass flow within the desired range with a quoted error by the manufacturer of 1%.

3.7 *Visual Record*

Each experiment was captured on two camcorders: One recorded the fire inside the compartment; the other recorded the gas sample valves to certify which sample lines were being analysed.

4 Observations

The purpose of this section is to give a qualitative account of the experiments conducted at McLeans Island. The following observations were made:

- As fire size increased, flame height increased.
- All fires hot gases contained soot particles, indicating incomplete combustion.
- As fire size increased, so did the level of soot generated by the fire.
- As fire size increased, flame height increased.
- In the fire room, the centrally located fires were all leaning away from the doorway. This behaviour has been observed previously (Quintiere et al., 1981). This is a result of incoming air's momentum pushing over the fire's flames.
- As fire size increased, radiation emitted by the fire increased. This was easily felt by standing in front of the compartment.
- The ceiling jet was clearly visible in the adjacent compartment. Since the adjacent compartment had no soffit, this prevented the build-up of hot gases.
- In the fire compartment, the production of hot, turbulent gases could be seen. This increased with an increase in fire size.
- A hot buoyant upper layer could be seen in the fire compartment. This hot upper layer was caused by the soffit constraining gas flow out of the fire compartment.
- The 110 kW corner fire's flames were the highest of all fires. The corner fire's flames reached and extended along the ceiling.
- The 110 kW corner fire's flames looked the 'smoothest' of all fires. The centrally located fire's flames were considerably more turbulent looking.



Figure 4.1 55 kW Fire



Figure 4.2 110 kW Fire



Figure 4.3 160 kW Fire



Figure 4.4 110 kW Corner Fire

5 Experimental Results and Discussion

Details relating to measurements made by the field thermocouple trees (commonly referred to as ‘trees’ throughout the rest of this report), corner thermocouples, surface thermocouples, and gas sample lines of the centrally located 55 kW, 110 kW, 160 kW fires, and the 110 kW corner fire are presented and discussed in this chapter.

5.1 Aims

This chapter aims to present steady state results from the data collected by the:

1. Field tree thermocouples,
2. Corner thermocouples,
3. Surface thermocouples, and
4. Gas sampling locations.

Details on how the above four sets of results are expressed, are discussed in Data Presentation and Analysis below.

5.2 Data Presentation and Analysis

This section discusses how data collected for the field trees (see Appendix 1 for tabulated results), corner thermocouples, surface thermocouples (see Appendix 2 for tabulated results), and gas sampling locations are presented and analysed.

5.2.1 Field Trees:

1. **Temperature profiles of the field trees are compared for the four fires.**
This is expressed as 9 Temperature vs. Height scatter graphs, one for each field tree with the temperature profiles for the four fires represented on each graph. The field trees are analysed in this manner so that an insight into how different fire sizes affect the vertical temperature profiles at each field tree location.

2. **Investigate the temperature variation from the average temperature during steady state for the thermocouple locations on each tree.** This is expressed on 9 bar graphs (with the four fires represented in each graph) where the standard deviation from the average temperature for each thermocouple tree during steady state, was recorded. The level and location of turbulence and/or mixing of ambient air with hot fire gases inside the compartment will be seen if the standard deviation during steady state is sizeable.
3. **An overall comparison per fire between field trees in each room.** This is expressed as 8 Temperature vs. Height scatter graphs with the field trees for each room on one graph, for each fire (Note: Trees 1, 2, 3 and 4 are in the fire room and trees 6, 7, 8, and 9 are in the adjacent room, with tree 5 situated in the doorway. See Section 3.2.1 for locations). This will give an insight to how vertical temperature profiles change within each room.

5.2.2 Corner Thermocouples

The average temperatures measured by the corner thermocouples located in the rear and front of the fire room, and in the adjacent room, are presented in tabular format. Each table represents one corner thermocouple set for each fire. The standard deviations for the temperatures measured over the steady state period are included to give an indication of the temperature variations for the thermocouples.

5.2.3 Surface Thermocouples:

The temperatures measured by the surface thermocouples are presented in four separate graphs. They are:

1. Temperature vs. Floor Thermocouple Location,
2. Temperature vs. Ceiling Thermocouple Location,
3. Temperature Difference Between Surface Thermocouple and Nearest Bare Bead Thermocouple on Thermocouple Tree vs. Thermocouple Location (two graphs, one for the ceiling thermocouples and one for the floor thermocouples).

These graphs are presented to gain an insight into temperature profiles by the surface thermocouples.

5.2.4 Gas Analysis

The concentration profiles of O₂ and CO₂ are presented in tabular format where the concentrations for each species at each sample point location for the trees which have sampling lines attached (see Section 3.3 for locations) are presented for the four fires. Included is the ratio of O₂ consumption to CO₂ production (see Appendix 4 for the background theory on the expected ratio of O₂ consumption to CO₂ production). This will give an indication of the efficiency of the LPG combustion within the compartment.

5.3 Method

5.3.1 General Method for the Field Trees, Corner Thermocouples and Surface Thermocouples

There were common data reduction techniques between aims 1, 2, and 3 as set out in the previous section. Previous experiments similar in nature to this experiment (but not in as greater detail) by Steckler et al. (1982) assumed steady state for their experiments occurred after 30 minutes. This allowed a constant heat and radiative flux to be established. Therefore, at steady state, instrumentation would not measure transient effects. Reports on field modelling results (Kerrison et al., 1994) of the Stecker et al. (1982) experiments suggest 30 minutes may not have been sufficient to allow the experiments to come to steady state. All thermocouples, field and surface, were analysed at steady state for this experiment. Steady state is assumed to begin at 45 minutes after the main burner had been ignited. From here, data was averaged over a 10 minute period. That is, for each thermocouple (type K24lt, type K24ht, and surface), temperatures measured were averaged over a 10 minute period. Since the temperature was measured every 5.2 – 5.3 seconds, this resulted in 115 measurements being averaged for each thermocouple. The minimum and maximum temperatures for every thermocouple on each tree was also noted for the 10 minute period and are

presented in Appendix 1. Note: The 110 kW corner fire is denoted as 110 kW c in all graph legends and in some tables throughout the rest of this report).

5.3.2 Method for Field Trees

Reduction Technique for Temperature Profile of the Field Trees for Different Fires

Thermocouple temperatures on each tree were averaged using the method mentioned in Section 5.3.1. One scatter graph is plotted for each field tree, illustrating its vertical temperature profile. Temperatures measured by each tree for the four fires, are represented on each graph.

Reduction Technique for the Variation in Temperature for the Field Trees during Steady State

The standard deviation for the 10 minute steady state period, was determined for the temperatures measured by the thermocouples on each tree, and then plotted on a bar graph. The horizontal axis represents the standard deviation for the temperature on each field tree, and the vertical axis represents the thermocouple height on each tree.

Comparisons Between Field Trees in Each Room per Fire

Thermocouple temperatures on each tree were averaged using the method mentioned in Section 5.3.1. Vertical temperature profiles for trees in each room are plotted on scatter graphs for the four fires.

5.3.3 Corner Thermocouples

Thermocouple temperatures in Tables 5.1 – 5.12 were averaged using the method mentioned in Section 5.3.1. Each table represents the average temperature and standard deviation of the temperatures (as an indication of temperature variation) measured for each corner thermocouple set per fire.

5.3.4 Surface Temperature Profiles

Temperature profiles for the surface thermocouples, both ceiling and floor, have been determined in a similar fashion to the tree thermocouples, that is, temperatures recorded were averaged over a ten minute period starting from the 45th minute into the experiments. Throughout this section, surface thermocouples on the ceiling and floor are referred to as ‘ceiling and floor thermocouples’.

5.3.5 Gas Analysis

Concentration profiles of O₂ and CO₂ were measured at various heights and locations (mentioned in Section 3.3) in the two-compartment structure.

During each experiment, sample point locations were sampled for three minutes, starting from the 13th minute of each experiment. To allow for the time lag associated with sampling lines, the concentration for each sample point location was determined by averaging measurements over the last minute. This gave each sample point two minutes for the gas species at that location to reach the gas analyser.

Gas species concentrations are presented as percent volume, with the measured gas concentrations subtracted from the ambient concentration (measured in the first three minutes of the experiment before the experiment started), that is, the gas concentrations are expressed as differences. Also, the ratio of oxygen consumed verses carbon dioxide formed is given at every height. Results are presented in tabular format, with gas concentrations for the fires presented for each tree with sample lines, plus the doorway.

5.4 Results

5.4.1 Field Trees

Temperature Profiles of Each Tree for Different Fires

Results for the temperature profiles of each tree for the four fires are listed below in Figures 5.1 – 5.9. Field trees are listed in numerical order.

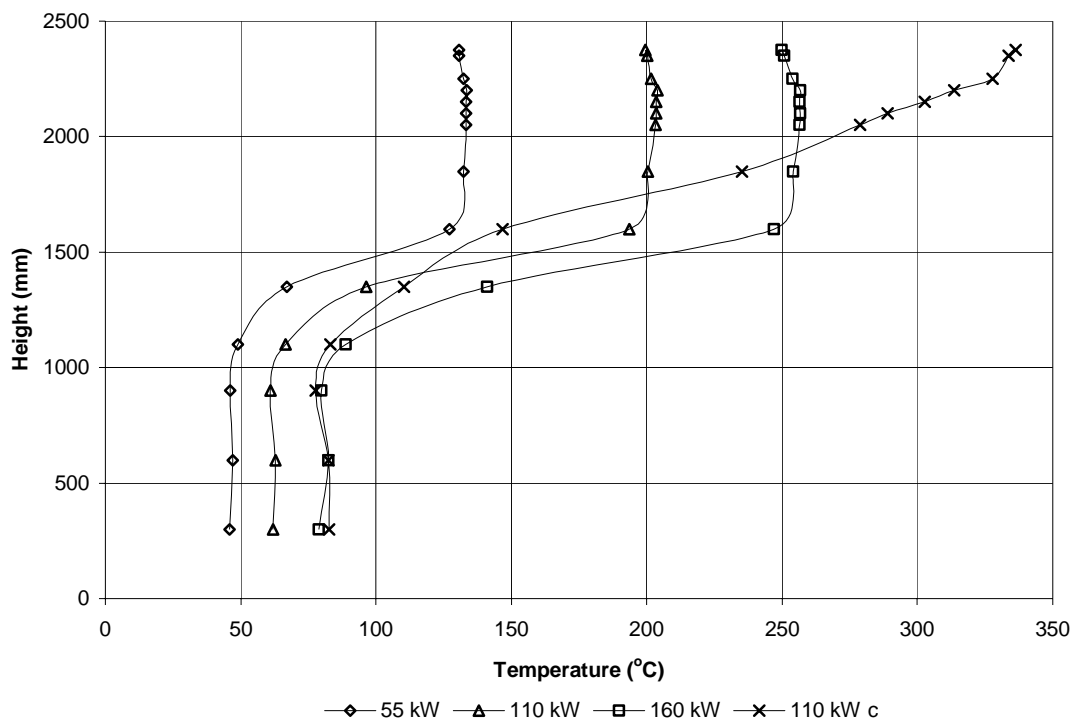


Figure 5.1 Temperature Profile for Tree 1 (All Fires)

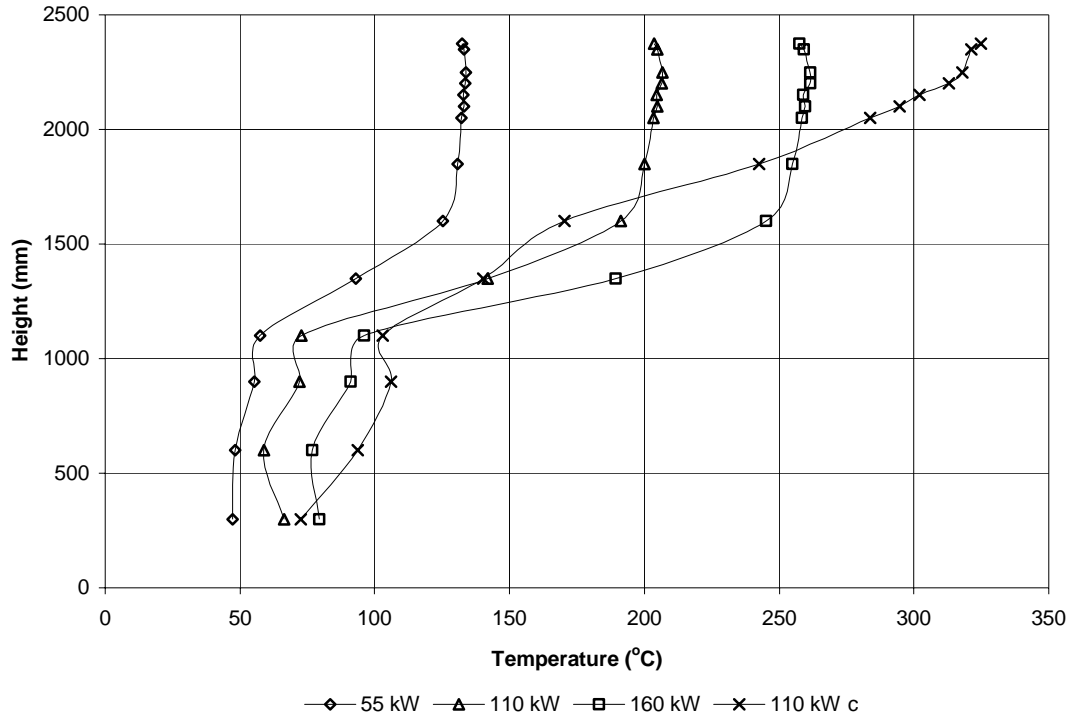


Figure 5.2 Temperature Profiles for Tree 2 (All Fires)

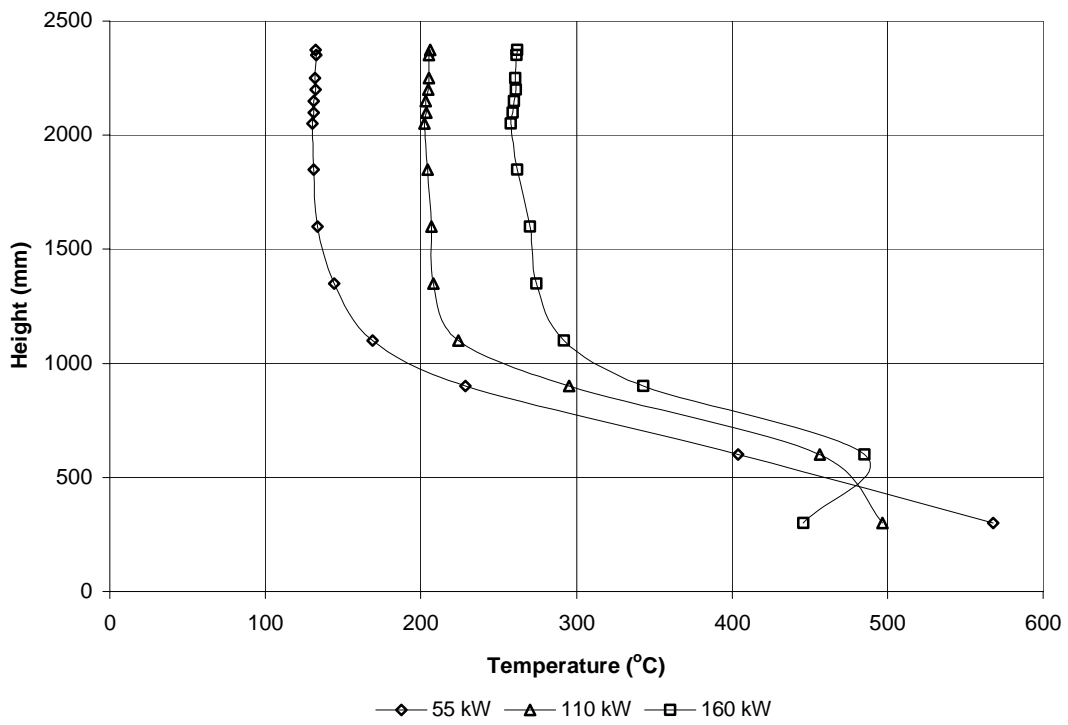


Figure 5.3 Temperature Profiles for Tree 3 (55 kW, 110 kW, and 160 kW fires)

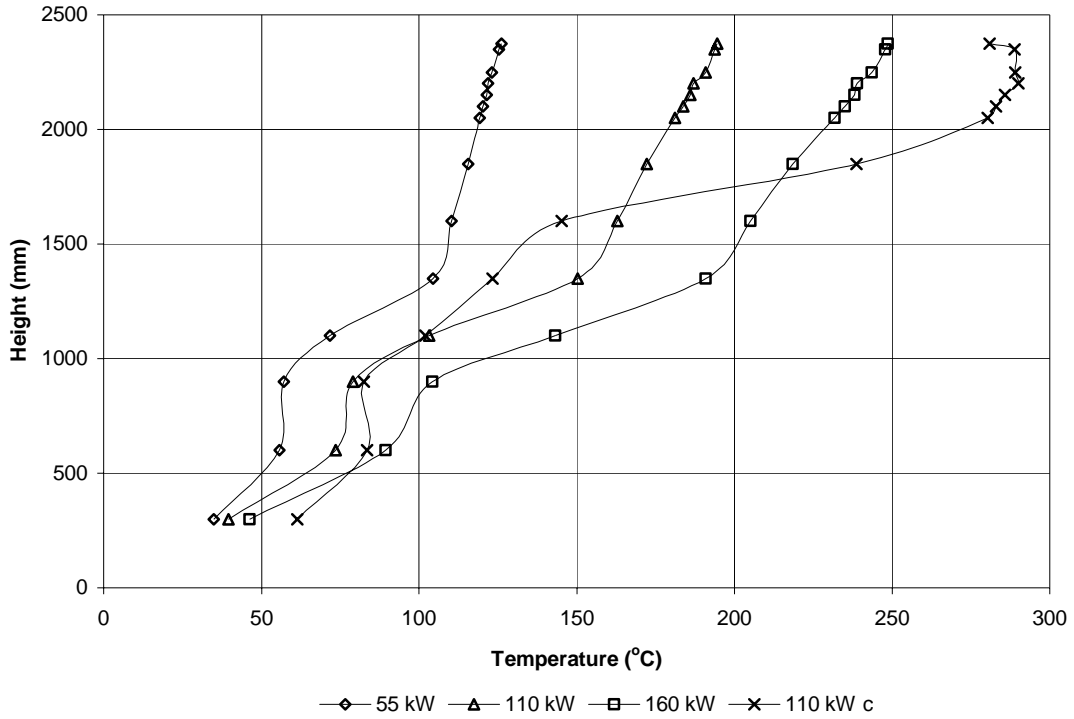


Figure 5.4 Temperature Profiles for Tree 4 (All Fires)

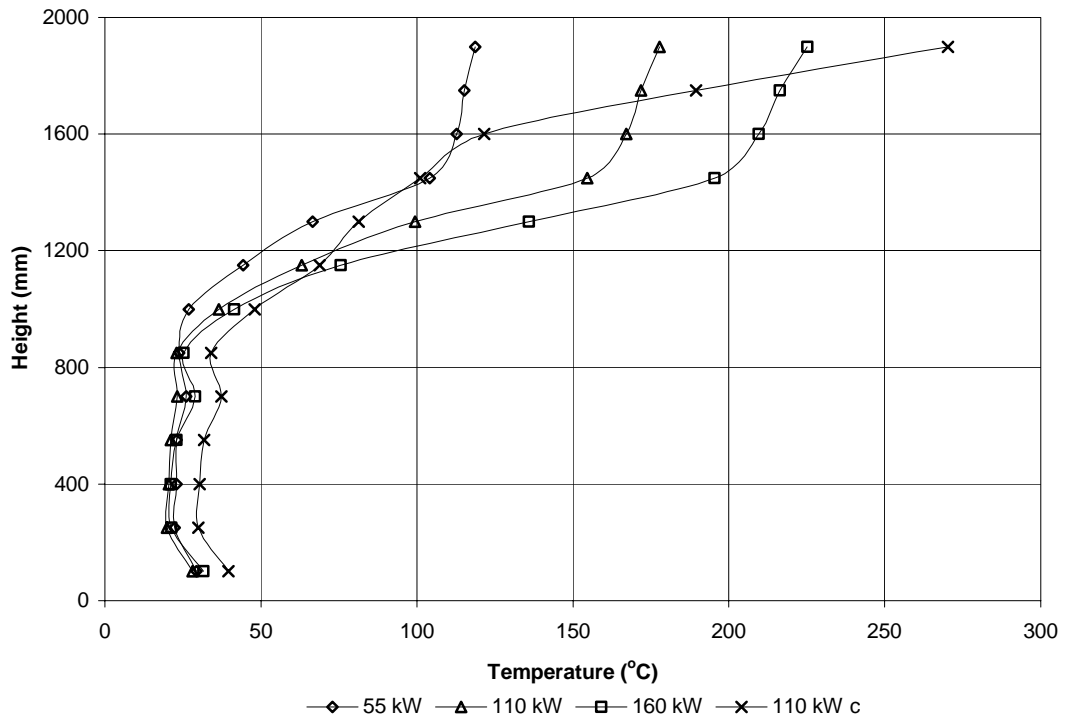


Figure 5.5 Temperature Profiles for Tree 5 (Doorway, All Fires)

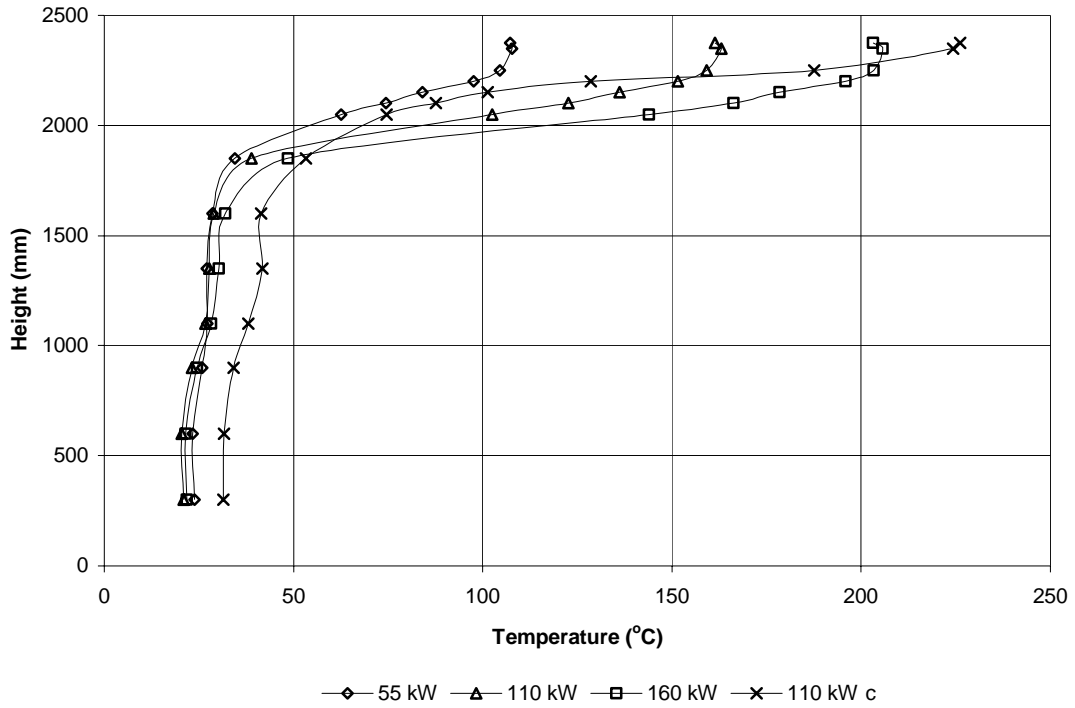


Figure 5.6 Temperature Profiles for Tree 6 (All Fires)

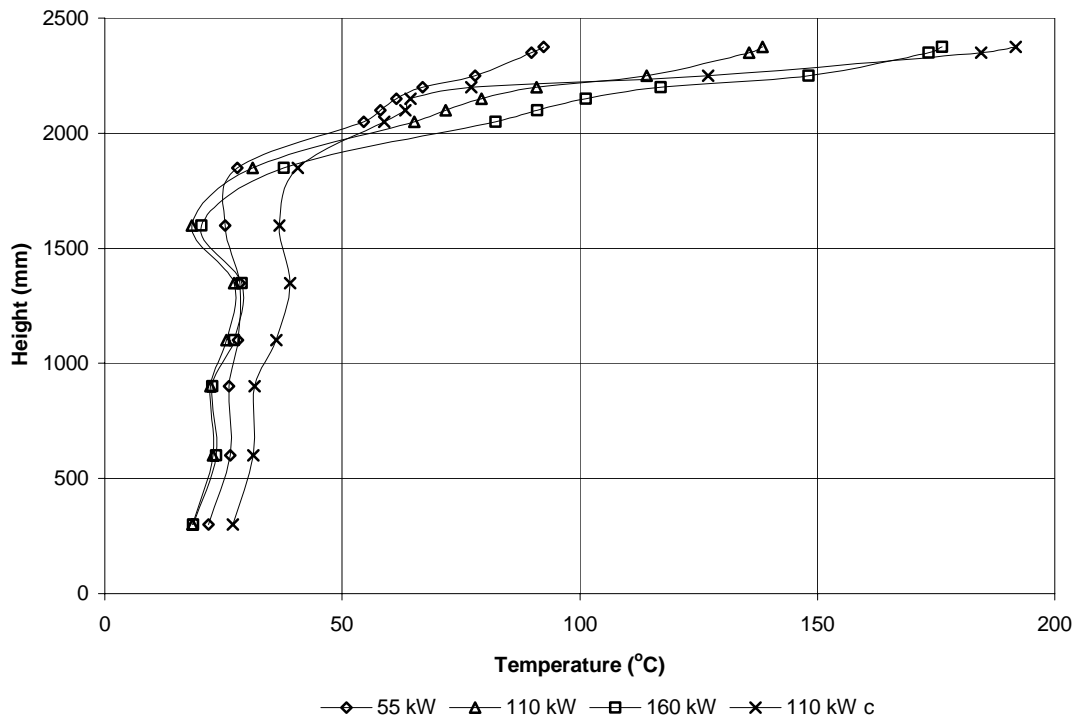


Figure 5.7 Temperature Profiles for Tree 7 (All Fires)

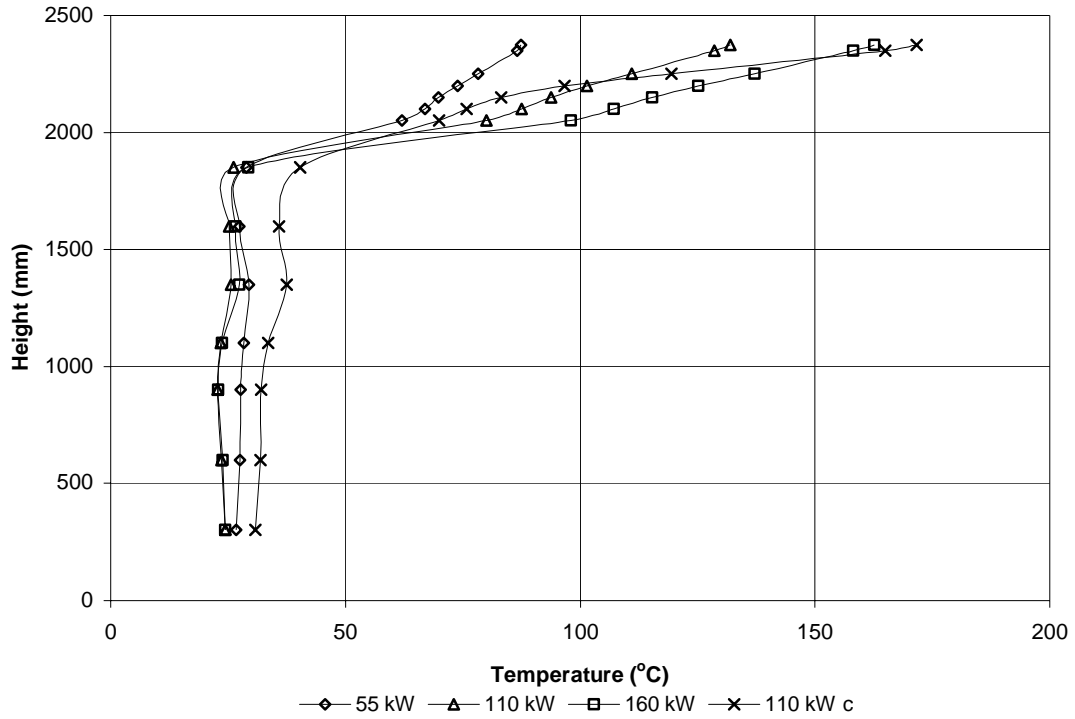


Figure 5.8 Temperature Profiles for Tree 8 (All Fires)

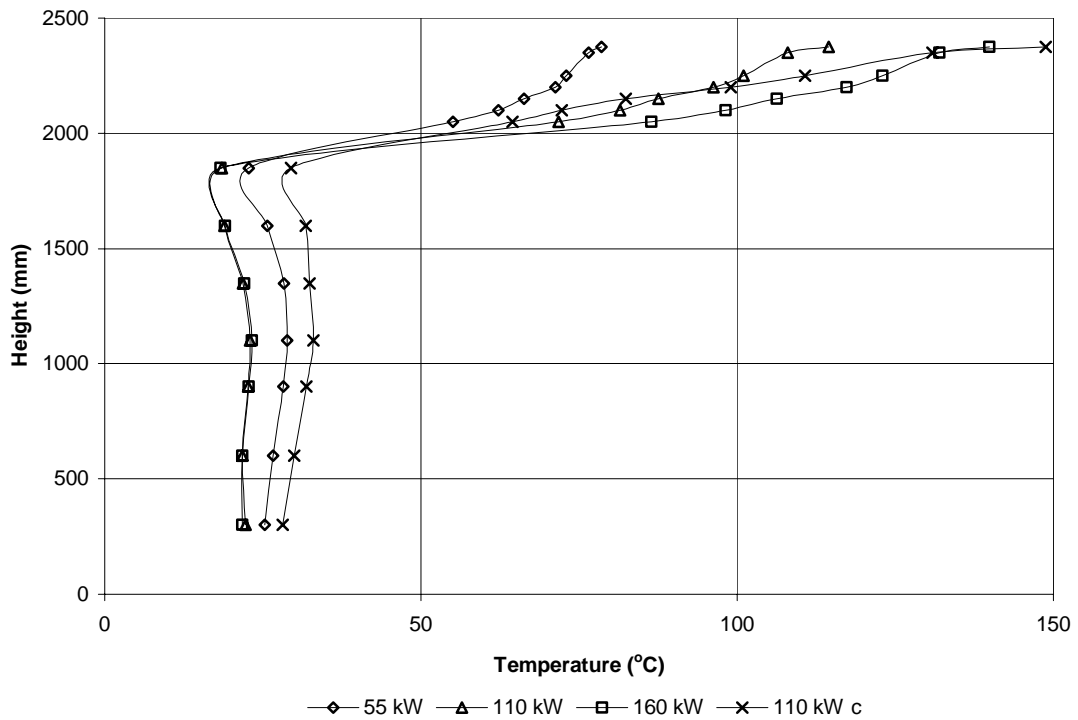


Figure 5.9 Temperature Profiles for Tree 9 (All Fires)

Variation in Temperature for Each Tree

Results for temperature variations (expressed as standard deviations) recorded over the 10 minute steady state period are listed below in Figures 5.10 – 5.18. Field trees are listed in numerical order.

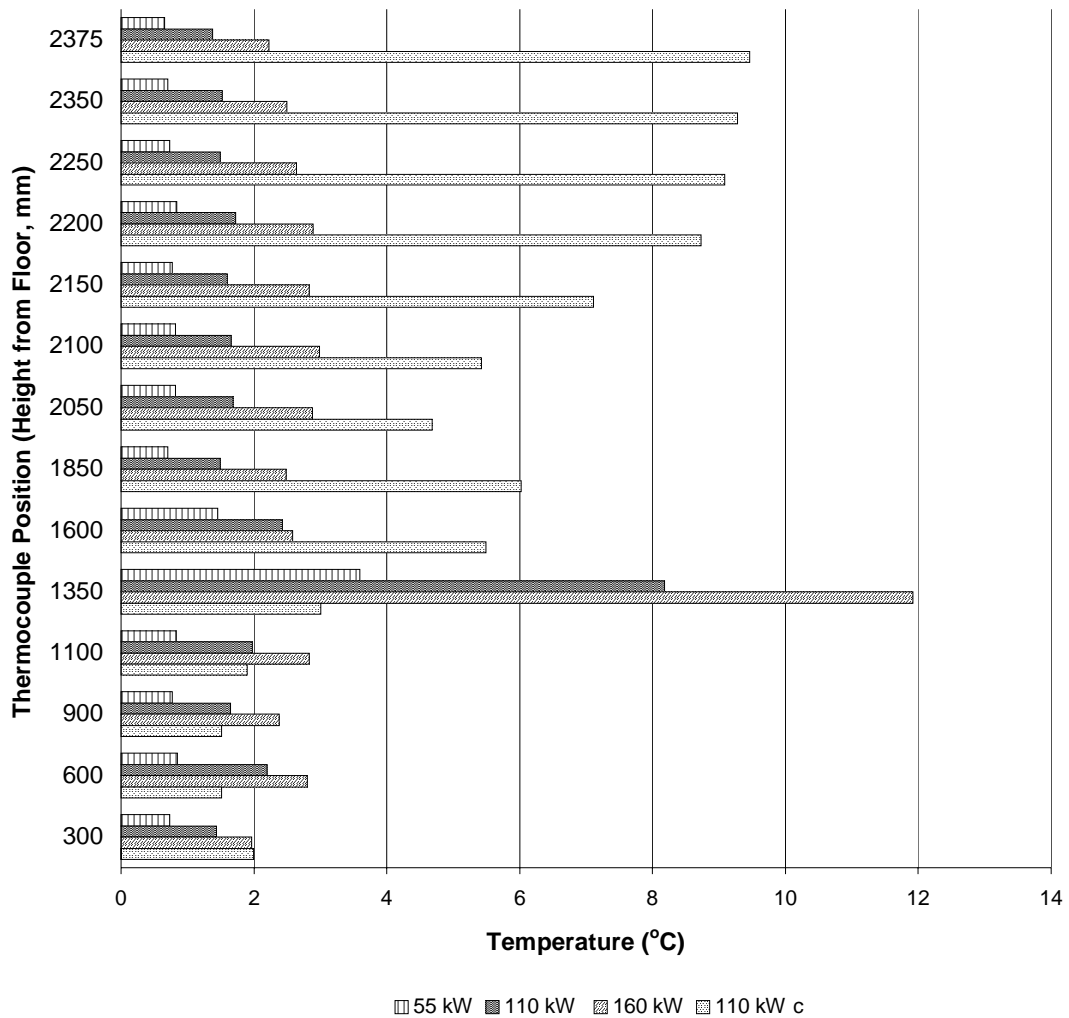


Figure 5.10 Temperature Variations For Tree 1 (All Fires)

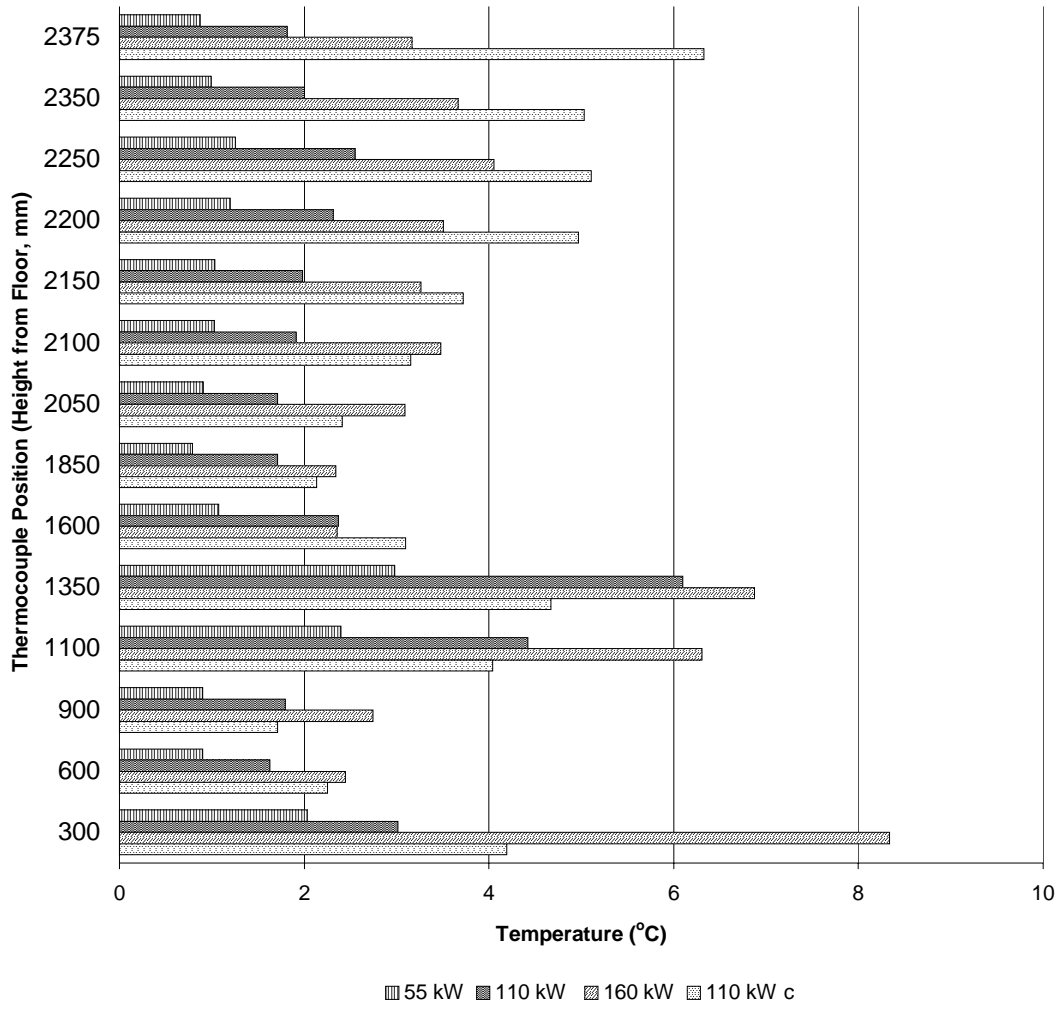


Figure 5.11 Temperature Variations for Tree 2 (All Fires)

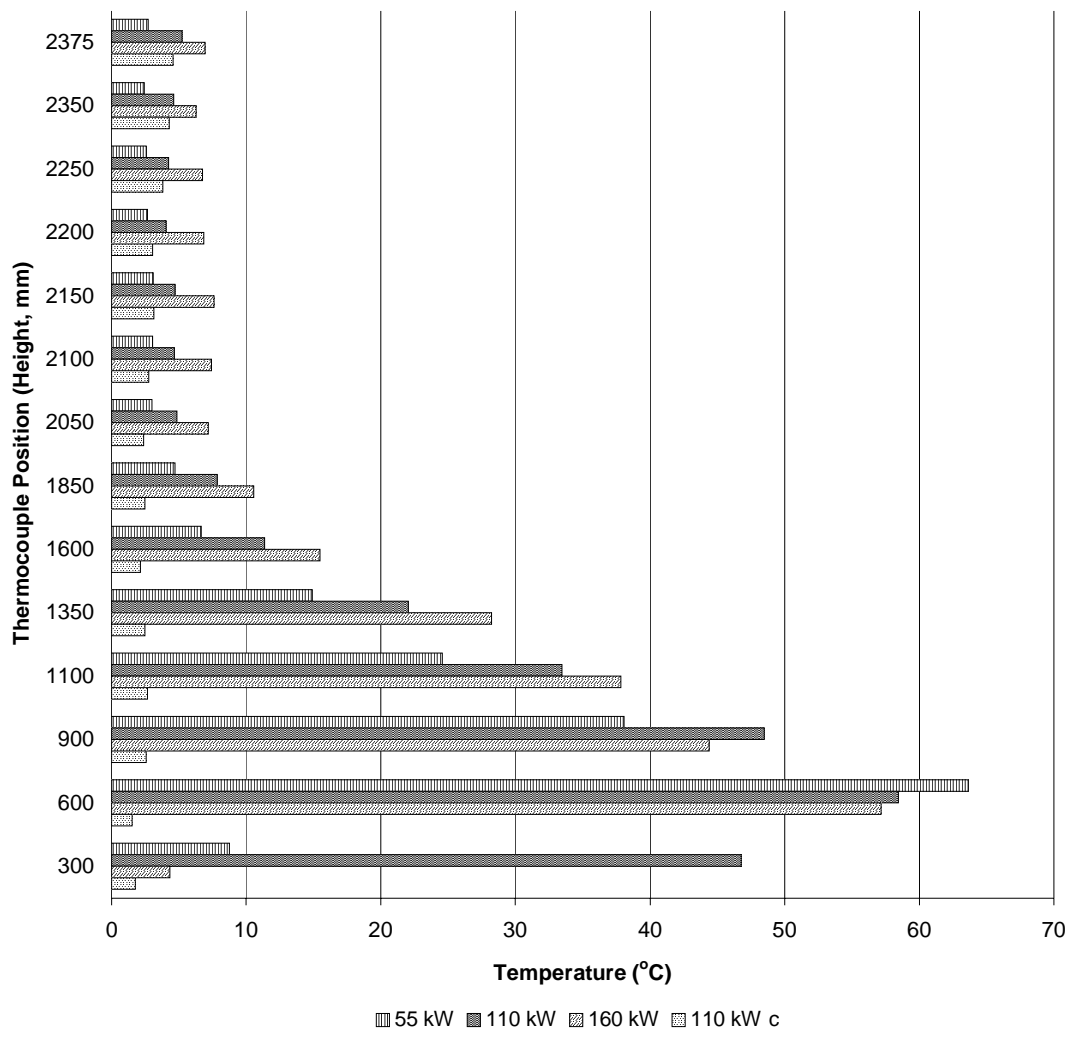


Figure 5.12 Temperature Variations for Tree 3 (55 kW, 110 kW, 160 kW fires)

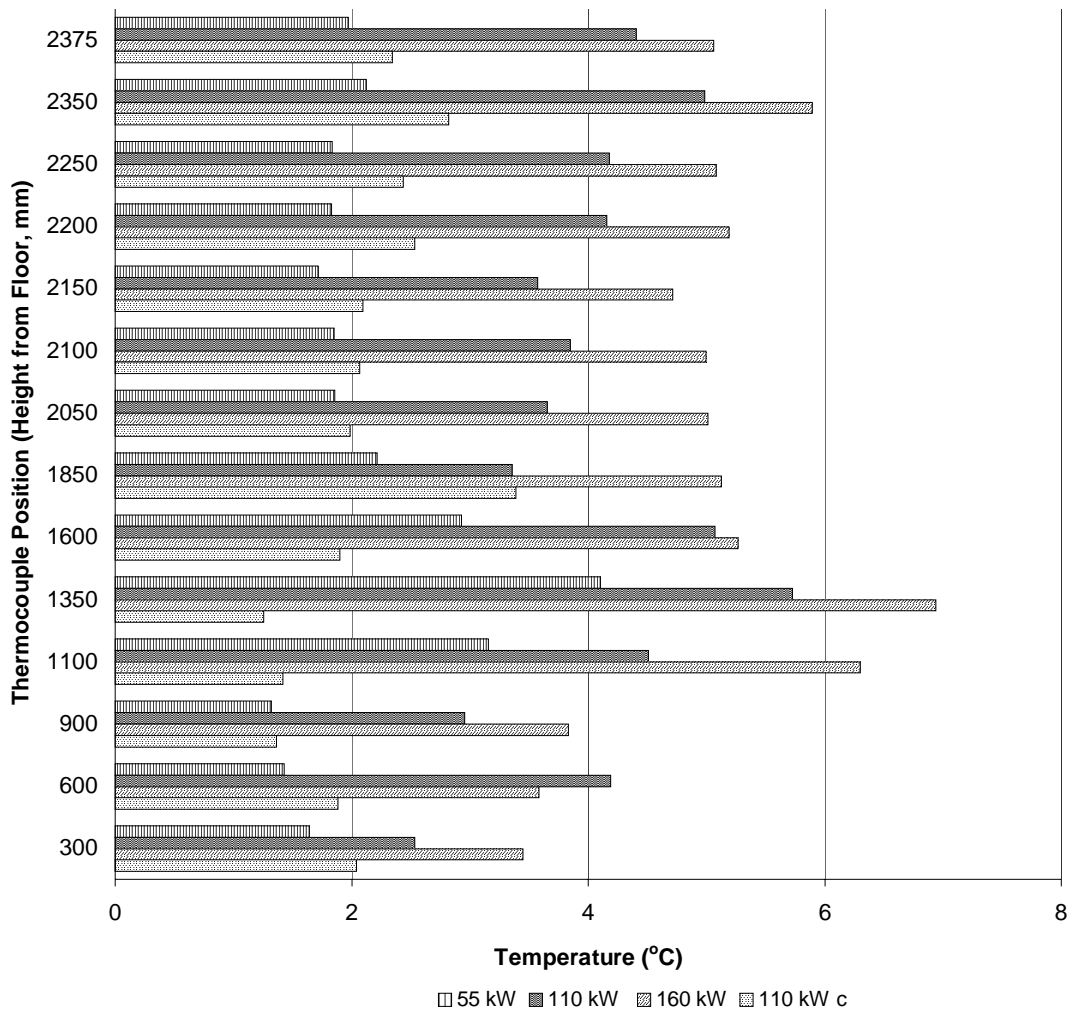


Figure 5.13 Temperature Variations for Tree 4 (All Fires)

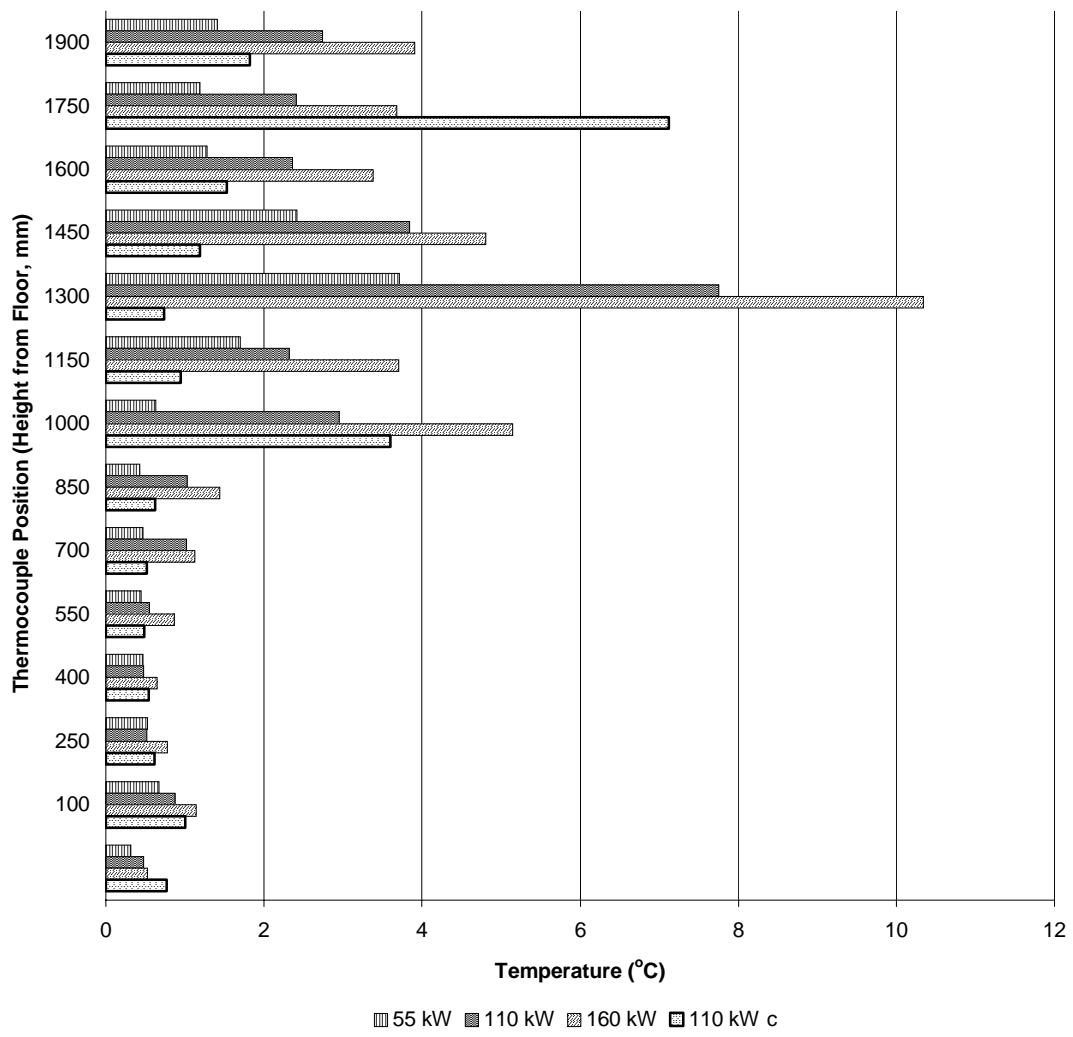


Figure 5.14 Temperature Variations for Tree 5 (Doorway, All Fires)

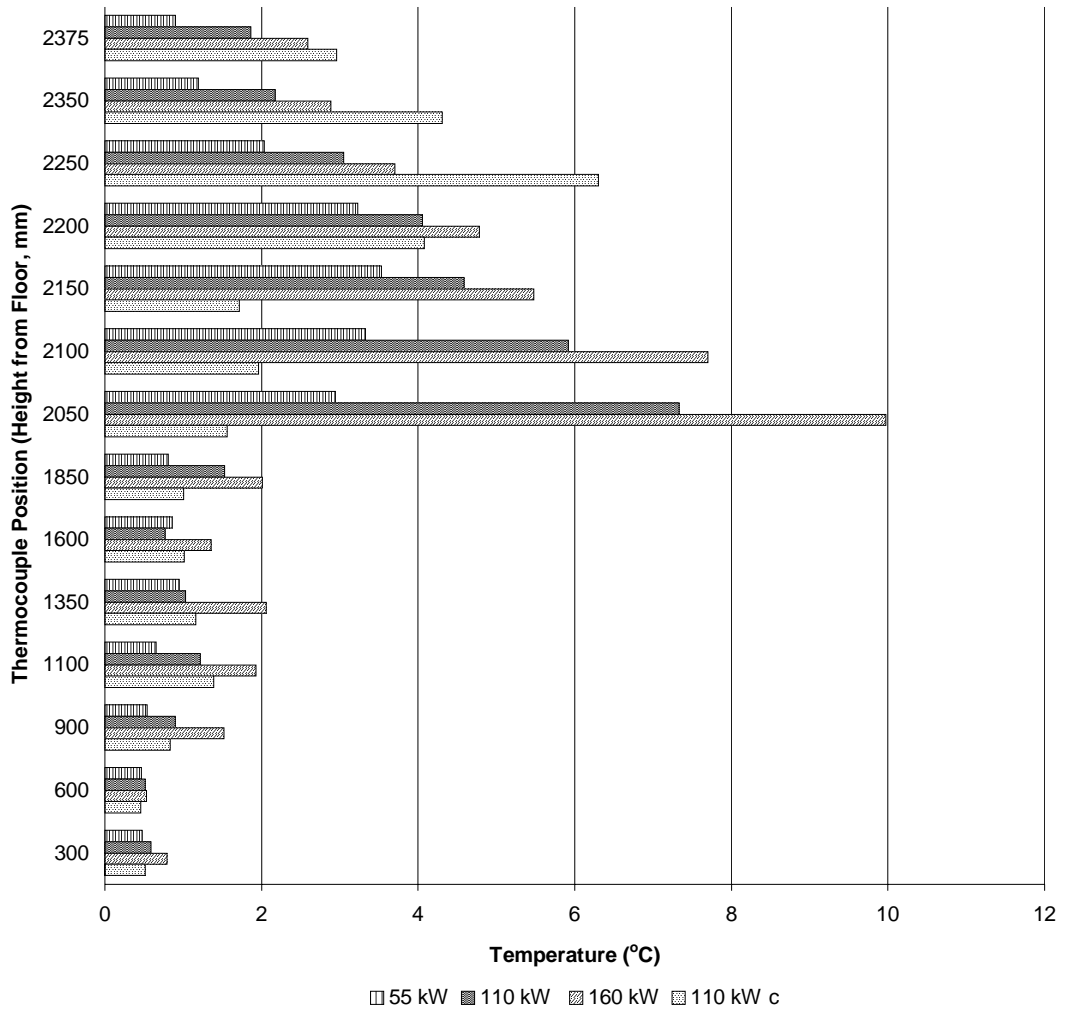


Figure 5.15 Temperature Variations for Tree 6 (All Fires)

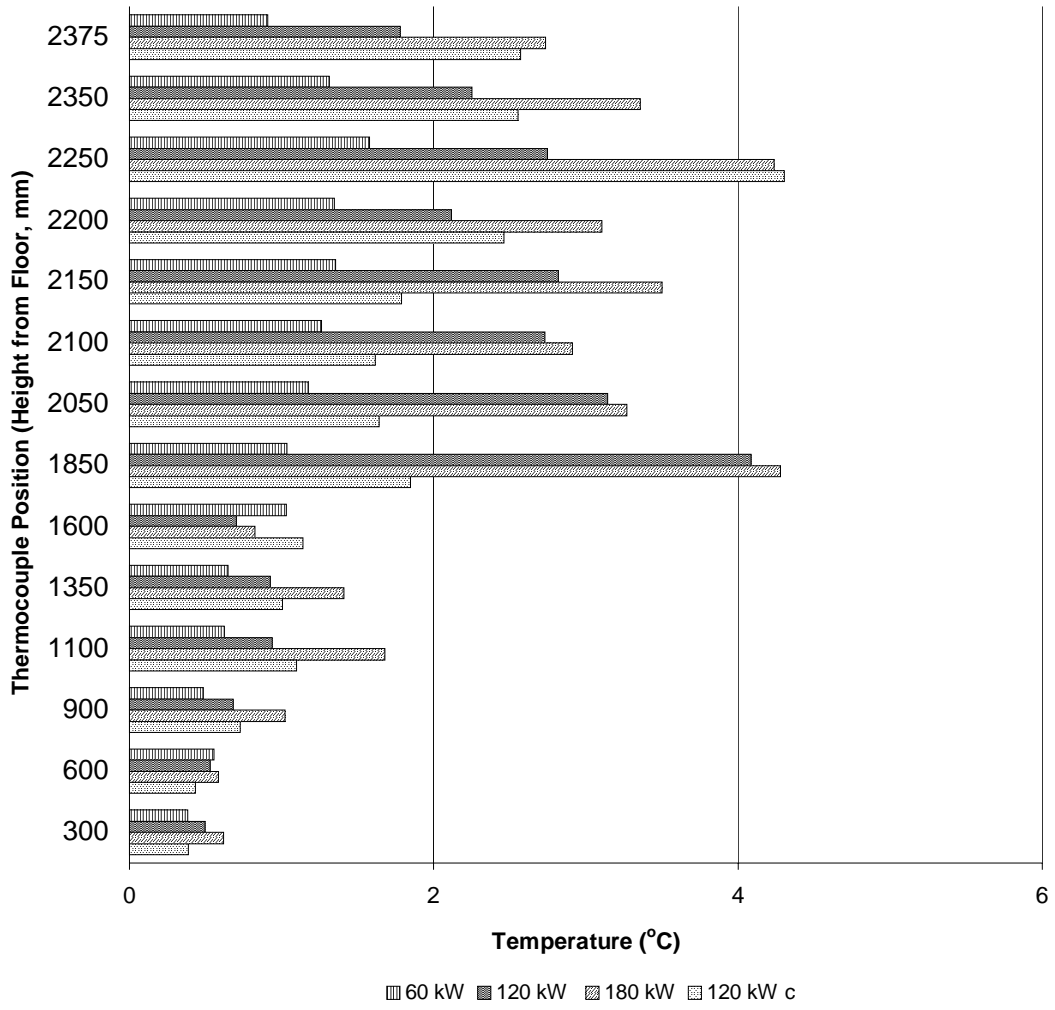


Figure 5.16 Temperature Variations for Tree 7 (All Fires)

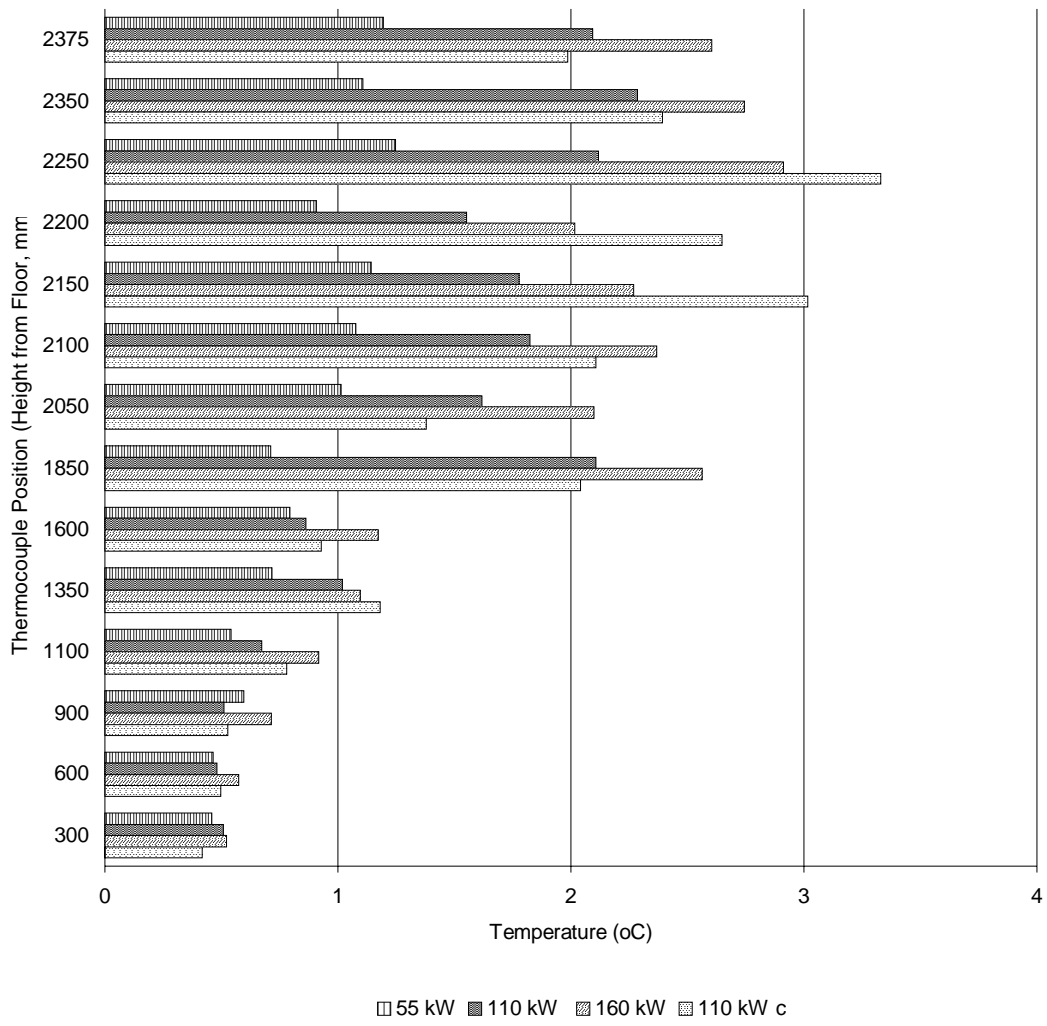


Figure 5.17 Temperature Variations for Tree 8 (All Fires)

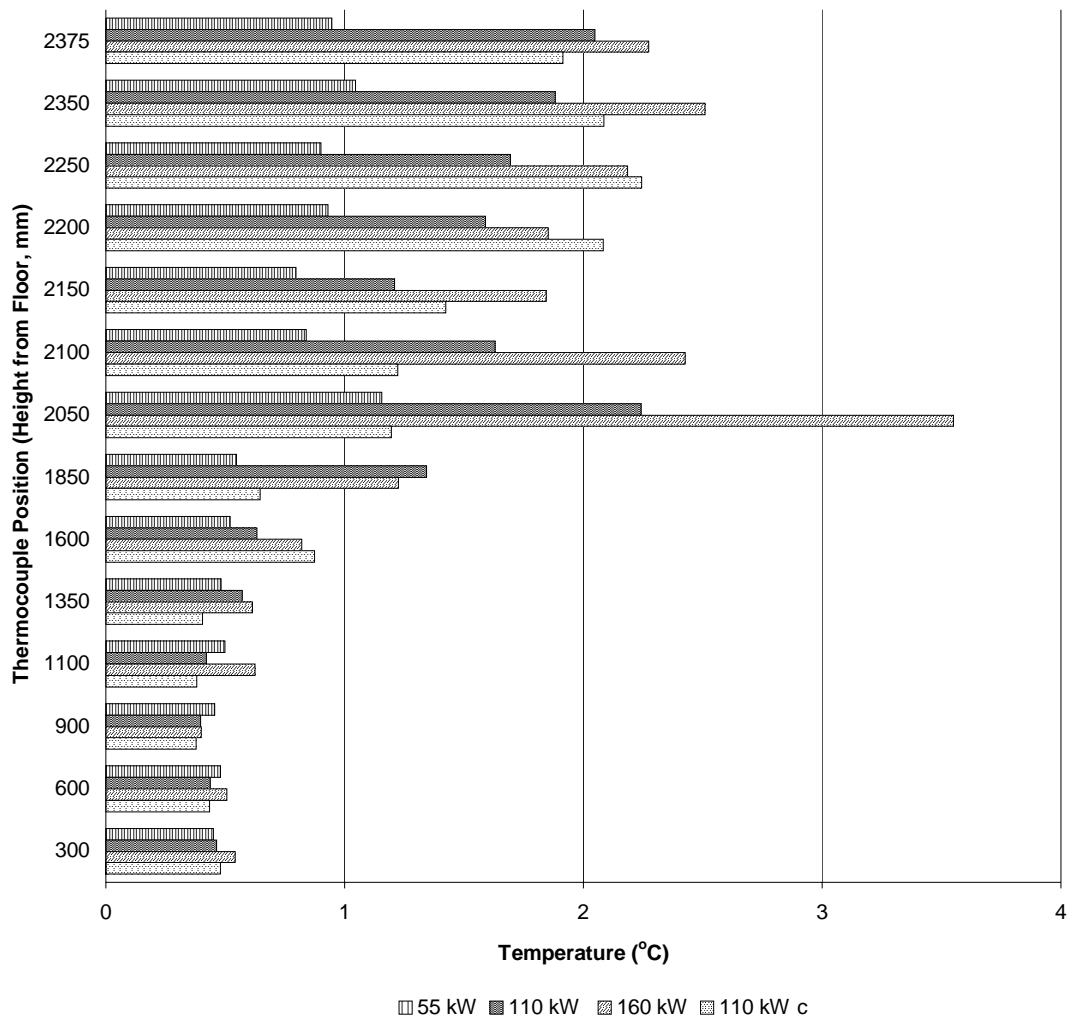


Figure 5.18 Temperature Variations for Tree 9 (All Fires)

Comparisons between Field Trees in Each Room per Fire

Comparisons between field trees in each room for each fire are listed below in Figures 5.19 – 5.26. Graphs are presented in order of increasing fire size.

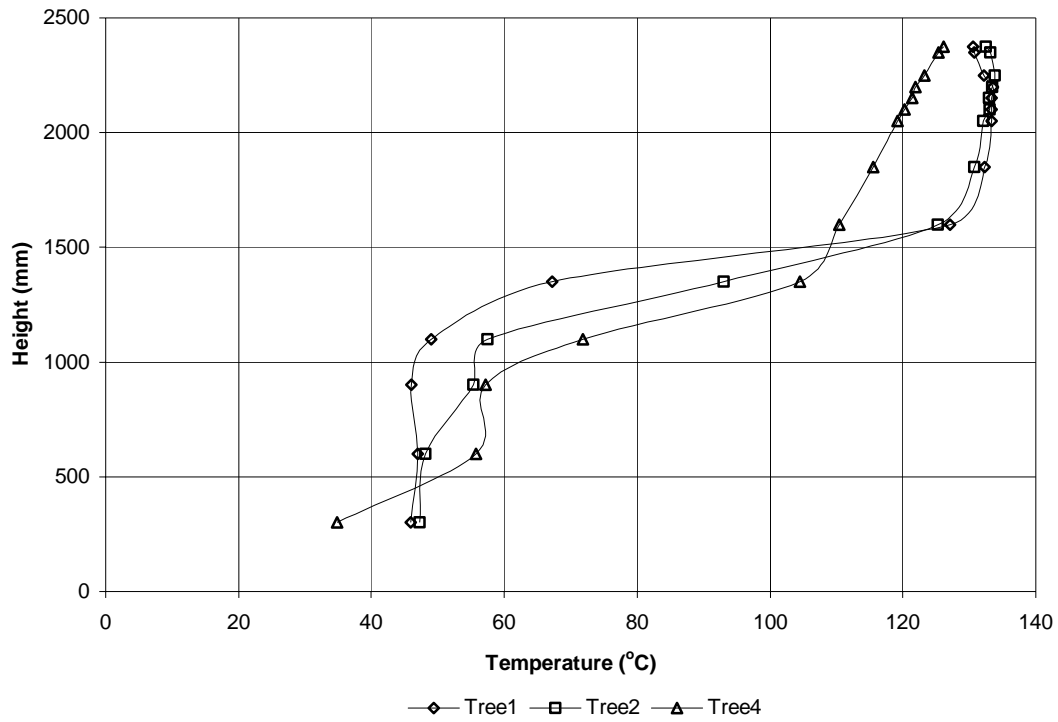


Figure 5.19 Temperature Profiles for Fire Room, 55 kW Fire

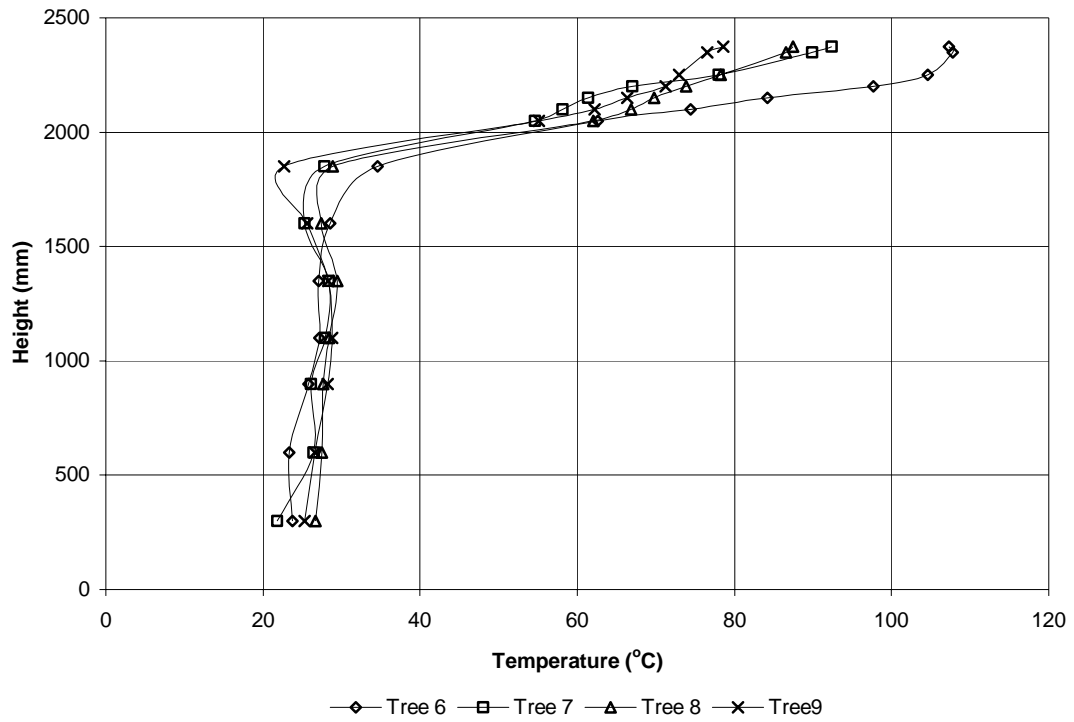


Figure 5.20 Temperature Profiles for the Adjacent Room, 55 kW Fire

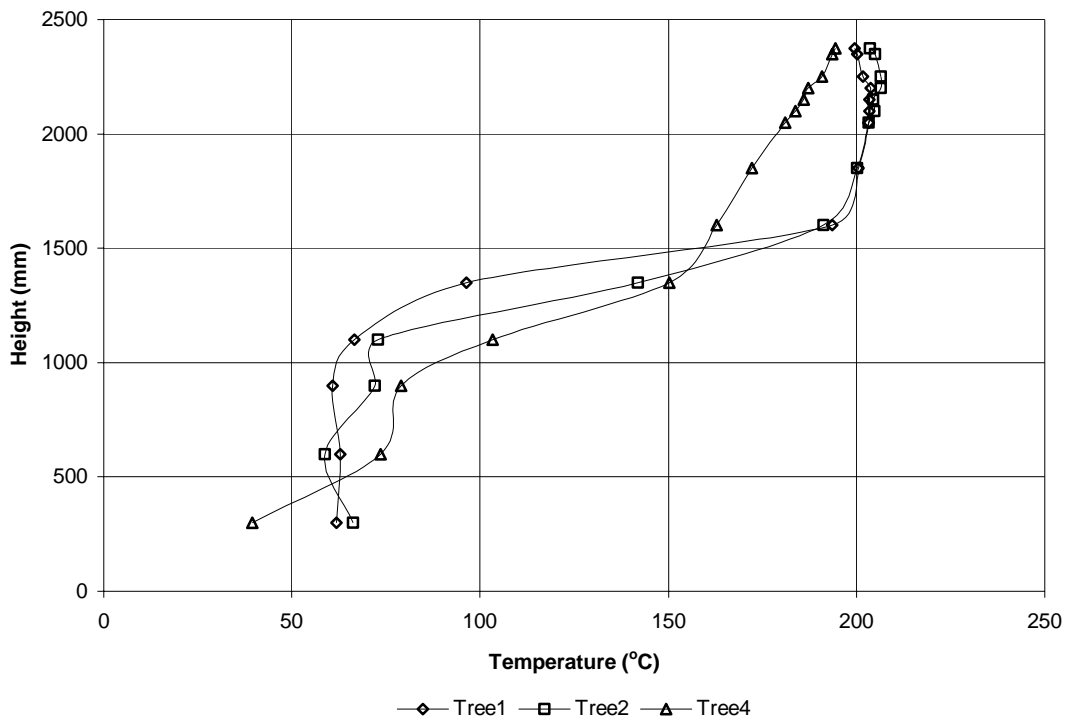


Figure 5.21 Temperature Profiles for the Fire Room, 110 kW Fire

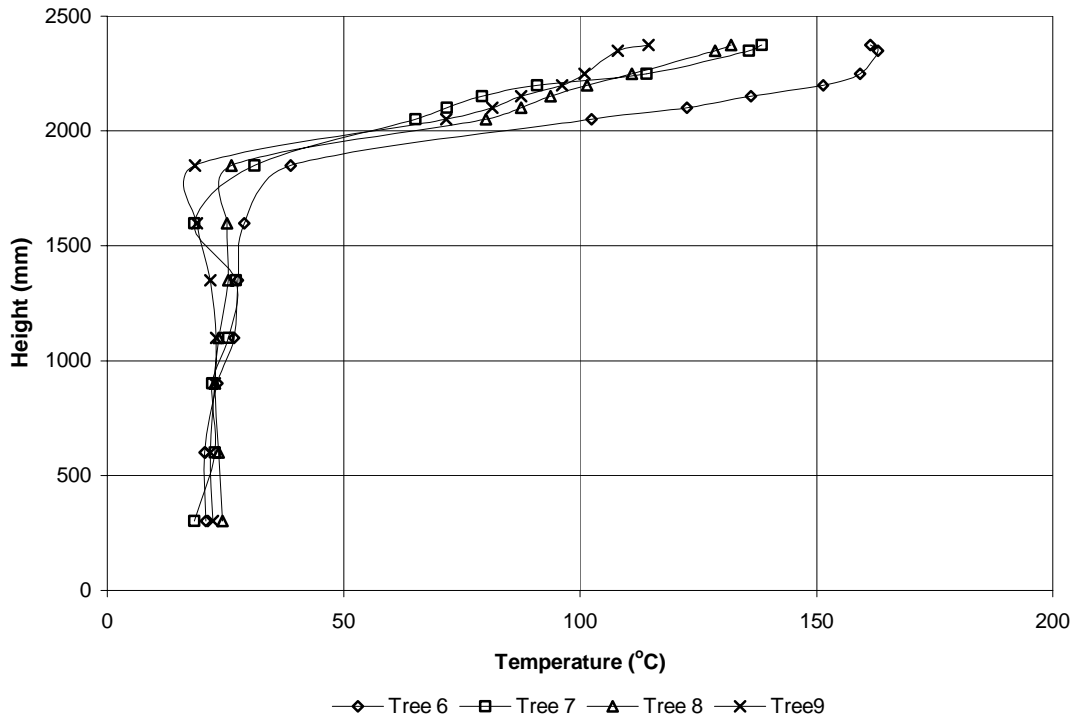


Figure 5.22 Temperature Profiles for the Adjacent Room, 110 kW Fire

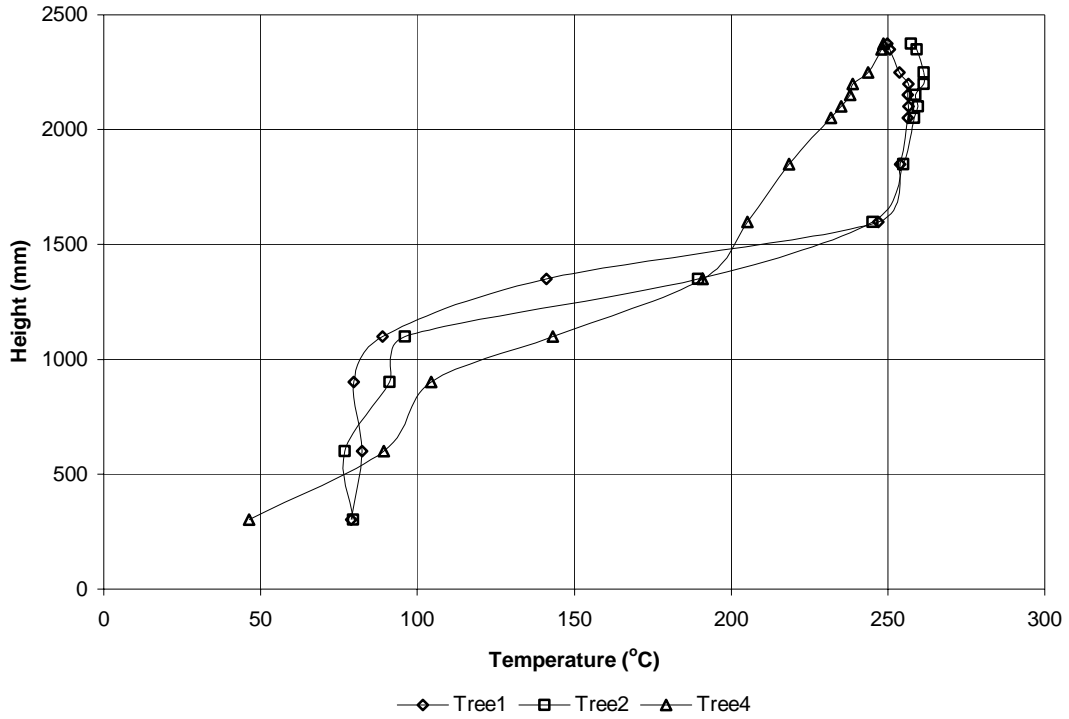


Figure 5.23 Temperature Profiles for the Fire Room, 160 kW Fire

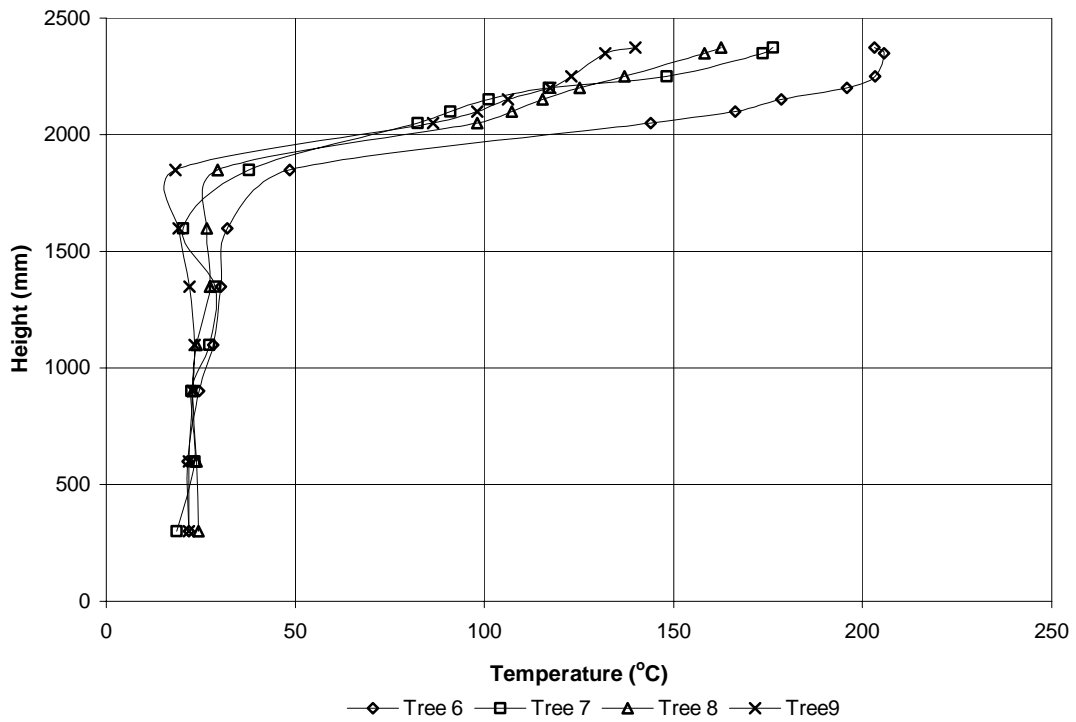


Figure 5.24 Temperature Profiles for the Adjacent Room, 160 kW Fire

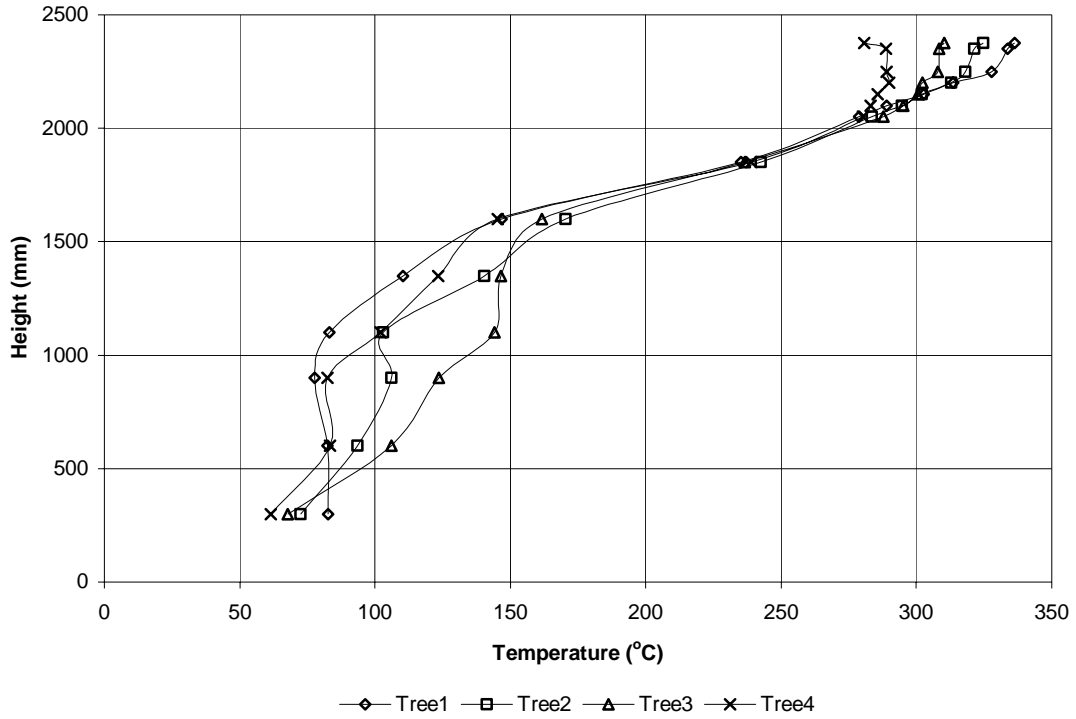


Figure 5.25 Temperature Profiles for the Fire Room, 110 kW Corner Fire

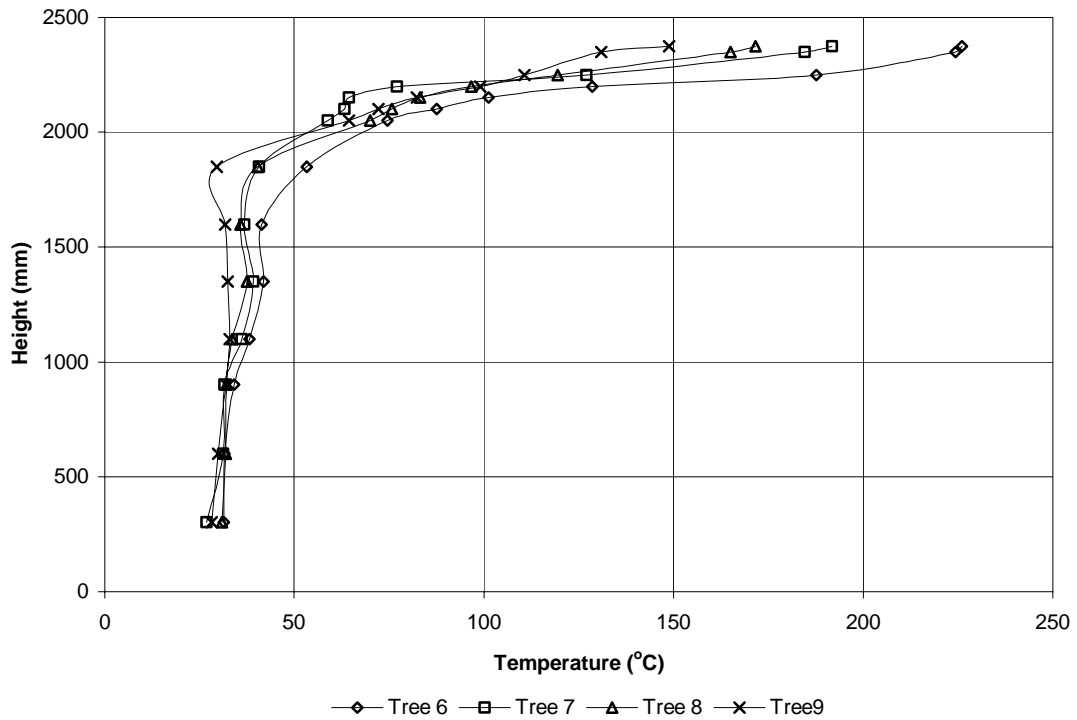


Figure 5.26 Temperature Profiles for the Adjacent Room, 110 kW Corner Fire

5.4.2 Corner Thermocouples

Results of the temperature profiles for the corner thermocouples are presented below for the four fires in Tables 5.1 – 5.24.

Table 5.1 Fire Room Rear Corner Temperatures (°C) for the 55 kW Fire

Distance from Ceiling	Distance from Wall				
	25 mm	75 mm	125 mm	175 mm	225 mm
25 mm	126.9	131.0	130.4	130.1	131.2
75 mm	129.3	132.0	131.4	130.9	
125 mm	130.0	133.0	131.8		
175 mm	130.7	132.5			
225 mm	132.4				

Table 5.2 Fire Room Rear Corner Temperature Standard Deviations (°C) for the 55 kW Fire

Distance from Ceiling	Distance from Wall				
	25 mm	75 mm	125 mm	175 mm	225 mm
25 mm	0.88	0.81	0.71	0.60	0.72
75 mm	0.82	0.70	0.71	0.59	
125 mm	0.74	0.72	0.66		
175 mm	0.68	0.75			
225 mm	0.72				

Table 5.3 Fire Room Front Corner Temperatures (°C) for the 55 kW Fire

Distance from Ceiling	Distance from Wall				
	25 mm	75 mm	125 mm	175 mm	225 mm
25 mm	124.0	122.6	118.0	117.9	122.3
75 mm	122.7	123.2	117.8	122.5	
125 mm	125.4	118.0	118.0		
175 mm	122.9	118.2			
225 mm	123.9				

Table 5.4 Fire Room Front Corner Temperature Standard Deviations (°C) for the 55 kW Fire

Distance from Ceiling	Distance from Wall				
	<i>25 mm</i>	<i>75 mm</i>	<i>125 mm</i>	<i>175 mm</i>	<i>225 mm</i>
<i>25 mm</i>	1.03	1.01	1.20	1.41	1.59
<i>75 mm</i>	1.27	1.31	1.55	1.53	
<i>125 mm</i>	1.35	1.36	1.50		
<i>175 mm</i>	1.38	1.27			
<i>225 mm</i>	1.37				

Table 5.5 Adjacent Room Corner Temperatures (°C) for the 55 kW Fire

Distance from Ceiling	Distance from Wall				
	<i>25 mm</i>	<i>75 mm</i>	<i>125 mm</i>	<i>175 mm</i>	<i>225 mm</i>
<i>25 mm</i>	101.7	102.2	102.5	106.0	105.2
<i>75 mm</i>	103.0	103.4	102.1	102.2	
<i>125 mm</i>	102.6	100.5	90.1		
<i>175 mm</i>	102.2	98.5			
<i>225 mm</i>	101.5				

Table 5.6 Adjacent Room Corner Temperature Standard Deviations (°C) for the 55 kW Fire

Distance from Ceiling	Distance from Wall				
	<i>25 mm</i>	<i>75 mm</i>	<i>125 mm</i>	<i>175 mm</i>	<i>225 mm</i>
<i>25 mm</i>	1.64	1.59	1.59	1.75	1.60
<i>75 mm</i>	1.64	1.67	1.55	1.79	
<i>125 mm</i>	1.65	1.54	1.49		
<i>175 mm</i>	1.54	1.41			
<i>225 mm</i>	1.64				

Table 5.7 Fire Room Rear Corner Temperatures (°C) for the 110 kW Fire

Distance from Ceiling	Distance from Wall				
	<i>25 mm</i>	<i>75 mm</i>	<i>125 mm</i>	<i>175 mm</i>	<i>225 mm</i>
<i>25 mm</i>	192.6	198.4	197.3	197.4	200.2
<i>75 mm</i>	196.5	199.2	200.5	199.4	
<i>125 mm</i>	197.3	200.5	201.3		
<i>175 mm</i>	198.0	200.0			
<i>225 mm</i>	200.0				

Table 5.8 Fire Room Rear Corner Temperature Standard Deviations (°C) for the 110 kW Fire

Distance from Ceiling	Distance from Wall				
	<i>25 mm</i>	<i>75 mm</i>	<i>125 mm</i>	<i>175 mm</i>	<i>225 mm</i>
<i>25 mm</i>	1.77	1.57	1.30	1.21	1.68
<i>75 mm</i>	1.56	1.48	1.63	1.33	
<i>125 mm</i>	1.31	1.44	1.50		
<i>175 mm</i>	1.36	1.31			
<i>225 mm</i>	1.30				

Table 5.9 Fire Room Front Corner Temperatures (°C) for the 110 kW Fire

Distance from Ceiling	Distance from Wall				
	<i>25 mm</i>	<i>75 mm</i>	<i>125 mm</i>	<i>175 mm</i>	<i>225 mm</i>
<i>25 mm</i>	186.4	186.4	178.0	178.1	186.9
<i>75 mm</i>	187.0	187.6	178.5	187.0	
<i>125 mm</i>	190.3	178.5	178.6		
<i>175 mm</i>	187.4	178.8			
<i>225 mm</i>	188.4				

Table 5.10 Fire Room Front Corner Temperature Standard Deviations (°C) for the 110 kW Fire

Distance from Ceiling	Distance from Wall				
	<i>25 mm</i>	<i>75 mm</i>	<i>125 mm</i>	<i>175 mm</i>	<i>225 mm</i>
<i>25 mm</i>	2.16	2.26	2.51	2.92	3.45
<i>75 mm</i>	2.76	2.82	3.19	3.13	
<i>125 mm</i>	2.92	2.85	2.93		
<i>175 mm</i>	2.87	2.70			
<i>225 mm</i>	2.91				

Table 5.11 Adjacent Room Corner Temperatures (°C) for the 110 kW Fire

Distance from Ceiling	Distance from Wall				
	<i>25 mm</i>	<i>75 mm</i>	<i>125 mm</i>	<i>175 mm</i>	<i>225 mm</i>
<i>25 mm</i>	155.1	156.0	156.2	161.7	162.3
<i>75 mm</i>	157.1	158.8	158.0	158.1	
<i>125 mm</i>	157.3	154.3	125.5		
<i>175 mm</i>	156.6	150.4			
<i>225 mm</i>	155.7				

Table 5.12 Adjacent Room Corner Temperature Standard Deviations (°C) for the 110 kW Fire

Distance from Ceiling	Distance from Wall				
	<i>25 mm</i>	<i>75 mm</i>	<i>125 mm</i>	<i>175 mm</i>	<i>225 mm</i>
<i>25 mm</i>	2.87	2.73	2.66	3.23	3.01
<i>75 mm</i>	3.05	3.02	2.82	3.04	
<i>125 mm</i>	2.96	2.77	2.26		
<i>175 mm</i>	2.93	2.66			
<i>225 mm</i>	2.95				

Table 5.13 Fire Room Rear Corner Temperatures (°C) for the 160 kW Fire

Distance from Ceiling	Distance from Wall				
	<i>25 mm</i>	<i>75 mm</i>	<i>125 mm</i>	<i>175 mm</i>	<i>225 mm</i>
<i>25 mm</i>	241.3	249.0	246.8	248.3	252.3
<i>75 mm</i>	247.6	250.1	253.2	251.5	
<i>125 mm</i>	249.0	252.0	253.9		
<i>175 mm</i>	250.6	251.6			
<i>225 mm</i>	252.1				

Table 5.14 Fire Room Rear Corner Temperature Standard Deviations (°C) for the 160 kW Fire

Distance from Ceiling	Distance from Wall				
	<i>25 mm</i>	<i>75 mm</i>	<i>125 mm</i>	<i>175 mm</i>	<i>225 mm</i>
<i>25 mm</i>	2.86	2.78	2.04	2.14	2.81
<i>75 mm</i>	2.75	2.64	2.72	2.55	
<i>125 mm</i>	2.63	2.61	2.76		
<i>175 mm</i>	2.65	2.43			
<i>225 mm</i>	2.62				

Table 5.15 Fire Room Front Corner Temperatures (°C) for the 160 kW Fire

Distance from Ceiling	Distance from Wall				
	<i>25 mm</i>	<i>75 mm</i>	<i>125 mm</i>	<i>175 mm</i>	<i>225 mm</i>
<i>25 mm</i>	237.8	238.1	230.3	230.0	238.5
<i>75 mm</i>	239.0	239.5	230.5	238.7	
<i>125 mm</i>	242.5	230.4	230.5		
<i>175 mm</i>	239.8	230.6			
<i>225 mm</i>	240.6				

Table 5.16 Fire Room Front Corner Temperature Standard Deviations (°C) for the 160 kW Fire

Distance from Ceiling	Distance from Wall				
	<i>25 mm</i>	<i>75 mm</i>	<i>125 mm</i>	<i>175 mm</i>	<i>225 mm</i>
<i>25 mm</i>	2.78	3.08	3.58	3.95	4.31
<i>75 mm</i>	3.81	3.82	4.30	4.27	
<i>125 mm</i>	3.95	4.00	4.23		
<i>175 mm</i>	3.98	3.89			
<i>225 mm</i>	4.12				

Table 5.17 Adjacent Room Corner Temperatures (°C) for the 160 kW Fire

Distance from Ceiling	Distance from Wall				
	<i>25 mm</i>	<i>75 mm</i>	<i>125 mm</i>	<i>175 mm</i>	<i>225 mm</i>
<i>25 mm</i>	181.9	183.2	184.7	191.8	190.6
<i>75 mm</i>	185.7	187.5	184.9	186.0	
<i>125 mm</i>	185.6	182.8	148.1		
<i>175 mm</i>	184.5	178.4			
<i>225 mm</i>	183.0				

Table 5.18 Adjacent Room Corner Temperature Standard Deviations (°C) for the 160 kW Fire

Distance from Ceiling	Distance from Wall				
	<i>25 mm</i>	<i>75 mm</i>	<i>125 mm</i>	<i>175 mm</i>	<i>225 mm</i>
<i>25 mm</i>	3.85	3.63	3.59	4.41	4.02
<i>75 mm</i>	4.02	4.12	3.77	4.12	
<i>125 mm</i>	4.00	3.99	3.42		
<i>175 mm</i>	3.79	3.56			
<i>225 mm</i>	3.85				

Table 5.19 Fire Room Rear Corner Thermocouple Temperatures (°C) for the 110 kW Corner Fire

Distance from Ceiling	Distance from Wall				
	25 mm	75 mm	125 mm	175 mm	225 mm
25 mm	345.2	344.7	333.6	322.0	322.3
75 mm	344.7	341.3	330.2	323.3	
125 mm	336.4	335.4	322.5		
175 mm	324.8	322.7			
225 mm	313.3				

Table 5.20 Fire Room Rear Corner Temperature Standard Deviations (°C) for the 110 kW Corner Fire

Distance from Ceiling	Distance from Wall				
	25 mm	75 mm	125 mm	175 mm	225 mm
25 mm	9.61	10.39	8.58	5.96	9.05
75 mm	10.27	9.77	9.71	7.28	
125 mm	8.93	9.46	9.02		
175 mm	7.82	7.53			
225 mm	7.57				

Table 5.21 Fire Room Front Corner Temperatures (°C) for the 110 kW Corner Fire

Distance from Ceiling	Distance from Wall				
	25 mm	75 mm	125 mm	175 mm	225 mm
25 mm	263.6	265.1	262.8	265.3	271.1
75 mm	269.4	271.4	270.5	274.4	
125 mm	274.2	269.9	274.2		
175 mm	272.7	270.7			
225 mm	275.8				

Table 5.22 Fire Room Front Corner Temperature Standard Deviations (°C) for the 110 kW Corner Fire

Distance from Ceiling	Distance from Wall				
	25 mm	75 mm	125 mm	175 mm	225 mm
25 mm	2.33	1.95	1.90	2.28	2.39
75 mm	2.35	2.19	2.51	2.32	
125 mm	2.23	2.25	2.32		
175 mm	2.12	1.95			
225 mm	2.09				

Table 5.23 Adjacent Room Corner Temperatures (°C) for the 110 kW Corner Fire

Distance from Ceiling	Distance from Wall				
	25 mm	75 mm	125 mm	175 mm	225 mm
25 mm	217.8	217.7	218.0	226.6	222.9
75 mm	222.2	214.5	209.0	208.0	
125 mm	216.5	202.7	191.7		
175 mm	214.9	195.8			
225 mm	212.3				

Table 5.24 Adjacent Room Corner Temperature Standard Deviations (°C) for the 110 kW Corner Fire

Distance from Ceiling	Distance from Wall				
	25 mm	75 mm	125 mm	175 mm	225 mm
25 mm	3.45	3.43	3.19	3.85	3.29
75 mm	3.70	4.18	4.21	4.72	
125 mm	3.42	3.86	4.52		
175 mm	3.09	3.27			
225 mm	3.23				

5.4.3 Surface Temperatures

Results of the temperature profiles for the surface thermocouples are presented below for the four fires in Figures 5.27 – 5.30.

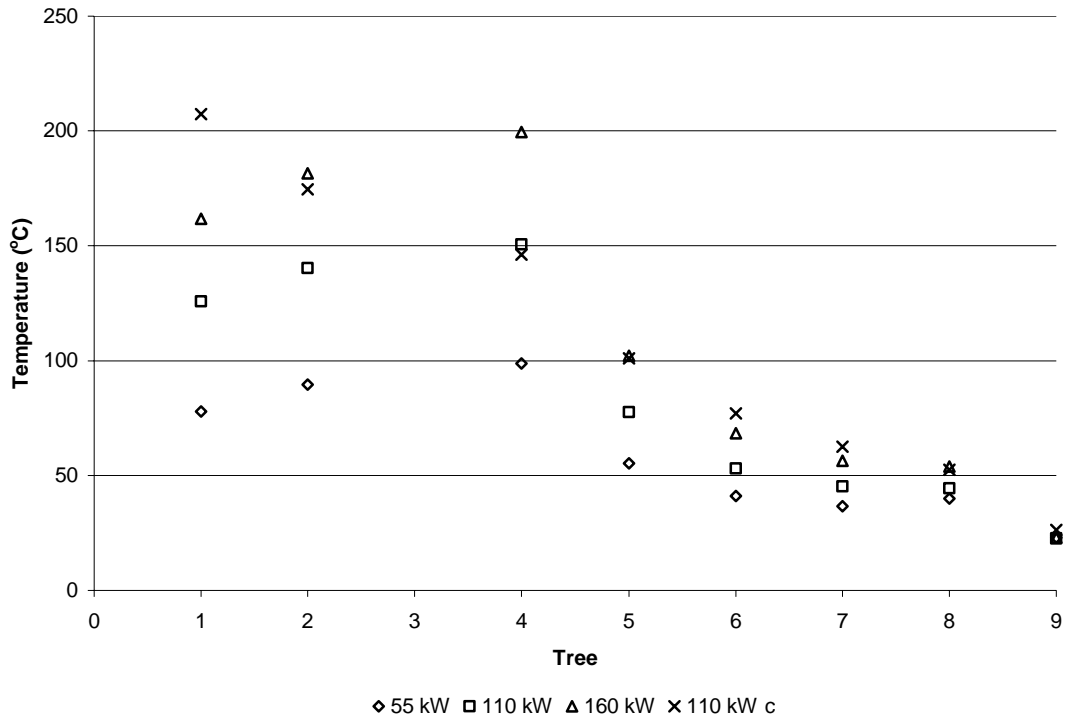


Figure 5.27 Floor Temperatures throughout Two-Compartment Structure

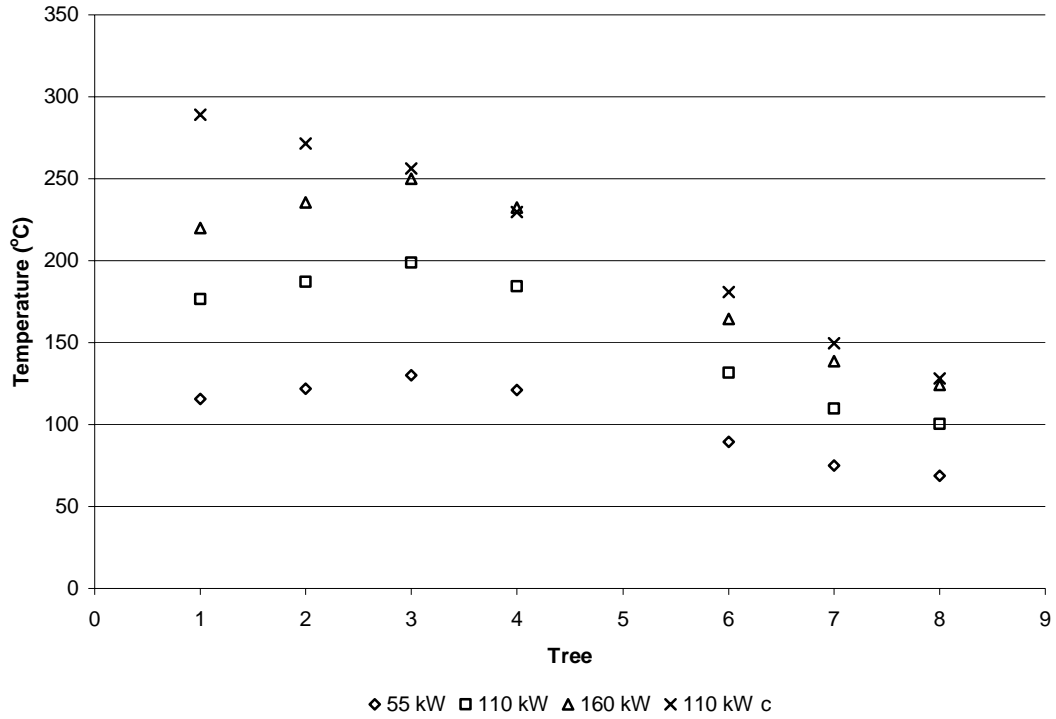


Figure 5.28 Ceiling Temperatures throughout Two-Compartment Structure

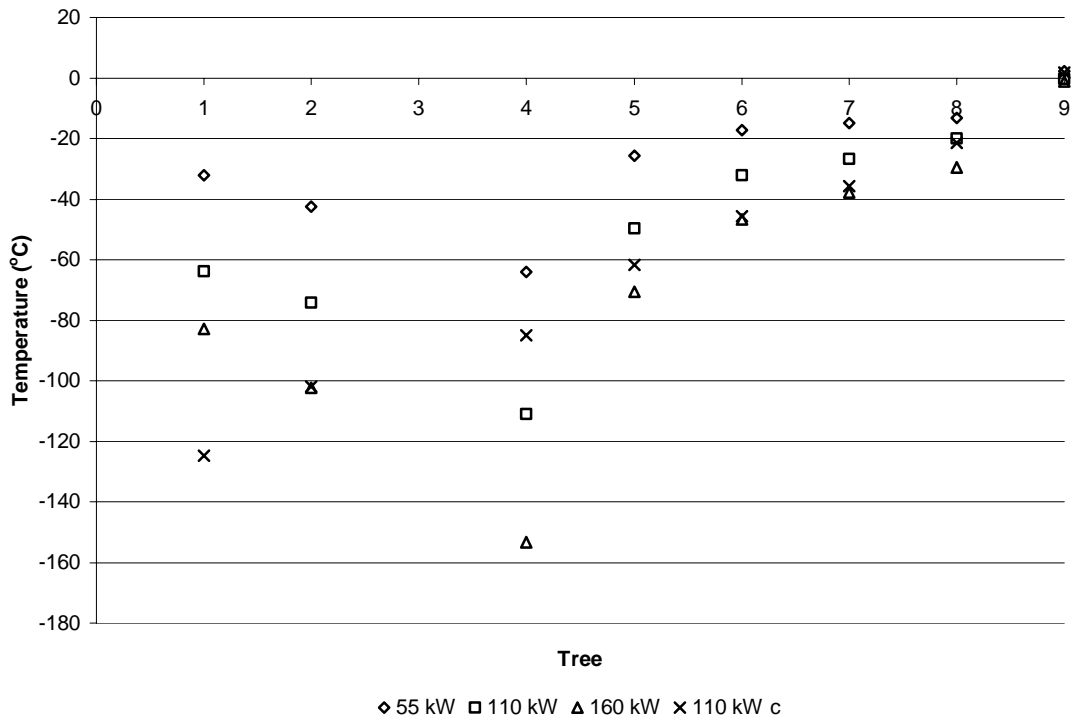


Figure 5.29 Temperature Difference between 300 mm TC and Floor TC

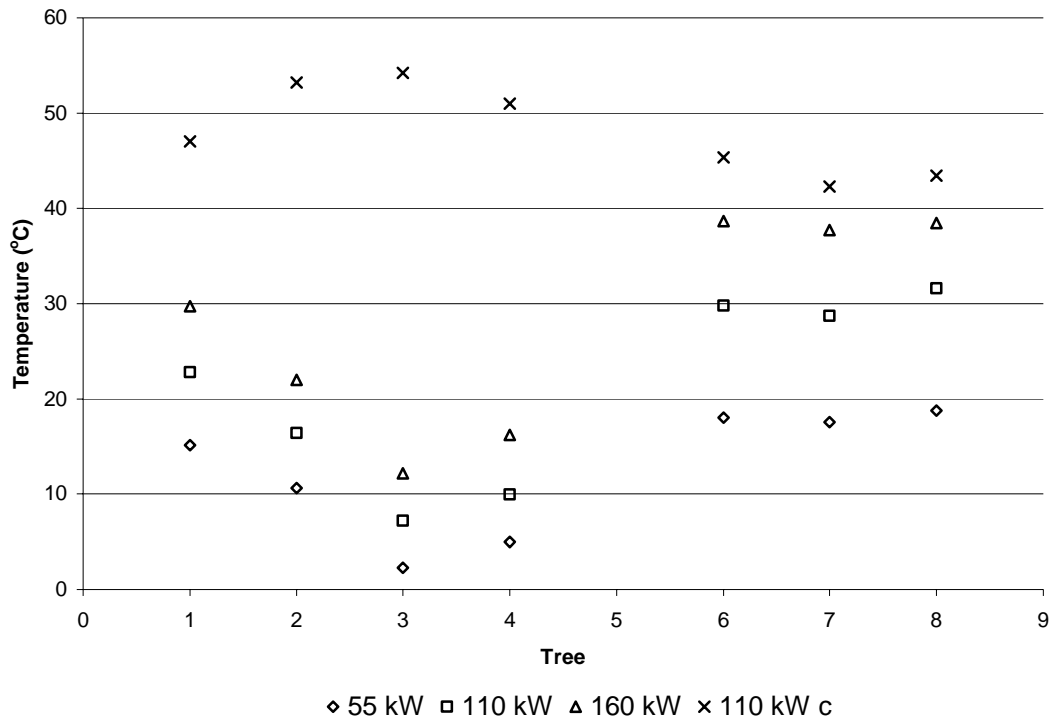


Figure 5.30 Temperature Difference between 2375 mm TC and Ceiling TC

5.4.4 Gas Analysis

Results are expressed below in Tables 5.13 – 5.16 for O₂ consumption and CO₂ production (% volume) for the sample points on each tree and the doorway. Note: N/A (Not Available) signifies O₂ consumption and CO₂ production concentrations were too low to be measured by the gas analyser.

Table 5.25 O₂ Consumption and CO₂ Production Profiles for Tree 2 (% vol)

Height (mm)	Gas Species	55 kW	110 kW	160 kW	110 kW corner
2250	O ₂	8.90E-01	1.50E+00	2.18E+00	2.78E+00
	CO ₂	5.92E-01	9.79E-01	1.42E+00	1.82E+00
	O ₂ :CO ₂	1.50	1.53	1.54	1.53
1950	O ₂	8.69E-01	6.55E-01	1.55E+00	1.80E+00
	CO ₂	5.78E-01	4.04E-01	1.35E+00	1.19E+00
	O ₂ :CO ₂	1.50	1.62	1.15	1.51
600	O ₂	N/A	2.16E-01	1.37E-02	N/A
	CO ₂	N/A	1.44E-01	8.29E-03	N/A
	O ₂ :CO ₂	N/A	1.5	1.65	N/A
300	O ₂	N/A	N/A	N/A	N/A
	CO ₂	N/A	N/A	N/A	N/A
	O ₂ :CO ₂	N/A	N/A	N/A	N/A

Table 5.26 O₂ Consumption and CO₂ Production Profiles for Tree 4 (% vol)

Height (mm)	Gas Species	55 kW	110 kW	160 kW	110 kW corner
2250	O ₂	7.09E-01	1.58E+00	1.79E+00	3.14E+00
	CO ₂	4.73E-01	1.02E+00	1.17E+00	2.06E+00
	O ₂ :CO ₂	1.50	1.55	1.53	1.52
1950	O ₂	6.68E-01	1.53E+00	1.55E+00	2.98E+00
	CO ₂	4.44E-01	1.00E+00	1.01E+00	1.97E+00
	O ₂ :CO ₂	1.50	1.53	1.53	1.51
600	O ₂	N/A	6.53E-03	3.29E-02	8.35E-03
	CO ₂	N/A	6.46E-03	2.02E-02	6.37E-03
	O ₂ :CO ₂	N/A	1.01	1.63	1.31
300	O ₂	N/A	N/A	N/A	N/A
	CO ₂	N/A	N/A	N/A	N/A
	O ₂ :CO ₂	N/A	N/A	N/A	N/A

Table 5.27 O₂ Consumption and CO₂ Production Profiles for Tree 7 (% vol)

Height (mm)	Gas Species	55 kW	110 kW	160 kW	110 kW corner
2250	O ₂	3.68E-01	1.30E+00	8.94E-01	1.38E-01
	CO ₂	2.47E-01	8.47E-01	5.82E-01	1.01E-01
	O ₂ :CO ₂	1.49	1.53	1.54	1.37
1950	O ₂	1.20E-01	1.14E+00	2.67E-01	4.59E-02
	CO ₂	8.27E-02	7.44E-01	1.75E-01	3.53E-02
	O ₂ :CO ₂	1.45	1.53	1.53	1.3
600	O ₂	N/A	N/A	N/A	N/A
	CO ₂	N/A	N/A	N/A	N/A
	O ₂ :CO ₂	N/A	N/A	N/A	N/A
300	O ₂	N/A	N/A	N/A	N/A
	CO ₂	N/A	N/A	N/A	N/A
	O ₂ :CO ₂	N/A	N/A	N/A	N/A

Table 5.28 O₂ Consumption and CO₂ Production Profiles for the Doorway (% vol)

Height (mm)	Gas Species	55 kW	110 kW	160 kW	110 kW corner
1900	O ₂	7.25E-01	1.30E+00	1.73E+00	3.08E+00
	CO ₂	4.87E-01	8.51E-01	1.13E+00	2.04E+00
	O ₂ :CO ₂	1.49	1.53	1.53	1.51
1600	O ₂	6.86E-01	1.16E+00	1.53E+00	5.77E-02
	CO ₂	4.54E-01	7.60E-01	9.93E-01	4.37E-02
	O ₂ :CO ₂	1.51	1.53	1.54	1.32
700	O ₂	N/A	N/A	N/A	N/A
	CO ₂	N/A	N/A	N/A	N/A
	O ₂ :CO ₂	N/A	N/A	N/A	N/A
400	O ₂	N/A	N/A	N/A	N/A
	CO ₂	N/A	N/A	N/A	N/A
	O ₂ :CO ₂	N/A	N/A	N/A	N/A

5.5 Discussion

Results regarding each section of analysis are discussed in detail below. The two rooms and the doorway between the rooms are discussed separately in their own subsections regarding the field tree analysis, with an overall discussion concluding the discussion.

5.5.1 General Behaviour for Field Trees

The field trees all exhibit general similarities/patterns. The following observations can be made from figures 5.1 – 5.24 for the temperature profiles and variations for each tree for the four fires:

- **The three centrally located fires' temperature profile increases with fire size.** This came as no surprise, as for this experiment, fire diameter was held constant. This meant that as the fire size increased, flame height must increase. This would in turn reduce the amount of cool air entrained into the fire and plume, as part or the whole of the plume for a larger fire would be in the hot upper layer.
- **Temperature fluctuations increase markedly where there is a temperature gradient.** The temperature gradient that occurs at approximately 1 m for the fire room and 1.8 m for the adjacent room is the beginning of where the interface is between the upper and lower layers. Colder, denser air enters the compartment at floor level, while hotter more buoyant air leaves at ceiling level. Shearing takes place at the interface where the hot gases are leaving and cold air is entering. This creates turbulence within this region. Consequently, a standard deviation increase in temperature over the 10 minute period indicates turbulence, since an increase in standard deviation suggests a larger distribution of temperatures from the average temperature during steady state. The turbulence from the hot gases leaving and the cold air entering creates a region where the temperature fluctuates markedly, as hot gases and cold ambient air are mixing in this turbulent region.
- **Trees located closer to the fire have a higher temperature than trees at a further distance.** Further from the fire, the hot gases in the upper layer are

cooler as a result of ambient air entrainment that occurs between the interface of the hot gases and ambient air. Heat is also conducted into the compartment surfaces, reducing the temperature.

5.5.2 Fire Room Field Trees

Temperature Profiles of Each Tree for Different Fires

Specific details of the temperature vs. height profiles (for different fires) are discussed below. Temperature profiles plotted in Figures 5.1 – 5.4 indicate:

- **As fire size increases for the centrally located fires, the temperature at 300 mm increases by about 25°C.** This illustrates that the lower layer rises in temperature with increasing fire size. Although there is very little mixing between the upper and lower layers, it is significant enough to increase the temperature in the lower layer when fire size is increased. Radiation from the fires also contributes to raising the temperature of the thermocouples at this height.
- **The temperatures for all centrally located fires are constant from approximately 0 - 1 m and 1600 - 2375 mm for tree 1, with a sharp temperature gradient in between. However, temperature profiles for trees 2 and 4 are not as constant between 0 – 1 m and 1600 – 2375 mm.** This indicates how well the upper and lower layers are mixed. Tree 1 is the furthest away from the fire and is between the back wall and the fire, away from where ambient air is entering the fire room to supply the fire with oxygen. Therefore at tree 1, the upper and lower layers are well mixed compared, to trees 2 and 4, as the hot gases and entrained air have had more time to form a uniform mixture. Tree 2 is also between the doorway and the fire, but is closer to the fire than tree 1, and so the upper layer, which is formed from the fire's gases and entrained ambient air, is not as well mixed as tree 1. Therefore, tree 2 shows a variation from the constant temperature profiles of tree 1, albeit small. Tree 4 shows an even greater variation from the constant temperature profile than tree 2. This is because tree 4 is located between the fire and the doorway (where ambient air is entering and hot gases are exiting). Shearing and mixing between ambient air and the hot gases will be greatest here, where the large

deviation from constant temperature profiles between the regions mentioned is attributed to insufficient mixing (particularly the upper region of 1600 – 2375 mm). Thus, tree 4 has the greatest variation from the constant temperature profile of tree 1.

- **Temperatures for tree 3 (located directly in the 55 kW, 110 kW, and 160 kW fires), illustrate a constant temperature profile from a height of 1350 mm.** The constant temperature indicates how the centreline temperature of the fire's plume changes little from this height to the ceiling. The constant temperature of the centreline of the fire's plume suggests that from 1350 mm, the fire's plume cannot entrain cool ambient air from this height onwards as the fire's plume is in the upper layer of hot gases.
- **Temperatures measured in the fire by tree 3 are lower than expected.** Typical temperatures within the fires flames should be at least 800°C (Drysdale, 1986). There are two reasons for lower than expected temperatures. The first is radiation. The thermocouples in the fire are very hot, and will therefore emit radiation which will reduce the temperature of the thermocouples. The second reason is that the thermocouples located in the upper part of the flame will be measuring the intermittent flame temperature. Note also that the temperature for the 160 kW fire at 300 mm is lower than the 55 kW and 110 kW fires at the same height. This is probably a result of uncombusted LPG lowering the temperature of the thermocouple, since the 160 kW fire requires the most LPG and it is not all combusted at 300 mm.
- **The temperature profile for the 110 kW corner fire is significantly hotter than the central fires.** The 110 kW fire produces considerably higher temperatures at most heights throughout the compartment compared to the equivalently sized 110 kW central fire, and produces the highest temperature 2 m and above for any fire. When there is no obstacle present, fires entrain air into the flames and plume from all directions, but air entrainment for the 110 kW corner fire is reduced by approximately 50% since the corner reduces entrainment surface area by 50%. This reduction in air entrainment increases plume temperature, and therefore upper layer temperature.
- **The temperature profile for the 110 kW corner fire differs significantly from the centrally located fires.** The temperature profile for the 110 kW

corner fire shows a constant temperature with height for the region between 0 – 1 m (similarly to the 55 kW, 110 kW, and 160 kW centre fires), but shows a temperature gradient from 1 m to the ceiling, rather than a constant temperature profile from about 1600 – 2375 mm. This is attributed to the 110 kW corner fire generating much lower levels of turbulence than the centrally located fires (Takahashi et al., 1997). Since the 110 kW corner fire's entrainment area is reduced by approximately 50%, air entrainment is less, therefore turbulence will be less, as lower quantities of hot gases are produced. This results in the upper layer not being as well mixed as the centrally located fires. Hence the hottest most buoyant gases will rise to the top of the ceiling, while cooler less buoyant combustion gases settle at a lower level. Thus, the low levels of turbulence reduce mixing between the hot gases (which will consequently have different densities and therefore different buoyancies), producing the temperature gradient shown.

Temperature Variations for Each Tree

Specific details of the temperature variations for each tree (for different fires) are discussed below. Temperature variations graphed in Figures 5.0 – 5.13 indicate:

- **Temperature variations for the central fires increase with increasing fire size.** Increasing the central fire's size increases the amount of air entrained. Thus, higher amounts of air entrained increases temperature variations, as it takes longer for the mixture to become uniform. Different trees and different points on individual trees show varying temperature fluctuations. A general trend for many points on each tree is that the 160 kW fire temperature variation is double that of the 55 kW fire, with the temperature variation for the 110 kW fire being somewhere between (often half way between the 55 kW and 160 kW fire).
- **The temperature variations for tree 3 decrease with height for the centrally located fires, with the intermittent flaming region responsible for the largest fluctuations.** A flame can be divided into two sections: the continuous flaming region and the intermittent flaming region (Drysdale, 1986). The intermittent region is located above the continuous region. When

increasing fire size, the location of the intermittent flaming region is higher. Evidence for this can be seen from Figure 5.12. At 600 mm, temperature variation is greatest for the 55 kW fire; at 900 mm, the 110 kW fire shows the greatest temperature variation, whereas at 1100 and 1350 mm the temperature variation is greatest for the 160 kW fire. The large temperature variations are also attributed to the flame swaying from its centreline. This swaying is more prevalent higher up the flame, therefore increasing the temperature variations nearer the tip of the continuous and intermittent flaming regions. Once the thermocouple locations are clearly out of the flaming regions (from 2050 mm) the temperature variations for each fire reduce considerably and are constant with height. Note: The temperature variation for the 110 kW fire at 300 mm is significantly larger than for the 55 kW or 160 kW fires. This is probably a result of uneven LPG distribution over the burner (as this was the only fire where sand was used to disperse LPG over the burner), creating temperature fluctuations across the surface of the burner.

- **Temperature variations increase for trees close to the fire.** Again, a lack of mixing between the fire's hot gases and entrained ambient air is responsible for this. As previously discussed (the first bullet point in 'Temperature Profiles of Each Tree for Different Fires', Section 5.5.2), the mixture of hot fire gases and ambient air close to the fire is not very homogeneous. The temperature variation is smallest for tree 1. Tree 2, being half the distance from the fire compared to tree 1, shows greater temperature variation. Generally, tree 2 shows double the temperature variation of tree 1. Tree 4 shows the greatest temperature variation. This results from tree 4 being situated between the doorway and the fire, where there is a high level of mixing with ambient air entering and hot gases leaving via the doorway.
- **The temperature variation for the 110 kW corner fire shows the greatest temperature variation nearer the ceiling.** The temperature variation is greatest on tree 1, with decreasing variations occurring on trees 2, 3 and 4. Tree 1 is nearest the 110 kW corner fire, therefore temperature variation will be greatest here as ambient air entrained into the fire's hot gases is not fully mixed with the fire's hot gases by the time it reaches tree 1. However, the mixture is more uniform by the time the mixture of hot gases and entrained air

reaches trees 2, 3 and 4. Also, the 110 kW corner fire produces the hottest temperature profile (particularly close to the ceiling), so any unmixed air entrained into the fire's gases will give rise to large temperature variations compared to the central fires where the temperature difference between the fire's hot gases and entrained air is not as high.

Overall Comparisons between Field Trees in Each Room per Fire

Specific details of the overall comparisons between each field tree in each room per fire are discussed below. Overall comparisons graphed in Figures 5.19, 5.21, 5.23, and 5.25 indicate:

- **Trees 1 and 2 follow similar temperature profiles for each central fire, whereas tree 4 differs considerably.** Trees 1 and 2 are located in similar positions, that is, they are between the back wall and the fire. Tree 4 however, is located between the doorway and the fire where hot gases are leaving and ambient air is entering the fire room. Therefore, tree 4 shows a different profile as it is exposed to different conditions.
- **At 300 mm from the floor tree 4 records the lowest temperature for each fire.** Tree 4 is closest to the doorway; therefore, as ambient air enters the fire room it enters close to the floor. This is due to the ambient air having a higher density than the exiting hot gases. Thus, the lowest part of tree 4 (300 mm from the floor) will record the lowest temperature.
- **All trees converge to similar temperatures (for equivalent fires) at the ceiling for the central fires.**
- **The temperature close to the ceiling increases markedly for increasing fire size (for the central fires).** Temperatures near the ceiling show that the 55 kW fire reaches ~ 125°C, the 110 kW fire reaches ~ 200°C, and the 160 kW fire reaches ~ 250°C.
- **The 110 kW corner fire's temperature near the ceiling is noticeably higher than the central fires.** As discussed before, the corner fire's entrainment area is reduced by approximately 50%. This increases the temperature of the fire's gases. The corner fire's ceiling temperature is between 50 – 100°C greater than the 160 kW central fire.

- **The trees do not converge to the same temperature for the 110 kW corner fire.** The ceiling temperature for trees 1 and 2 are very similar demonstrating a ceiling jet. However, temperature profile at the ceiling trees 3 and 4 becomes more constant with height than trees 1 and 2. This constant temperature profile results from mixing (which does occur for the 110 kW corner fire, but to a lesser extent than for the centrally located fires) in the upper layer, producing an average upper layer temperature. Evidence of this can be seen from a height of 2200 mm, where the temperature profile for trees 3 and 4 become more constant with height.

5.5.3 The Adjacent Room Field Trees

Temperature Profiles of Each Tree for Different Fires

Specific details of the temperature vs. height profiles (for different fires) are discussed below. Temperature profiles plotted in Figures 5.6 – 5.9 indicate:

- **The upper layer height of the adjacent room is higher than the fire room.** A doorway with a soffit separated the fire room from the adjacent room. The soffit increases the depth of the upper layer as it acts as a barrier that the hot gases must ‘rise’ over. Therefore, since the adjacent room does not have a soffit, the upper layer does not increase in depth. The temperature gradient where the upper layer begins in the adjacent room starts at approximately 1850 mm from the floor for all trees in the adjacent room, whereas the temperature gradient for the fire room begins at approximately 1100 mm.
- **All trees in the adjacent room show a constant temperature up to a height of 1850 mm.** The temperature is low up to this height as high density ambient air occupies this space, while the less dense hot gases are exiting above.
- **A temperature gradient exists up to the ceiling for all trees beyond 1850 mm.** The central fires exhibited a constant temperature profile above approximately 1600 mm for the fire room, whereas in the adjacent room a temperature gradient begins at 1850 mm, with no constant temperature profile above this height. This suggests little mixing of the upper layer in the adjacent room. The reduced mixing results from there being no fire in the room that

generates turbulence, which in turn promotes mixing. Also, without the presence of a soffit, the residence time for the hot gases is less than for the fire room, therefore a uniform upper layer temperature is unable to be formed. The temperature profile in the adjacent room above 1850 mm is typical of a ceiling jet.

- **The temperature at 300 mm for the centrally located fires increases marginally as fire size increases.** Temperatures increase for tree 6 by about 10°C between the ‘coldest fire’ (55 kW) and the ‘hottest fire’ (110 kW corner). There is a gradual decay in temperature differences for each tree that is further away until tree 9 is reached, where the difference between the ‘hottest fire’ (110 kW corner) and the ‘coldest fire’ (55 kW) is about 6°C. The increase in temperature at this height is likely to be a result of radiation from the fire, not from hot gases raising the temperature of the lower layer.
- **The temperature of the upper layer at 2375 mm is highest at tree 6 and decreases for each tree along the adjacent room.** The temperature is highest at tree 6 as this tree is closest to the fire room. The temperature decreases along the length of the adjacent room. The reduction in temperature along the adjacent room results from heat transfer through the ceiling.
- **The temperature drop across the thermocouples closest to the ceiling along the adjacent room is greatest for the hottest fire (110 kW corner), and lowest for the coldest fire (55 kW).** The temperature difference between the 2375 mm thermocouples from tree 6 to tree 9 for the 55 kW fire is approximately 30°C, whereas temperature difference for the 110 kW for the corner fire for the same thermocouples is approximately 75°C, with the 110 kW and 160 kW fires being in between these values. This drop in temperature indicates heat transfer across the ceiling. From basic heat transfer principles, if the temperature gradient is increased, heat flux will increase. The temperature gradient across the ceiling for the 110 kW corner fire is greater than that for the 55 kW fire, since the exterior of the compartment is exposed to ambient conditions which do not vary significantly between experiments. Therefore, the temperature drop along the trees for the adjacent room in the upper layer for the 110 kW corner fire, is greater than the 55 kW fire.

Temperature Variations for Each Tree

Specific details of the temperature variation from the mean for each tree (for different fires) are discussed below. Temperature variations graphed in Figures 5.15 – 5.18 indicate:

- **The temperature variations for the central fires increase with increasing fire size.** As previously discussed in section 5.5.2, an increase in fire size increases temperature variations. This trend continues in the adjacent room.
- **Temperature variations increase for trees closer to the fire.** Tree 6 shows the greatest temperature fluctuations, with trees 7, 8, and 9 reducing in temperature variations respectively. The temperature variation of tree 9 is approximately 50 % less than tree 6 (generally), with trees 7 and 8 showing temperature fluctuations between the values of trees 6 and 9. This reduction in temperature variation along the length of the adjacent room is a result of the mixture of entrained air and fire gases becoming more uniform.
- **Temperature variations for all trees increase by up to 100 % or more at and beyond 1850 – 2050 mm.** Temperatures increase in this region. Temperature variations are low below this height. The temperature variations increase as a result of the hot upper layer moving through the adjacent room, shearing and mixing with ambient air below the hot upper layer, creating a non-uniform mixture of hot and cold gases.

Overall Comparisons between Field Trees in Each Room per Fire

Specific details of the overall variation between each field tree in each room per fire are discussed below. Overall comparisons graphed in Figures 5.20, 5.22, 5.24 and 5.26 indicate:

- **The temperature profile for all trees is constant up to a height of 1600 mm.** The constant temperature profile shows that mostly cooler ambient air is below 1600 mm; the cooler ambient air is denser than the outgoing lower density hot gases.
- **The temperature profile for all trees are very similar for each fire, up to a height of 1600 mm.** This confirms the previous conclusion that the thermocouples are measuring the ambient air temperature.

- **A temperature gradient emerges for all trees and for each fire at a height of approximately 1850 mm.** The increase in temperature illustrates how the hotter, more buoyant gases are leaving the compartment. The temperature gradient continues up to the ceiling, suggesting a ceiling jet.
- **Tree 6 records the highest temperature nearest the ceiling for each fire, with a reduction in temperature along the compartment for trees 7, 8, and 9.** As hot gases leave the compartment, cooler air is being entrained along the length of the compartment as a result of the shearing and mixing between the hot upper layer and cool lower layer, as well as heat transfer into the ceiling. Therefore, as it approaches the opening the upper layer decreases in temperature.
- **The 110 kW corner fire produces the highest temperature near the ceiling.** As discussed earlier in section 5.5.2, the 110 kW corner fire continues to generate the highest temperature profile (as a result of restricted air entrainment), particularly near the ceiling. In fact, as the fire size increases (or in the case of the corner fire – entrainment is decreased) the temperature difference increases between trees at the 2375 mm thermocouple. For example, the temperature difference between tree 6 and tree 7 for the 55 kW fire is approximately 20°C, whereas for the 110 kW corner fire the temperature difference between the same trees is approximately 35°C.

5.5.4 Doorway Field Tree

Temperature Profiles of the Doorway Tree for Different Fires

Specific details of the temperature vs. height profiles (for different fires) are discussed below. Temperature profiles plotted in Figure 5.5 indicate:

- **The temperature profiles for trees 4 and 5 are similar up to 2 m where the soffit stops any hot gases from leaving the fire room** (reasons behind the temperature profiles of the fire room, particularly tree 4 was pointed out in Section 5.5.2). When comparing Figure 5.4 with Figure 5.5, the temperature at in the doorway 1900 mm is close to the temperature recorded by the

thermocouple at 1850 mm for tree 4, with the temperature profile from 1850 mm downwards on tree 4 almost matching the doorway temperature profile.

- **The doorway tree shows a constant temperature profile up to 1 m.** This illustrates how the cooler, higher density ambient air is entering the room below 1 m. Above 1 m, hot lower density gases are exiting through the doorway.
- **The doorway temperature gradient from 1000 mm is more continuous than that from the same height on tree 4.** The doorway separating the fire room from the adjacent room constrains air flow in and out of the fire room. Therefore, shear between the hot low density gases and cool high density ambient air will be highest at the doorway and between the interface of the two gases of different densities. The resulting shear between the two layers promotes mixing, producing a more continuous temperature gradient, i.e. a less constant temperature in the upper layer.
- **An increase in temperature at 1900 mm is observed for increasing fire size, with the 110 kW corner fire producing the highest temperature.** The 55 kW fire produces the lowest temperature at 1900 mm of $\sim 120^{\circ}\text{C}$, the 110 kW fire's temperature increases by $\sim 60^{\circ}\text{C}$ to $\sim 180^{\circ}\text{C}$, the 160 kW fire's temperature increases by a further $\sim 45^{\circ}\text{C}$ to $\sim 225^{\circ}\text{C}$, with the 110 kW fire producing the highest temperature of $\sim 270^{\circ}\text{C}$.

Temperature Variation from the Mean for the Doorway

Specific details of the temperature variation from the mean for the doorway (for different fires) are discussed below. Temperature variations graphed in Figure 5.14 indicate:

- **Temperature variations for the central fires increase with increasing fire size.** As discussed previously in Section 5.5.2, increasing the fire size increases the amount of air entrained, increasing temperature variations of the mixture. This trend continues for the doorway thermocouple tree.
- **Temperature variations increase by up to 100 % or more at and beyond 1000 mm.** The temperature variations increase at and beyond 1000 mm as a result of shear between the hot upper layer and the cool lower layer, previously discussed in Section 5.5.2. The maximum temperature variation

occurs at 1300 mm with variations from the mean of up to 20°C for the 160 kW fire.

5.5.5 Corner Thermocouples

Specific details of the temperature profiles for the corner thermocouples presented in Tables 5.1 – 5.12 are discussed below.

General Patterns

The following are general patterns that were observed for the corner thermocouples in the fire and adjacent rooms.

- **The temperatures increase with increasing fire size.** This behaviour remains consistent with what was observed for the field trees when the fire size was increased.
- **Temperature variations increase with increasing fire size.** Again, this is consistent with what was observed for the field trees when the fire size was increased.
- **The fire room rear corner thermocouples records slightly higher temperatures than the fire room front corner thermocouples for the centrally located fires.** Usually the temperature difference between the rear and the front corners is about 5°C overall. Both corner thermocouples are at an equivalent distance from the central fires. Since the fire entrains ambient air from the front of the compartment, this area of the compartment will be cooler, resulting in the front corner having a lower temperature than the rear corner. This is consistent with what is observed when comparing trees 2 and 4.
- **A considerable temperature drop occurs between the corner thermocouples in the fire room and the adjacent room.** Overall, the temperature drop is about 25 - 30°C for the 55 kW fire, 30 – 35°C for the 110 kW fire, 60 – 70°C for the 160 kW fire, and 50 – 60°C for the 110 kW corner fire. This drop in temperature is a result of the exiting hot gases passing through the doorway, entraining ambient air, and recirculating around the adjacent corner thermocouples.

Specific Corner Profiles

This section discusses specific behaviour observed for each of the three corner thermocouples.

Fire Room Rear Corner Thermocouples

The rear corner thermocouples temperature profile of the fire room shows a temperature gradient that decreases as the wall and ceiling are approached. This is caused by shear wall stresses that reduce the turbulence generated by the fire. This reduction in turbulence near the wall in turn allows heat transfer to occur between the comparatively more stagnant hot gases and the compartment surface. Thermocouples located on the outer edge of the corner thermocouple sets are all similar in temperature, demonstrating how the upper layer is well mixed, as discussed in Section 5.5.2.

Fire Room Front Corner Thermocouples

The front corner thermocouples in the fire room do not illustrate the temperature gradient seen with the rear corner thermocouples in the fire room. Generally, there seems to be a constant temperature profile across all thermocouples, suggesting that this corner is not as stagnant as the rear corner in the fire room. Thermocouples DW75DC125 (**D**istance from **W**all 75 mm, **D**istance from **C**eiling 125 mm), DW75DC175, DW125DC25, DW125DC75, DW125DC125, and DW175DC25 are about 5 – 10°C lower than the other thermocouples. This is an unexpected result.

Adjacent Room Corner Thermocouples

The adjacent room corner thermocouples show a different temperature profile to the previous corners discussed. The thermocouples show a reduction in temperature in the corner and along the wall/soffit, with a temperature increase along the ceiling. The reduction in temperature in the corner, and along the wall, is a result of low turbulence from wall shear stress. Consequently, the hot gases have longer residence times which allows heat transfer to the surface of the compartment (this has already been discussed). Also, as the hot fire gases spill out of the fire room, flow is directed towards the opening of the adjacent compartment, where an increase in temperature is

seen along the thermocouples further away from the wall. Therefore, a smaller amount of the hot gases recirculate back to the corner of the adjacent room.

5.5.6 Surface Temperatures

Specific details of the surface temperatures recorded by the ceiling and floor thermocouples are discussed below. The following conclusions can be drawn from Figures 5.27 – 5.30:

- **The high floor temperatures are a result of radiation from the fire.** At every field tree location, the gas temperature at 300 mm from the floor is lower than the floor thermocouples. Therefore, the fire's radiation must be the cause of high floor temperatures. Figure 5.29 illustrates this point where all values of the difference between floor temperatures and the 300 mm thermocouple are positive.
- **Increasing the fire size increases the temperature of the floor thermocouples.** This shows (Figure 5.27) that the greater the fire size, the greater the radiation output of the fire.
- **The floor thermocouple temperatures are higher closer to the fire.** Figure 5.27 illustrates this point where thermocouples 2 and 4 record the highest temperature of all floor thermocouples (with the exception of the 110 kW corner fire where the closest thermocouple, which records the highest temperature, is 1).
- **Floor thermocouples 2 and 4 are the same distance away from the centrally located fires, however, in every case, thermocouple 4 records a slightly higher temperature.** For example, thermocouple 2 for the 160 kW fire is 20°C lower (180°C) than thermocouple 4 (200°C). Initially, thermocouple 2 was expected to produce a higher temperature than thermocouple 4, since air enters the compartment and blows the fire over slightly towards thermocouple 2. This places flames closer to thermocouple 2, increasing incident radiation on thermocouple 2 and decreasing radiation on thermocouple 4. This outcome of thermocouple 2 measuring a lower temperature than thermocouple 4 was unexpected.
- **Thermocouple 4 has the greatest temperature difference in Figure 5.29.** Thermocouple 4, located between the fire and the doorway, is exposed to the fire's radiation and incoming air. The large temperature difference at this location is a result of the incoming cooler air at tree 4 entering the fire room below the hot

exiting gases. This keeps the thermocouple temperature at 300 mm low (close to ambient), while radiation from the fire raises the temperature of thermocouple 4. This occurs for all fires except the 110 kW corner fire, which is much further away from thermocouple 4. Therefore, radiation is not as high at this location as for the centrally located fires.

- **The ceiling thermocouple temperatures are higher closer to the fire.**
- **The ceiling thermocouples produce higher temperatures than the floor thermocouples at the same locations.** The ceiling thermocouples are not only exposed to radiation from the fire, but also to the convected heat released from the fire. Figure 5.28 illustrates this point where the 110 kW corner fire produces the highest temperature at the ceiling. As previously discussed (Section 5.5.2), the 110 kW corner fire produces the hottest temperatures, producing the highest ceiling temperatures.
- **Ceiling temperatures in the adjacent room do not decay as rapidly as the floor temperatures.** The ceiling jet is the main source of heat in the adjacent room for the ceiling thermocouples. This raises the temperature of the ceiling thermocouples considerably. On the other hand, the floor thermocouples only source of heat is radiation from the fire. The intensity of radiation from the fire decays rapidly with distance, which results in the floor thermocouples temperature decaying more rapidly than the ceiling thermocouples. This can be seen when comparing Figures 5.27 and 5.28
- **Figure 5.30 (The Temperature Difference between the 2375 mm thermocouple and the ceiling) shows a drop in temperature across the compartments for all ceiling thermocouple locations.** This shows that the heat resulting from radiation and convection is being transferred through the ceiling. The greatest temperature gradient occurs for the 110 kW corner fire. The 110 kW corner fire produces the highest temperatures for all fires. Therefore, with ambient temperature varying a maximum of 5°C for each fire, heat conduction through the ceiling will be the greatest for the 110 kW corner fire (i.e. the greater the temperature difference, the greater the heat transfer). Heat transfer through the ceiling decreases with decreasing fire size for the 160 kW, 110 kW, and 55 kW fires.

- **The temperature difference in Figure 5.30 (temperature difference between the 2375 mm thermocouple and the ceiling) does not decay significantly along the length of the room.** This shows that heat transfer is occurring across the entire ceiling of the compartment.
- **Thermocouples 2 and 4 show the lowest temperature difference in Figure 5.30 (temperature difference between the 2375 mm thermocouple and the ceiling).** Ceiling thermocouples 2 and 4 are closest to the fire. Heat transfer will be the greatest here, but so is the heat output from the fire. Therefore, the temperature gradient is lowest between the thermocouple at 2375 mm (the highest thermocouple on trees 2 and 4) and the ceiling thermocouple.

5.5.7 Gas Analysis

O₂ and CO₂ Concentration Profiles

Results of the concentration profiles for O₂ and CO₂ are discussed below. For all observations, comments will mostly regard O₂ consumption, since CO₂ production is directly proportional to O₂ consumption (see Appendix 4). The following observations for O₂ and CO₂ concentration profiles can be made:

- **O₂ consumption increases with increasing fire size for the centrally located fires.** For these experiments, fire size was increased by increasing the supply of LPG to the fire. By increasing the fire size, more O₂ must be consumed. This is observed by an increase in O₂ consumption. Also, smaller fire sizes result in smaller flame heights (see Chapter 4 Observations). This in turn allows more air to be entrained into the fire's plume, increasing the O₂ concentration.
- **O₂ consumption increases with height.** As air is entrained into the fire and its plume, the outer edges of the plume and fire entrain more air than within the plume and fire, as the edge of the plume and fire are in direct contact with ambient air. As a result of entraining more air, this part of the plume will be cooler, and therefore less dense than the hotter gases within. Hence this cooler air, which has entrained more air and therefore has a higher O₂ concentration, will be situated lower than the hotter air which has not entrained as much air. This explains why, with decreasing height, sample lines measure a decrease in O₂ concentration.

- **O₂ depletion for the 110 kW corner fire is the highest for all fires.** Entrainment into the fire and plume is restricted for the corner fire; this will reduce the amount of O₂ entrained, hence in the amount of O₂ consumed increases. The increase in O₂ consumption corresponds to an increase in CO₂ production. Note also, that the O₂ consumption of the 110 kW corner fire is approximately double that of the centrally located 110 kW fire. This suggests that the corner fire's entrainment rate is approximately halved.
- **Tree 2 records the highest consumption of O₂, with a decrease in O₂ consumption for trees 4 and 7 respectively.** At each equivalent sample point height for trees 2, 4, and 7, a decrease in O₂ consumption is observed. Tree 2, located between the fire and the back wall, records the highest amount of O₂ consumption since ambient air is not supplied to the fire via this tree from outside the compartment. Ambient air enters the compartment via trees 4 and 7. Therefore, these trees measure a lower amount of O₂ consumption, with tree 4 measuring a higher O₂ consumption than tree 7, as tree 4 is closer to the fire (which consumes O₂).
- **The O₂ consumption for the 110 kW corner fire decreases with height more rapidly than for the centrally located fires.** Lower quantities of hot gases are leaving the compartment since the 110 kW corner fire entrains less air than the centrally located fires. Therefore, the drop off in O₂ consumption with height is higher than for the centrally located fires.
- **O₂ consumption is very low or nil below 600 mm for trees 2, 4 and 7, and 700 mm for the doorway.** This indicates that at these heights, ambient, higher density air is mostly present.
- **The ratio of O₂ consumption to CO₂ production is approximately 1.5 for most gas sampling locations.** As explained in Appendix 4, the consumption of O₂ is directly proportional to CO₂ production, with an approximate ratio of 1.4. The ratio of O₂ consumption to CO₂ production measured at most sample points is very close to the theoretical ratio. The slightly higher value of 1.5 indicates that perfect combustion is not occurring, with minor amounts of CO, un-combusted and partially combusted LPG are contributing to a slightly lower ratio.

5.6 Overall Discussion

From the analysis of the experimental data above, the following conclusions for the behaviour of the compartmentalized fires can be drawn:

- **There is a difference in behaviour between the fire compartment and the adjacent compartment for all experiments.** For all experiments the temperature profiles, temperature variations, surface temperatures, and gas concentrations gave different results for each compartment. This difference was primarily caused by the presence of a soffit between the fire compartment and adjacent compartment, while there was no soffit separating the adjacent compartment and outside the compartment. The effect of the soffit caused the hot buoyant gases produced in the fire compartment to build up, increasing the depth of the hot upper layer. This build-up of hot gases in the fire compartment increased the temperature profile of the fire room, created an upper layer that illustrated a constant temperature profile with height, lowered the height where CO₂ was measured compared with the adjacent room, and increased the ceiling surface temperature. Whereas in the adjacent room the upper layer was located significantly higher than in the fire room. The temperature profile here was lower with correspondingly lower surface temperatures.
- **Increasing the fire size for the centrally located fires increased temperature profiles, temperature variations, surface temperatures and CO₂ concentrations in both the fire and adjacent compartments.**
- **The 110 kW corner fire produced distinctive results when compared to the centrally located fires.** The distinct results were a direct consequence of the corner fire's reduction in entrainment area by approximately 50%. This reduction in entrainment increased temperature profiles in the fire and adjacent compartments (particularly near the ceiling), generated significantly different temperature profiles along the fire compartments centre-line, reduced temperature variations as a result of the corner fire generating less turbulence, and increased the CO₂ concentration in both compartments.

5.7 Limitations and Assumptions

There are important limitations and assumptions that must be acknowledged regarding this chapter. These regard the thermocouples and fire size.

Thermocouples

- **Thermal lag by the thermocouples prevented the true temperature variations from being measured.** Thermocouple response time is on the order of 5 – 10 seconds (Holman, 1978). Since each thermocouple head was welded manually, the thermocouples will also have a distribution of response times. Therefore, significant temperature deviations that occurred, particularly in regions such as the upper and lower layers, may not be read accurately if the frequency of temperature fluctuations (which has not been looked at for these experiments) is higher than the thermocouple response time. Therefore it should be recognized that the standard deviation, determined from the temperature fluctuations, should only be taken qualitatively and used to compare between other thermocouples, rather than as an absolute value.
- **Thermocouple temperatures are uncorrected for radiation.** The thermocouples were unable to be corrected for radiation using the aspirated thermocouples as it was discovered that the amount of air pumped through the aspirated thermocouples was insufficient. The effect of radiation on the thermocouples depends on their location relative to the fire. If the thermocouples are close to the fire but not exposed to the fire's hot gases (such as in the lower layer), then the thermocouple can absorb radiation from the fire, increasing its temperature, thereby not measuring the surrounding gas temperature correctly. The other scenario is when the thermocouple is at a very high temperature (such as in the fire, or in the upper layer near the fire). This will result in the thermocouple emitting radiation, thereby reducing its temperature; again the thermocouple will not measure the surrounding gas temperature correctly. These effects should not be significant for the thermocouples in the adjacent compartment, since the temperatures are not very high. Therefore, they will not emit significant levels of radiation which would reduce their temperature, nor are they close enough to the fire so that

radiation would be absorbed. However, in the fire compartment, thermocouples located in the fire (tree 3), in the lower layer near the fire (eg the thermocouples at 300 mm for trees 2 and 4), and near the fire (trees 2 and 4) will be subjected to the effects of radiation. Therefore, these radiation effects should be remembered when looking at the temperatures measured by the thermocouples in these and similar locations. The up side to this is that it is unlikely the temperature profiles for any of the trees are affected to the point where a qualitative analysis does not hold.

- **The temperature profiles plotted may not give a high resolution along the length of the field trees.** Vertical thermocouple spacing varied from 25 mm to 300 mm; therefore temperature profiles plotted may not reveal exact temperature profiles in regions where there is wider thermocouple spacing.
- **The position of each thermocouple varies slightly from the positions quoted.** It was impossible to align every thermocouple to the exact millimetre quoted. From experience, the error for each thermocouple would be no more than 10 mm after the thermocouples were aligned.

6 SMARTFIRE Introduction and Overview

The purpose of this chapter is to provide an overview of the SMARTFIRE program. The general reference for the material presented in this chapter is the SMARTFIRE User Manual (Galea et al. 1998). This report does not detail the differential equations used for field modelling programs such as SMARTFIRE. Readers wishing to familiarize themselves with the theory associated with field modelling are referred to work from authors such as Hinze (1957), Versteeg and Malalasekera (1995), Patankar (1980), and Markatos et al. (1982).

6.1 Introduction

Fire models are becoming popular with Fire Engineers as they can be used at little cost to examine fire and smoke movement for buildings that are or have yet to be constructed. From this the necessary fire safety systems, tenability and evacuation times can be determined. Also, many countries are now adopting performance based building codes, allowing the use of fire models to meet the required criteria for building design.

Essentially, there are two methods for simulating fires: zone models and field models. Zone models use experimentally derived correlations to predict fire and smoke movement within an enclosure. The heavy reliance of empirical data implies the possibility for inaccurate modelling results for scenarios that do not have experimentally derived correlations. However, field models rely on the fundamental principles of fluid dynamics to determine fire and smoke movement within a compartment, with little reliance on empirically derived data. So a greater reliance can be placed on the accuracy of a field models' result.

There are, however, downsides to using field modelling as opposed to zone models. Field models are usually expensive to buy and require powerful computers to process simulations, compared to a zone model. They are very difficult to use, requiring an extensive knowledge of fire dynamics, and a good understanding of the specialist

knowledge associated with the Computational Fluid Dynamics (CFD) used to solve for the conservation of mass, energy and momentum.

Most fire engineers are very competent in fire dynamics, but they do not have specialist knowledge in CFD, making it difficult for them to apply field models successively. SMARTFIRE has been specifically developed to help fire engineers overcome this problem by providing a user interface that does not require extensive CFD knowledge, thus making field modelling less complicated.

6.2 Overview of the SMARTFIRE System

The SMARTFIRE field modelling program is composed of four main components:

- Front end user interface,
- Expert system,
- Grid generator, and
- CFD code.

For a simulation, the four main components are used in the order above. The front end user interface is used to define the geometry and fire scenario; the expert system specifies an appropriate mesh; the grid generator generates the 3D grid; and the CFD code simulates the scenario. Figure 6.1 illustrates how each component of the SMARTFIRE program interacts. Each component will now be described in greater detail.

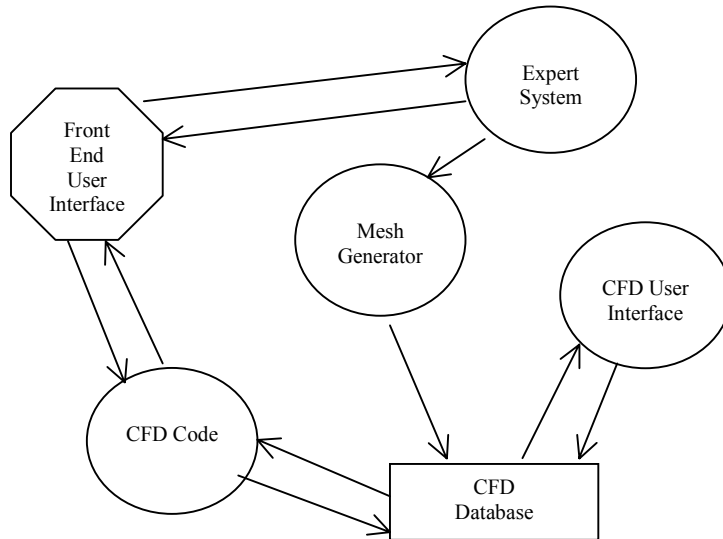


Figure 6.1 SMARTFIRE Block Diagram

6.2.1 Front End User Interface

SMARTFIRE has been designed with the intention of having a Windows front end user interface to allow users easy communication with the program. This version is limited to defining a single “box-shaped” region. This region can be divided up into sub-regions by creating obstruction partitions. It is here where the user can specify dimensions of the compartment, fire properties, vents (windows and doors), obstructions, user specified cell budget, and the various (and to what extent) Physics models (such as six-flux radiation or radiosity models) are used.

The fire is specified as a volumetric heat source. The fire’s physical size must be specified, along with its location and heat output. The fire can be specified as a constant heat release rate or as an equation based transient heat release rate. The equation based fire’s expression is:

$$P = A + Bt + Ct^2 + De^{Et} \quad (6.1)$$

Where: P is the total power output of the fire (kW),
t is the current simulation time (s),
A is the constant heat release coefficient (kW),

B is the heat release coefficient with time (kWs^{-1}),
C is the heat release coefficient with t^2 (kWs^{-1}),
D is the exponential heat release coefficient (kW), and
E is the exponential term modifier with time (s^{-1}).

So for a typical t^2 fire, variables A, B, and D would be assigned a value of zero with C being the fire growth parameter for the t^2 fire.

When the scenario has been completely specified, the mesh specification KBS tool is launched. A cell budget will be presented which can be accepted, increased, or decreased. It must be recognized that a high cell budget will increase the accuracy of the solution but is likely to significantly increase computational time, with the final solution not necessarily being markedly more accurate. With a low cell budget, a reduced computational is likely to come with the expense of inaccurate results.

6.3 Knowledge Based System (KBS)

6.3.1 Overview of Mesh Generation by KBS

The KBS's purpose is to aid the user to assign an appropriate number of cells to the problem and distribute the cells appropriately. This process is called "mesh generation". The distribution of cells is a powerful technique that, when applied correctly, improves the accuracy of the solution without increasing computational time. Some areas within a compartment require finer resolution than others, since some areas change more in temperature and smoke concentration than others. For example: temperatures at the ceiling will increase more rapidly than near the floor. Therefore, to improve accuracy for a simulation, more important areas should have finer cell resolution. Conversely, areas that are not likely to change do not need as high a resolution and can have the number of cells reduced without threatening accuracy. Using this method potentially means greater accuracy while maintaining the cell budget, without increasing computational time. Figure 6.2 below shows an example of efficient cell distribution.

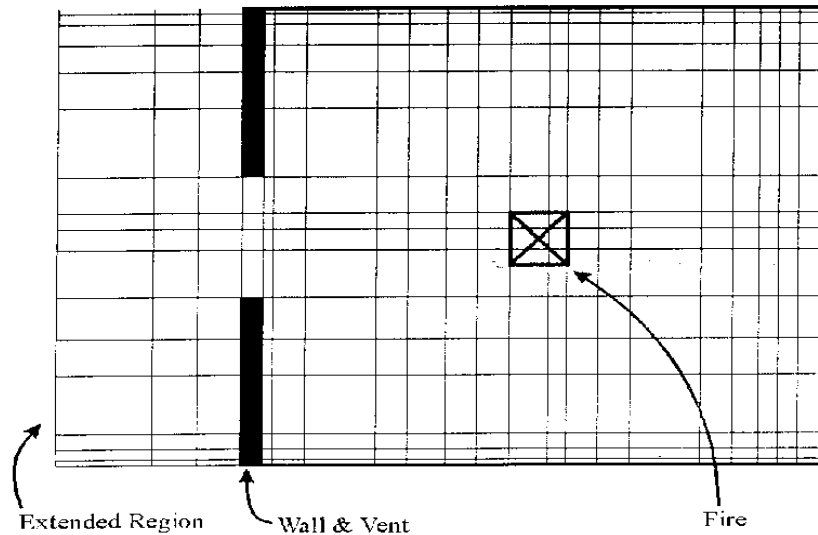


Figure 6.2 Example of Efficient Cell Distribution

As can be seen, the grid is not evenly distributed. Cells have been refined within the fire and towards the walls. Refinement near the wall is important if wall-functions e.g. turbulent wall layer, are to be used to define interactions such as heat transfer coefficients from local flow conditions. Note also, an area outside the vent has been meshed. This “extended region” is required for vents (doors and windows) as flows through vents are usually bi-directional. It is necessary to extend the grid past the vent as a correct solution can only be found by removing the free surface boundary away to a considerable distance beyond the vent. The next section describes how SMARTFIRE assigns a non-uniform grid to improve simulation accuracy without trading off computational time.

6.3.2 Knowledge Acquisition

To enable SMARTFIRE to assign a suitable mesh for most scenarios, a system was developed called Case Base Reasoning (CBR). CBR is based on the idea that human experts rely on experience for their understanding. By interviewing experts, suitable meshing of different scenarios evolved, with patterns emerging as to how to assign appropriate grids to various scenarios. However, the patterns observed were not sufficient to enable different scenarios to be meshed correctly. The solution was to also incorporate previous cases of similar geometry. These cases are stored in a

library where they are accessed by a retrieval algorithm which finds the case most similar to the problem specified. Past cases have been developed based on the Steckler et al., (1982) room fire experiments. The CBR cycle is shown in Figure 6.3 below.

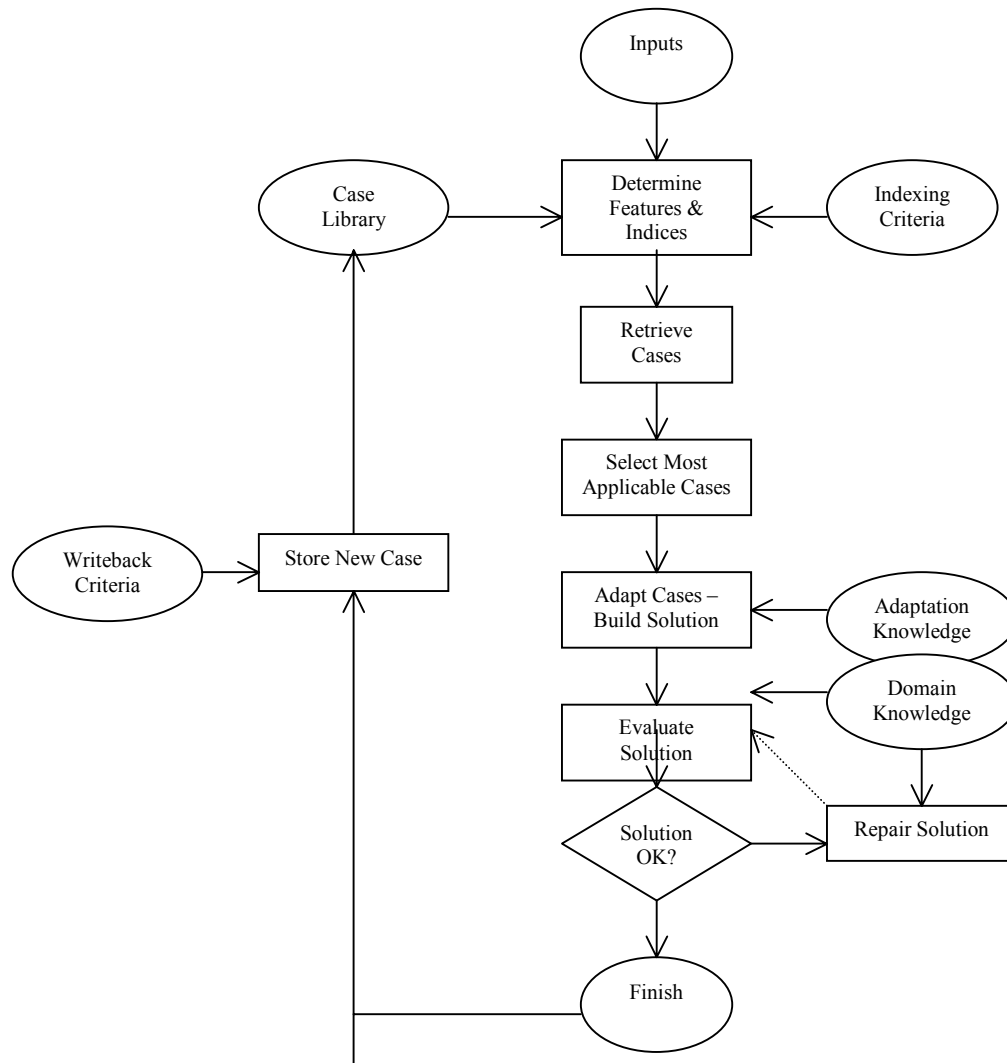


Figure 6.3 SMARTFIRE CBR Cycle

Here, cases are retrieved on search indices. These are significant pieces of information that separate one case from another. SMARTFIRE looks for relationships such as fire location, relative vent, vent location on its wall, fire size, and vent size between the current specified scenario and its library of previous cases. The most applicable case is then chosen. Once retrieved, they are adapted to account for differences between the scenario and retrieved case. For SMARTFIRE, adaptation occurs when the

scenario has more than one vent or fire, since the library cases are based on single fire and vent experiments. For each combination of fire and vent in the scenario, the retrieval algorithm retrieves most applicable cases. Meshing instructions are then superimposed over the scenario.

General meshing instructions that apply to most scenarios, are then applied to the scenario, such as the fire must have more than one cell in any direction and there must be a fine cell next to a wall. Cells in the mesh are then checked for adjacency aspect ratios. Figure 6.4 below illustrates some examples of adjacency aspect ratios.

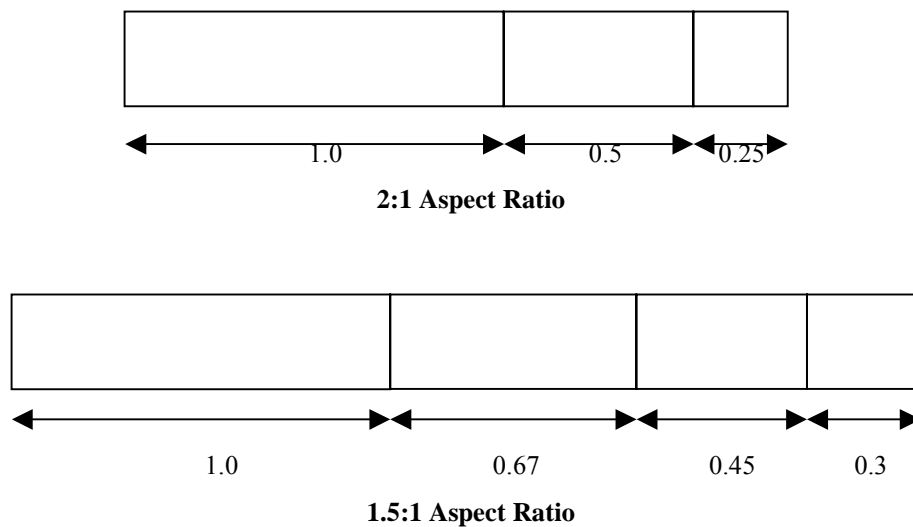


Figure 6.4 Adjacency Aspect Ratio Examples

The less abrupt the adjacency aspect ratio, the more accurate the solution is likely to be. Clearly, a 2:1 aspect ratio is far more abrupt than a 1.5:1 aspect ratio. SMARTFIRE attempts to keep these aspect ratios as smooth as possible. For instance, near walls and extended regions, a single power law is applied.

Internal aspect ratios of all cells must also be checked. The internal aspect ratio is the ratio between two sides of a cell at 90° to each other. This is necessary as long thin cells are undesirable. Internal aspect ratios are compared along the XYZ axes. If any ratio is above three or below one third (the inverse of three), then the cell is at least three times longer in one direction than the other. Usually, SMARTFIRE will splice the cells that violate the internal aspect ratio rule, increasing the number of cells. This will not sacrifice accuracy of the simulation. Exceptions might occur when the cell

budget is very large, and SMARTFIRE will merge violating cells together to form larger, squarer cells.

Overall, the process is an iterative one, with SMARTFIRE altering the mesh to comply with adjacency and internal aspect rules when a suitable cases along with general meshing principles, have been chosen.

7 SMARTFIRE Simulation Methodology and Parameters

The purpose of this chapter is to specify the methodology and parameters implemented for the SMARTFIRE simulations of the four fires conducted at McLeans Island.

7.1 Introduction

Eight simulations have been carried out for the four different fires conducted at McLeans Island, two for each fire – one simulation with the six-flux radiation employed, and one without. This has been done to see if using the six-flux radiation model produces superior results.

Due to the late arrival of the SMARTFIRE program, SMARTFIRE simulations have mostly been based on recommended default settings, as there was insufficient time available to determine the best settings for the scenarios.

7.2 Computer Hardware and Software

SMARTFIRE Version 2.01 was used to simulate the four fire experiments conducted at McLeans Island. Temperatures associated with field tree locations were then input into an Excel 2000 Spreadsheet, where temperatures were plotted against height. All simulations were carried out on a 450 MHz Pentium III computer with 128 MB RAM, running on Windows NT operating system.

7.3 SMARTFIRE Variables

7.3.1 Fire Properties

The physical fire size must be specified for each simulation. The height and width of each fire was estimated from video footage taken, which can be seen in Chapter 4 Observations. Table 7.1 below lists the dimensions for each fire.

Table 7.1 Fire Dimensions for Simulations

Fire Size	Flame Height (m)	Flame Width (m)	Flame Breadth (m)	Elevation (m)
<i>55 kW</i>	0.6	0.3	0.3	0.3
<i>110 kW</i>	0.9	0.3	0.3	0.3
<i>160 kW*</i>	1.2	0.4	0.4	0.3
<i>110 kW_c</i>	1.5	0.3	0.3	0.3

*The 160 kW fire appeared to produce a diameter larger than the size of the burner's base (0.3 m square). Thus, the size of the 160 kW fire was increased to 0.4 m square.

All fires were modelled as steady-state simulations, i.e. fires were modelled as instantaneous fires with no growth phase to reach desired fire size.

7.3.2 Surface Material

Surface materials were modelled as gypsum plasterboard for all the SMARTFIRE simulations, as this was the closest material to what was used for the experiments.

7.3.3 Temperature

The temperature for each simulation must be specified (in Kelvin) and was set to the ambient temperature recorded for each experiment. Table 7.2 lists the ambient temperatures for each fire specified for the simulations.

Table 7.2 Ambient Temperatures for Simulations

Fire	Ambient Temperature (K)
<i>55 kW</i>	293
<i>110 kW</i>	289
<i>160 kW</i>	288
<i>110 kW_c</i>	293.5

7.3.4 Grid Generation

For every simulation, the KBS system assigned the appropriate grid. As described previously in Section 6.3, the KBS system determines the appropriate grid so an appropriate number of cells are assigned to the problem, as well as distributing cells in

regions that require higher resolution. It was assumed that the KBS system chose the appropriate grid resolution given time constraints for the SMARTFIRE simulations.

7.3.5 Convergence Limits and Radiation Issues

Since each simulation was run as a steady state fire, simulations were required to be defined by a set number of iterations, not by a simulation time. Consequently, the number of iterations set for each simulation was 1000.

Convergence for each iteration was based on setting the convergence tolerance value to 0.0001. This means that SMARTIFIRE will not move onto the next iteration until all simulation variables have converged to a value equal to or lower than 0.0001.

For the simulations where the six-flux radiation model was incorporated, absorption coefficient values need to be entered for the fuel type used in the experiments. Values of 5.97 and 11.94 were entered as minimum and maximum absorption coefficients respectively for propane. Since LPG (used in the experiments) is 80% propane and 20% butane, the absorption coefficients used should be suitable.

7.3.6 Running the Simulation

After all the necessary procedures have been completed, the simulation may be started. Starting the simulation is done by pressing the run command in the CFD engine. From here each iteration is swept through until all iterations have been completed.

7.3.7 Data Exploration and Exporting

After each simulation was complete, temperature profiles relating to field tree locations were noted and input into a Microsoft Excel 2000 Spreadsheet.

8 SMARTFIRE Results and Discussion

The purpose of this chapter is to present and discuss the results of the SMARTFIRE simulations of the four fire experiments conducted at McLeans Island.

The results presented comprise of visual contours along the centre-line of the room, inline with the locations of the field trees. The visual contours of the entire two-compartment structure will be presented first, followed by visual contours of the fire room and adjacent room. This is done so an overall representation can be examined, followed by a more detailed profile of each room. The visual contours will include results for the simulations, with and without the six-flux radiation sub-model.

Temperature contours plotted represent temperature profiles in units of Kelvin. Each visual contour plot also includes the mesh displaying the cell profile along the centreline of the compartment. Grid statistics and computer run times for each simulation will be presented and discussed following the visual contour results.

8.1 Results

8.1.1 55 kW Fire

Results of the visual contour profiles for the SMARTFIRE simulations of the 55 kW fire are presented below in Figures 8.1 – 8.6. The visual contour profile for the entire two-compartment structure is presented first, followed by the fire room and the adjacent room. The simulation without the six-flux radiation sub-model is presented first for each visual profile segment of the structure.

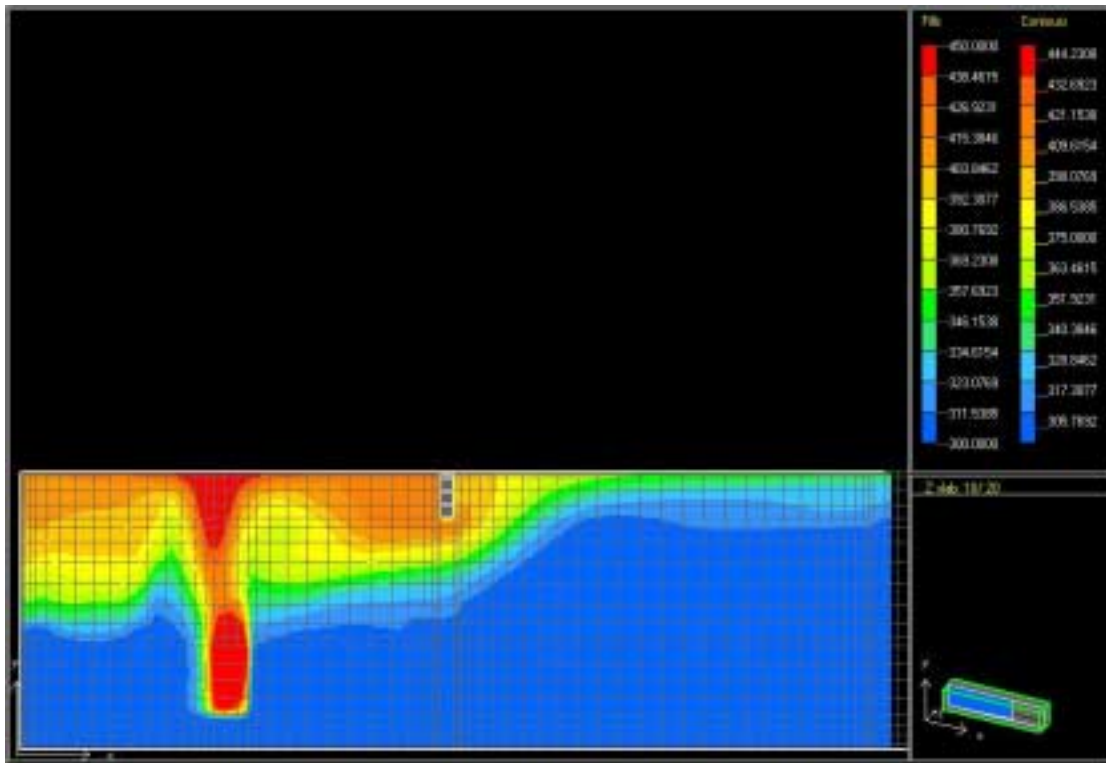


Figure 8.1 Visual Contour Profile for the Two-compartment Structure (55 kW Fire without Six-flux Radiation Sub-model)

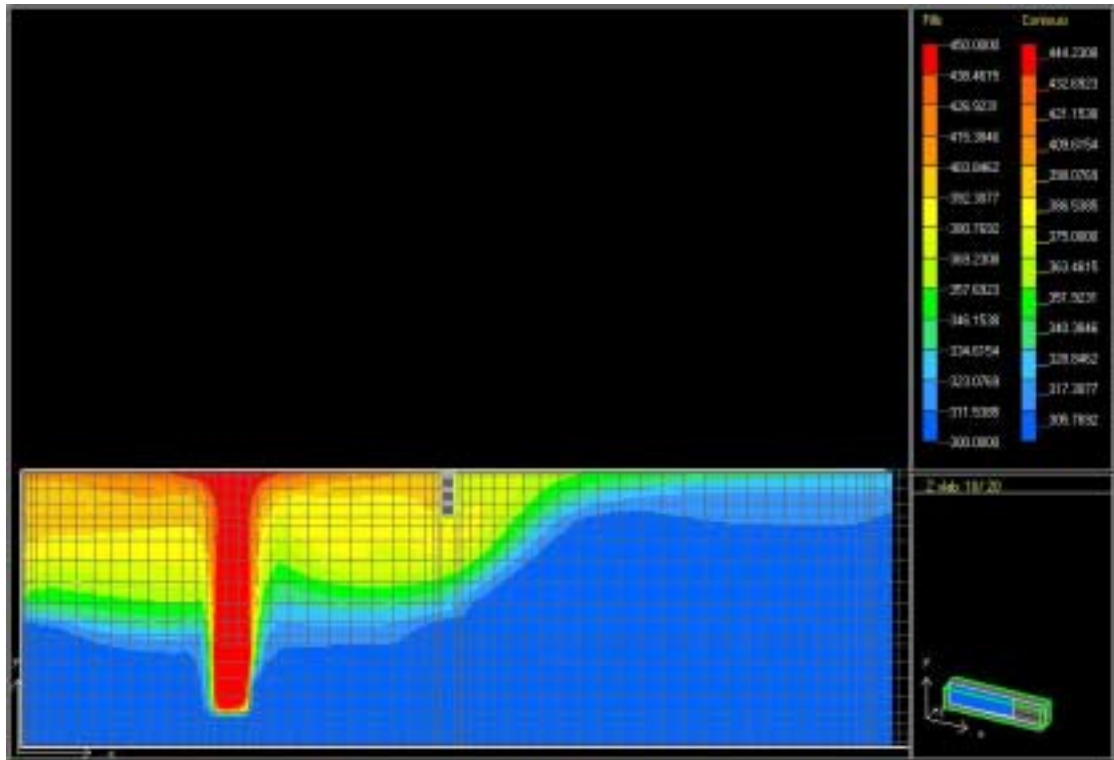


Figure 8.2 Visual Contour Profile for the Two-compartment Structure (55 kW Fire with Six-flux Radiation Sub-model)

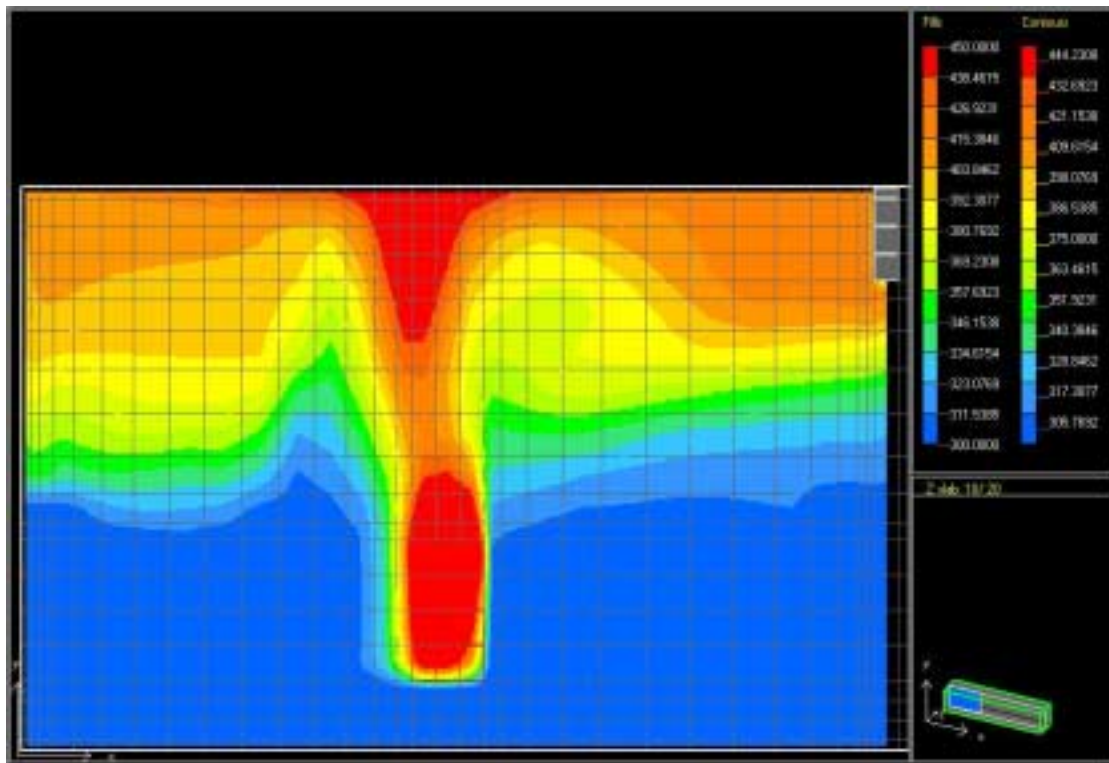


Figure 8.3 Visual Contour Profile for the Fire Room (55 kW Fire without Six-flux Radiation Sub-model)

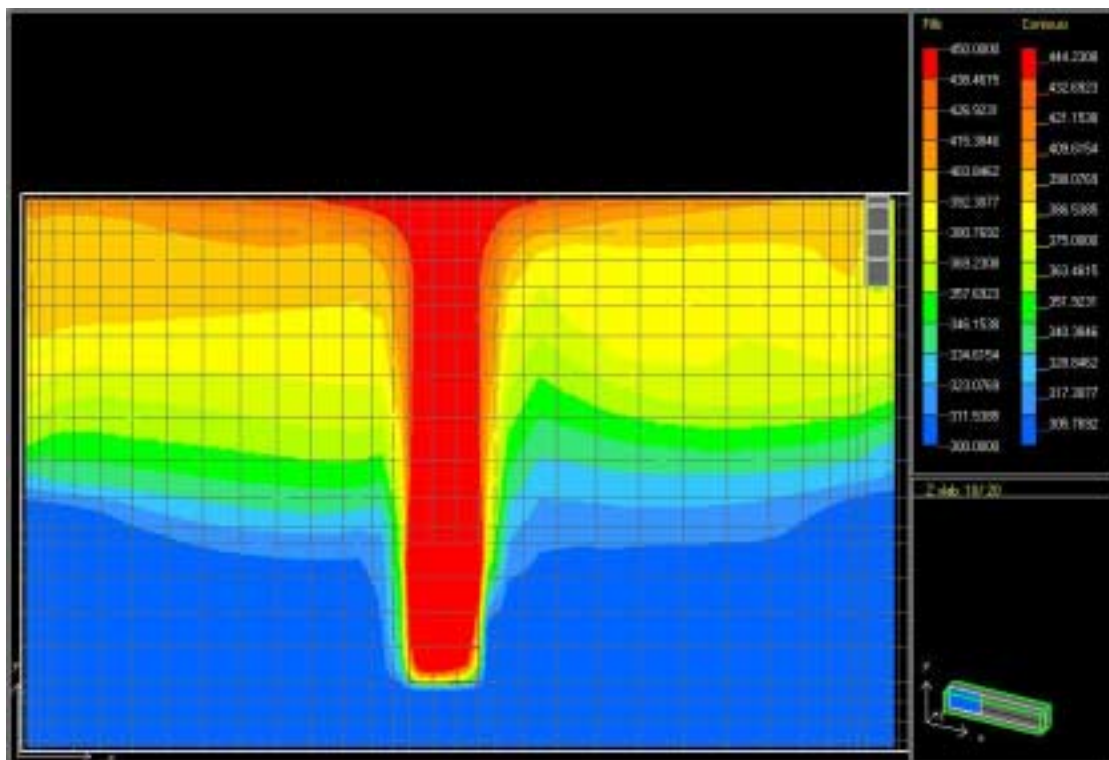


Figure 8.4 Visual Contour Profile for the Fire Room (55 kW Fire with Six-flux Radiation Sub-model)

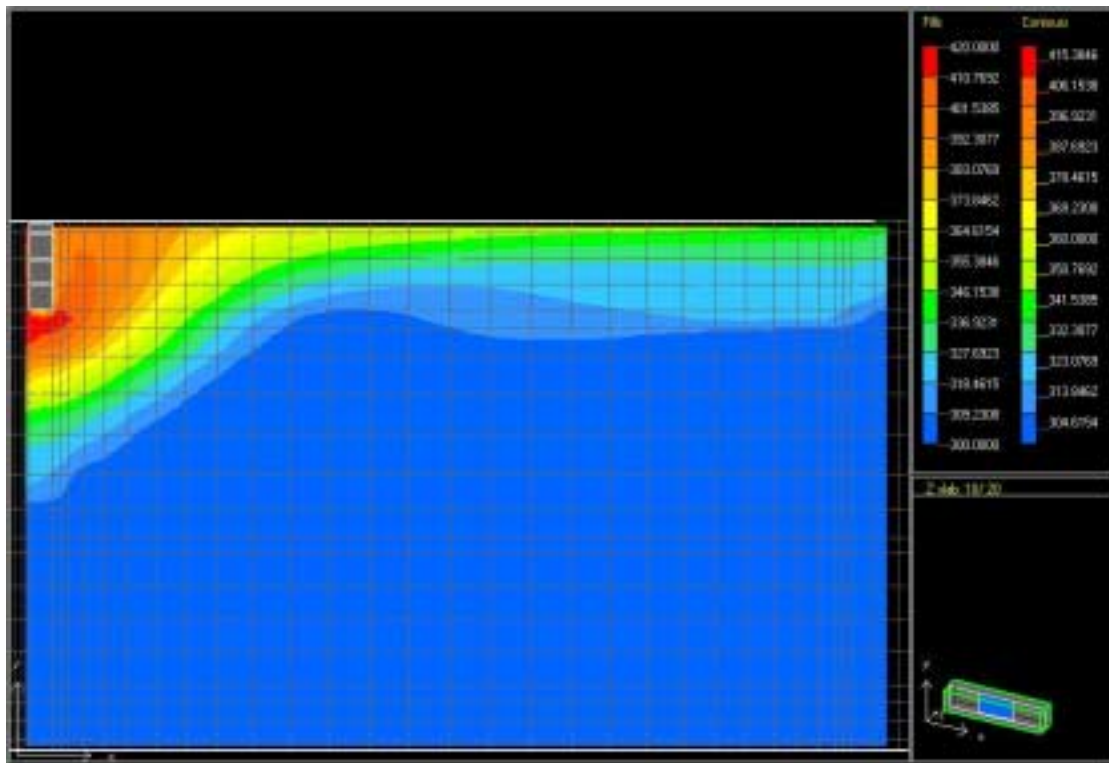


Figure 8.5 Visual Contour Profile for the Adjacent Room (55 kW Fire without Six-flux Radiation Sub-model)

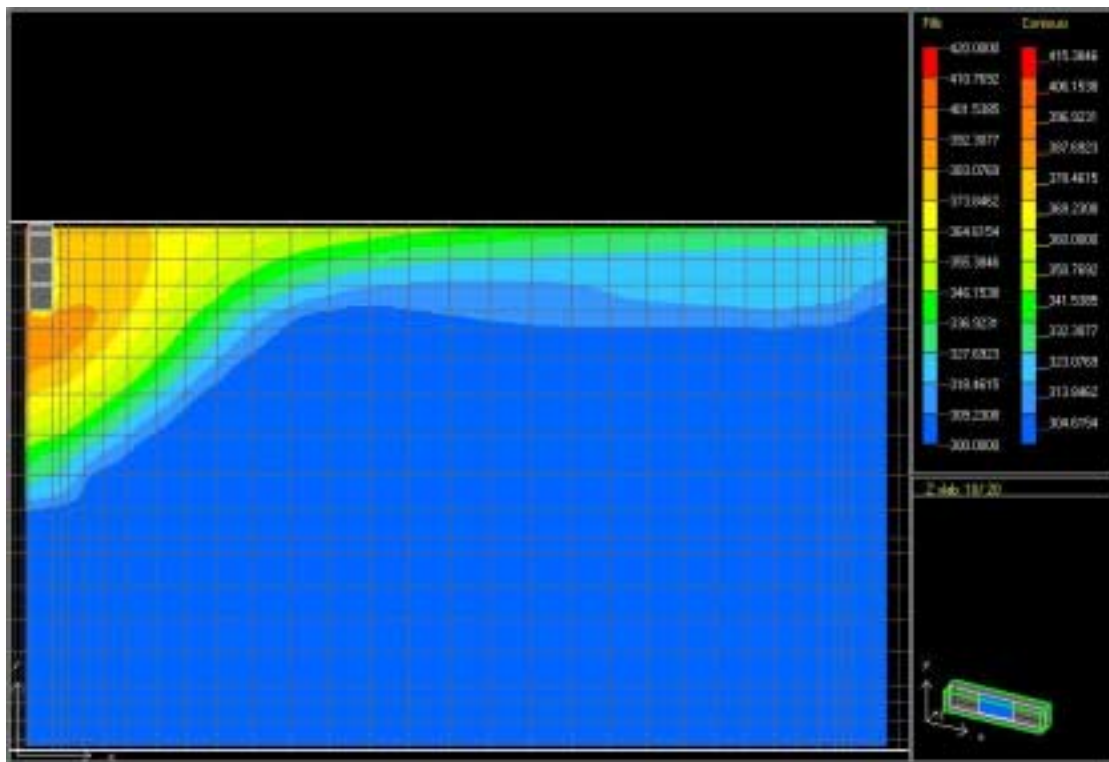


Figure 8.6 Visual Contour Profile for the Adjacent Room (55 kW Fire with Six-flux Radiation Sub-model)

8.1.2 110 kW Fire

Results of the visual contour profiles for the SMARTFIRE simulations of the 110 kW fire are presented below in Figures 8.7 – 8.12. The visual contour profile for the entire two-compartment structure is presented first, followed by the fire room and the adjacent room. The simulation without the six-flux radiation sub-model is presented first for each visual profile segment of the structure.

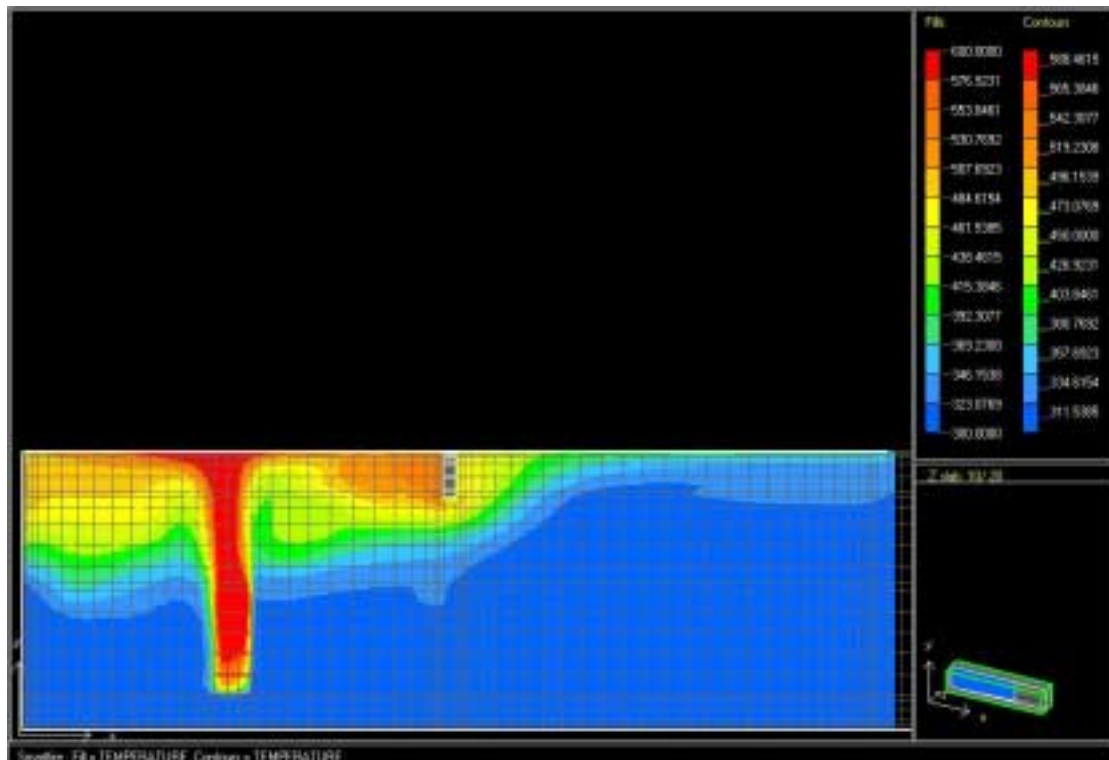


Figure 8.7 Visual Contour Profile for the Two-compartment Structure (110 kW Fire without Six-flux Radiation Sub-model)

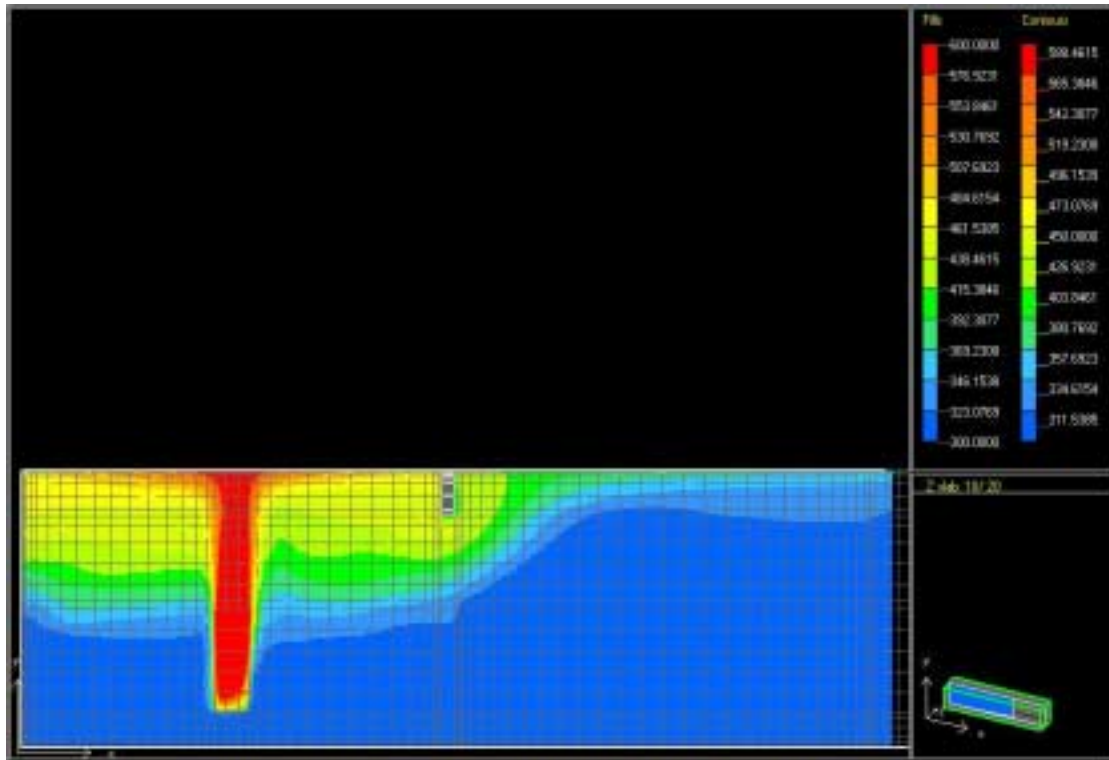


Figure 8.8 Visual Contour Profile for the Two-compartment Structure (110 kW Fire with Six-flux Radiation Sub-model)

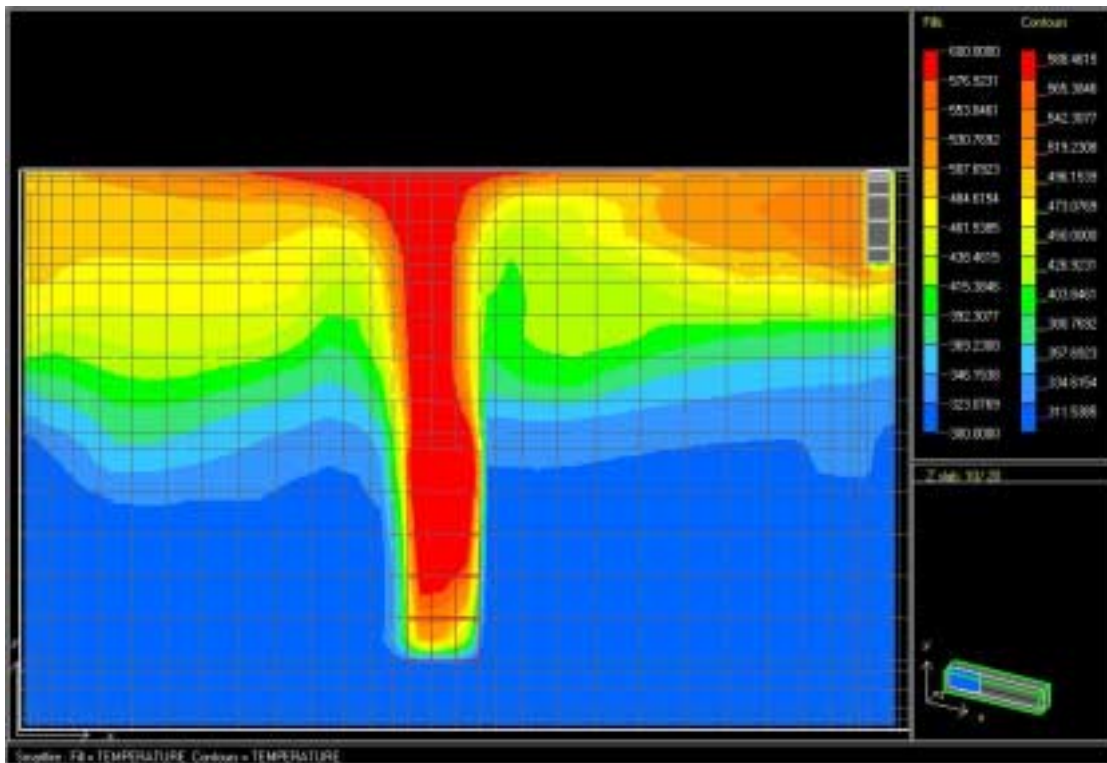


Figure 8.9 Visual Contour Profile for the Fire Room (110 kW Fire without Six-flux Radiation Sub-model)

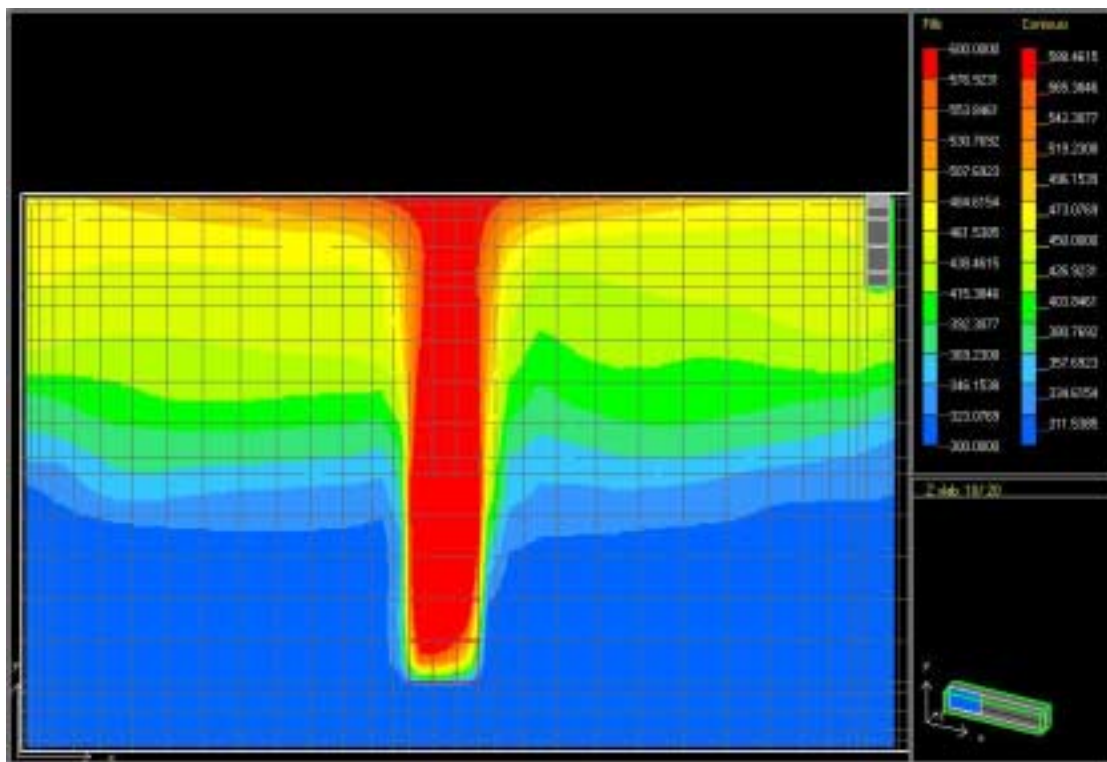


Figure 8.10 Visual Contour Profile for the Fire Room (110 kW Fire with Six-flux Radiation Sub-model)

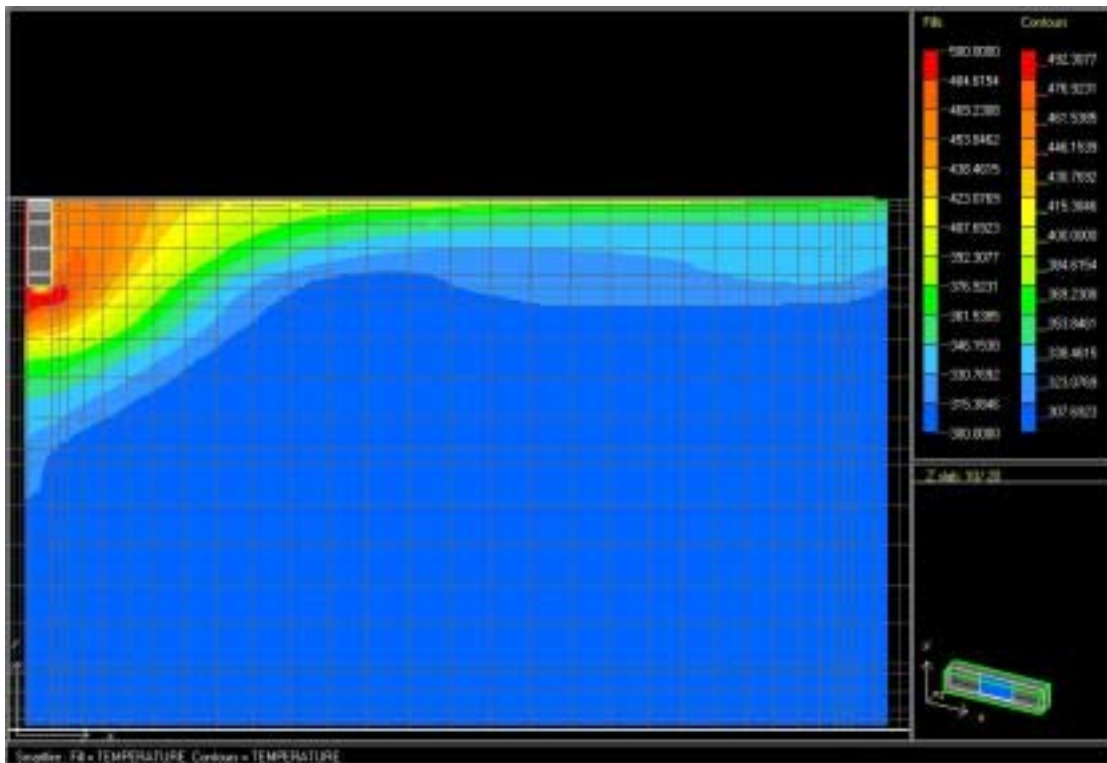


Figure 8.11 Visual Contour Profile for the Adjacent Room (110 kW Fire without Six-flux Radiation Sub-model)

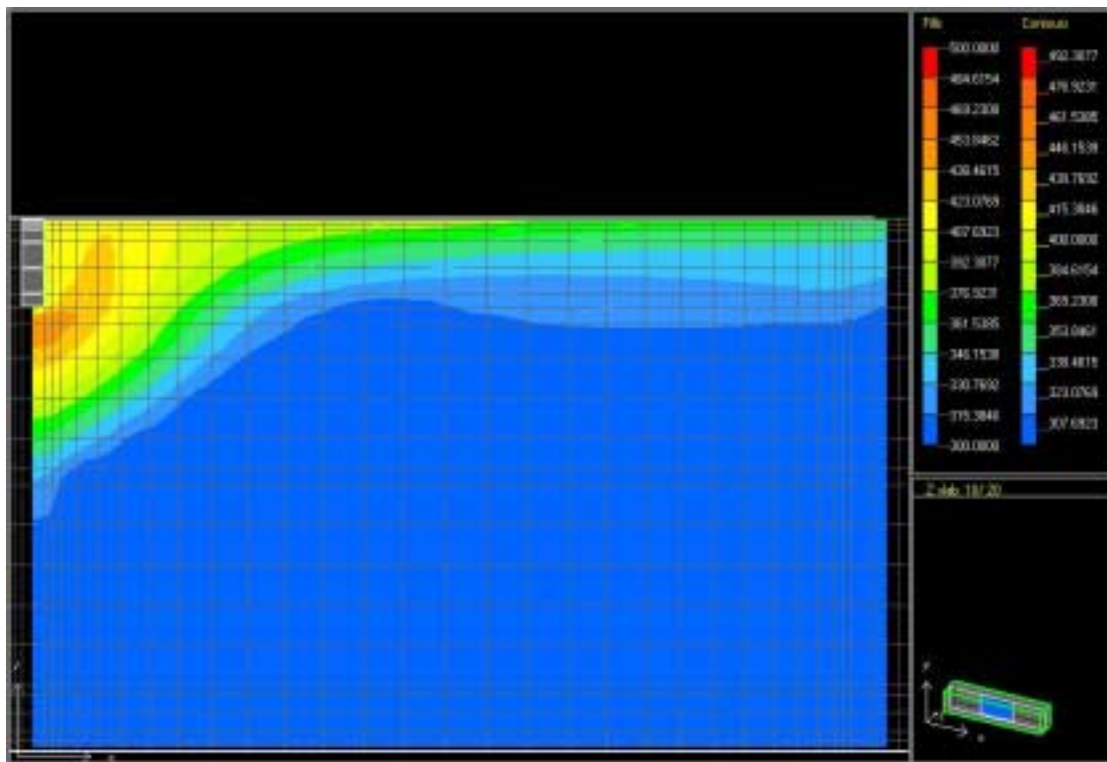


Figure 8.12 Visual Contour Profile for the Adjacent Room (110 kW Fire with Six-flux Radiation Sub-model)

8.1.3 160 kW Fire

Results of the visual contour profiles for the SMARTFIRE simulations of the 160 kW fire are presented below in Figures 8.13 – 8.18. The visual contour profile for the entire two-compartment structure is presented first, followed by the fire room and the adjacent room. The simulation without the six-flux radiation sub-model is presented first for each visual profile segment of the structure.

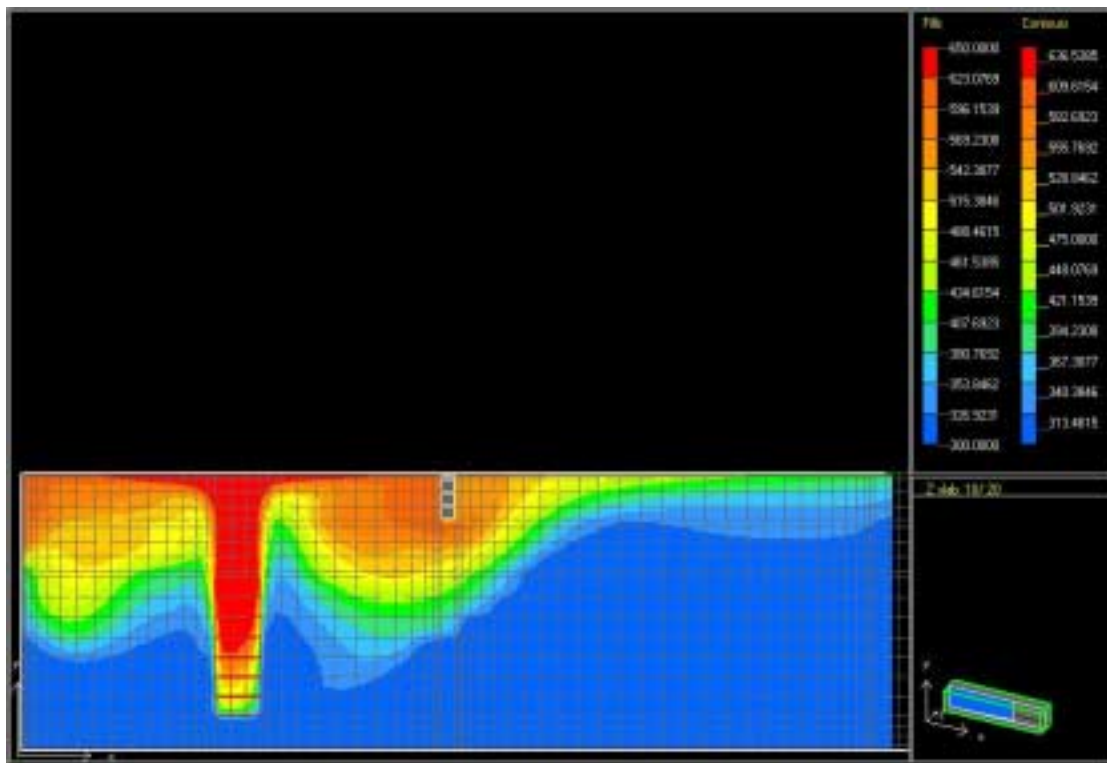


Figure 8.13 Visual Contour Profile for the Two-compartment Structure (160 kW Fire without Six-flux Radiation Sub-model)

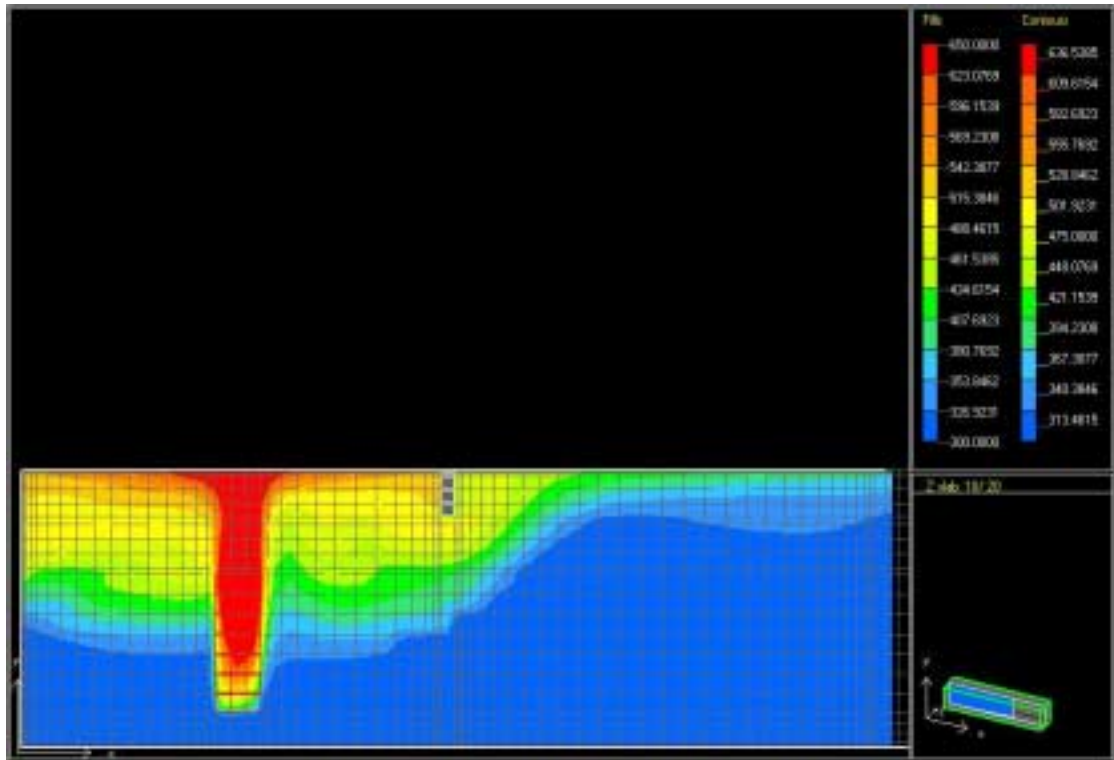


Figure 8.14 Visual Contour Profile for the Two-compartment Structure (160 kW with Six-flux Radiation Sub-model)

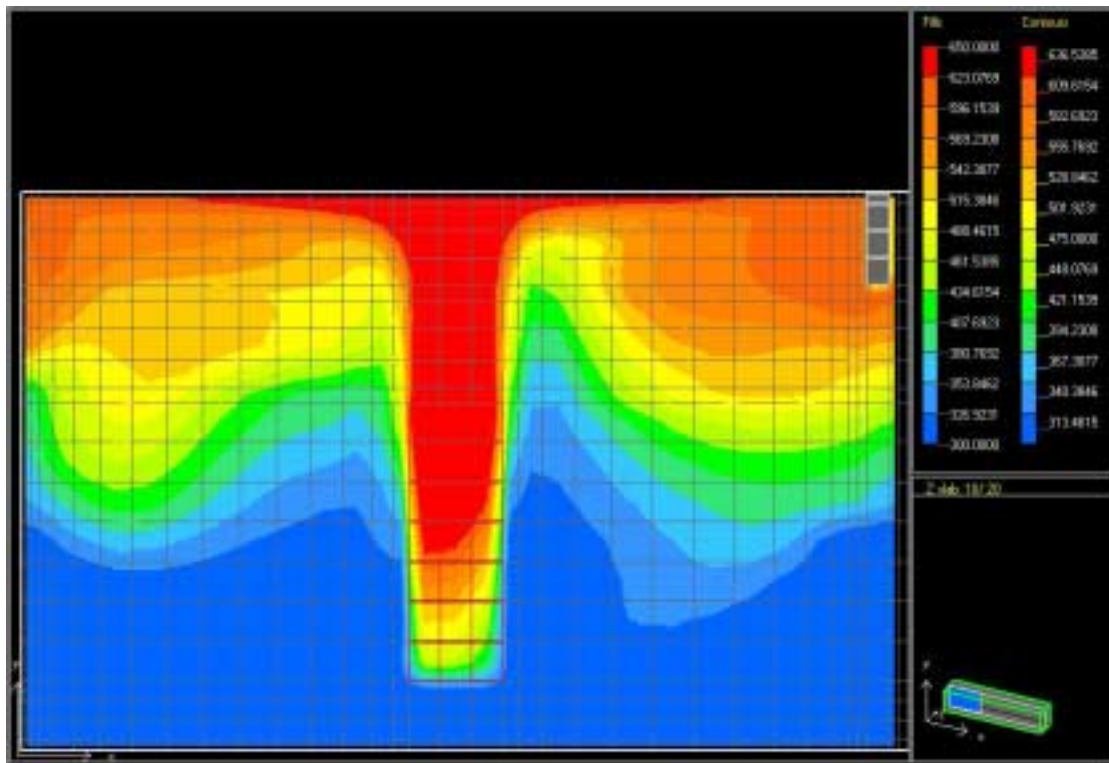


Figure 8.15 Visual Contour Profile for the Fire Room (160 kW Fire without Six-flux Radiation Sub-model)

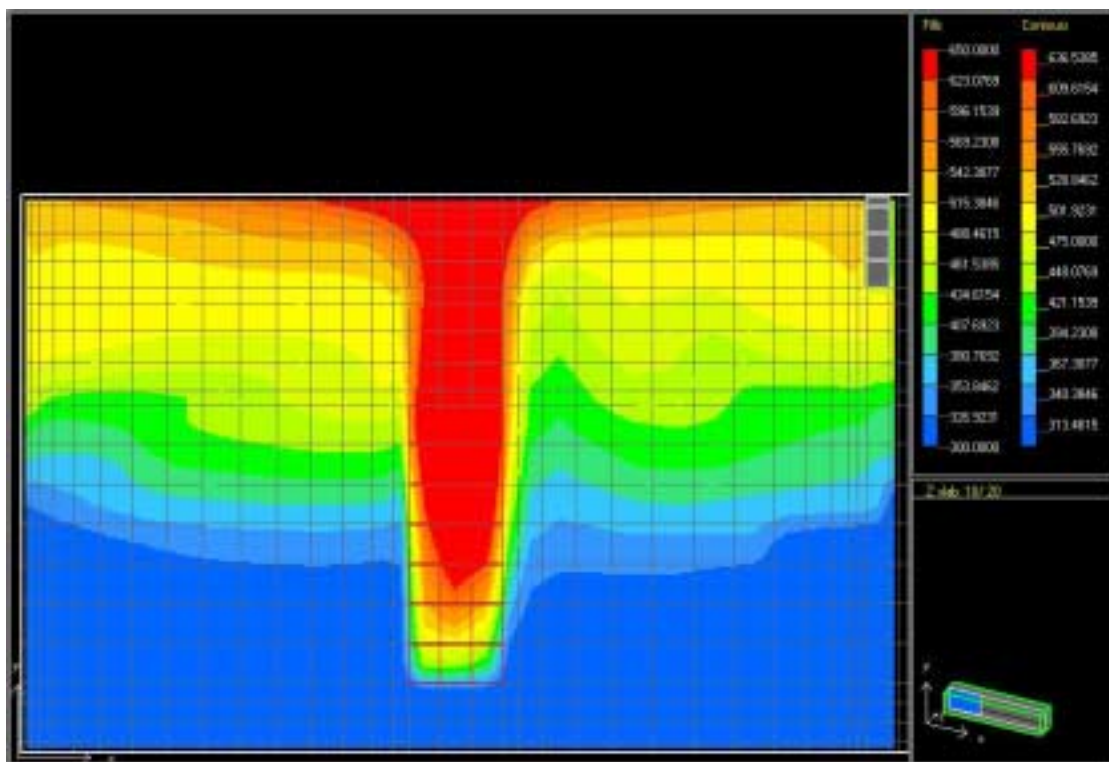


Figure 8.16 Visual Contour Profile for the Fire Room (160 kW Fire with Six-flux Radiation Sub-model)

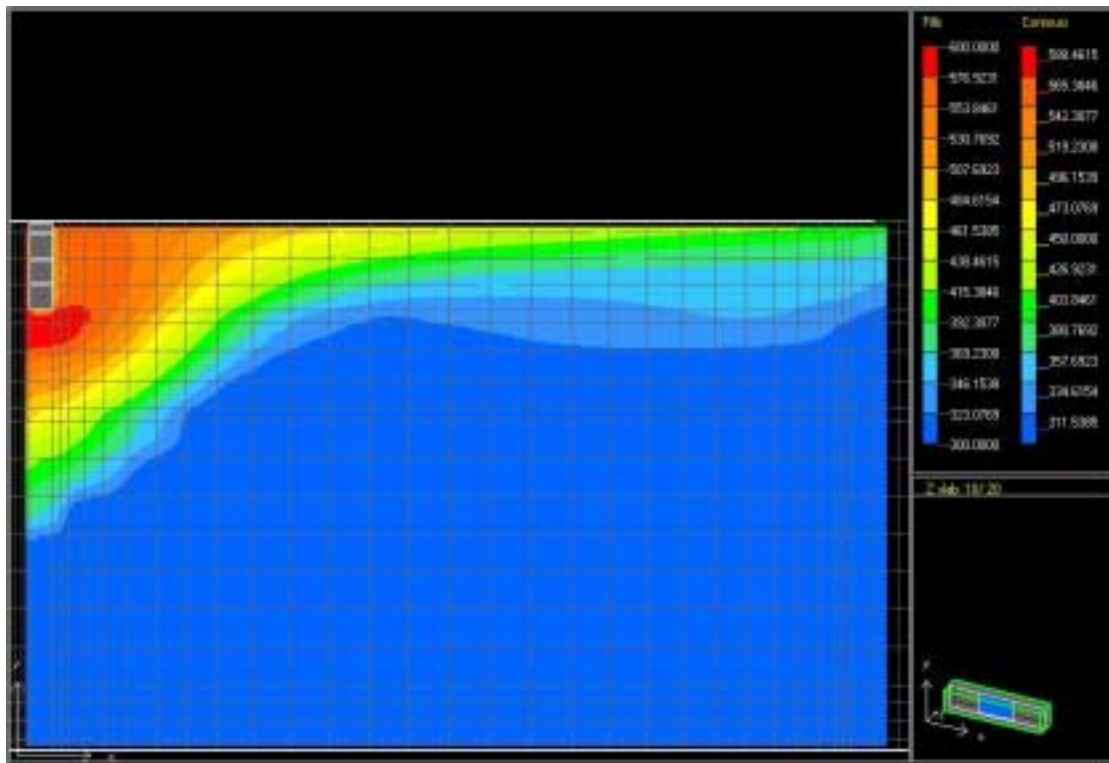


Figure 8.17 Visual Contour Profile for the Adjacent Room (160 kW Fire without Six-flux Radiation Sub-model)

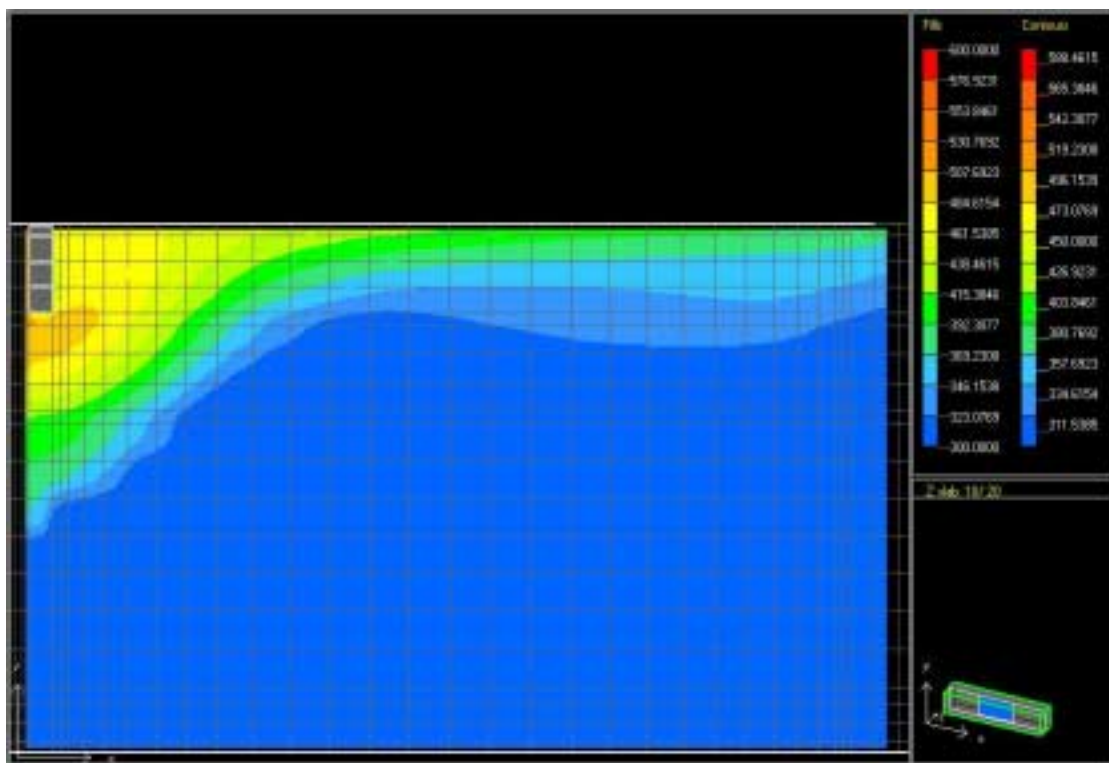


Figure 8.18 Visual Contour Profile for the Adjacent Room (160 kW Fire with Six-flux Radiation Sub-model)

8.1.4 110 kW Corner Fire

Results of the visual contour profiles for the SMARTFIRE simulations of the 110 kW corner fire are presented below in Figures 8.19 – 8.24. The visual contour profile for the entire two-compartment structure is presented first, followed by the fire room and the adjacent room. The simulation without the six-flux radiation sub-model is presented first for each visual profile segment of the structure.

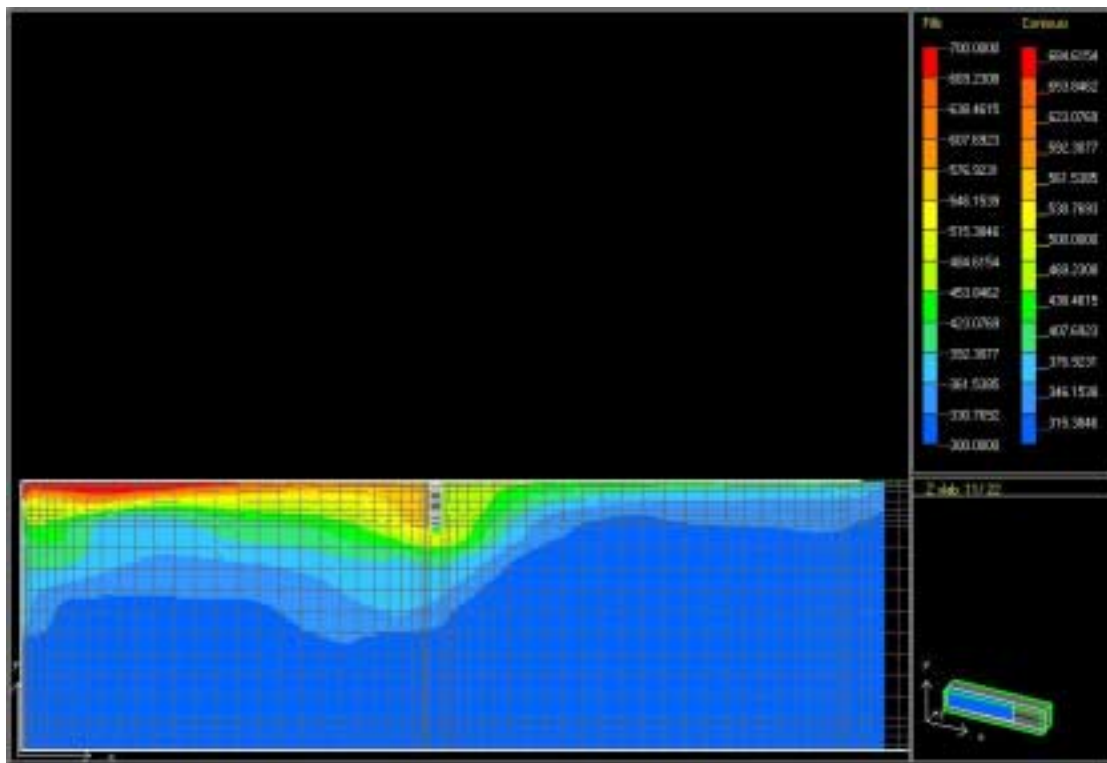


Figure 8.19 Visual Contour Profile for the Two-compartment Structure (110 kW Corner Fire without Six-flux Radiation Sub-model)

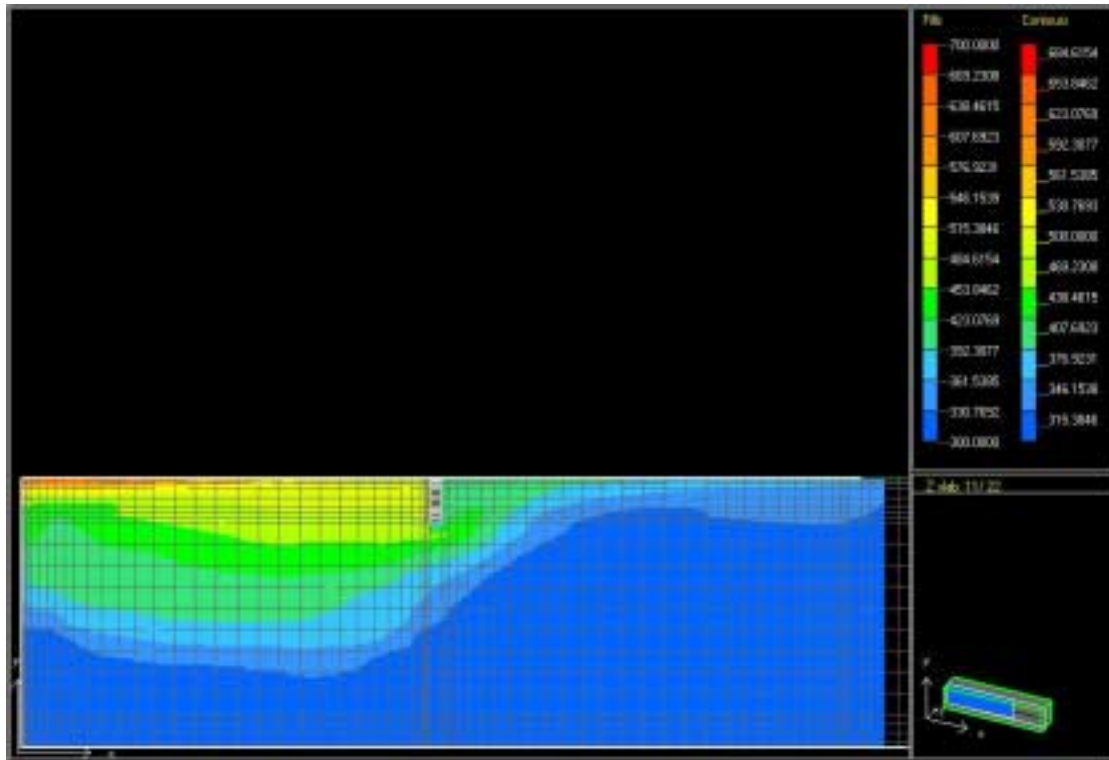


Figure 8.20 Visual Contour Profile for the Two-compartment Structure (110 kW Corner Fire with Six-flux Radiation Sub-model)

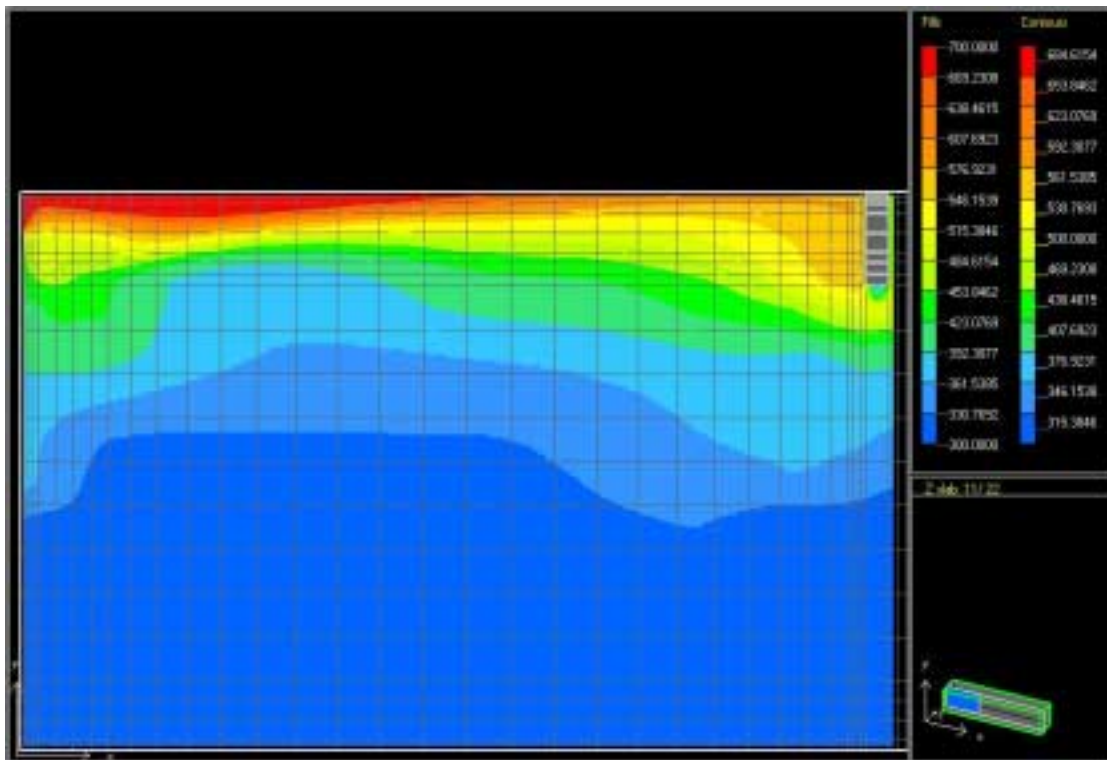


Figure 8.21 Visual Contour Profile for the Fire Room (110 kW Corner Fire without Six-flux Radiation Sub-model)

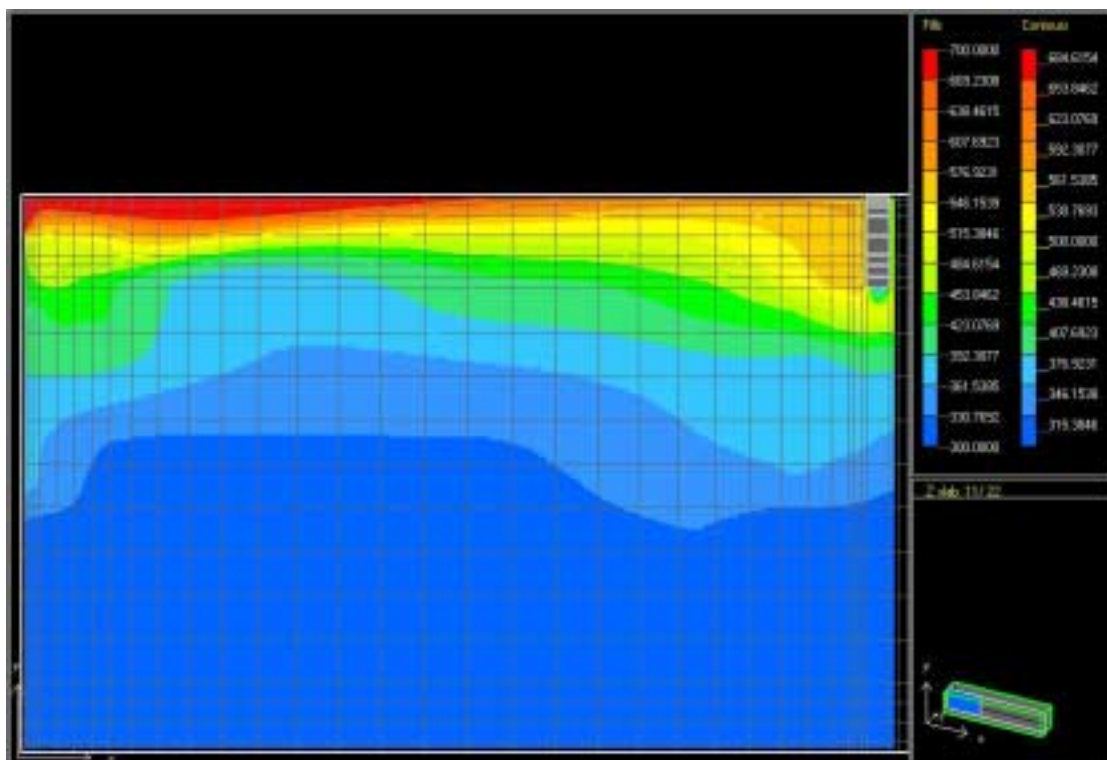


Figure 8.22 Visual Contour Profile for the Fire Room (110 kW Corner Fire with Six-flux Radiation Sub-model)

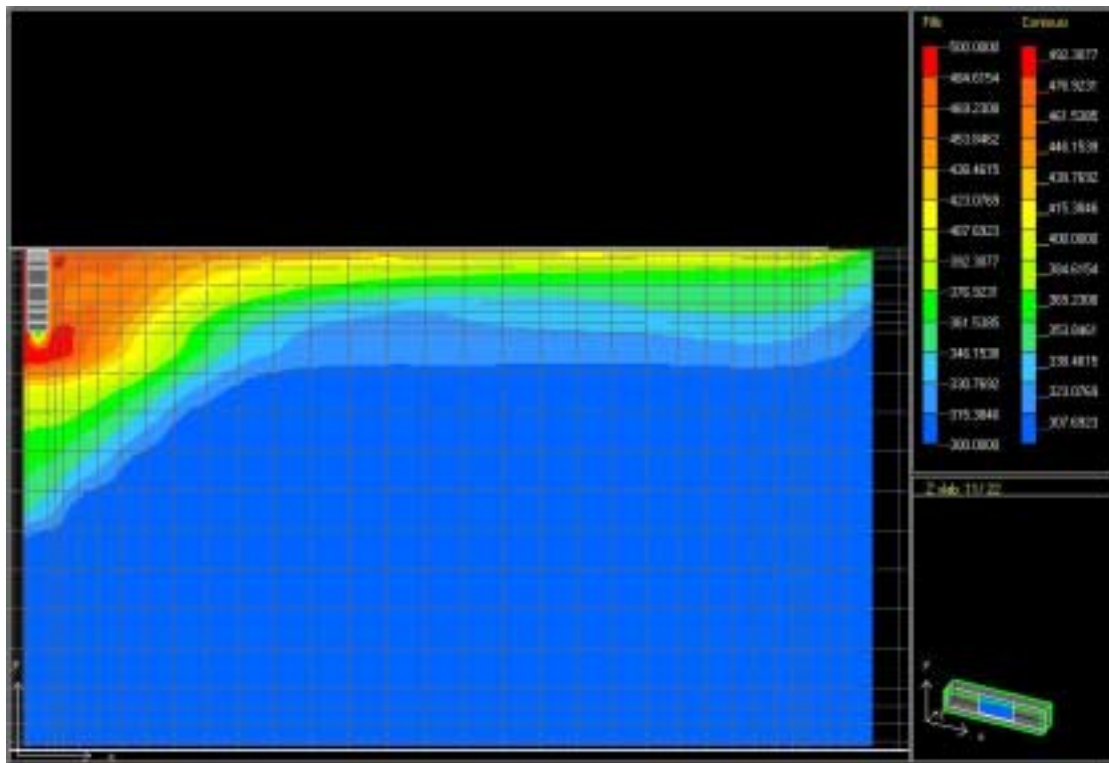


Figure 8.23 Visual Contour Profile for the Adjacent Room (110 kW Corner Fire without Six-flux Radiation Sub-model)

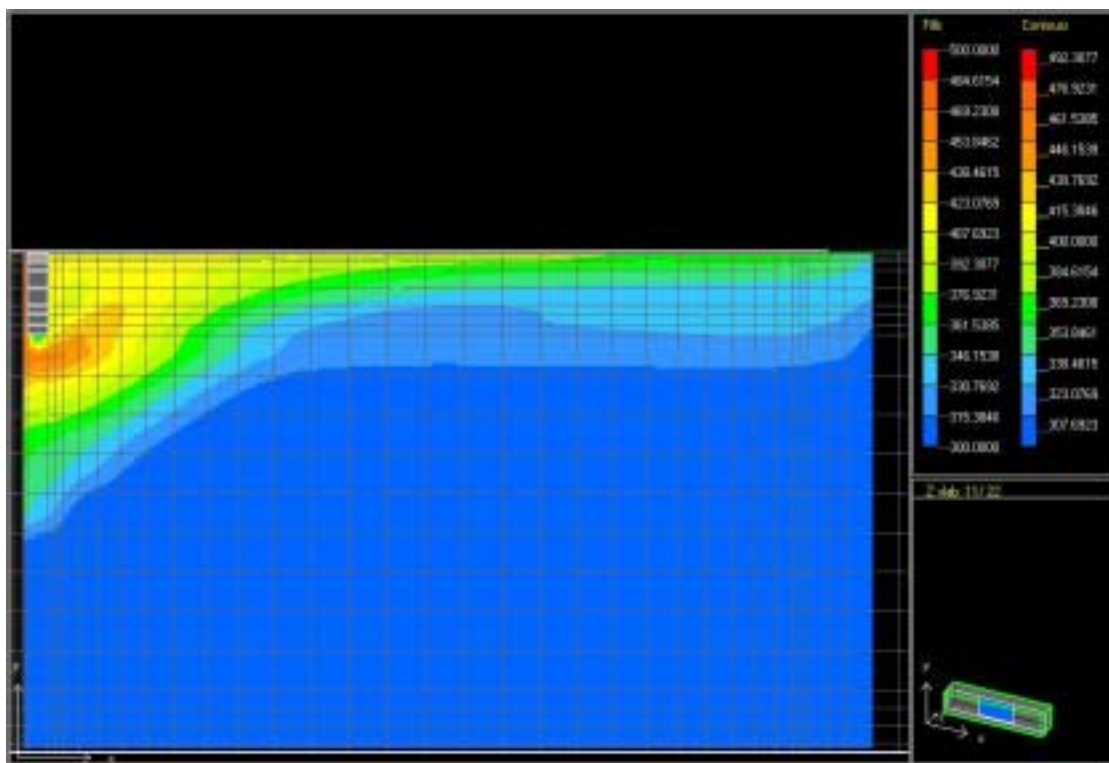


Figure 8.24 Visual Contour Profile for the Adjacent Room (110 kW Corner Fire with Six-flux Radiation Sub-model)

8.2 Grid Statistics for the Fire Simulations

Table 8.1 below presents the number of cells in each direction for the fire simulations.

Table 8.1 Grid Statistics for Each Simulation

Fire Size	Number of Cells in Each Direction of Compartment			Total Number of Cells
	<i>Length</i>	<i>Width</i>	<i>Height</i>	
<i>55 kW</i>	67	20	20	26800
<i>110 kW</i>	67	20	20	26800
<i>160 kW</i>	67	20	20	26800
<i>110 kW c</i>	67	20	20	26800

8.3 Computer Simulation Times

Table 8.2 below presents the time taken to simulate the four fires on a Pentium III 450 MHz computer with 128 MB RAM.

Table 8.2 Computer Simulation Times for the Four Fires

Fire Size	Computer Simulation Time (hours:minutes)	
	<i>Without Six-Flux Radiation Sub-model</i>	<i>With Six-Flux Radiation Sub-model</i>
<i>55 kW</i>	2:40	3:05
<i>110 kW</i>	3:01	3:29
<i>160 kW</i>	2:40	3:07
<i>110 kW c</i>	3:09	3:42

8.4 Discussion

8.4.1 Fire Simulation Visual Profiles

The following comments can be made on the visual temperature profiles for the fires presented in Figures 8.1 – 8.24:

- **With increasing the fire size, the upper layer temperature increases.** This is evident when studying the upper layer temperatures for the 55 kW, 110 kW,

and 160 kW centrally located fires. The temperature of 110 kW corner fire is highest nearer the ceiling, and decreases rapidly with reducing height when compared with the centrally located fires.

- **There is a constant temperature profile in the lower region of both compartments.** This indicates the presence of a lower layer that is associated with pre-flashover fires. Air entering the fire compartment is cooler, therefore is denser than the hot, fire gases. Visualisations show how the cooler air enters the compartment below the hot fire gases, and is entrained into the fire.
- **Temperature increases begin from a lower height in the fire compartment than in the adjacent room.** This illustrates how the soffit in the fire room reduces the interface height between the upper and lower layers, as in the adjacent compartment where there is no soffit, the upper layer is higher up.
- **The temperatures in the upper layer are higher in the fire room than in the adjacent room.**
- **Simulations modelled without the six-flux radiation sub-model produce higher temperature profiles in the upper layer than when the six-flux radiation sub-model is incorporated into the simulations.** Usually, 30 – 40% of the total energy released by a buoyancy driven fire is released as radiation (Heskestad, 1995). For the simulations without the inclusion of a radiation model, the fire's convective energy is probably higher, producing higher upper layer temperatures. This is evident for both the fire room and adjacent room.
- **The corner temperatures near the soffit in the adjacent room are higher for the simulations without the six-flux radiation sub-model than the simulations with the six-flux sub-model.** This trend is directly a result of higher temperatures in the upper layer for the simulations without the six-flux radiation sub-model.
- **The inclination of the fire plume is only evident for the simulations of the centrally located fires when modelled without incorporating the six-flux radiation sub-model for the 55 kW and 110 kW fires.** As air enters the fire room, the fire's combustible gases are blown away from the burner towards the back wall (this effect has been noted previously in experiments by Quintiere et al., 1981). The absence of an inclined fire plume for the

simulations with the inclusion of the six-flux radiation sub-model is unexpected. Note: Neither simulation for the 160 kW fire predicts an inclined fire plume. This is probably because SMARTFIRE requires the user to specify the flame height, therefore assigning the fire as a number of vertically aligned cells. Because the flame enters the upper layer of the 160 kW fire, so does the plume. Therefore the plume is not blown over by air entering the compartment as the cooler denser air enters below the hot upper layer.

- **Temperature profiles in the upper layer are non-uniform.** This indicates that the upper layer is not well mixed; therefore, a constant temperature profile does not occur in the upper layer for these simulations.
- **Temperature profiles in the fire room for the simulations without the inclusion of the six-flux radiation sub-model appear less horizontal than for the simulations with the six-flux radiation sub-model.** Such considerable differences between the simulations are surprising.
- **For the 110 kW corner fire, temperature increases start at a lower height for the simulation with the six-flux radiation sub-model than the simulation without the six-flux radiation sub-model.** However, the simulation without the six-flux radiation sub-model produces a higher temperature nearer the ceiling. The simulation without the six-flux radiation sub-model also produces a higher temperature in the adjacent room.

8.4.2 Grid Statistics for the Fire Simulations

The KBS system assigned each simulation with identical cell numbers in all directions. However, on further inspection, cell resolution differed between the central fires and the corner fire (a detailed analysis to see if the KBS system has applied an appropriate cell resolution has not been undertaken for these simulations).

8.4.3 Computer Simulation Time

Computer simulation times show that simulation time increased correspondingly with increasing fire size. This shows that steady state was reached earlier for the smaller fire size; therefore, iteration convergence time is less. The simulations of the 110 kW corner fire required the longest time, as it was not located along a plane of symmetry

the way the centrally located fires were. The 160 kW fire's shorter simulation time than the 110 kW fire was unexpected.

Generally, the simulations which included the six-flux radiation sub-model required an additional 30 minutes. The additional time required to simulate with the six-flux radiation sub-model was expected, as when the six-flux radiation sub-model is included in the simulation, the number of variables for each cell to be calculated by the CFD engine increases by six (as the model calculates the radiative flux in the six orthogonal directions from each cell and links these six extra solved variables to the thermal energy computations).

9 Comparisons

The purpose of this chapter is to compare temperature profiles obtained from the SMARTFIRE field modelling program with the experimental temperature profiles.

9.1 Aim

The aim of this chapter is the following:

1. Present the method for comparing experimental results with the simulations.
2. Present the results of the comparisons.
3. Discuss the results of the comparisons.

9.2 Method

Temperature profiles obtained from the experiments conducted at McLeans Island during the period 26 November and 1 December for the 55 kW, 110 kW, 160 kW, and 110 kW corner fires are plotted on scatter graphs together with temperature profiles from the SMARTFIRE simulations. This is presented as one scatter graph for each tree per fire. Each graph presents the experimental temperature profile (denoted as Exp on the graph legend), the SMARTFIRE simulation without the six-flux radiation sub-model incorporated into the simulation (denoted as SF on the graph legend), and the SMARTFIRE simulation with the six-flux radiation sub-model incorporated into the simulation (denoted as SFR on the graph legend).

9.3 Results

Results for the comparisons between the experiments and the SMARTFIRE simulations are presented below. Results are presented for the 55 kW, 110 kW, 160 kW, and 110 kW corner fires respectively, with field trees presented in numerical order.

9.3.1 55 kW Fire Comparisons

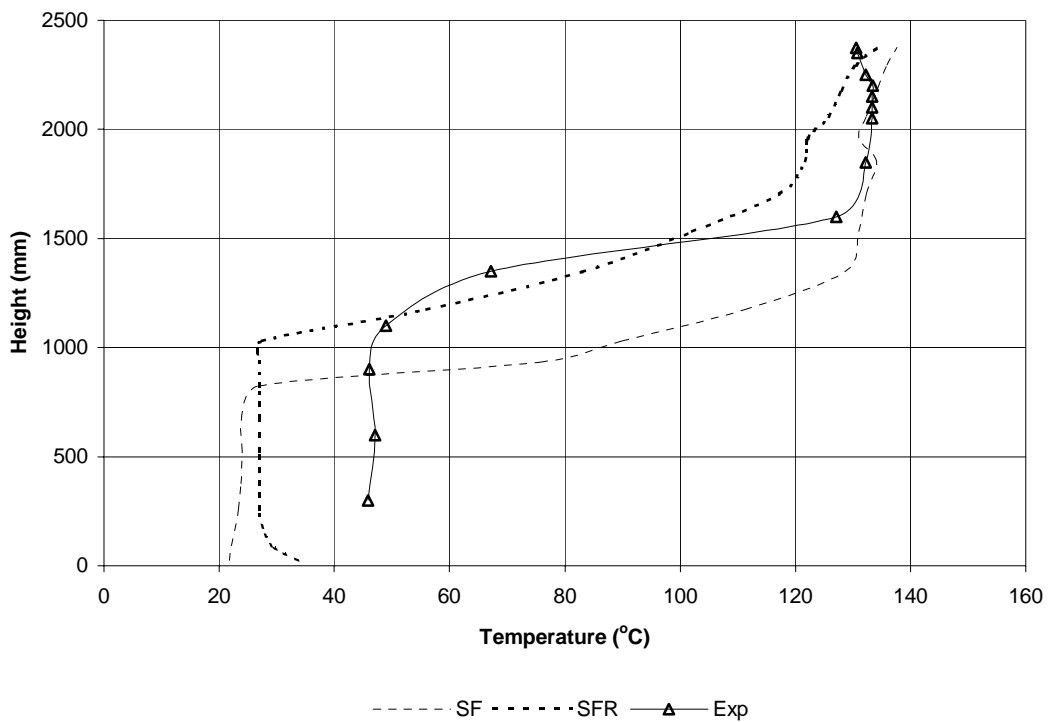


Figure 9.1 Comparisons for Tree 1 (55 kW Fire)

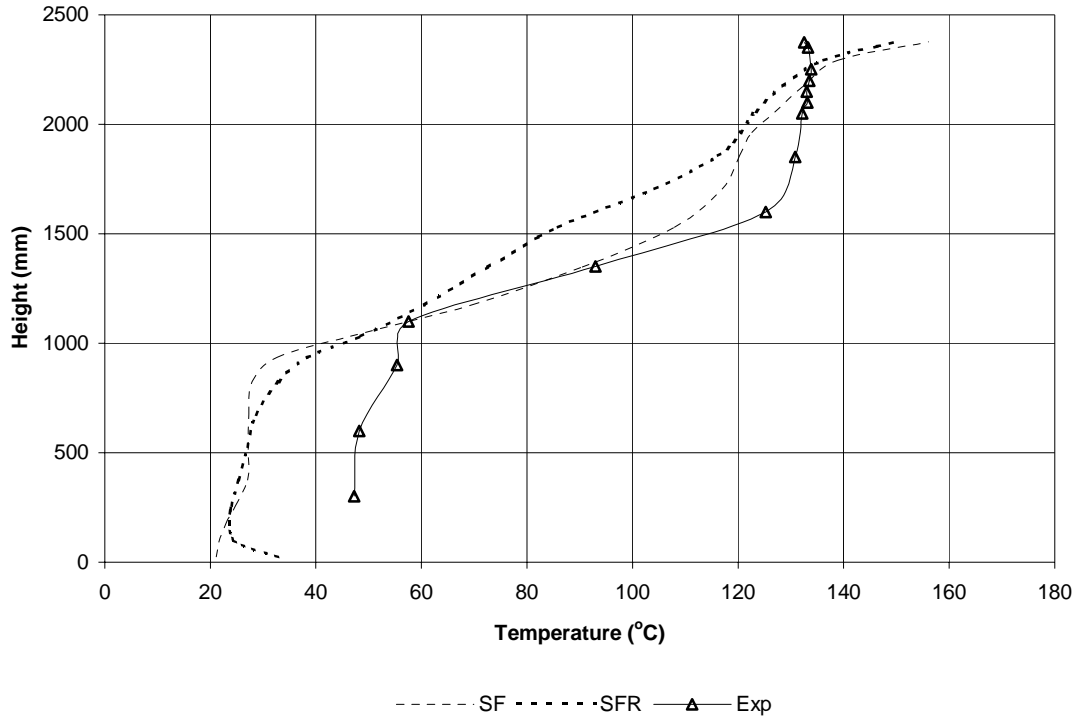


Figure 9.2 Comparisons for Tree 2 (55 kW Fire)

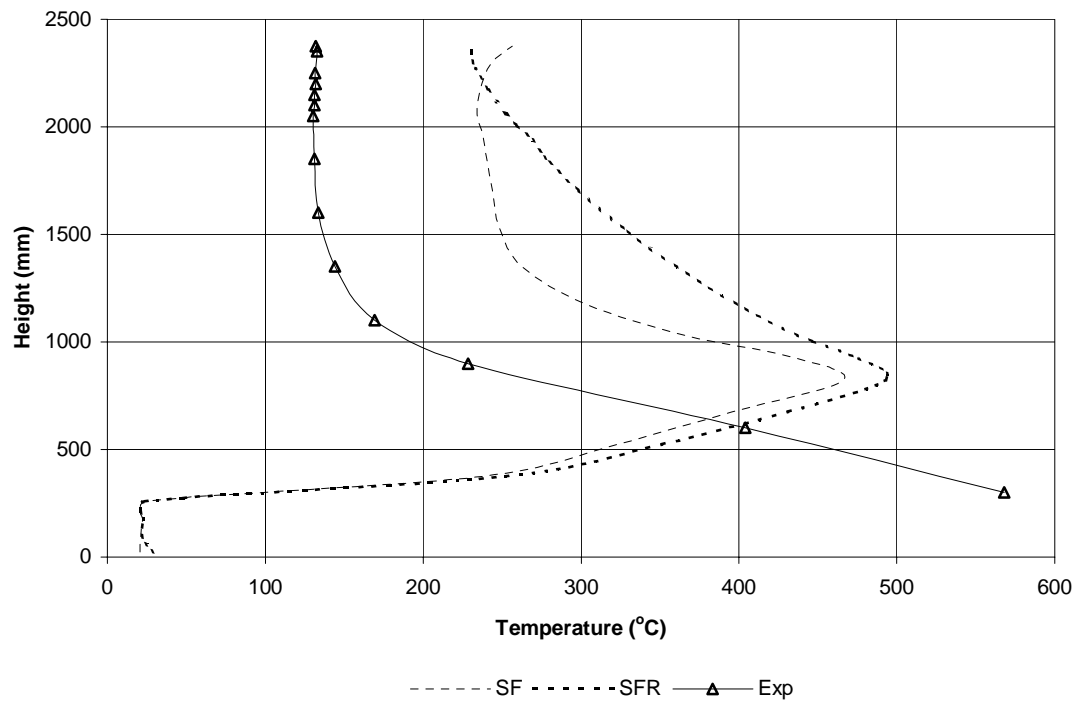


Figure 9.3 Comparisons for Tree 3 (55 kW Fire)

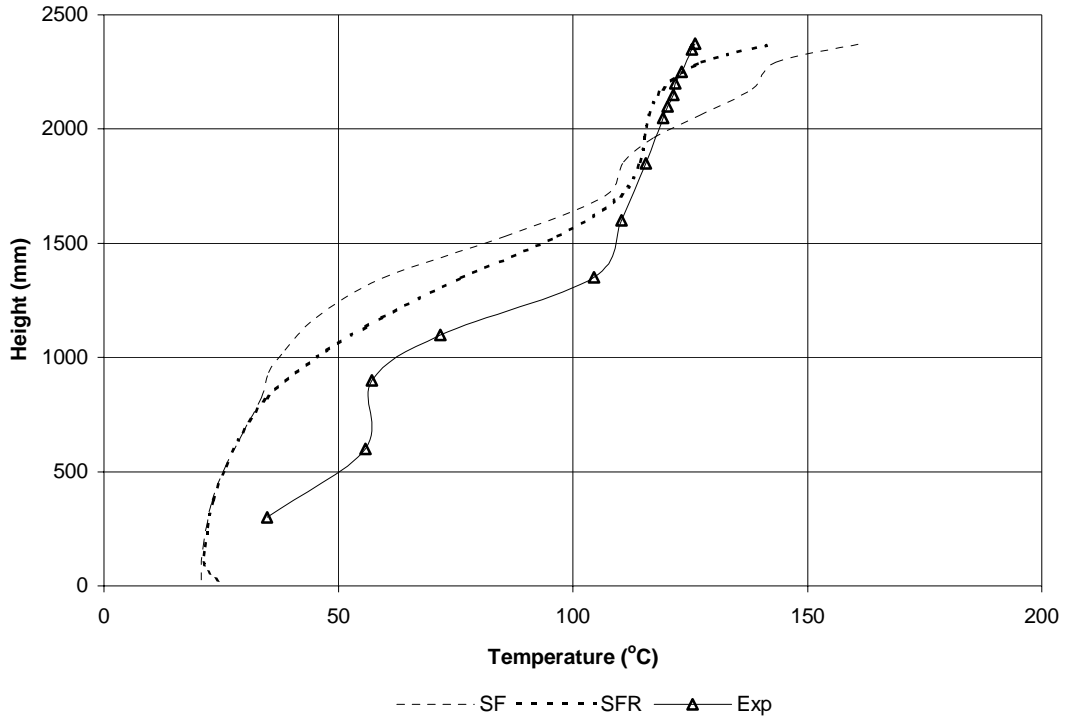


Figure 9.4 Comparisons for Tree 4 (55 kW Fire)

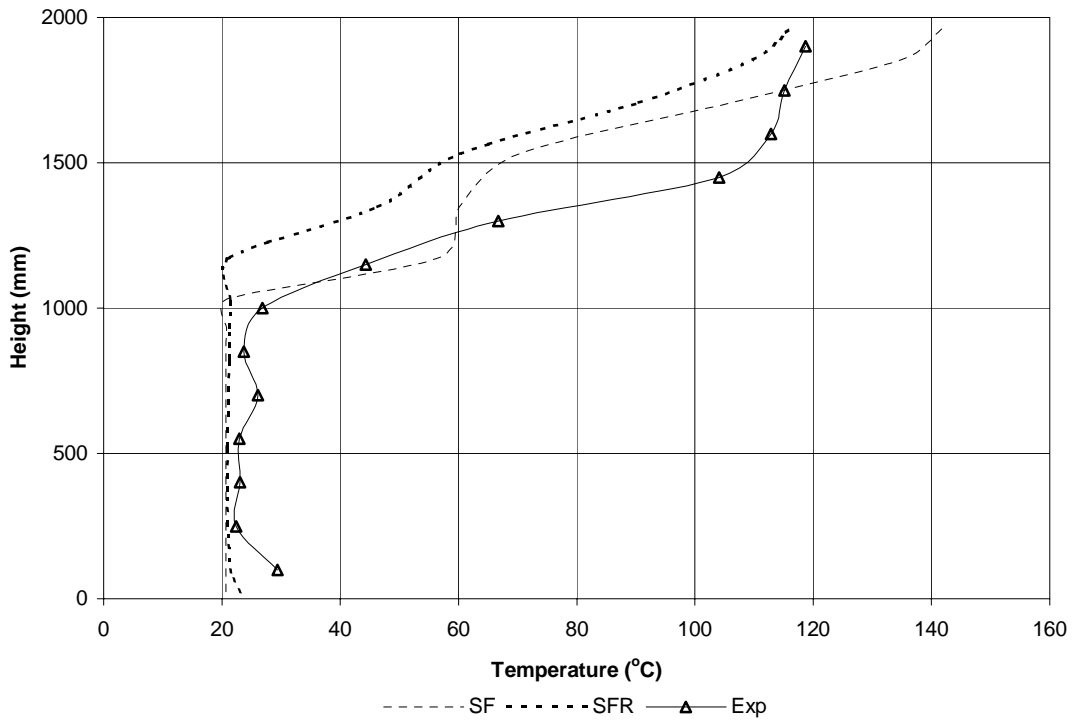


Figure 9.5 Comparisons for Tree 5 (Doorway, 55 kW Fire)

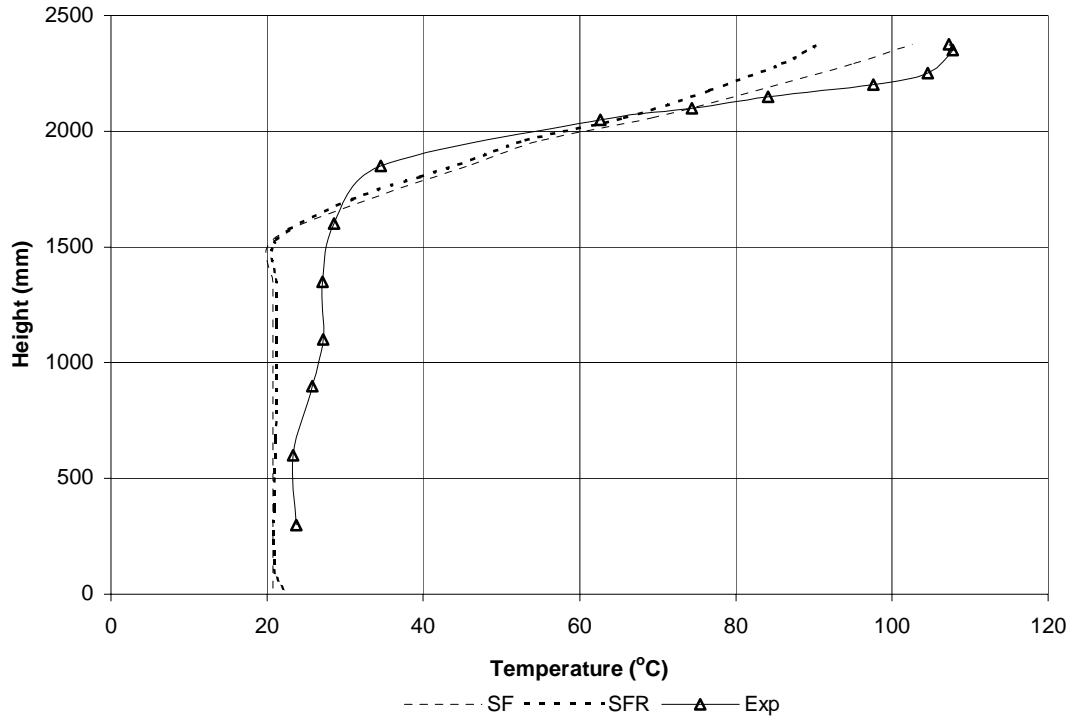


Figure 9.6 Comparisons for Tree 6 (55 kW Fire)

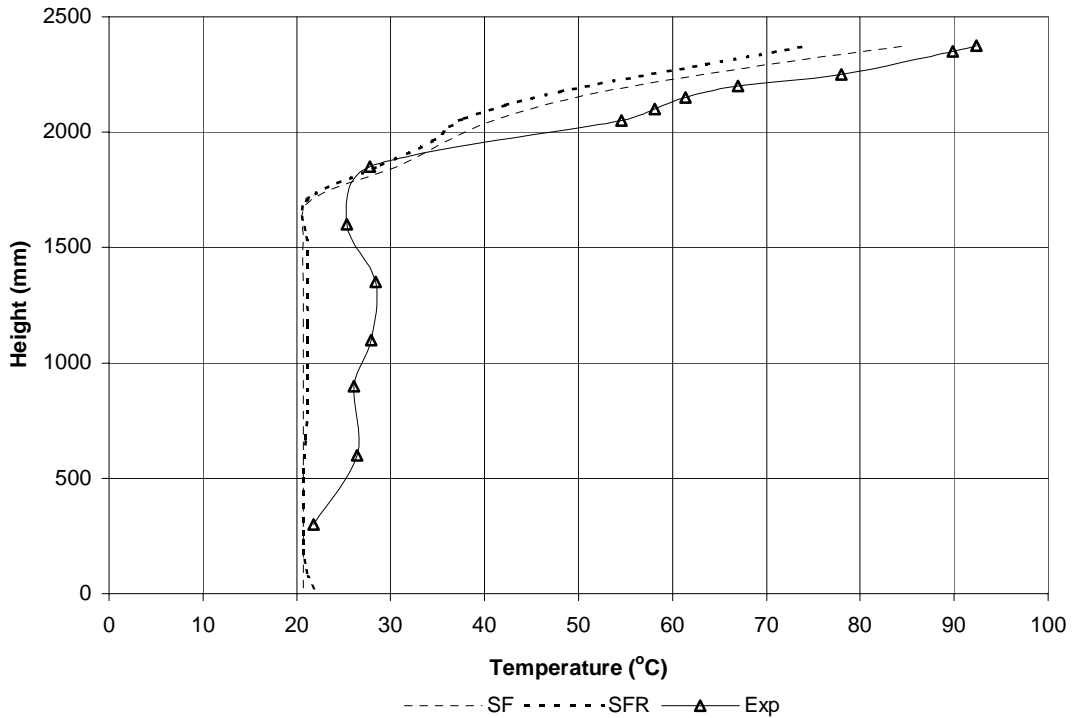


Figure 9.7 Comparisons for Tree 7 (55 kW Fire)

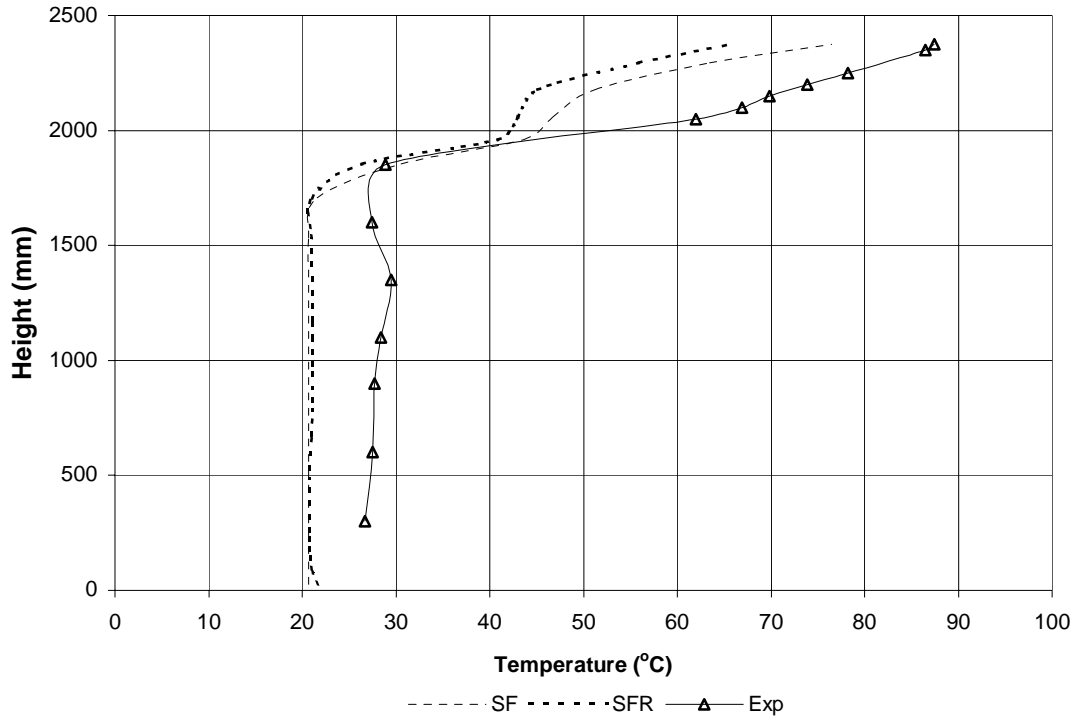


Figure 9.8 Comparisons for Tree 8 (55 kW Fire)

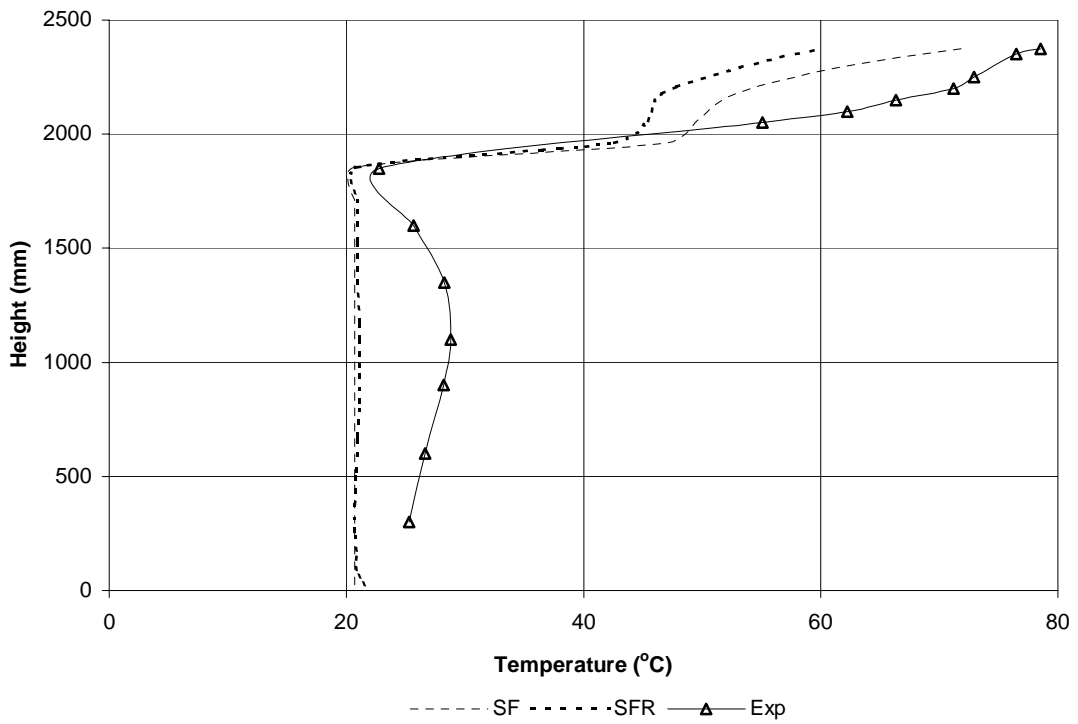


Figure 9.9 Comparisons for Tree 9 (55 kW Fire)

9.3.2 110 kW Fire Comparisons

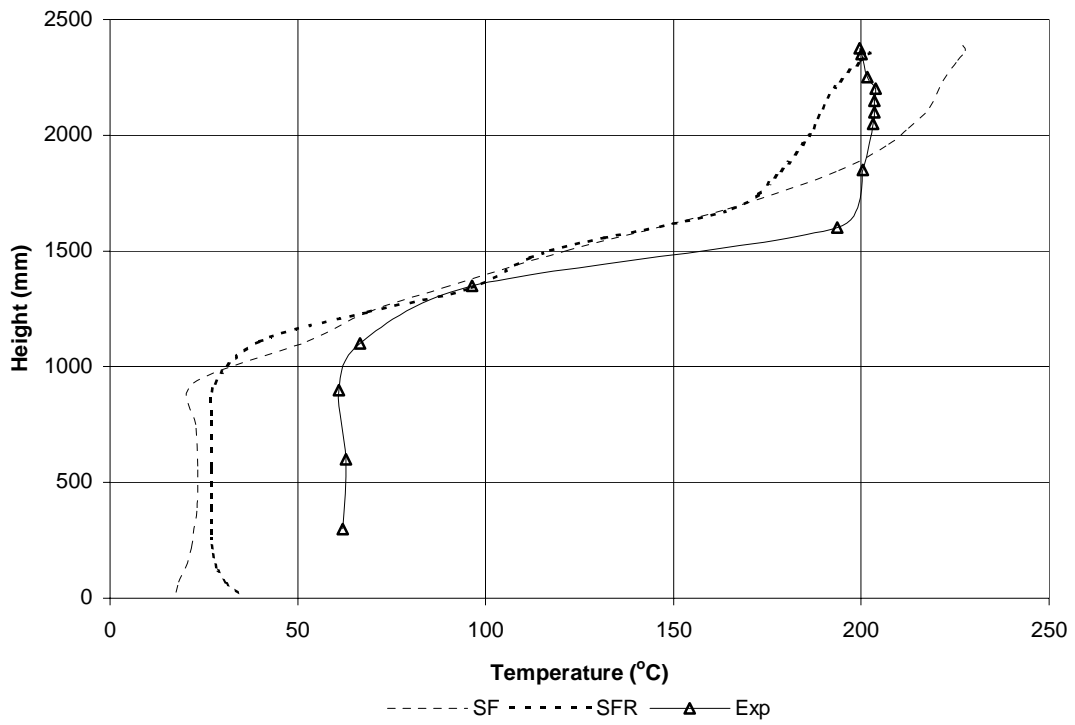


Figure 9.10 Comparisons for Tree 1 (110 kW Fire)

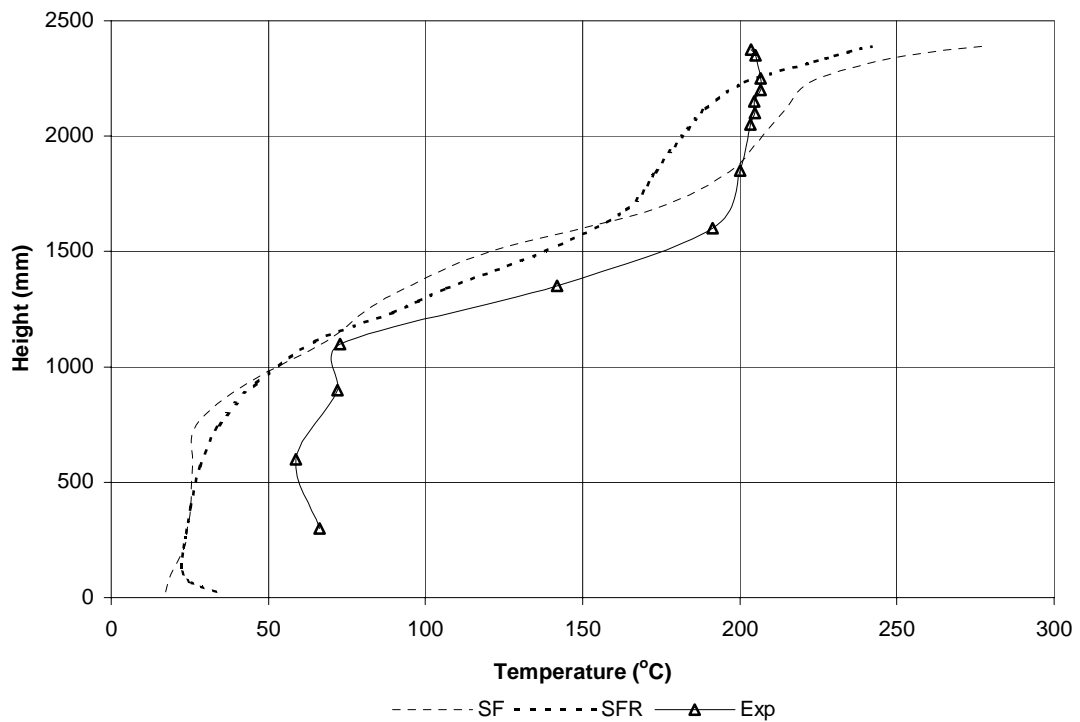


Figure 9.11 Comparisons for Tree 2 (110 kW Fire)

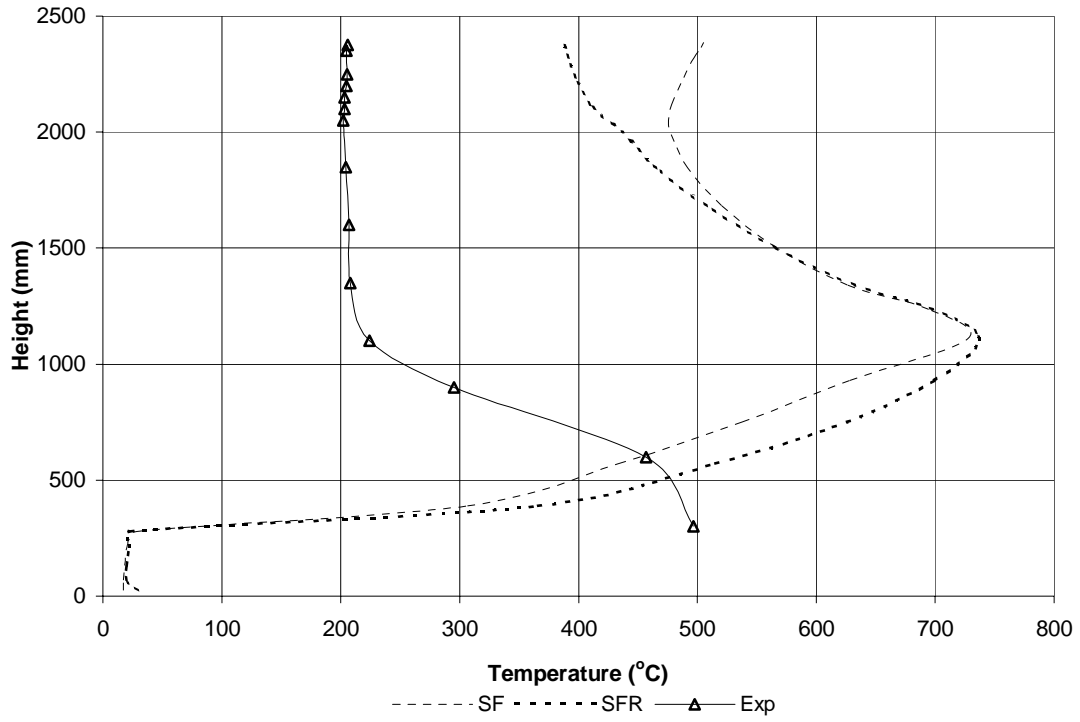


Figure 9.12 Comparisons for Tree 3 (110 kW Fire)

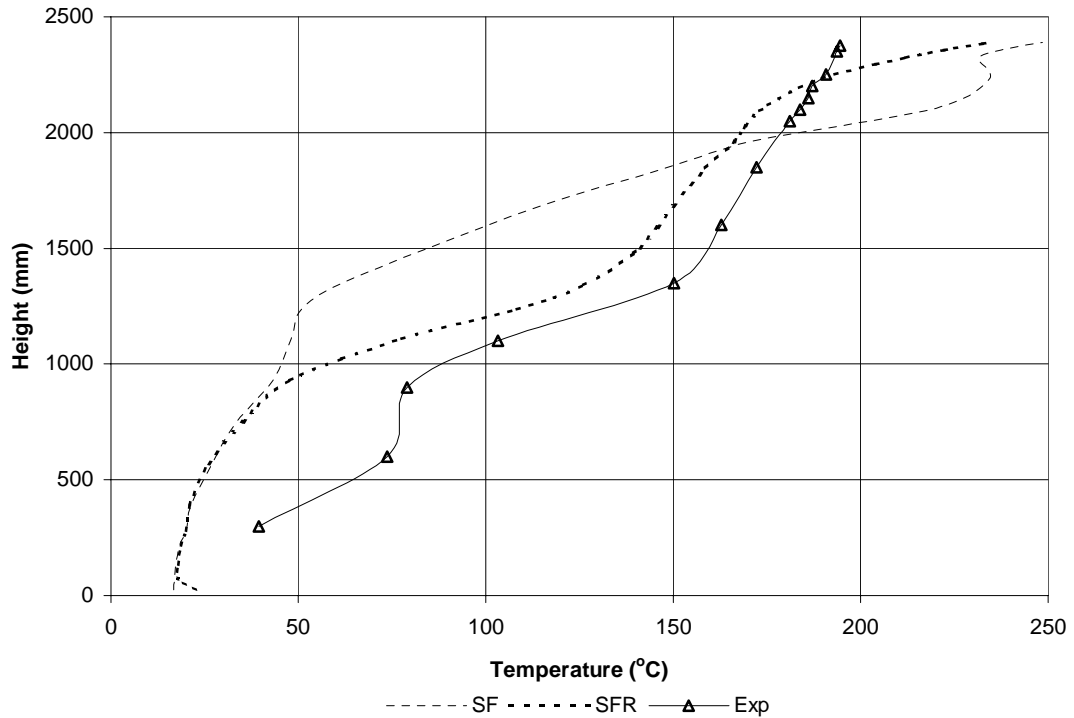


Figure 9.13 Comparisons for Tree 4 (110 kW Fire)

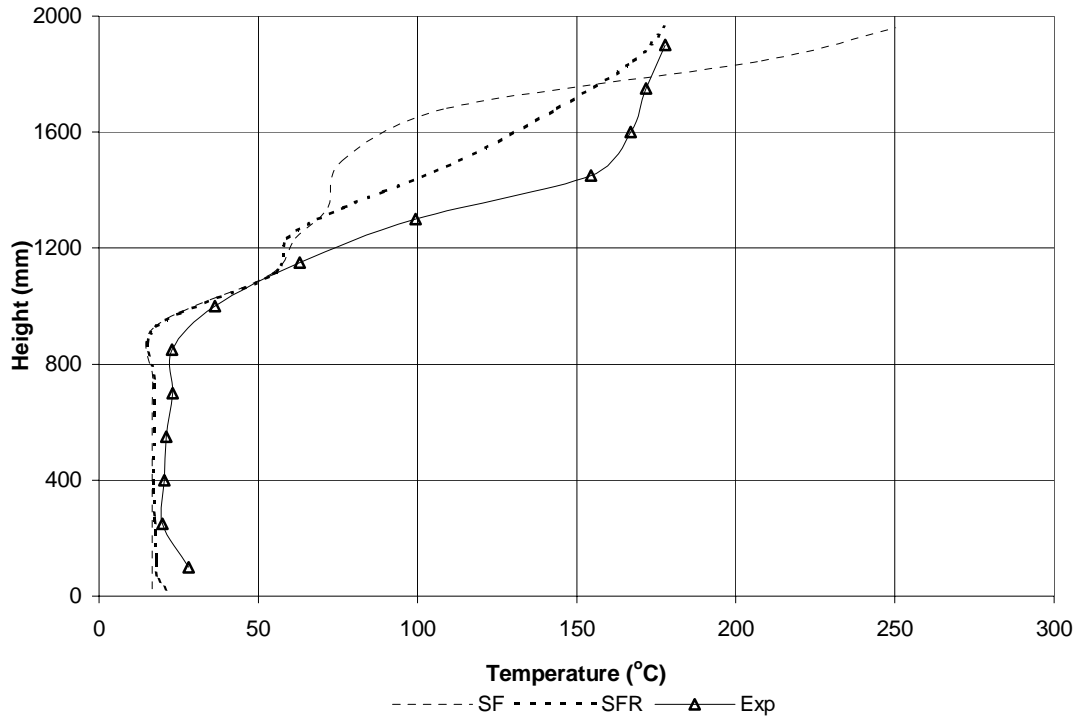


Figure 9.14 Comparisons for Tree 5 (Doorway, 110 kW Fire)

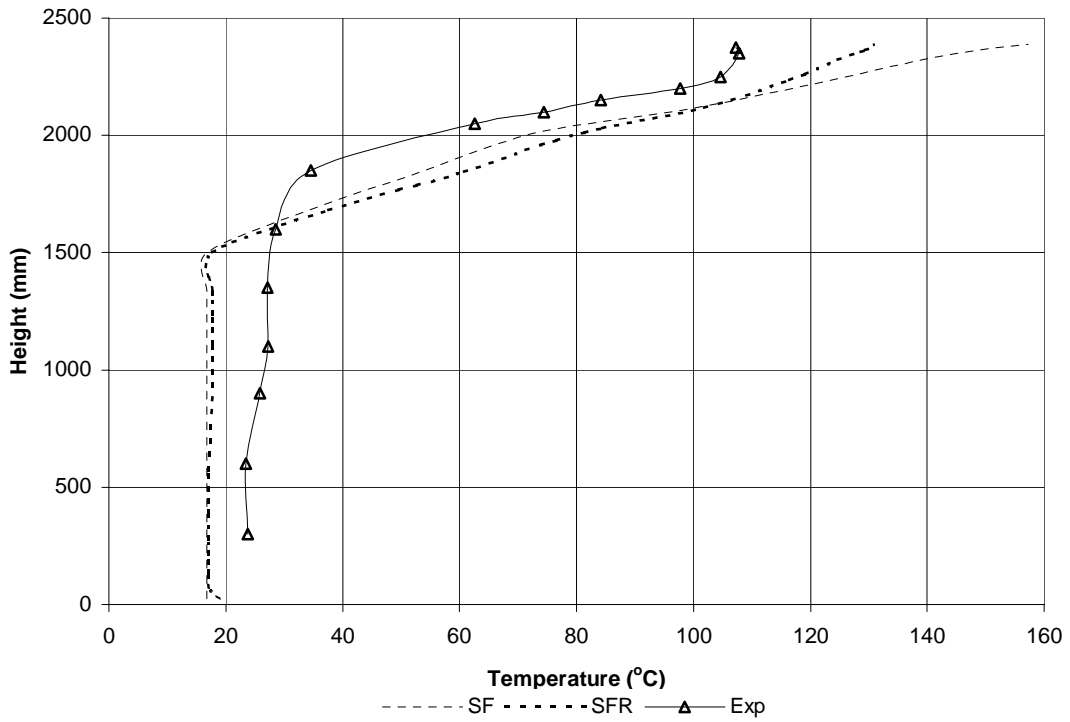


Figure 9.15 Comparisons for Tree 6 (110 kW Fire)

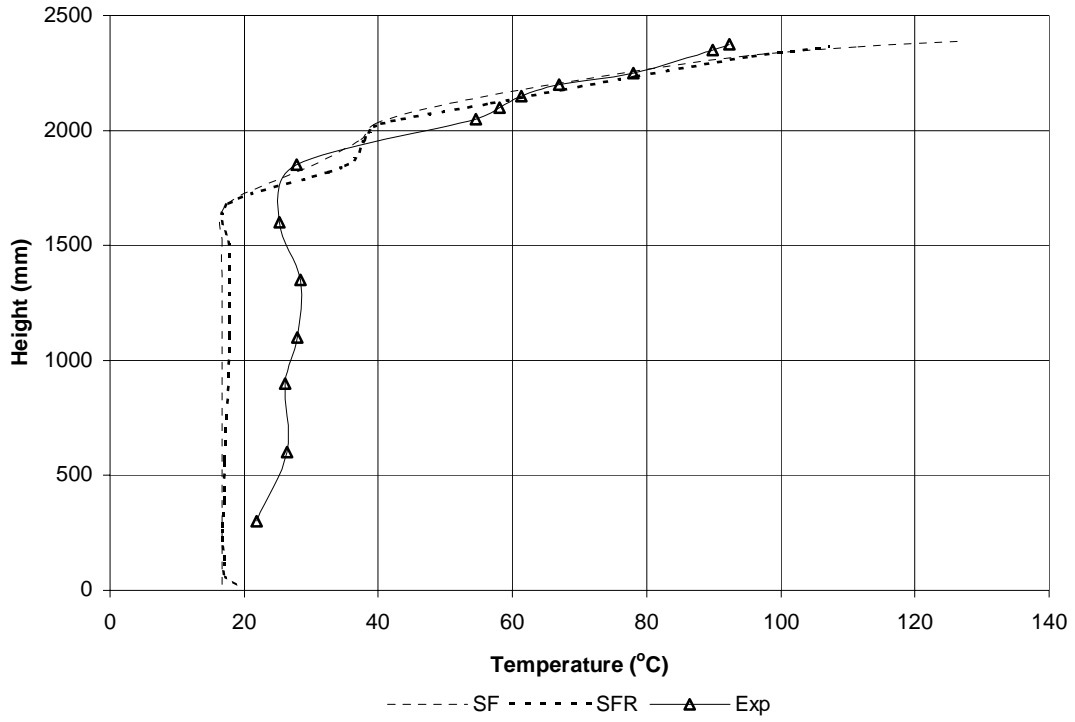


Figure 9.16 Comparisons for Tree 7 (110 kW Fire)

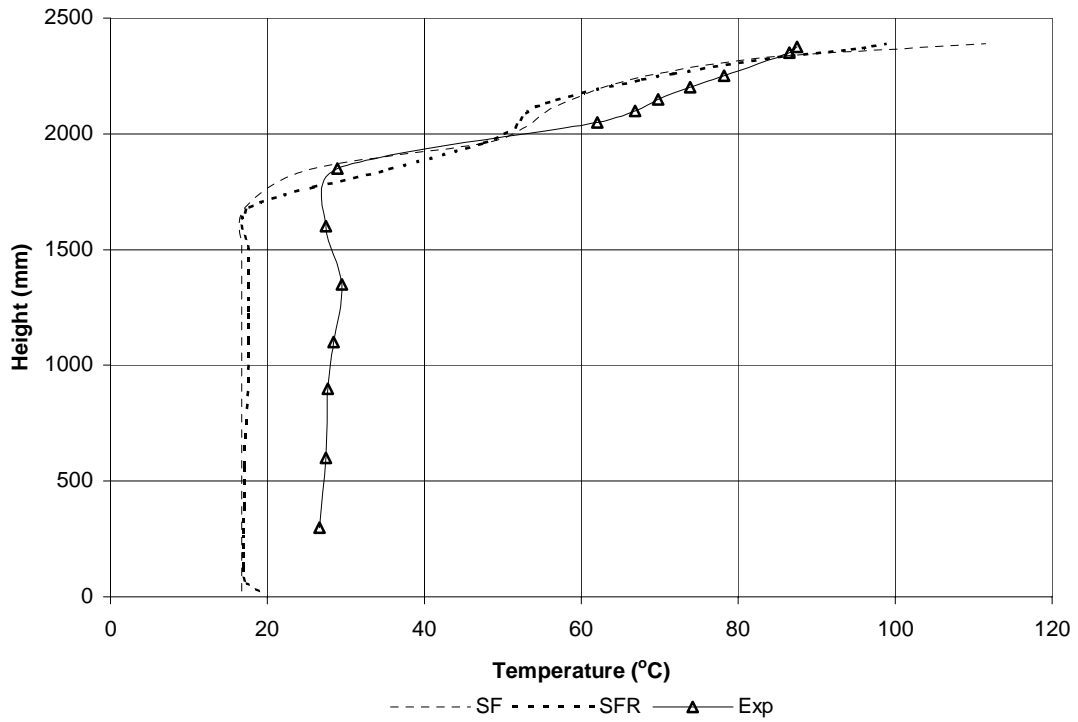


Figure 9.17 Comparisons for Tree 8 (110 kW Fire)

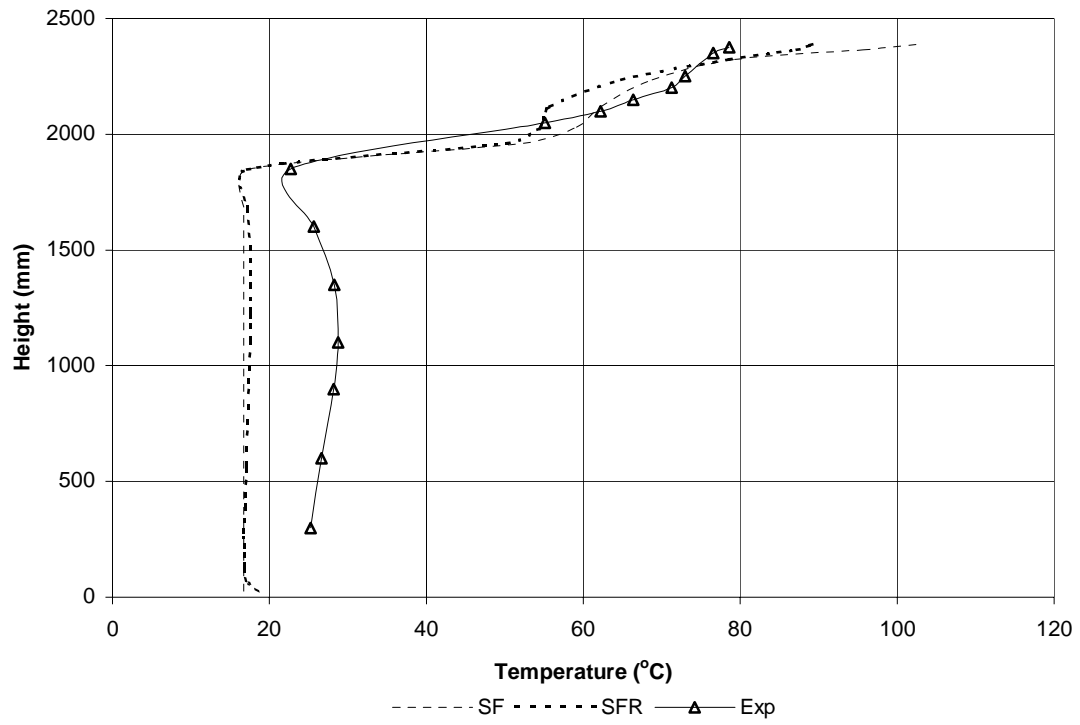


Figure 9.18 Comparisons for Tree 9 (110 kW Fire)

9.3.3 160 kW Fire Comparisons

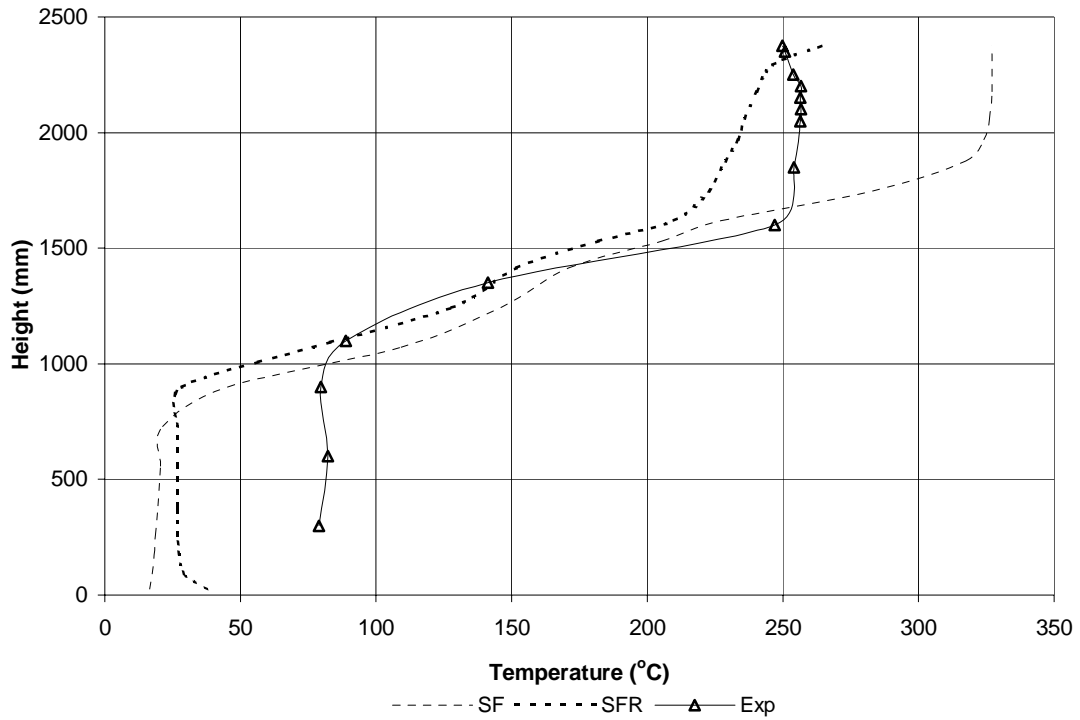


Figure 9.19 Comparisons for Tree 1 (160 kW Fire)

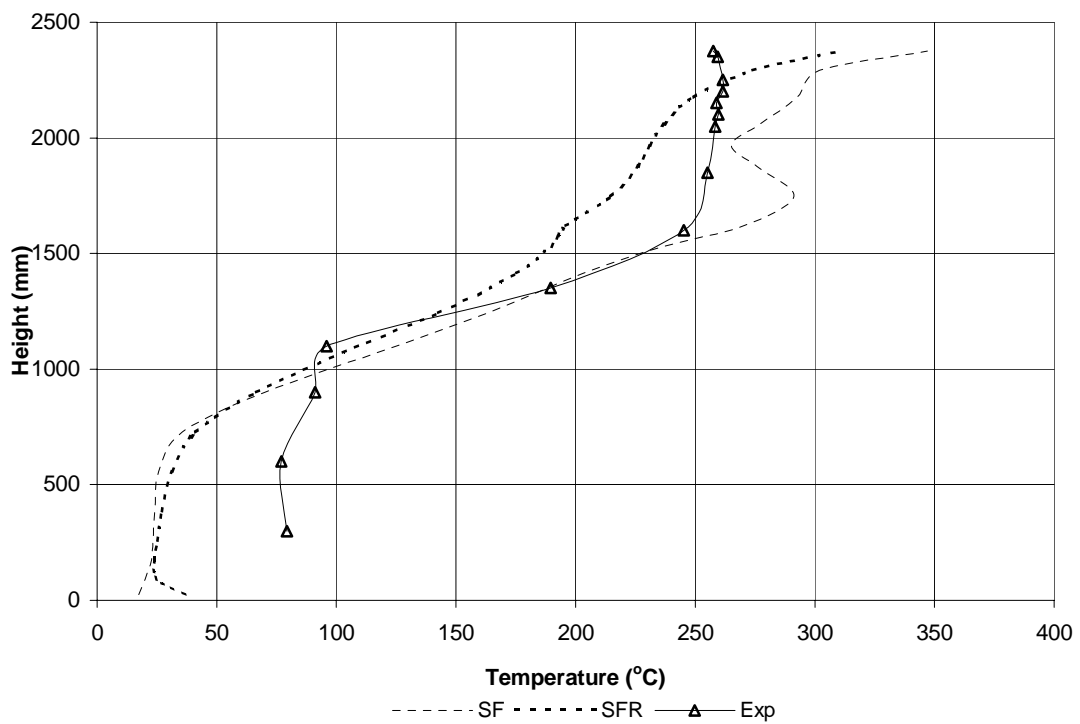


Figure 9.20 Comparisons for Tree 2 (160 kW Fire)

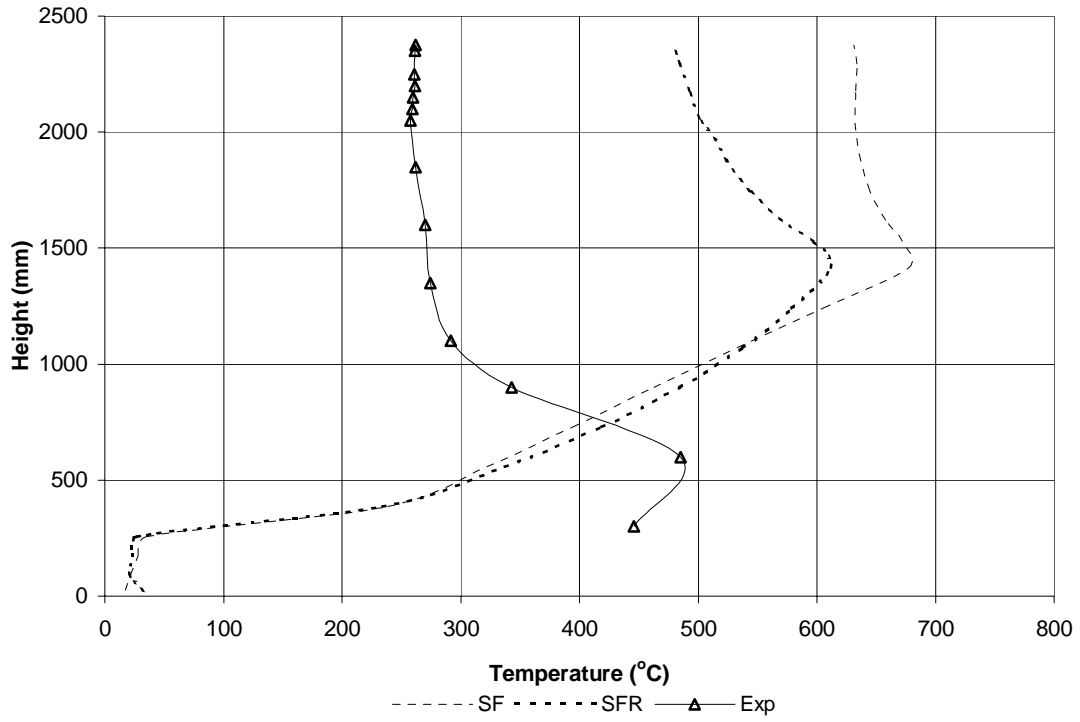


Figure 9.21 Comparisons for Tree 3 (160 kW Fire)

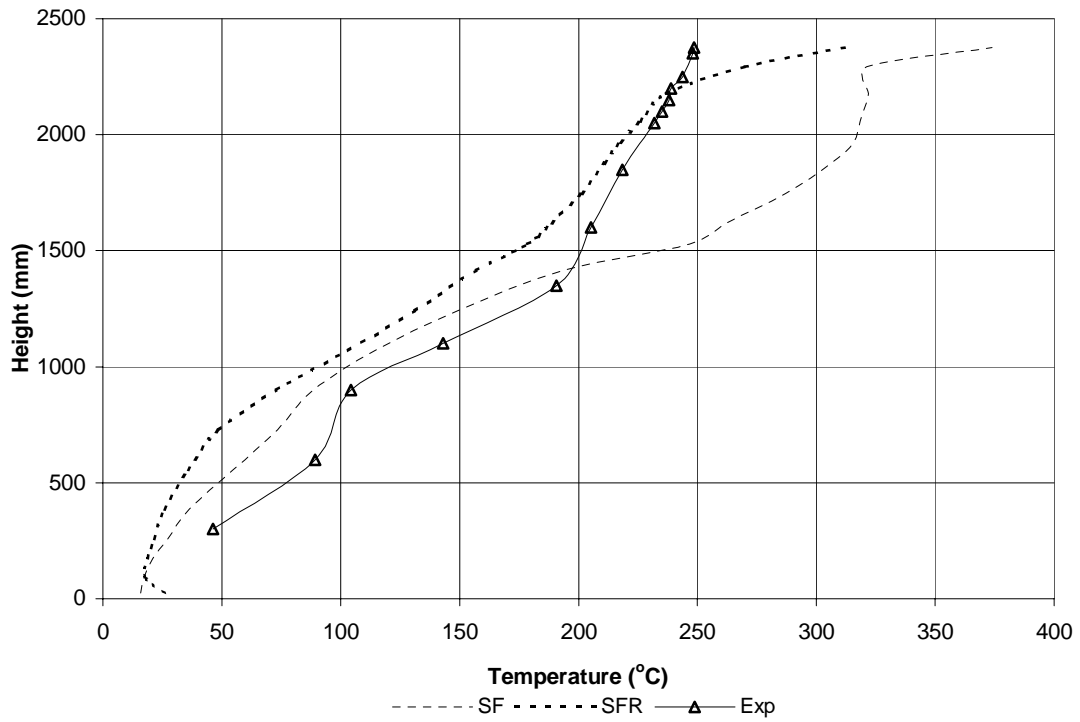


Figure 9.22 Comparisons for Tree 4 (160 kW Fire)

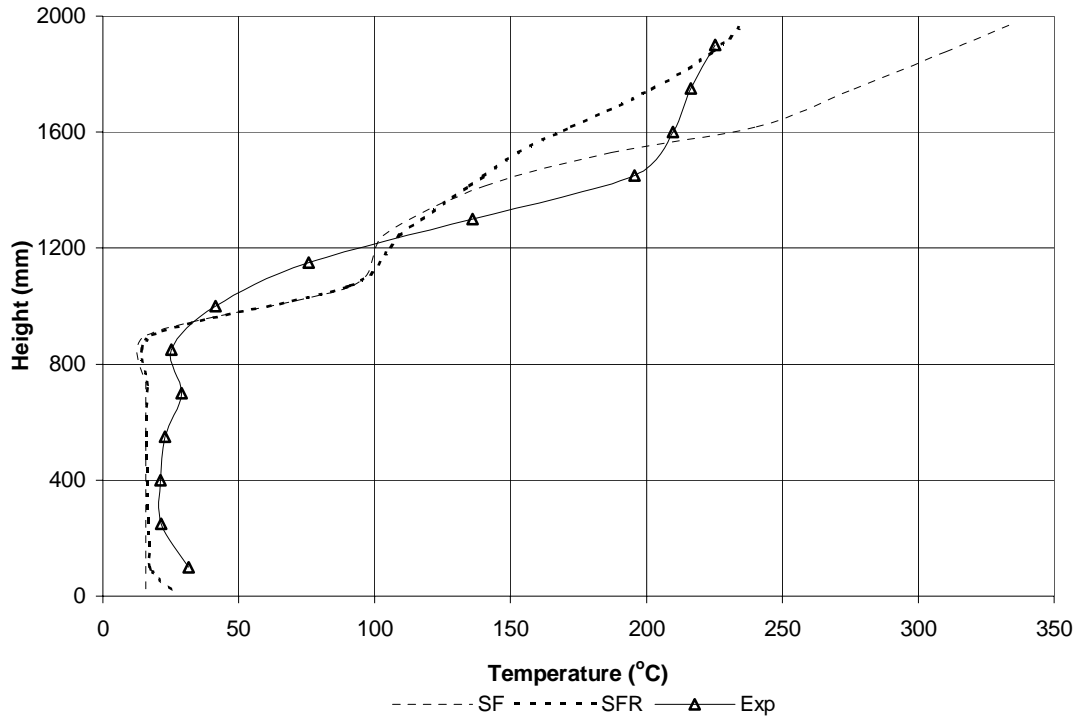


Figure 9.23 Comparisons for Tree 5 (Doorway, 160 kW Fire)

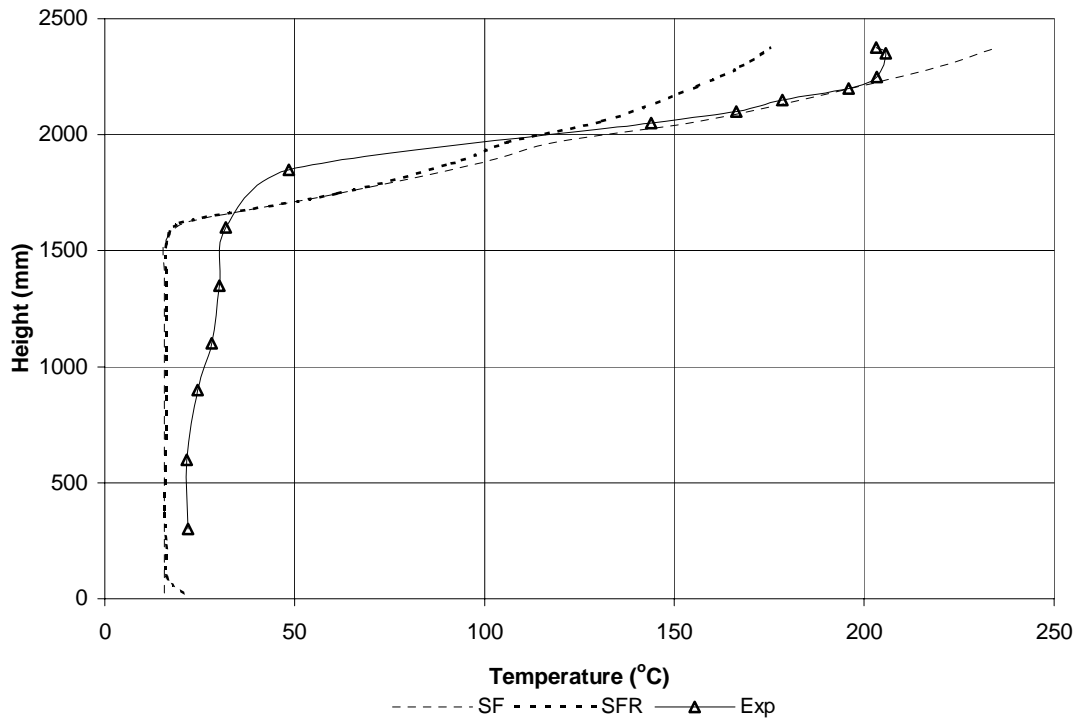


Figure 9.24 Comparisons for Tree 6 (160 kW Fire)

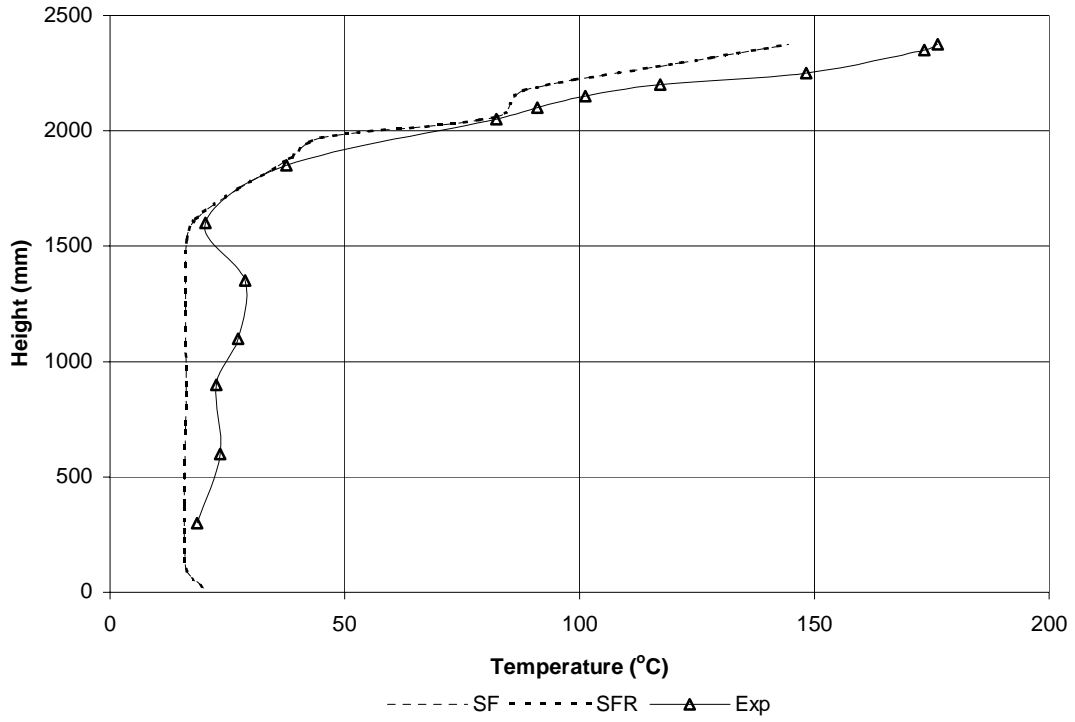


Figure 9.25 Comparisons for Tree 7 (160 kW Fire)

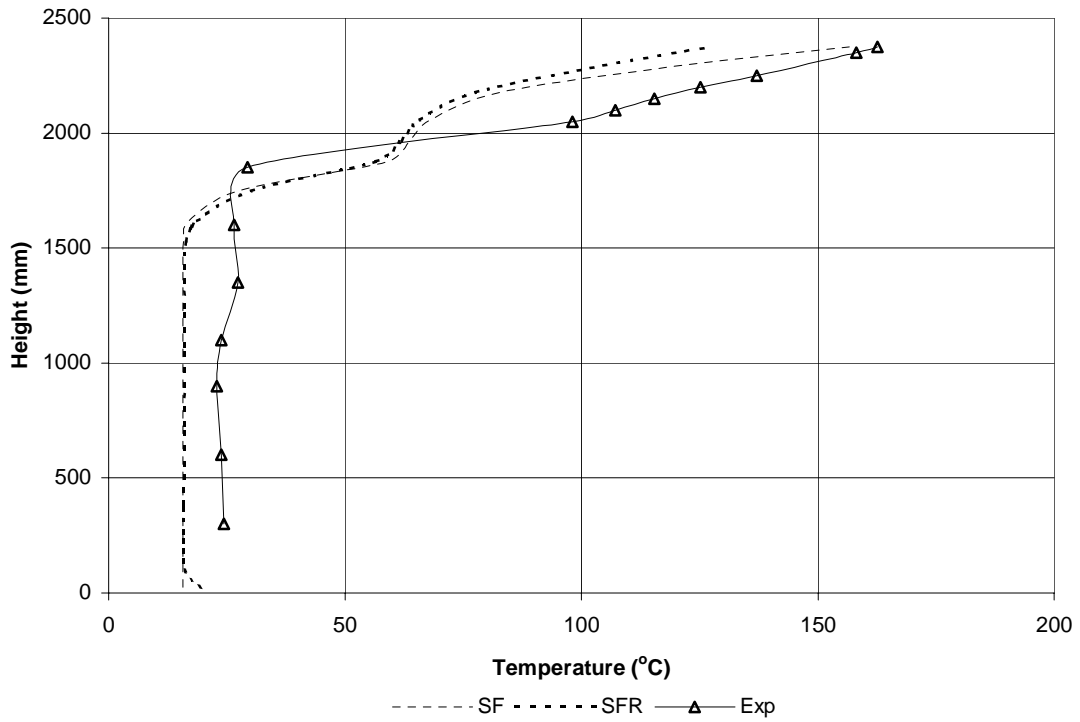


Figure 9.26 Comparisons for Tree 8 (160 kW Fire)

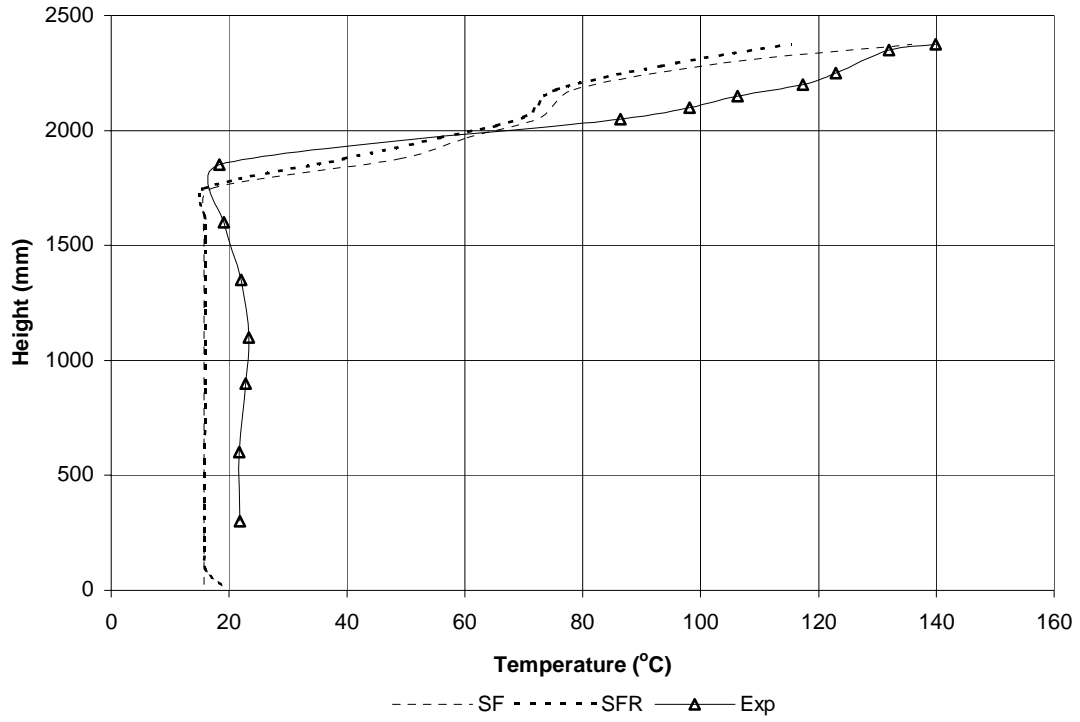


Figure 9.27 Comparisons for Tree 9 (160 kW Fire)

9.3.4 110 kW Corner Fire Comparisons

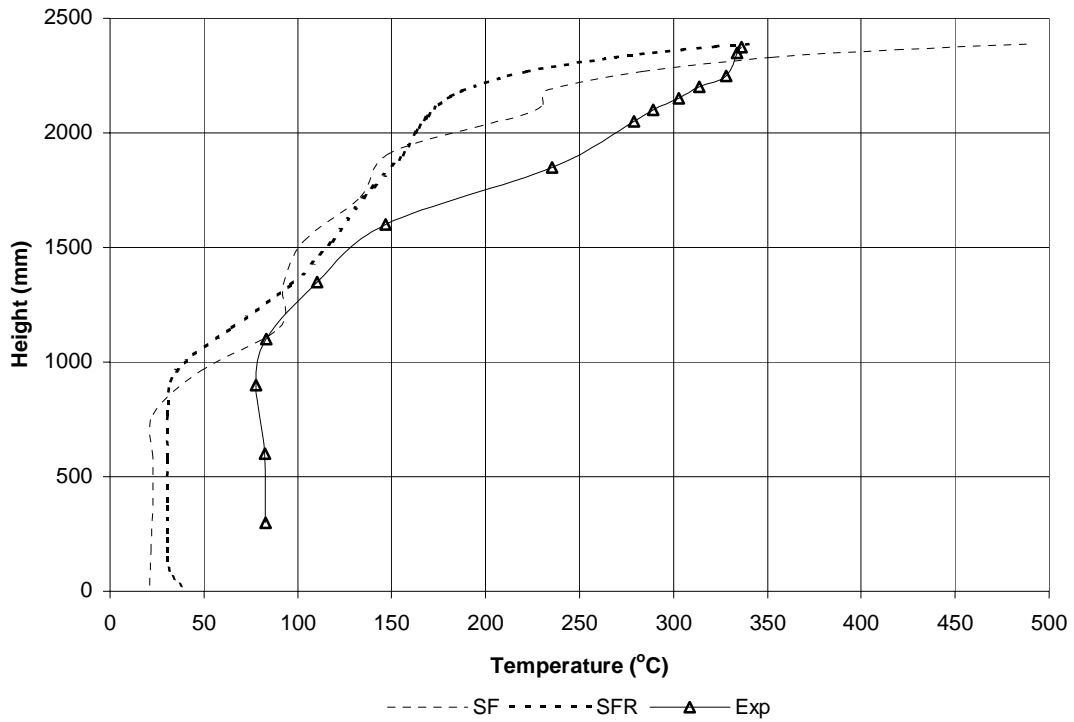


Figure 9.28 Comparisons for Tree 1 (110 kW Corner Fire)

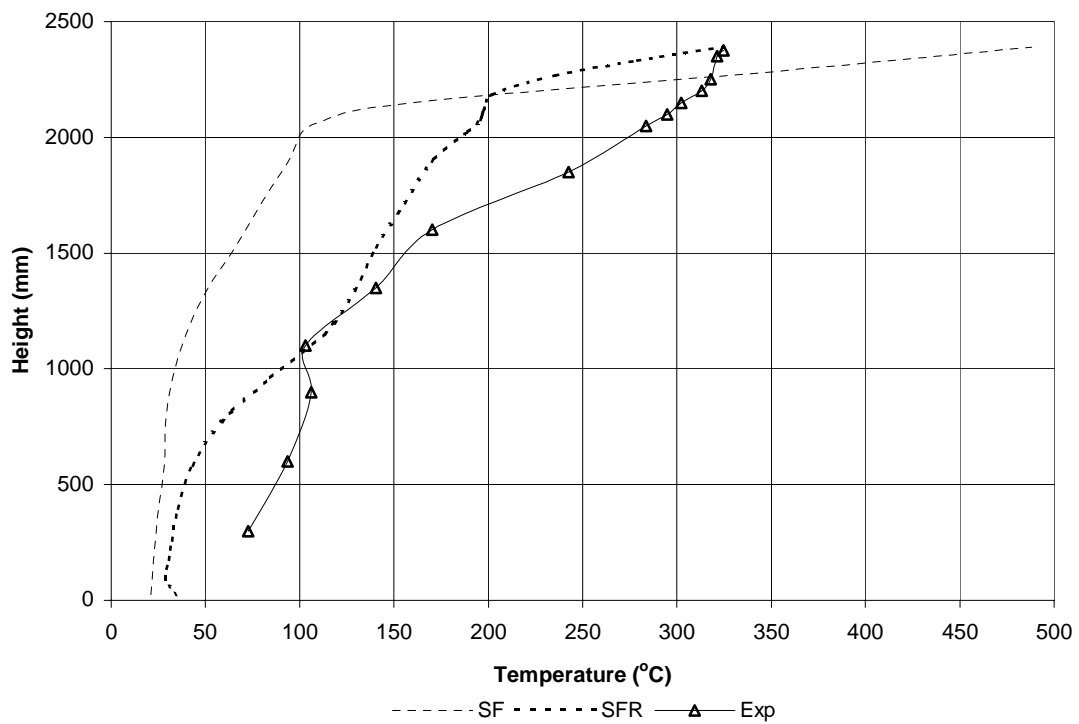


Figure 9.29 Comparisons for Tree 2 (110 kW Corner Fire)

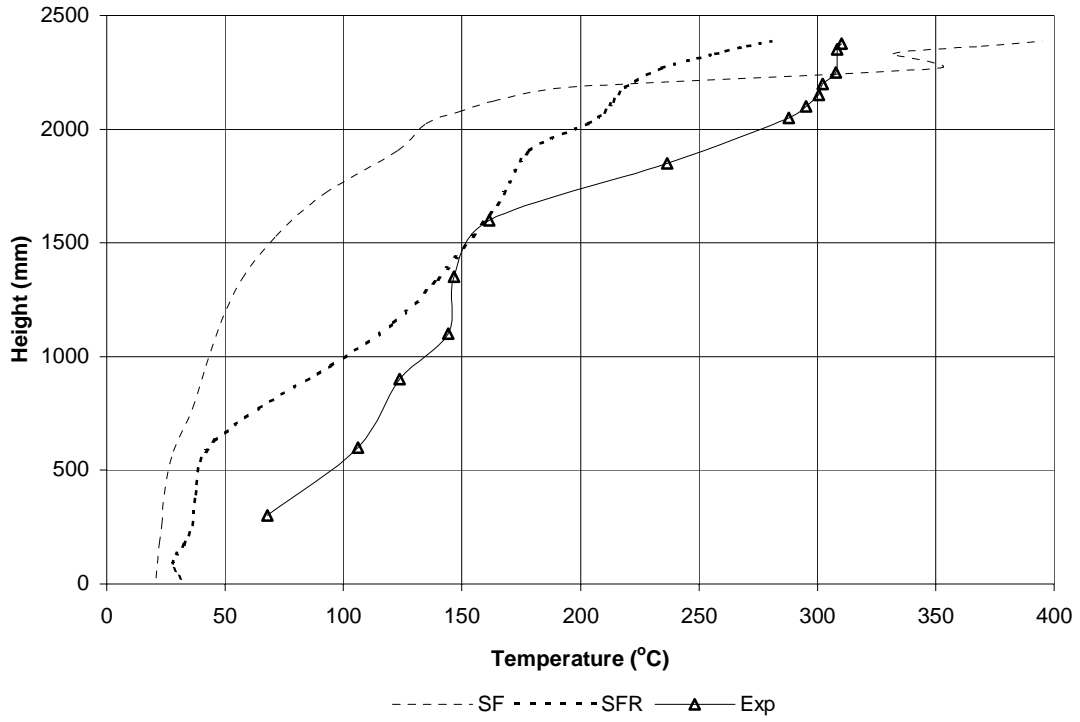


Figure 9.30 Comparisons for Tree 3 (110 kW Corner Fire)

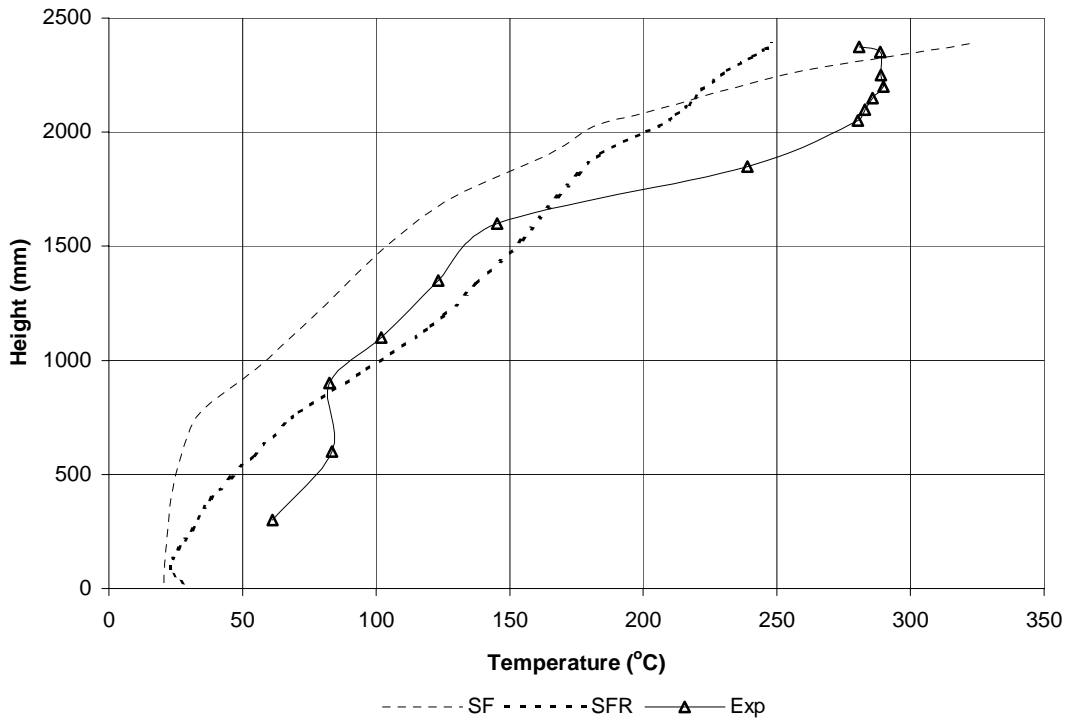


Figure 9.31 Comparisons for Tree 4 (110 kW Corner Fire)

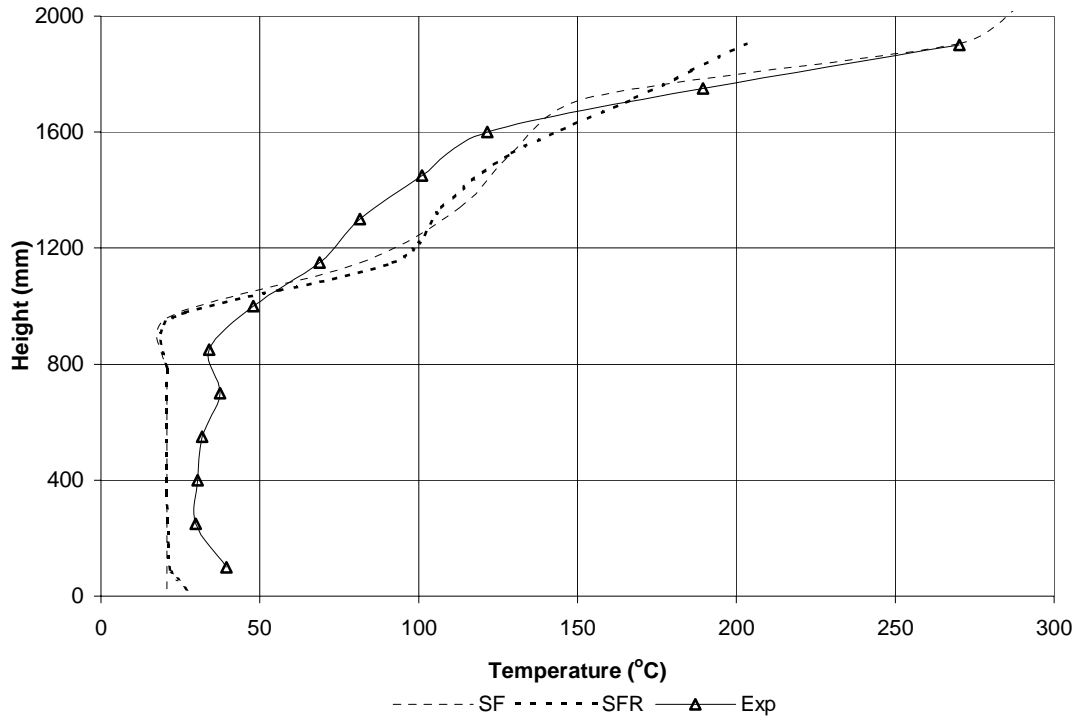


Figure 9.32 Comparisons for Tree 5 (Doorway, 110 kW Corner Fire)

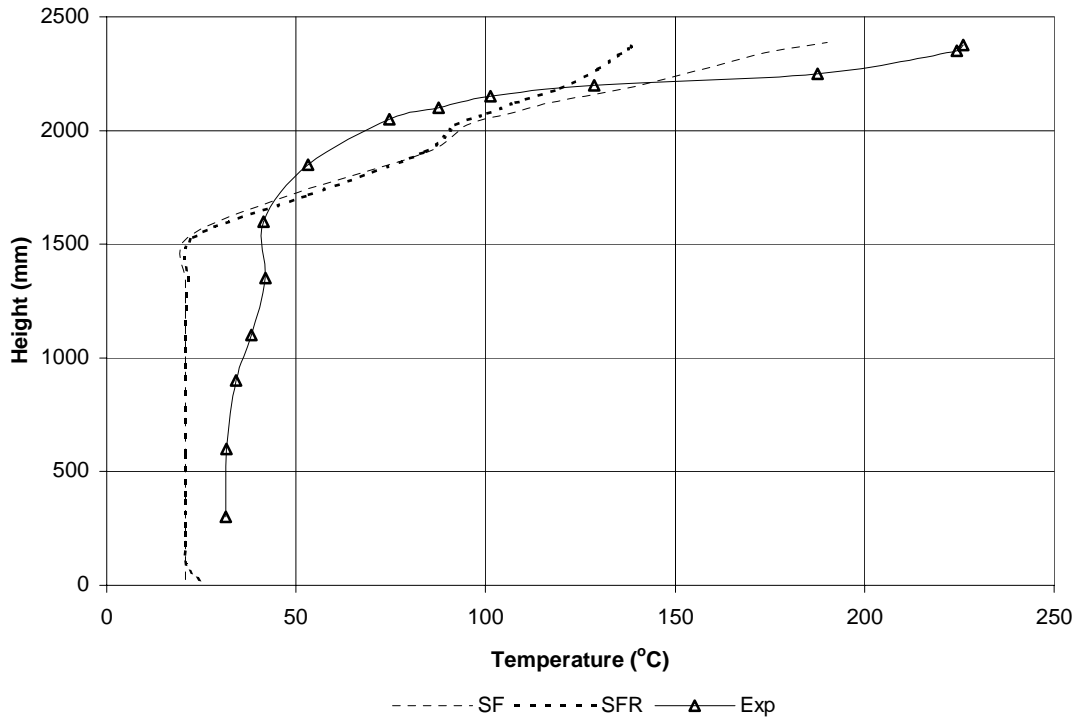


Figure 9.33 Comparisons for Tree 6 (110 kW Corner Fire)

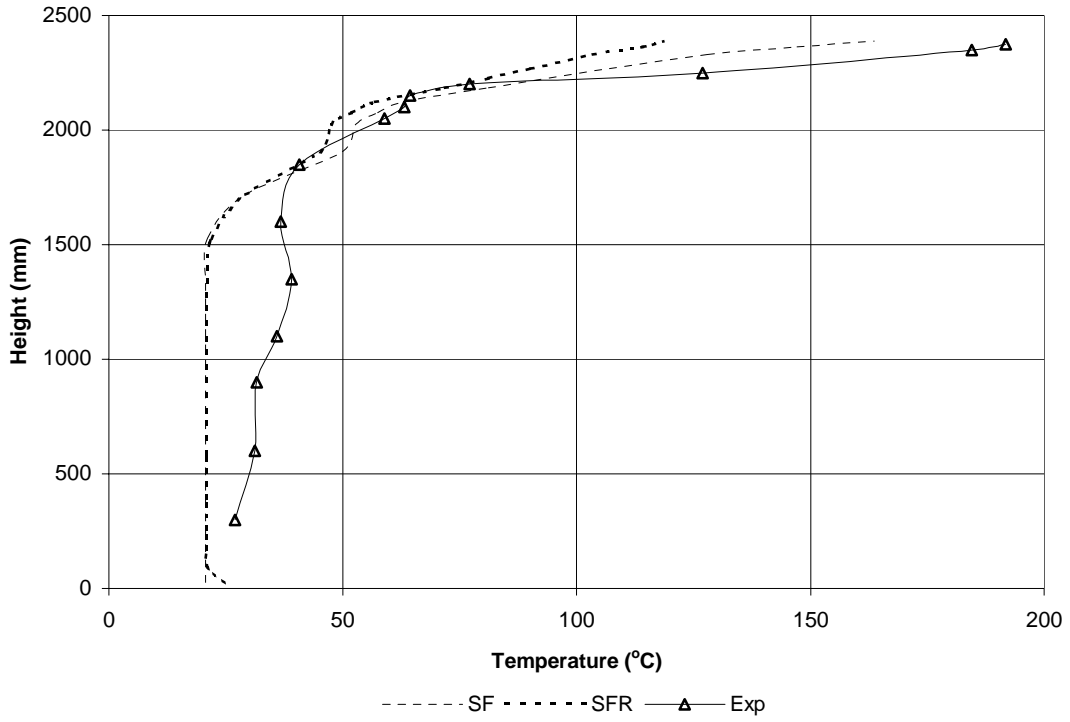


Figure 9.34 Comparisons for Tree 7 (110 kW Corner Fire)

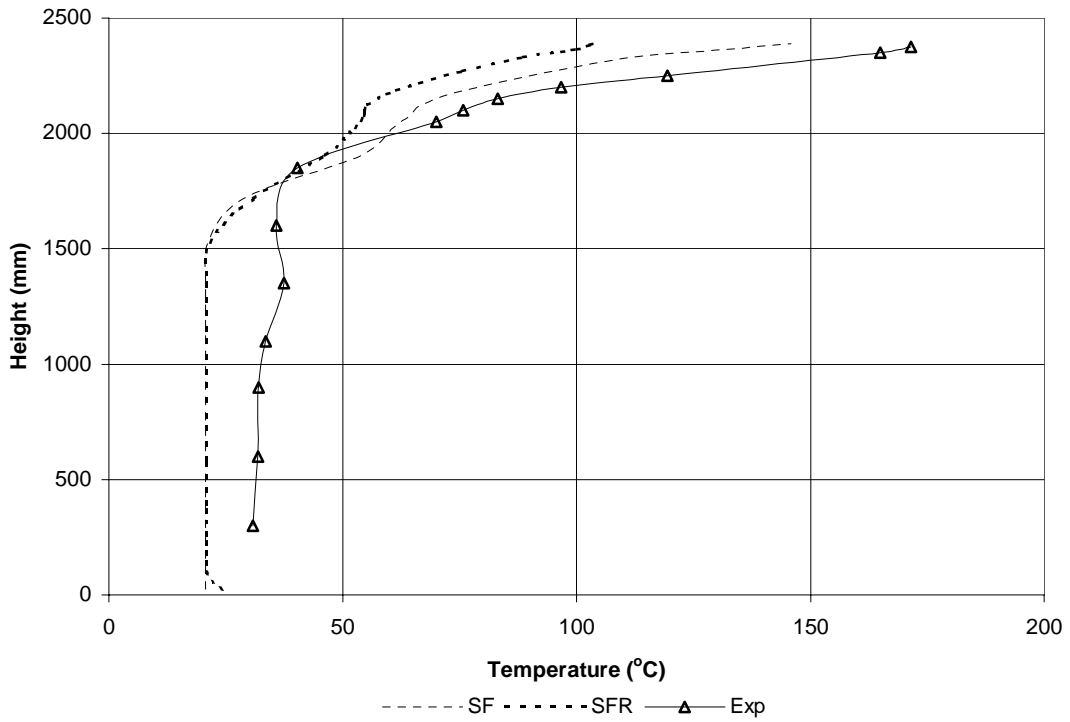


Figure 9.35 Comparisons for Tree 8 (110 kW Corner Fire)

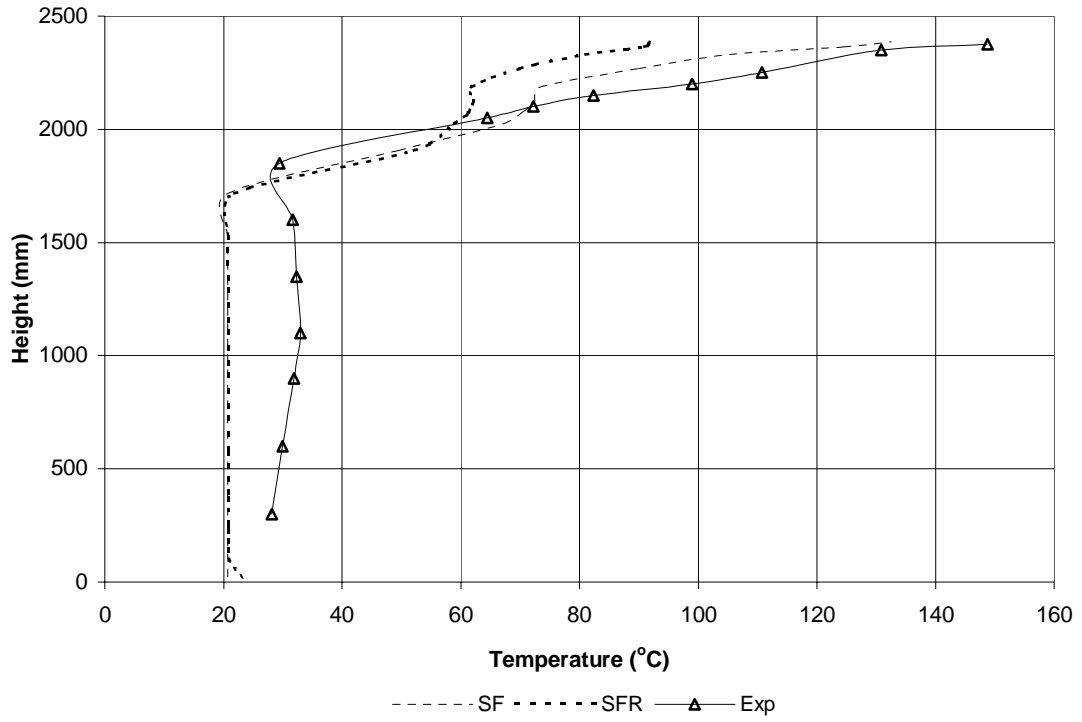


Figure 9.36 Comparisons for Tree 9 (110 kW Corner Fire)

9.4 Discussion

Results regarding the comparisons between the SMARTFIRE simulations and the experimental results for each fire is discussed below, followed by an overall discussion.

9.4.1 Discussion Structure

The structure for the discussions regarding the comparisons are as follows:

- Comparisons for each fire are presented in a format where the fire room, adjacent room, and the doorway are discussed separately.
- Comparisons for each room and the doorway are structured in a fashion where the temperature profiles are broken down into segments and are compared independently. These segments are the lower layer temperature profile, temperature gradient between the upper and lower layers, and the upper layer profile. The starting points are also compared where the temperature gradient begins between the upper and lower layers.

9.4.2 Comparisons for the 55 kW Fire

Specific details of the temperature profile comparisons in Figures 9.1 – 9.9 for the 55 kW fire are discussed below.

Fire Room

Both SMARTFIRE simulations underestimate the temperature of the lower layer in the fire room. SMARTFIRE simulations suggest that the lower layer is very close to the ambient temperatures, which is inaccurate, as temperatures in the lower layer are expected to be greater than ambient. Radiation from the fire increases the temperature measured by the thermocouples in the lower layer, creating an error for the temperature measured; however, this increase from radiation is not the reason why the simulations appear to be underestimating the lower layer temperature. The SMARTFIRE run with the inclusion of the radiation sub-model estimated a slightly higher lower layer temperature, but is still lower than the experimental value. Both simulations predict reasonably constant temperature profiles in the lower layer. This is

in line with what is seen experimentally. The temperature gradient between the upper and lower layers begins at a slightly lower height than the experimental temperature profiles, with the exception of the simulation with radiation for tree 1. The temperature profiles of the simulations follow an almost parallel temperature profile to that of the experimental profile. In this region the simulation that includes radiation generally produces a profile that is closer to the experimental gradient. The experimental temperature profiles in the upper layer are constant for trees 1 and 2, suggesting a well mixed and uniform upper layer temperature which is not demonstrated by the simulations. Instead, a temperature gradient in this region continues towards the ceiling. Temperatures nearer the ceiling tend to be overestimated, with the simulation results for tree 1 the most accurate, and tree 4 the most inaccurate.

Adjacent Room

Generally, simulated temperature profiles for the adjacent room are more accurate than those for the fire room. Lower layer temperature profiles for both simulations are constant with height, with little difference between them. When compared to the experimental profile, temperatures are underestimated slightly. This is probably a result of the thermocouples in the adjacent room absorbing radiation from the fire, thereby not measuring the true lower layer gas temperature, which is likely to be ambient. The height where the temperature gradient begins for both simulations is similar to experimental results. From here, the temperature gradients for the simulations follow similar profiles to the experimental. Temperatures in the very upper layer close to the ceiling of the adjacent room are to some extent underestimated, with the simulation without radiation producing more accurate results. It appears that the experimental results nearer the ceiling consistently diverge from the simulated results.

Doorway

The temperature profiles for both simulations in the lower layer are constant with height, and consistent with what is observed experimentally. Temperatures are also very close to the experimental results, with little difference between the two simulations. The temperature gradient begins at a slightly higher height for the simulation that includes radiation, whereas the temperature gradient for the simulation

with without radiation begins at an almost identical height compared with the experimental. Temperature gradients for both simulations follow a similar profile to that of the experimental. The simulation with radiation produces a more agreeable result nearer the soffit, with the non-radiation simulation overestimating the temperature.

9.4.3 Comparisons for the 110 kW Fire

Specific details of the temperature profile comparisons in Figures 9.10 – 9.18 for the 110 kW fire are discussed below.

Fire Room

Both simulations underestimate temperatures in the lower layer of the fire room, and in most cases the simulation with radiation calculates a slightly higher temperature. Both simulations predict similar temperature profiles to the experimental results in the lower layer, with near constant profiles at trees 1 and 2. Predictions for tree 4 do not match the experimental profile very well, with the experimental profile showing a temperature increase at the 600 mm and 900 mm thermocouples. The temperature gradient for both simulations between the upper and lower layer begins at a slightly lower height, with the exception of tree 4. Here the simulation with radiation predicts the beginning of the temperature gradient well, while the simulation without radiation overestimates the height where the temperature gradient begins. The steepness of the temperature gradient corresponds well with experimental gradients; however, these gradients extend further than the experimental profiles. The upper layer profiles are not predicted well by either simulation, with the upper layer for trees 1 and 2 exhibiting temperature gradients rather than constant temperature profiles. This indicates that both simulations underestimate how the upper layer at these locations is uniform in temperature. For tree 4, the experimental upper layer temperature profile illustrates more of a temperature gradient, which is simulated more accurately by the simulation with radiation. Both simulations overestimate the upper layer temperature nearer the ceiling, suggesting a steep temperature gradient, typical of a ceiling jet. The simulation without radiation tends to over predict the temperature more so than the simulation with radiation.

Adjacent Room

The simulated temperature profiles of the lower layer are constant, and consistent with the experimental profiles. The temperatures are underestimated, however, this is probably a result of the thermocouples absorbing radiation, and incorrectly increasing measured gas temperatures. Both simulations predict reasonably well where the temperature gradient between the upper and lower layers begin, with the exception of tree 6. Here the location predicted by both simulations is underestimated. The profile of the temperature gradient corresponds well with experimental observations. Both simulations display near identical profiles. The temperatures also correspond well to experimental temperatures. Temperatures very close to the ceiling are overestimated, more so by the simulation without radiation. The exception to this trend is tree 6, where temperatures very close to the ceiling tend to diverge slightly away from experimental values.

Doorway

Temperature profiles for both simulations in the lower layer are constant with height and consistent with what is observed experimentally. Temperatures are also very similar to the experimental results, with little difference between the two simulations. The temperature gradient for both simulations, between the lower and upper layers, begins at almost identical heights, and corresponds well to what is seen experimentally. The temperature gradient for both simulations follows a similar profile to the experimental. The simulation with radiation produces a more agreeable result nearer the soffit, whereas the simulation without radiation overestimates the temperature.

9.4.4 Comparisons for the 160 kW Fire

Specific details of the temperature profile comparisons in Figures 9.19 – 9.27 for the 160 kW fire are discussed below.

Fire Room

Both simulations predict constant temperature profiles for the lower layer and consistent with what is observed experimentally. The simulations predict temperatures near ambient, underestimating the lower layer temperature. Gas temperatures (insignificantly affected by radiation) in the lower layer will be above ambient. Again, radiation from the fire will be responsible for raising thermocouple temperatures in the lower layer; however, this increase from radiation is not the reason why the simulations appear to be underestimating the lower layer temperature. Temperatures in the lower layer for trees 1 and 2 are underestimated. The simulation with radiation predicts a slightly higher temperature in the lower layer for tree 1 than the simulation without radiation, while there appears to be little difference between simulations at tree 2. Also the simulation without radiation predicts a closer temperature to the experimental results for tree 4. The height where the temperature gradient between the lower and upper layers begins is slightly underestimated for both simulations for all trees, with little difference between simulations. The steepness of the temperature gradient corresponds well to the experimental profiles. The upper layer profiles are not predicted well by either simulation, with the upper layer for trees 1 and 2 exhibiting temperature gradients rather than constant temperature profiles. This indicates that both simulations do not predict how the upper layer at these locations is uniform in temperature. For tree 1 the simulation with radiation is significantly more accurate than the simulation without. For tree 2 the simulation with radiation under predicts the temperature whilst the simulation without over predicts (both by similar quantities). The simulation that includes radiation over predicts the temperature nearer the ceiling. For tree 4, the experimental upper layer temperature profile illustrates more of a temperature gradient, which is simulated well by the radiation simulation. Again, the temperature gradient nearer the ceiling increases significantly, suggesting a ceiling jet.

Adjacent Room

The simulated temperature profiles of the lower layer show a constant temperature with height, similar with what is observed for the experimental profiles. The temperatures are underestimated, however, once again this is probably a result of the thermocouples absorbing radiation, and incorrectly increasing measured gas temperatures. Both simulations predict near identical starting points where the temperature gradient begins between the lower and upper layers. For trees 6 and 8 the starting point for the temperature gradient is underestimated, for tree 9 it is insignificantly overestimated, whilst for tree 7 the starting point is good. The profiles of the temperature gradients correspond well with experimental observations, with both simulations displaying near identical profiles. The temperatures also correspond well with experimental temperatures. For trees 7, 8, and 9, temperatures close to the ceiling are underestimated, mostly by the radiation simulations. The non-radiation simulations predict the upper layer temperature gradients well.

Doorway

The temperature profiles for both simulations in the lower layer are constant with height and consistent with what is observed for the experimental profile. Temperatures are also very similar to the experimental results, with little difference between the two simulations. The temperature gradient between the lower and upper layer begins at almost identical heights for both simulations, and corresponds well with what is seen experimentally. The temperature gradient for both simulations follows a similar profile to the experimental. The simulation with radiation produces a more agreeable result nearer the soffit, with the non-radiation simulation diverging away from the experimental results, and overestimates the temperature nearer the ceiling.

9.4.5 Comparisons for the 110 kW Corner Fire

Specific details of the temperature profile comparisons in Figures 9.20 – 9.36 for the 160 kW fire are discussed below.

Fire Room

The simulated temperature profiles in the lower layer generally match experimental profiles for trees 1 and 2. Lower layer temperature profiles for trees 3 and 4 are not as well simulated. Temperatures measured on tree 3, at heights of 600 mm and 900 mm of the experimental profiles, appear to be too high and are probably incorrect. This is more than likely a result of these thermocouples being affected by the experiments with the central fires (which were located directly under tree 3), as the temperatures at these heights are higher than any other tree. The simulated temperature profiles for the lower layer at tree 4 vary greatly, with the radiation simulation showing little or no constant temperature profile in the lower layer, whilst the simulation without radiation does. As mentioned earlier, temperatures measured in the lower layer are likely to be affected by radiation, thus increasing their temperature. Nevertheless, the simulations underestimate lower layer temperatures. Overall, the simulation with radiation predicts a higher temperature, giving a better result than the simulation without. The starting point for the temperature gradient of the corner fire between the upper and lower layer is not as clearly defined for some of the trees for the experimental profiles. It appears that the starting point for the temperature gradient for all trees between the upper and lower layer is underestimated by both simulations, with the radiation simulation predicting a slightly higher starting point for trees 1 and 3 than the non-radiation simulation. The reverse applies for trees 2 and 4. The profiles of the temperature gradients do not correspond well to the experimental profiles, particularly for the non-radiation simulations at trees 2 and 3. The experimental upper layer temperature profile of the corner fire is not constant as is seen with the centrally located fires (reasons are given in Section 5.5.2). In the upper section of the fire compartment (from about 1500 mm), both simulations predict an upper temperature profile where the curvature is opposite to that which is seen experimentally. Closer to the ceiling, experimental temperatures converge with the simulated, particularly for

the simulation with radiation. Here, the simulation without radiation produces a much higher temperature profile close to the ceiling.

Adjacent Room

Once again the simulated temperature profiles of the lower layer are constant, similar with what is observed for the experimental profiles. The temperatures are underestimated. Again, this is probably a result of the thermocouples absorbing radiation, and incorrectly increasing measured temperatures. There appears to be no significant temperature difference between simulations. Both simulations predict near identical starting points where the temperature gradient begins between the lower and upper layers. For all trees, except 6, the starting point of the temperature gradient is underestimated. Most of the profiles of the simulated temperature gradients correspond well with experimental observations; only the simulation profiles for tree 6 display a lower temperature gradient than what is observed experimentally. Generally the temperatures correspond well with experimental temperatures. However, for all trees temperatures very close to the ceiling are underestimated, more so by the radiation simulations than the non-radiation simulations.

Doorway

The temperature profiles for both simulations in the lower layer are constant with height and consistent with what is observed for the experimental profile. Temperatures are also very similar to the experimental results, with the small difference probably attributed to radiation increasing the experimental profile. For both simulations the temperature gradients between the lower and upper layers begin at almost identical heights, with the starting point for the temperature gradient for both simulations being slightly over predicted. The temperature gradient for both simulations follows a similar profile to that of the experimental, with little difference between the two simulations. The simulation without radiation predicts a higher temperature result nearer the soffit, with both simulations under predicting the temperature nearer the soffit.

9.5 Overall Discussion

Fire Room

For all simulations, the lower layer temperature of the fire room was underestimated. Without being able to quantify the effects of radiation on the thermocouples, the accuracy of the simulations can only be qualitatively discussed. The simulation including radiation performed better than the simulation without. The height at where the temperature gradient between the lower and upper layers begins is predicted well by both simulations, with modest differences between the two simulations and experimental results. The slope of the temperature gradient most tree locations is predicted with reasonable accuracy for by both simulations. Generally the temperatures along the temperature gradient between the upper and lower layers are close to what is seen experimentally, with the 110 kW corner fire simulations displaying the worst results. For the centrally located fires, experimental results revealed a constant temperature profiles, particularly for trees 1 and 2. This shows how the upper layer was uniform in temperature. Neither simulation predicts this well, with both simulations generating upper layer profiles with temperature gradients, often with very high temperatures close to the ceiling, indicating a ceiling jet. The simulation with radiation produced slightly better results in the upper layer. Overall, the simulation with radiation predicts the best profile in the adjacent room.

Adjacent Room

Temperature profiles by both simulations are predicted with more accuracy than the fire room. The lower layer temperature profiles show a constant temperature. This is close to what is seen experimentally, especially if the effects of radiation on the thermocouples are taken into account. The height where the temperature gradient between the lower and upper layer begins is predicted well by both simulations, often with little difference between them. The temperatures in the upper layer are also predicted well, however, temperatures are often under predicted closer to the ceiling.

Doorway

Temperature profiles in the lower layer are modelled well by both simulations. The height where the temperature gradient begins between the lower and upper layer

agrees with what is seen experimentally. The temperature gradient's profile and temperatures for both simulations generally agree with the experimental profiles and temperatures. Nearer the soffit, the simulation without radiation over predicts the temperature for all but the 110 kW corner fire. Overall, the simulation with radiation produces the best results.

Overall

Capping off, running the simulations with the six-flux radiation sub-model simulates temperatures and temperature profiles more accurately than the simulation without the six-flux radiation model.

10 Conclusions

Firstly this report has examined the characteristics of pre-flashover fire experiments for centrally located 55 kW, 110 kW, 160 kW fires, and a 110 kW corner fire, all of which were conducted in a two-compartment structure 7.2 m long × 2.4 m wide × 2.4 m high. Secondly, the accuracy of preliminary SMARTFIRE simulations for these fires was determined.

10.1 Conclusions from the Pre-flashover Fire Experiments

The following conclusions were reached from the pre-flashover fire experiments conducted at McLeans Island:

Overall:

- Temperature profiles in the two-compartment structure comprised of a hot upper layer and a cool lower layer, with a temperature gradient between the layers.
- Temperature profiles in the fire room varied significantly from the adjacent room.
- Lower layer temperatures in the fire room were significantly higher than the adjacent room.
- The 110 kW corner fire produced higher temperatures and higher CO₂ concentrations in the upper layer than the equivalently sized 110 kW central fire (approximately double the concentration of CO₂).
- The 110 kW corner fire produced a temperature profile in the fire room that varied significantly from the centrally located fires.
- Temperature variations occurred in areas of large temperature gradients and non-uniform mixtures between the hot fire gases and ambient air.
- Radiation from the fire increased the floor surface thermocouples temperature.
- Ceiling surface thermocouples illustrated how heat is conducted into the ceiling.

Fire Room:

- Temperature profiles on trees 1 and 2 for the centrally located fires produced well-defined upper and lower layers of constant temperature, with a temperature gradient between the layers starting at 1350 mm.
- Temperature fluctuations increased markedly at the temperature gradient between the upper and lower layers.
- Temperatures in the upper layer for the centrally located fires reached 130°C for the 55 kW fire, 200°C for the 110 kW fire, and 250°C for the 160 kW fire.
- The 110 kW corner fire produced the highest temperature nearer the ceiling reaching 335°C.
- The upper layer temperature profile of the 110 kW corner fire did not display a constant temperature profile as seen with the central fires.
- Corner temperatures at the back of the fire room illustrated slightly higher temperatures than the front corner thermocouples, with the difference in most cases being 5°C overall.

Adjacent Room:

- Temperature profiles for all trees showed a well-defined constant temperature lower layer near the ambient temperature, with an upper layer displaying a temperature gradient up to the ceiling. For all fires, temperatures increased for the upper layer, starting at 1850 mm.
- Temperature variations increased considerably above 1850 mm, and continued to remain high beyond this height.
- Temperatures in the upper layer for the centrally located fires reached 110°C for the 55 kW fire, 160°C for 110 kW fire, and 200°C for the 160 kW fire.
- The 110 kW corner fire produced the highest temperature in the upper layer, reaching up to 225°C at tree 6.
- The temperatures of the adjacent room corner thermocouples were lower than the fire room corner thermocouples. Overall the drop was about 25 – 30°C for the 55 kW fire, 30 – 35°C for the 110 kW fire, 60 – 70°C for the 160 kW fire, and 50 – 60°C for the 110 kW corner fire.

10.2 Conclusions from the SMARTFIRE Simulations

- Predicted temperature profiles suggested the formation of upper and lower layers associated with pre-flashover fires.
- The temperature profile for all simulations in the upper layer in the fire room displayed a temperature gradient rather than a constant temperature profile.
- The upper layer height in the fire room was predicted to be lower than the adjacent room upper layer height.
- Simulations, including the simulation with the six-flux radiation sub-model, produced lower temperatures in the upper layer than the simulations without the six-flux radiation sub-model.
- Upper layer temperature profiles were more horizontal for the simulations which included the six-flux radiation sub-model.
- Close to the ceiling the 110 kW corner fire simulations produced the highest temperatures, which rapidly decreased with descending height.
- By specifying the fire as a volumetric block, SMARTFIRE was unable to simulate flame layback as a result of incoming air, with little or no layback of the fire's plume.
- Simulations where the six-flux radiation sub-model was incorporated required more computational time than simulations without the six-flux radiation model.

10.3 Conclusions from the Comparisons

Fire Room:

- All simulations predicted constant lower layer temperature profiles, but underestimated lower layer temperatures.
- All simulations for the centrally located fires predicted a temperature gradient in the upper layer for trees 1 and 2, rather than the constant temperature profile seen experimentally.
- Temperatures close to the ceiling were often overestimated by both simulations, with the simulations predicting a temperature profile of a ceiling jet not seen experimentally.

- Simulations for the 110 kW corner fire produced corresponded the least with experimental temperatures.

Adjacent Room:

- Both simulations under predicted the lower layer temperature slightly.
- The simulated upper layer temperature profiles generally corresponded well with experimental results.

Doorway:

- Both simulations predicted the lower layer temperature well.
- Upper layer temperature profiles were generally simulated with reasonable accuracy.

10.4 Further Research

Experiments at McLeans Island:

1. Aspirated thermocouples need to be used to determine the magnitude of the effects of radiation on the thermocouples.
2. The location of the fire should be varied throughout the fire compartment, eg against the back wall. Also, experiments need to be carried out, whereby for each experiment, the fire's position is moved in increments away from the wall or corner.
3. Experiments should be conducted with the inclusion of a doorway and a soffit on the adjacent compartment.

SMARTFIRE simulations:

1. An investigation needs to be carried out to determine the best settings for the simulations.
2. The sensitivity of the solution's dependence on grid size needs to be investigated.
3. Simulations using the radiosity sub-model should be carried out and compared with the six-flux radiation simulations.

11 Nomenclature

A	constant heat release coefficient (kW),
B	heat release coefficient with time (kWs ⁻¹),
C	heat release coefficient with t ² (kWs ⁻¹),
D	exponential heat release coefficient (kW), and
E	exponential term modifier with time (s ⁻¹)
g	gravitational constant (ms ⁻²)
M	molecular mass (kg/mol),
p	pressure (N/m ²),
P	power output (kW),
r	Radius (m)
R	universal gas constant (8134 J/kg.mol.K)
T	time (s),
T	Temperature (°C).
V	velocity (ms ⁻¹),

Greek Symbols

Δ	“drop”
ρ	density (kg/m ³).

12 References

- BIA (1992) *New Zealand Building Code and Approved Documents*, Building Industry Authority, Wellington, New Zealand
- Blevins, L., G. (1999) Behaviour of Bare and Aspirated Thermocouples in Compartment Fires, *Proc. 33rd Nat. Heat Trans. Con.*, August 15-17.
- Buchanan, A., H. (1999) Implementation of Performance-based Fire Codes, *Fire Safety J.*, **32**, 377-383.
- Cox, G. (1994) The Challenge of Fire Modelling, *Fire Safety J.*, **23**, 123-132.
- Drysdale, D. (1986) *An Introduction to Fire Dynamics*. A Wiley-Interscience publication. U.K 1986.
- Emmons, H., W. (1995) Vent Flows, chapter 5 section 2 in *The SFPE Handbook of Fire Protection Engineering*, second edition, Society of Fire Protection Engineers and National Fire Protection Association, Quincy, Massachusetts, USA.
- Galea, E.R., Knight, B., Patel, M.K., Ewer, J., Pitridis, M., and Taylor, S., SMARTFIRE V2.0 USER GUIDE AND TECHNICAL MANUAL. Fire Safety Engineering Group, University of Greenwich, UK, 1998.
- Heskestad, G. (1995) Fire Plumes, chapter 2 section 2 in *The SFPE Handbook of Fire Protection Engineering*, second edition, Society of Fire Protection Engineers and National Fire Protection Association, Quincy, Massachusetts, USA.
- Hinze, J., O. (1957) *Turbulence – An Introduction to Its Mechanism and Theory*, McGraw-Hill, New York, New York, USA.
- Holman, J, P. (1978) *Experimental Methods for Engineers*. McGraw-Hill, Inc. USA.

Kerrison, L., Galea, E. R., Hoffman, N., and Patel M. K. (1994b) A Comparison of a FLOW 3D Based Fire Model with Experimental Compartment Data, *Fire Safety J.*, **23**, 387-411

Markatos N.C., Malin, M. R., Cox G. (1982) Mathematical Modelling for the Buoyancy Induced Smoke Flow in Enclosures, *Int. J. Heat Mass Transfer*, **25** (1), 63.

McCaffrey, B. (1995) Flame Height, chapter 1 section 2 in *The SFPE Handbook of Fire Protection Engineering*, second edition, Society of Fire Protection Engineers and National Fire Protection Association, Quincy, Massachusetts, USA.

Patankar, S., V. (1980) *Numerical Heat Transfer and Fluid Flow*. McGraw-Hill, New York, USA

Quintiere, J. G, Rinkinen, W. J, and Jones, W. W. (1981) The effect of Room Openings on Fire Plume Entrainment, *Comb. Sci. Tech.*, **26**, 193-201.

Steckler, K. D., Quintiere, J. G. and Rinkinen, W. J., Flow Induced by Fire in a Compartment. NBSIR 82-2520, National Bureau of Standards, Washington, September 1982.

Stroup, D. W. (1995) Using Field Modelling to Simulate Enclosure Fires, chapter 3 section 8 in *The SFPE Handbook of Fire Protection Engineering*, second edition, Society of Fire Protection Engineers and National Fire Protection Association, Quincy, Massachusetts, USA.

Takahashi, B., Tanaka, H., Sugawa, O., and Ohtake, M. (1997) Flame and Plume Behaviour in and near a Corner of Walls, *Proc. Fifth International Symp. Fire Safety Science*, 261-284.

Versteeg, H., K., and Malalasekera, W. (1995) *An Introduction to Computational Fluid Dynamics – The Finite Volume Method*, Longman Scientific & Technical, Essex CM20 2JE, England.

Weaver, S. D. (2000) *A Comparison of Data Reduction Techniques for Zone Model Validation*, Fire Engineering Research Report 98/6, Department of Civil Engineering, University of Canterbury, New Zealand.

Appendix 1: Tabulated Experimental Field Tree Temperatures

Run 1: 110 kW Fire

Tables A.1 – A.4 below lists the average, minimum, maximum, and standard deviations of the temperatures recorded by the field trees for run number 1 (110 kW fire) during the 10 minute period starting from the 45th minute (results from this experiment were analysed in this report). Ambient temperature at the start of the experiment was 16°C.

Table A.1 Run 1 Temperatures for Field Trees 1, 2, and 3

TC Height (mm)	Tree 1 Temperatures (°C)				Tree 2 Temperatures (°C)				Tree 3 Temperatures (°C)			
	Ave	Min	Max	SD	Ave	Min	Max	Std	Ave	Min	Max	SD
<i>Ceiling</i>	176.7	175.3	177.7	0.5	187.2	185.9	188.3	0.5	198.7	197.7	200.6	0.6
2375	199.5	196.5	203.5	1.4	203.6	200.0	209.4	1.8	206.0	195.9	222.3	5.2
2350	200.1	196.5	204.1	1.5	204.9	200.0	210.6	2.0	205.1	196.5	219.9	4.6
2300	201.7	198.3	205.3	1.5	206.6	200.6	216.4	2.6	205.3	195.9	216.4	4.2
2250	203.9	200.0	207.6	1.7	206.5	202.4	212.9	2.3	204.8	193.6	215.8	4.0
2200	203.5	199.4	207.1	1.6	204.5	201.2	211.2	2.0	203.4	190.6	218.8	4.7
2150	203.4	199.4	207.1	1.7	204.8	201.2	211.2	1.9	203.5	192.4	219.9	4.7
2100	203.2	198.8	207.1	1.7	203.3	200.0	208.2	1.7	202.4	190.6	218.8	4.8
1850	200.5	197.1	204.1	1.5	200.1	195.3	204.7	1.7	204.2	185.3	225.8	7.8
1600	193.7	187.1	200.0	2.4	191.2	182.4	196.5	2.4	207.0	183.6	246.2	11.3
1350	96.3	83.2	121.9	8.2	141.9	126.0	158.3	6.1	208.0	163.0	272.4	22.1
1100	66.6	61.6	72.1	2.0	72.9	65.6	84.3	4.4	224.2	169.5	314.0	33.4
900	60.9	55.2	64.5	1.7	72.0	69.1	77.9	1.8	295.3	200.6	424.3	48.5
600	62.9	58.1	69.1	2.2	58.8	54.0	62.7	1.6	456.7	330.1	574.4	58.4
300	61.9	58.1	65.6	1.4	66.3	59.2	75.0	3.0	496.7	399.5	630.3	46.8
<i>Floor</i>	125.8	124.8	127.1	0.6	140.5	139.5	141.2	0.4	0.0	0.0	0.0	0.0

Table A.2 Run 1 Temperatures for Field Trees 4, 6, and 7

TC height (mm)	Tree 4 Temperatures (°C)				Tree 6 Temperatures (°C)				Tree 7 Temperatures (°C)			
	<i>Ave</i>	<i>Min</i>	<i>Max</i>	<i>SD</i>	<i>Ave</i>	<i>Min</i>	<i>Max</i>	<i>SD</i>	<i>Ave</i>	<i>Min</i>	<i>Max</i>	<i>SD</i>
<i>Ceiling</i>	184.6	183.6	185.9	0.5	131.6	130.1	132.4	0.5	109.7	108.9	110.7	0.4
<i>2375</i>	194.5	184.7	207.1	4.4	161.4	157.1	165.4	1.9	138.5	134.2	144.2	1.8
<i>2350</i>	193.7	181.8	210.6	5.0	163.1	158.3	168.3	2.2	135.7	130.1	143.6	2.3
<i>2300</i>	190.8	180.6	202.9	4.2	159.2	151.2	167.7	3.0	114.1	107.2	123.6	2.7
<i>2250</i>	187.0	175.9	200.0	4.2	151.5	143.0	163.0	4.1	90.9	86.1	97.2	2.1
<i>2200</i>	185.9	177.7	195.9	3.6	136.1	123.6	148.3	4.6	79.3	72.1	86.1	2.8
<i>2150</i>	183.8	173.6	194.1	3.8	122.6	110.7	139.5	5.9	71.8	63.9	78.5	2.7
<i>2100</i>	181.1	170.1	190.6	3.7	102.5	88.4	124.8	7.3	65.2	54.0	71.5	3.1
<i>1850</i>	172.2	164.8	183.6	3.4	38.8	36.0	45.9	1.5	31.1	23.3	39.5	4.1
<i>1600</i>	162.8	150.1	175.3	5.1	29.0	27.3	30.8	0.8	18.4	16.9	20.4	0.7
<i>1350</i>	150.2	131.3	158.9	5.7	27.7	25.0	30.2	1.0	27.2	25.0	29.1	0.9
<i>1100</i>	103.3	90.8	113.0	4.5	26.8	23.9	29.6	1.2	25.6	23.9	27.9	0.9
<i>900</i>	79.1	71.5	89.0	3.0	23.2	21.5	26.2	0.9	22.2	20.4	23.9	0.7
<i>600</i>	73.6	65.1	88.4	4.2	20.5	19.2	22.1	0.5	22.7	21.5	23.9	0.5
<i>300</i>	39.5	33.7	47.0	2.5	20.9	19.8	22.7	0.6	18.4	17.5	19.8	0.5
<i>Floor</i>	150.6	149.5	151.8	0.6	52.9	52.3	54.0	0.4	45.3	44.7	45.9	0.3

Table A.3 Run 1 Temperatures for Field Trees 8 and 9

TC height (mm)	Tree 8 Temperatures (°C)				Tree 9 Temperatures (°C)			
	<i>Ave</i>	<i>Min</i>	<i>Max</i>	<i>SD</i>	<i>Ave</i>	<i>Min</i>	<i>Max</i>	<i>SD</i>
<i>Ceiling</i>	100.3	99.6	101.3	0.4	0.0	0.0	0.0	0.0
<i>2375</i>	132.0	126.0	137.1	2.1	114.4	109.5	120.1	2.0
<i>2350</i>	128.5	123.0	133.0	2.3	108.0	103.7	113.0	1.9
<i>2300</i>	111.0	106.0	116.6	2.1	101.0	97.8	104.8	1.7
<i>2250</i>	101.4	97.8	104.8	1.6	96.3	92.5	100.1	1.6
<i>2200</i>	93.8	90.2	97.8	1.8	87.6	84.3	90.8	1.2
<i>2150</i>	87.5	83.8	91.4	1.8	81.4	75.0	84.9	1.6
<i>2100</i>	80.1	76.2	83.8	1.6	71.7	65.1	77.3	2.2
<i>1850</i>	26.2	23.9	40.6	2.1	18.5	16.4	23.3	1.3
<i>1600</i>	25.3	23.3	27.9	0.9	18.9	17.5	21.0	0.6
<i>1350</i>	25.6	23.3	28.5	1.0	21.8	21.0	23.3	0.6
<i>1100</i>	23.5	22.1	25.0	0.7	23.0	22.1	23.9	0.4
<i>900</i>	22.8	21.5	24.4	0.5	22.7	22.1	23.3	0.4
<i>600</i>	23.5	22.1	25.0	0.5	21.8	20.4	22.7	0.4
<i>300</i>	24.3	23.3	25.6	0.5	22.3	21.0	23.3	0.5
<i>Floor</i>	44.4	44.1	45.3	0.3	22.6	21.5	23.3	0.4

Table A.4 Run 1 Temperatures for Field Tree 5 (Doorway)

TC height (mm)	Tree 5 Temperatures (°C)			
	<i>Ave</i>	<i>Min</i>	<i>Max</i>	<i>SD</i>
<i>1900</i>	177.8	171.2	183.6	2.7
<i>1750</i>	171.8	164.8	176.5	2.4
<i>1600</i>	167.0	161.8	173.0	2.4
<i>1450</i>	154.5	144.2	164.2	3.8
<i>1300</i>	99.4	83.8	120.1	7.8
<i>1150</i>	63.2	58.1	68.6	2.3
<i>1000</i>	36.4	29.6	44.1	3.0
<i>850</i>	23.0	20.4	26.2	1.0
<i>700</i>	23.1	21.0	26.7	1.0
<i>550</i>	21.1	19.8	22.1	0.5
<i>400</i>	20.4	19.2	21.5	0.5
<i>250</i>	20.0	18.7	21.5	0.5
<i>100</i>	28.1	26.2	30.2	0.9
<i>Floor</i>	77.6	76.7	79.1	0.5

Run 2: 160 kW Fire

Tables A.5 – A.8 below lists the average, minimum, maximum, and standard deviations of the temperatures recorded by the field trees for run number 2 (160 kW fire) during the 10 minute period starting from the 45th minute. Ambient temperature at the start of the experiment was 15°C.

Table A.5 Run 2 Temperatures for Field Trees 1, 2, and 3

TC height (mm)	Tree 1 Temperatures (°C)				Tree 2 Temperatures (°C)				Tree 3 Temperatures (°C)			
	<i>Ave</i>	<i>Min</i>	<i>Max</i>	<i>SD</i>	<i>Ave</i>	<i>Min</i>	<i>Max</i>	<i>SD</i>	<i>Ave</i>	<i>Min</i>	<i>Max</i>	<i>SD</i>
<i>Ceiling</i>	227.4	226.4	229.3	0.5	242.5	241.6	243.9	0.5	260.4	259.1	262.5	0.9
<i>2375</i>	260.0	254.4	266.0	2.5	267.8	260.8	277.1	3.3	275.7	262.0	293.8	7.5
<i>2350</i>	260.3	254.4	266.6	2.5	270.1	262.5	279.4	3.7	273.8	262.0	289.8	6.7
<i>2300</i>	263.7	257.9	269.5	2.5	273.1	265.4	284.6	4.1	273.0	261.4	292.7	6.7
<i>2250</i>	267.0	260.2	273.6	2.9	273.3	266.0	283.4	3.7	273.1	262.0	292.1	6.7
<i>2200</i>	266.9	259.6	273.0	2.9	270.4	263.1	279.4	3.4	272.7	260.2	293.3	7.6
<i>2150</i>	267.4	260.2	273.6	3.1	271.0	263.7	281.1	3.3	272.6	258.5	295.0	7.9
<i>2100</i>	266.8	260.2	272.4	3.0	268.7	262.5	275.3	2.9	271.4	255.6	293.8	7.7
<i>1850</i>	263.6	259.6	267.8	2.2	264.4	259.6	268.4	2.3	277.3	252.6	313.5	11.8
<i>1600</i>	255.0	248.0	260.8	2.9	252.4	245.1	257.9	2.7	286.2	243.3	333.0	15.7
<i>1350</i>	139.6	116.0	165.9	9.5	183.9	155.4	204.1	9.1	271.2	231.1	335.3	23.5
<i>1100</i>	88.8	83.8	93.7	2.1	98.5	86.7	113.0	5.9	282.0	228.1	380.3	32.1
<i>900</i>	79.9	75.0	85.5	2.1	95.1	90.2	104.8	3.0	332.1	259.1	496.5	47.7
<i>600</i>	84.1	78.5	91.4	2.5	73.6	68.6	81.4	2.7	466.4	331.8	698.0	68.6
<i>300</i>	81.2	75.6	87.3	2.1	83.6	73.2	90.8	4.1	700.1	601.2	823.5	43.4
<i>Floor</i>	160.9	159.5	163.0	0.6	173.7	173.0	175.3	0.5	0.0	0.0	0.0	0.0

Table A.6 Run 2 Temperatures for Field Trees 4, 6, and 7

TC height (mm)	Tree 4 Temperatures (°C)				Tree 6 Temperatures (°C)				Tree 7 Temperatures (°C)			
	<i>Ave</i>	<i>Min</i>	<i>Max</i>	<i>SD</i>	<i>Ave</i>	<i>Min</i>	<i>Max</i>	<i>SD</i>	<i>Ave</i>	<i>Min</i>	<i>Max</i>	<i>SD</i>
<i>Ceiling</i>	243.4	241.6	245.1	0.8	170.6	169.5	171.8	0.4	144.2	143.0	145.4	0.5
<i>2375</i>	264.9	248.0	284.6	6.4	216.1	209.4	223.5	3.1	186.7	178.3	197.1	3.1
<i>2350</i>	264.5	245.7	286.3	7.3	218.2	209.4	227.0	3.6	183.7	174.2	197.7	3.9
<i>2300</i>	259.6	244.5	273.6	5.8	214.5	202.4	225.8	5.1	153.5	144.2	165.9	4.7
<i>2250</i>	254.5	240.4	270.1	5.8	205.9	185.9	219.9	6.6	119.6	110.1	131.3	3.8
<i>2200</i>	252.5	239.8	267.2	5.3	185.4	165.4	201.8	7.0	102.6	90.2	115.4	4.0
<i>2150</i>	248.9	235.1	269.5	5.6	171.1	147.1	195.3	9.1	90.7	80.8	99.6	3.1
<i>2100</i>	245.4	234.6	269.5	5.4	146.9	121.3	173.0	10.5	81.2	72.6	92.5	3.3
<i>1850</i>	228.3	210.6	249.7	5.3	48.1	44.1	59.2	2.3	34.4	25.0	47.0	4.2
<i>1600</i>	210.0	188.9	227.5	6.9	31.9	29.1	34.8	1.1	19.9	18.1	22.1	0.7
<i>1350</i>	186.7	165.9	208.2	7.9	31.7	26.7	34.8	1.5	29.0	27.3	32.0	1.1
<i>1100</i>	135.7	120.1	149.5	6.1	29.0	25.6	33.1	2.0	26.7	23.3	31.4	1.9
<i>900</i>	104.3	94.9	113.0	4.0	24.2	21.5	28.5	1.7	21.8	20.4	25.0	1.1
<i>600</i>	93.8	84.9	101.9	2.9	21.0	19.8	22.7	0.6	22.0	21.0	23.3	0.4
<i>300</i>	49.2	41.8	56.3	3.5	20.7	19.2	22.7	0.7	17.4	16.4	18.7	0.5
<i>Floor</i>	192.9	190.6	194.7	1.1	69.4	68.6	70.3	0.4	57.9	56.9	58.7	0.3

Table A.7 Run 2 Temperatures for Field Trees 8 and 9

TC height (mm)	Tree 8 Temperatures (°C)				Tree 9 Temperatures (°C)			
	<i>Ave</i>	<i>Min</i>	<i>Max</i>	<i>SD</i>	<i>Ave</i>	<i>Min</i>	<i>Max</i>	<i>SD</i>
<i>Ceiling</i>	129.0	128.3	130.1	0.5	0.0	0.0	0.0	0.0
<i>2375</i>	171.5	163.6	178.3	2.9	146.8	140.1	153.0	2.5
<i>2350</i>	166.7	156.5	176.5	3.4	137.5	130.7	143.0	2.3
<i>2300</i>	142.6	133.6	151.2	3.1	128.1	122.4	133.0	2.1
<i>2250</i>	129.2	122.4	135.4	2.2	121.6	117.2	126.0	1.8
<i>2200</i>	118.4	112.5	124.2	2.4	109.7	105.4	113.0	1.8
<i>2150</i>	109.6	103.7	115.4	2.5	101.0	89.0	106.6	3.0
<i>2100</i>	100.1	91.4	106.0	2.4	88.9	71.5	97.2	4.8
<i>1850</i>	31.4	25.6	48.8	4.9	18.1	15.2	22.7	1.2
<i>1600</i>	26.3	24.4	30.2	1.4	17.8	16.4	19.8	0.7
<i>1350</i>	26.2	23.3	28.5	1.1	20.7	19.8	21.5	0.4
<i>1100</i>	22.8	21.0	25.6	0.8	21.9	21.0	22.7	0.4
<i>900</i>	21.8	20.4	23.3	0.5	21.3	20.4	22.1	0.4
<i>600</i>	22.6	21.5	23.9	0.5	20.3	19.2	21.5	0.4
<i>300</i>	23.2	22.1	24.4	0.5	20.6	19.8	21.5	0.3
<i>Floor</i>	53.5	52.8	54.6	0.3	24.8	24.4	25.6	0.4

Table A.8 Run 2 Temperatures for Field Tree 5 (Doorway)

TC height (mm)	Tree 5 Temperatures (°C)			
	<i>Ave</i>	<i>Min</i>	<i>Max</i>	<i>SD</i>
<i>1900</i>	238.4	228.1	252.1	4.3
<i>1750</i>	227.8	216.4	239.8	4.7
<i>1600</i>	218.3	204.7	227.5	3.5
<i>1450</i>	200.0	183.0	211.2	5.6
<i>1300</i>	134.8	111.9	157.1	10.6
<i>1150</i>	84.2	74.4	97.8	4.0
<i>1000</i>	51.4	37.7	61.6	5.6
<i>850</i>	25.9	22.7	29.6	1.6
<i>700</i>	24.2	22.1	29.1	1.4
<i>550</i>	22.8	21.5	27.3	1.0
<i>400</i>	20.7	19.2	22.1	0.5
<i>250</i>	20.1	18.7	21.5	0.6
<i>100</i>	29.9	28.5	33.1	0.8
<i>Floor</i>	102.5	100.7	103.7	0.7

Run 3: 160 kW Fire

Tables A.9 – A.12 below lists the average, minimum, maximum, and standard deviations of the temperatures recorded by the field trees for run number 3 (160 kW fire) during the 10 minute period starting from the 45th minute (results from this experiment were analysed in this report). Ambient temperature at the start of the experiment was 15°C.

Table A.9 Run 3 Temperatures for Field Trees 1, 2, and 3

TC height (mm)	Tree 1 Temperatures (°C)				Tree 2 Temperatures (°C)				Tree 3 Temperatures (°C)			
	<i>Ave</i>	<i>Min</i>	<i>Max</i>	<i>SD</i>	<i>Ave</i>	<i>Min</i>	<i>Max</i>	<i>SD</i>	<i>Ave</i>	<i>Min</i>	<i>Max</i>	<i>SD</i>
<i>Ceiling</i>	220.0	218.8	221.7	0.7	235.4	234.0	236.9	0.7	249.9	248.0	252.1	1.3
<i>2375</i>	249.7	245.7	256.7	2.2	257.4	250.3	266.0	3.2	262.0	245.7	280.5	6.9
<i>2350</i>	250.7	245.7	257.9	2.5	259.2	251.5	269.5	3.7	261.4	245.7	278.2	6.3
<i>2300</i>	253.7	248.6	261.4	2.6	261.5	252.6	273.6	4.1	260.9	242.7	277.6	6.8
<i>2250</i>	256.6	250.3	264.9	2.9	261.4	253.2	270.7	3.5	261.3	242.7	280.0	6.9
<i>2200</i>	256.4	250.3	264.3	2.8	258.9	251.5	266.6	3.3	259.8	241.0	278.8	7.6
<i>2150</i>	256.6	250.9	264.9	3.0	259.6	252.1	267.2	3.5	259.3	241.6	277.1	7.4
<i>2100</i>	256.3	250.3	264.9	2.9	258.3	251.5	266.0	3.1	258.0	238.1	277.6	7.2
<i>1850</i>	254.0	249.2	261.4	2.5	255.0	249.2	260.2	2.3	262.0	234.6	305.4	10.6
<i>1600</i>	247.0	241.6	253.2	2.6	245.1	238.1	252.1	2.4	270.0	241.0	353.5	15.5
<i>1350</i>	141.2	109.5	170.1	11.9	189.5	174.2	205.3	6.9	274.2	225.2	383.1	28.2
<i>1100</i>	88.8	80.2	96.0	2.8	96.0	82.6	117.7	6.3	291.9	228.1	401.8	37.8
<i>900</i>	79.8	73.2	85.5	2.4	91.2	87.3	104.8	2.7	343.0	257.3	470.8	44.4
<i>600</i>	82.4	73.8	88.4	2.8	76.9	72.1	82.6	2.4	485.1	365.5	633.7	57.2
<i>300</i>	79.0	73.2	84.3	2.0	79.5	63.9	93.1	8.3	445.8	436.7	464.1	4.3
<i>Floor</i>	161.7	160.6	163.0	0.8	181.7	180.6	183.0	0.5	0.0	0.0	0.0	0.0

Table A.10 Run 3 Temperatures for Field Trees 4, 6, and 7

TC height (mm)	Tree 4 Temperatures (°C)				Tree 6 Temperatures (°C)				Tree 7 Temperatures (°C)			
	<i>Ave</i>	<i>Min</i>	<i>Max</i>	<i>SD</i>	<i>Ave</i>	<i>Min</i>	<i>Max</i>	<i>SD</i>	<i>Ave</i>	<i>Min</i>	<i>Max</i>	<i>SD</i>
<i>Ceiling</i>	232.4	230.5	234.0	0.8	164.4	163.0	166.5	0.7	138.5	137.1	140.7	0.7
<i>2375</i>	248.6	236.9	260.8	5.1	203.1	197.7	211.7	2.6	176.3	170.6	184.7	2.7
<i>2350</i>	247.9	234.6	266.0	5.9	205.6	200.0	215.8	2.9	173.5	165.4	183.0	3.4
<i>2300</i>	243.6	230.5	256.1	5.1	203.3	195.3	213.5	3.7	148.2	136.5	160.6	4.2
<i>2250</i>	238.9	227.0	252.6	5.2	195.8	184.7	207.6	4.8	117.1	108.9	125.4	3.1
<i>2200</i>	238.0	227.5	250.3	4.7	178.4	166.5	190.0	5.5	101.2	92.5	109.5	3.5
<i>2150</i>	235.1	221.7	248.0	5.0	166.3	148.9	183.6	7.7	91.0	82.6	97.2	2.9
<i>2100</i>	231.8	219.4	245.7	5.0	143.9	120.1	166.5	10.0	82.3	73.8	90.8	3.3
<i>1850</i>	218.4	204.7	234.0	5.1	48.5	44.7	54.0	2.0	37.7	28.5	47.0	4.3
<i>1600</i>	205.1	188.3	219.9	5.3	31.9	27.3	34.8	1.4	20.3	18.1	22.7	0.8
<i>1350</i>	190.8	172.4	207.1	6.9	30.2	24.4	34.3	2.1	28.8	24.4	32.0	1.4
<i>1100</i>	143.1	124.8	154.8	6.3	28.2	23.9	32.0	1.9	27.2	23.9	31.4	1.7
<i>900</i>	104.4	95.5	117.2	3.8	24.5	22.1	29.1	1.5	22.6	21.0	25.6	1.0
<i>600</i>	89.4	83.2	101.3	3.6	21.6	20.4	22.7	0.5	23.4	22.1	25.0	0.6
<i>300</i>	46.2	37.7	53.4	3.4	21.8	20.4	23.9	0.8	18.6	17.5	20.4	0.6
<i>Floor</i>	199.5	198.3	201.2	0.7	68.4	68.0	69.1	0.4	56.4	55.7	56.9	0.3

Table A.11 Run 3 Temperatures for Field Trees 8 and 9

TC height (mm)	Tree 8 Temperatures (°C)				Tree 9 Temperatures (°C)			
	<i>Ave</i>	<i>Min</i>	<i>Max</i>	<i>SD</i>	<i>Ave</i>	<i>Min</i>	<i>Max</i>	<i>SD</i>
<i>Ceiling</i>	124.2	123.6	125.4	0.4	0.0	0.0	0.0	0.0
2375	162.6	155.9	170.1	2.6	139.9	135.4	147.1	2.3
2350	158.2	151.2	165.4	2.7	132.0	125.4	139.5	2.5
2300	137.1	128.9	145.4	2.9	122.9	117.7	130.1	2.2
2250	125.2	119.5	129.5	2.0	117.4	113.0	123.0	1.9
2200	115.4	109.5	120.1	2.3	106.2	101.9	111.9	1.8
2150	107.2	100.7	113.0	2.4	98.2	90.8	104.2	2.4
2100	98.0	93.1	103.1	2.1	86.4	73.8	93.1	3.5
1850	29.4	25.6	37.2	2.6	18.3	15.8	21.5	1.2
1600	26.5	24.4	29.6	1.2	19.1	16.9	21.5	0.8
1350	27.4	24.4	30.2	1.1	22.1	20.4	24.4	0.6
1100	23.8	22.1	26.7	0.9	23.3	22.1	24.4	0.6
900	22.9	21.5	25.0	0.7	22.8	21.5	23.9	0.4
600	23.8	22.7	25.6	0.6	21.7	21.0	23.3	0.5
300	24.4	23.3	25.6	0.5	21.8	19.8	22.7	0.5
<i>Floor</i>	54.0	51.7	55.2	0.8	22.9	22.1	23.9	0.4

Table A.12 Run 3 Temperatures for Field Tree 5 (Doorway)

TC height (mm)	Tree 5 Temperatures (°C)			
	<i>Ave</i>	<i>Min</i>	<i>Max</i>	<i>SD</i>
<i>1900</i>	225.2	217.0	237.5	3.9
<i>1750</i>	216.3	207.6	227.0	3.7
<i>1600</i>	209.6	200.0	220.5	3.4
<i>1450</i>	195.5	180.0	204.1	4.8
<i>1300</i>	136.0	107.2	157.7	10.3
<i>1150</i>	75.7	65.6	86.7	3.7
<i>1000</i>	41.4	29.1	52.3	5.1
<i>850</i>	25.3	22.7	28.5	1.4
<i>700</i>	28.9	26.2	32.0	1.1
<i>550</i>	22.9	21.0	25.6	0.9
<i>400</i>	21.2	19.8	22.7	0.6
<i>250</i>	21.3	19.2	23.9	0.8
<i>100</i>	31.5	29.6	34.3	1.1
<i>Floor</i>	102.1	101.3	103.7	0.5

Run 4: 55 kW Fire

Tables A.13 – A.16 below lists the average, minimum, maximum, and standard deviations of the temperatures recorded by the field trees for run number 4 (55 kW fire) during the 10 minute period starting from the 45th minute. Ambient temperature at the start of the experiment was 17.5°C.

Table A.13 Run 4 Temperatures for Field Trees 1, 2, and 3

TC height (mm)	Tree 1 Temperatures (°C)				Tree 2 Temperatures (°C)				Tree 3 Temperatures (°C)			
	<i>Ave</i>	<i>Min</i>	<i>Max</i>	<i>SD</i>	<i>Ave</i>	<i>Min</i>	<i>Max</i>	<i>SD</i>	<i>Ave</i>	<i>Min</i>	<i>Max</i>	<i>SD</i>
<i>Ceiling</i>	114.2	113.0	114.8	0.4	120.8	120.1	121.3	0.4	129.9	127.1	131.8	1.1
<i>2375</i>	129.3	127.1	132.4	1.1	131.6	127.7	135.4	1.5	131.9	123.0	141.2	4.0
<i>2350</i>	129.5	127.1	132.4	1.2	132.2	128.3	135.4	1.7	132.4	124.2	140.7	3.6
<i>2300</i>	131.0	128.3	134.2	1.2	132.5	128.3	136.5	1.8	131.6	123.0	141.2	3.6
<i>2250</i>	132.2	128.9	135.4	1.3	132.2	128.3	136.0	1.6	131.9	122.4	141.8	3.6
<i>2200</i>	132.2	128.9	134.8	1.2	131.8	128.9	135.4	1.5	130.9	121.9	141.2	3.9
<i>2150</i>	132.2	129.5	136.0	1.3	131.8	128.9	136.0	1.5	131.0	121.9	140.7	3.9
<i>2100</i>	132.3	129.5	136.0	1.3	131.0	127.7	134.8	1.5	130.0	120.1	138.3	4.0
<i>1850</i>	131.1	127.7	134.2	1.4	129.6	126.6	132.4	1.4	131.3	117.2	144.8	5.7
<i>1600</i>	125.5	121.3	128.9	1.7	123.6	119.5	127.1	1.6	134.3	115.4	154.2	7.7
<i>1350</i>	65.5	55.2	77.9	4.8	83.9	74.4	93.1	4.6	147.9	118.9	197.1	17.0
<i>1100</i>	45.1	42.4	47.6	1.0	56.9	48.8	65.1	4.2	172.4	127.7	258.5	27.1
<i>900</i>	41.9	39.5	44.1	0.9	52.2	48.8	58.7	2.3	233.6	169.5	341.0	41.6
<i>600</i>	43.0	39.5	45.3	1.2	43.4	40.1	47.6	1.5	405.2	293.8	614.6	67.2
<i>300</i>	42.1	38.3	45.3	1.6	43.4	40.1	47.6	1.7	630.3	593.9	692.9	22.5
<i>Floor</i>	74.1	72.6	75.6	0.6	88.3	87.3	89.0	0.5	0.0	0.0	0.0	0.0

Table A.14 Run 4 Temperatures for Field Trees 4, 6, and 7

TC height (mm)	Tree 4 Temperatures (°C)				Tree 6 Temperatures (°C)				Tree 7 Temperatures (°C)			
	<i>Ave</i>	<i>Min</i>	<i>Max</i>	<i>SD</i>	<i>Ave</i>	<i>Min</i>	<i>Max</i>	<i>SD</i>	<i>Ave</i>	<i>Min</i>	<i>Max</i>	<i>SD</i>
<i>Ceiling</i>	119.9	118.3	121.3	0.8	87.6	86.1	89.0	0.6	70.2	69.1	70.9	0.3
<i>2375</i>	124.7	118.3	132.4	2.9	105.8	102.5	108.9	1.4	88.1	84.9	91.9	1.2
<i>2350</i>	123.7	117.7	131.3	3.2	105.8	103.1	109.5	1.4	85.3	82.0	89.6	1.5
<i>2300</i>	121.6	116.0	128.3	2.9	101.9	96.6	106.6	2.1	72.8	67.4	76.7	1.9
<i>2250</i>	120.0	114.2	126.6	3.1	94.9	86.1	101.9	3.4	60.0	55.7	65.1	2.1
<i>2200</i>	119.7	114.2	125.4	2.9	81.4	73.8	91.4	3.9	53.6	48.8	58.7	2.2
<i>2150</i>	118.6	111.9	125.4	3.0	71.6	63.3	85.5	4.2	49.8	44.1	55.2	2.4
<i>2100</i>	117.6	111.3	124.2	3.1	59.0	49.9	75.0	4.0	45.8	40.6	51.7	2.1
<i>1850</i>	114.1	105.4	121.3	3.6	29.8	27.9	33.7	1.0	24.0	18.7	29.6	2.3
<i>1600</i>	108.4	98.4	118.3	4.2	23.5	21.0	25.6	1.2	17.1	14.6	18.7	0.7
<i>1350</i>	97.5	86.1	106.0	4.5	21.9	18.1	24.4	1.4	23.6	21.0	25.6	1.2
<i>1100</i>	64.3	59.2	69.7	2.5	22.7	19.8	25.0	1.4	23.2	21.0	25.6	1.1
<i>900</i>	51.2	48.2	54.6	1.4	20.7	18.7	22.7	1.0	21.1	19.8	22.7	0.8
<i>600</i>	50.8	47.0	56.9	1.7	18.4	16.9	19.2	0.5	21.9	20.4	22.7	0.5
<i>300</i>	31.9	27.3	37.7	2.2	19.2	18.1	20.4	0.6	18.0	16.9	19.2	0.5
<i>Floor</i>	94.8	93.7	95.5	0.4	36.8	36.0	37.2	0.3	32.3	31.4	33.1	0.4

Table A.15 Run 4 Temperatures for Field Trees 8 and 9

TC height (mm)	Tree 8 Temperatures (°C)				Tree 9 Temperatures (°C)			
	<i>Ave</i>	<i>Min</i>	<i>Max</i>	<i>SD</i>	<i>Ave</i>	<i>Min</i>	<i>Max</i>	<i>SD</i>
<i>Ceiling</i>	66.3	65.6	66.8	0.3	0.0	0.0	0.0	0.0
<i>2375</i>	85.4	83.2	87.8	1.2	76.3	73.2	79.7	1.2
<i>2350</i>	84.5	80.8	87.3	1.3	73.3	70.9	77.3	1.3
<i>2300</i>	74.4	70.3	77.9	1.6	69.0	66.2	72.1	1.2
<i>2250</i>	69.4	66.2	72.1	1.2	66.7	63.9	69.7	1.2
<i>2200</i>	64.5	61.6	68.0	1.4	60.9	58.1	63.9	1.2
<i>2150</i>	61.1	58.7	63.9	1.3	55.4	49.9	59.2	1.9
<i>2100</i>	55.5	53.4	58.7	1.1	47.3	40.1	51.7	2.6
<i>1850</i>	23.2	21.0	27.9	1.3	17.6	15.8	22.1	1.0
<i>1600</i>	22.0	18.7	23.9	1.1	19.5	18.7	21.0	0.6
<i>1350</i>	24.2	22.1	26.7	1.1	22.3	21.0	23.3	0.5
<i>1100</i>	23.3	21.5	24.4	0.7	23.1	22.1	23.9	0.5
<i>900</i>	22.6	21.5	23.9	0.5	22.8	21.5	23.9	0.5
<i>600</i>	23.0	22.1	23.9	0.5	21.9	20.4	22.7	0.5
<i>300</i>	23.6	22.1	25.0	0.6	21.8	19.8	23.3	0.8
<i>Floor</i>	34.8	33.1	36.0	0.7	20.9	20.4	21.5	0.3

Table A.16 Run 4 Temperatures for Field Tree 5 (Doorway)

TC height (mm)	Tree 5 Temperatures (°C)			
	<i>Ave</i>	<i>Min</i>	<i>Max</i>	<i>SD</i>
<i>1900</i>	116.9	111.9	121.3	2.3
<i>1750</i>	112.7	107.8	118.3	2.3
<i>1600</i>	109.7	106.0	116.0	2.1
<i>1450</i>	96.8	83.8	104.8	3.9
<i>1300</i>	55.4	43.0	72.6	5.5
<i>1150</i>	35.3	30.2	40.1	2.2
<i>1000</i>	21.8	18.1	26.2	1.9
<i>850</i>	18.2	16.4	20.4	0.8
<i>700</i>	20.8	18.7	22.7	0.9
<i>550</i>	18.0	16.9	19.2	0.6
<i>400</i>	18.2	16.4	19.2	0.6
<i>250</i>	17.8	16.4	19.2	0.7
<i>100</i>	24.7	22.7	26.7	1.0
<i>Floor</i>	53.0	51.1	54.6	1.0

Run 5: 55 kW Fire

Tables A.17 – A.20 below lists the average, minimum, maximum, and standard deviations of the temperatures recorded by the field trees for run number 5 (55 kW fire) during the 10 minute period starting from the 45th minute (results from this experiment were analysed in this report). Ambient temperature at the start of the experiment was 20°C.

Table A.17 Run 5 Temperatures for Field Trees 1, 2, and 3

TC height (mm)	Tree 1 Temperatures (°C)				Tree 2 Temperatures (°C)				Tree 3 Temperatures (°C)			
	<i>Ave</i>	<i>Min</i>	<i>Max</i>	<i>SD</i>	<i>Ave</i>	<i>Min</i>	<i>Max</i>	<i>SD</i>	<i>Ave</i>	<i>Min</i>	<i>Max</i>	<i>SD</i>
<i>Ceiling</i>	115.4	114.2	116.0	0.4	121.9	120.7	123.0	0.4	130.0	128.9	130.7	0.4
<i>2375</i>	130.6	128.9	132.4	0.7	132.5	130.7	134.8	0.9	132.2	124.2	139.5	2.7
<i>2350</i>	130.7	128.9	132.4	0.7	133.2	130.7	135.4	1.0	132.8	126.0	138.9	2.4
<i>2300</i>	132.2	130.1	133.6	0.7	133.8	130.7	137.1	1.3	131.8	125.4	138.3	2.6
<i>2250</i>	133.5	131.3	135.4	0.8	133.5	130.7	137.1	1.2	132.3	124.8	138.9	2.7
<i>2200</i>	133.3	131.3	135.4	0.8	132.9	130.7	136.5	1.0	131.2	123.0	138.3	3.1
<i>2150</i>	133.4	131.8	135.4	0.8	133.1	130.7	136.0	1.0	131.3	122.4	137.7	3.0
<i>2100</i>	133.4	131.8	135.4	0.8	132.1	130.1	134.2	0.9	130.3	121.9	137.1	3.0
<i>1850</i>	132.3	131.3	134.2	0.7	130.8	128.9	132.4	0.8	131.3	120.1	141.8	4.7
<i>1600</i>	127.1	123.6	130.7	1.5	125.2	122.4	127.1	1.1	133.7	121.3	150.1	6.7
<i>1350</i>	67.2	59.2	76.7	3.6	93.0	84.9	99.0	3.0	144.4	116.6	187.1	14.9
<i>1100</i>	48.96	47.0	51.1	0.8	57.5	53.4	63.9	2.4	169.2	120.7	228.7	24.5
<i>900</i>	46.05	44.1	47.6	0.8	55.4	53.4	58.1	0.9	228.6	154.2	322.1	38.1
<i>600</i>	47.04	44.7	49.4	0.9	48.2	46.4	51.1	0.9	404.0	273.6	612.9	63.6
<i>300</i>	45.9	43.5	47.6	0.7	47.3	43.0	50.5	2.0	568.0	549.4	605.7	8.8
<i>Floor</i>	77.97	76.7	79.1	0.4	89.7	89.0	90.8	0.3	0.0	0.0	0.0	0.0

Table A.18 Run 5 Temperatures for Field Trees 4, 6, and 7

TC height (mm)	Tree 4 Temperatures (°C)				Tree 6 Temperatures (°C)				Tree 7 Temperatures (°C)			
	<i>Ave</i>	<i>Min</i>	<i>Max</i>	<i>SD</i>	<i>Ave</i>	<i>Min</i>	<i>Max</i>	<i>SD</i>	<i>Ave</i>	<i>Min</i>	<i>Max</i>	<i>SD</i>
<i>Ceiling</i>	121.2	120.1	121.9	0.4	89.3	88.4	89.6	0.3	74.8	74.4	75.6	0.3
<i>2375</i>	126.1	119.5	130.7	2.0	107.3	104.8	109.5	0.9	92.4	89.6	94.3	0.9
<i>2350</i>	125.3	118.3	130.7	2.1	107.8	104.2	110.7	1.2	89.8	85.5	93.1	1.3
<i>2300</i>	123.2	117.7	127.7	1.8	104.6	99.6	108.9	2.0	78.0	74.4	82.6	1.6
<i>2250</i>	121.9	117.2	126.6	1.8	97.7	89.0	103.1	3.2	67.0	63.3	70.3	1.3
<i>2200</i>	121.4	117.7	126.6	1.7	84.1	75.0	91.9	3.5	61.3	58.1	63.9	1.4
<i>2150</i>	120.2	116.6	126.0	1.9	74.4	67.4	82.0	3.3	58.1	55.7	61.0	1.3
<i>2100</i>	119.2	115.4	123.6	1.9	62.6	56.3	70.3	2.9	54.6	51.7	57.5	1.2
<i>1850</i>	115.5	110.1	121.3	2.2	34.6	33.1	37.2	0.8	27.8	26.2	30.8	1.0
<i>1600</i>	110.4	101.3	115.4	2.9	28.6	26.2	30.2	0.9	25.3	22.7	27.9	1.0
<i>1350</i>	104.5	91.9	111.9	4.1	27.1	25.6	29.6	0.9	28.4	26.7	30.2	0.6
<i>1100</i>	71.8	65.1	82.0	3.2	27.2	25.6	29.1	0.7	28.0	26.7	29.6	0.6
<i>900</i>	57.2	53.4	59.8	1.3	25.8	24.4	27.3	0.5	26.1	25.0	27.3	0.5
<i>600</i>	55.7	52.3	59.2	1.4	23.4	22.1	24.4	0.5	26.4	25.0	27.9	0.6
<i>300</i>	34.8	32.0	40.1	1.6	23.8	22.7	25.0	0.5	21.8	21.0	22.7	0.4
<i>Floor</i>	98.9	97.8	99.6	0.4	41.1	40.1	41.8	0.4	36.7	36.0	37.7	0.4

Table A.19 Run 5 Temperatures for Field Trees 8 and 9

TC height (mm)	Tree 8 Temperatures (°C)				Tree 9 Temperatures (°C)			
	<i>Ave</i>	<i>Min</i>	<i>Max</i>	<i>SD</i>	<i>Ave</i>	<i>Min</i>	<i>Max</i>	<i>SD</i>
<i>Ceiling</i>	68.7	68.0	69.1	0.3	0.0	0.0	0.0	0.0
2375	87.4	84.3	90.8	1.2	78.6	76.2	80.8	0.9
2350	86.5	83.8	90.2	1.1	76.5	73.8	79.1	1.0
2300	78.2	75.6	82.0	1.2	73.0	70.9	75.6	0.9
2250	73.9	72.1	76.7	0.9	71.2	68.6	73.8	0.9
2200	69.8	67.4	72.6	1.1	66.3	64.5	68.6	0.8
2150	66.9	64.5	69.1	1.1	62.2	59.8	64.5	0.8
2100	62.0	59.8	64.5	1.0	55.1	52.3	57.5	1.2
1850	28.9	27.3	31.4	0.7	22.7	21.5	24.4	0.5
1600	27.5	25.6	29.6	0.8	25.7	24.4	26.7	0.5
1350	29.5	27.9	32.0	0.7	28.3	27.3	29.6	0.5
1100	28.4	27.3	29.6	0.5	28.8	27.9	29.6	0.5
900	27.7	26.2	29.1	0.6	28.2	27.3	29.1	0.5
600	27.5	26.2	28.5	0.5	26.6	25.6	28.5	0.5
300	26.7	25.6	27.9	0.5	25.3	23.9	26.2	0.5
<i>Floor</i>	39.8	38.9	40.6	0.3	23.0	22.7	23.9	0.3

Table A.20 Run 5 Temperatures for Field Tree 5 (Doorway)

TC height (mm)	Tree 5 Temperatures (°C)			
	<i>Ave</i>	<i>Min</i>	<i>Max</i>	<i>SD</i>
<i>1900</i>	118.7	116.6	122.4	1.4
<i>1750</i>	115.1	113.0	118.3	1.2
<i>1600</i>	112.9	108.9	116.6	1.3
<i>1450</i>	104.1	93.7	109.5	2.4
<i>1300</i>	66.7	58.7	80.8	3.7
<i>1150</i>	44.4	39.5	47.6	1.7
<i>1000</i>	26.8	25.6	29.1	0.6
<i>850</i>	23.7	22.7	25.0	0.4
<i>700</i>	26.1	25.0	27.3	0.5
<i>550</i>	22.9	22.1	23.9	0.4
<i>400</i>	23.0	22.1	23.9	0.5
<i>250</i>	22.4	21.0	23.3	0.5
<i>100</i>	29.4	27.3	30.8	0.7
<i>Floor</i>	55.1	54.6	55.7	0.3

Run 6: 160 kW Fire

Tables A.21 – A.24 below lists the average, minimum, maximum, and standard deviations of the temperatures recorded by the field trees for run number 6 (160 kW fire) during the 10 minute period starting from the 45th minute. Ambient temperature at the start of the experiment was 15°C.

Table A.21 Run 6 Temperatures for Field Trees 1, 2, and 3

TC height (mm)	Tree 1 Temperatures (°C)				Tree 2 Temperatures (°C)				Tree 3 Temperatures (°C)			
	<i>Ave</i>	<i>Min</i>	<i>Max</i>	<i>SD</i>	<i>Ave</i>	<i>Min</i>	<i>Max</i>	<i>SD</i>	<i>Ave</i>	<i>Min</i>	<i>Max</i>	<i>SD</i>
<i>Ceiling</i>	223.4	222.3	224.6	0.5	237.8	236.9	238.7	0.4	255.7	254.4	256.7	0.6
<i>2375</i>	254.5	250.9	259.1	1.7	262.6	257.3	270.7	2.6	268.5	256.1	285.2	6.0
<i>2350</i>	255.7	251.5	260.2	1.9	265.2	258.5	273.6	3.0	268.2	256.7	284.6	5.5
<i>2300</i>	258.9	253.2	264.9	2.1	267.7	259.6	282.9	3.6	268.0	253.8	288.6	6.2
<i>2250</i>	261.8	255.6	269.5	2.4	266.5	259.6	278.2	2.9	268.9	253.2	297.3	6.4
<i>2200</i>	261.7	256.7	268.9	2.2	264.8	259.1	275.3	2.5	267.9	248.6	300.8	6.9
<i>2150</i>	262.0	256.7	269.5	2.2	265.9	259.6	277.1	2.6	267.6	247.4	302.5	6.9
<i>2100</i>	261.9	257.3	268.4	2.1	264.4	258.5	270.1	2.2	266.9	249.2	305.4	7.3
<i>1850</i>	259.6	255.6	264.9	1.7	260.7	256.1	266.6	1.9	271.5	245.7	334.1	11.2
<i>1600</i>	252.6	244.5	258.5	2.6	251.0	243.9	258.5	2.7	279.9	248.6	367.2	16.3
<i>1350</i>	141.8	118.9	174.8	11.2	197.9	177.7	209.4	6.2	278.5	231.6	386.5	26.9
<i>1100</i>	91.9	84.3	97.2	3.0	98.2	87.3	109.5	5.0	292.9	232.2	438.3	38.3
<i>900</i>	83.3	76.2	89.6	2.7	96.0	90.2	103.7	2.5	338.4	266.6	499.2	43.8
<i>600</i>	85.5	77.9	93.1	3.3	82.8	76.7	88.4	2.3	454.2	342.7	643.8	60.3
<i>300</i>	82.7	77.9	88.4	2.1	88.2	80.2	97.2	4.5	456.2	446.7	471.9	3.8
<i>Floor</i>	164.9	163.0	165.9	0.7	182.3	181.2	183.0	0.5	0.0	0.0	0.0	0.0

Table A.22 Run 6 Temperatures for Field Trees 4, 6, and 7

TC height (mm)	Tree 4 Temperatures (°C)				Tree 6 Temperatures (°C)				Tree 7 Temperatures (°C)			
	<i>Ave</i>	<i>Min</i>	<i>Max</i>	<i>SD</i>	<i>Ave</i>	<i>Min</i>	<i>Max</i>	<i>SD</i>	<i>Ave</i>	<i>Min</i>	<i>Max</i>	<i>SD</i>
<i>Ceiling</i>	237.0	235.7	238.1	0.5	168.3	167.1	168.9	0.4	143.8	143.0	145.4	0.6
<i>2375</i>	257.1	243.3	270.7	5.0	204.4	200.0	210.6	2.1	179.8	175.3	187.7	2.3
<i>2350</i>	256.6	241.6	271.3	5.8	208.0	202.4	215.3	2.5	177.1	172.4	187.1	2.7
<i>2300</i>	251.5	240.4	266.6	4.7	206.4	197.7	214.7	3.3	153.0	143.6	164.2	3.4
<i>2250</i>	248.0	236.3	262.5	4.6	198.1	184.7	208.2	4.1	125.0	118.3	131.8	2.5
<i>2200</i>	246.7	239.2	259.6	4.1	180.5	167.7	191.8	4.7	110.6	103.7	119.5	2.9
<i>2150</i>	243.5	233.4	257.9	4.5	168.0	151.2	185.3	6.2	101.4	93.7	108.9	3.0
<i>2100</i>	239.8	229.3	252.6	4.4	145.9	126.0	168.3	8.0	93.5	84.9	101.3	3.0
<i>1850</i>	226.6	217.0	238.7	3.8	53.6	48.8	59.2	1.9	48.6	41.2	55.7	3.1
<i>1600</i>	213.7	199.4	225.8	4.8	36.7	34.8	38.9	0.8	26.8	25.0	30.2	1.0
<i>1350</i>	200.0	187.7	215.3	5.8	34.7	30.8	37.7	1.5	31.6	29.6	34.3	0.9
<i>1100</i>	152.9	138.9	166.5	6.0	29.4	27.9	31.4	0.9	28.2	26.7	29.6	0.5
<i>900</i>	111.8	103.1	121.3	3.8	26.5	25.6	28.5	0.6	24.6	23.3	25.6	0.5
<i>600</i>	96.9	89.6	108.9	3.6	24.9	23.9	26.2	0.5	28.8	27.3	30.2	0.6
<i>300</i>	59.7	48.2	68.0	3.6	25.7	24.4	26.7	0.6	21.9	20.4	23.3	0.5
<i>Floor</i>	201.7	200.6	202.4	0.4	73.6	72.6	74.4	0.4	60.3	58.7	61.0	0.4

Table A.23 Run 6 Temperatures for Field Trees 8 and 9

TC height (mm)	Tree 8 Temperatures (°C)				Tree 9 Temperatures (°C)			
	<i>Ave</i>	<i>Min</i>	<i>Max</i>	<i>SD</i>	<i>Ave</i>	<i>Min</i>	<i>Max</i>	<i>SD</i>
<i>Ceiling</i>	126.0	125.4	126.6	0.3	0.0	0.0	0.0	0.0
<i>2375</i>	163.4	156.5	171.2	2.4	141.7	136.5	147.1	2.0
<i>2350</i>	160.0	153.0	167.1	2.3	134.9	129.5	140.7	2.1
<i>2300</i>	141.0	136.0	145.9	2.2	126.0	123.0	129.5	1.6
<i>2250</i>	129.6	126.6	133.0	1.6	121.5	118.3	125.4	1.4
<i>2200</i>	120.8	116.6	126.6	1.9	110.9	107.8	113.6	1.3
<i>2150</i>	113.2	108.3	118.9	1.9	103.2	100.1	106.6	1.2
<i>2100</i>	104.8	100.1	109.5	1.6	93.5	89.6	97.2	1.6
<i>1850</i>	31.8	29.6	39.5	1.8	24.0	22.1	25.6	0.6
<i>1600</i>	32.6	29.1	35.4	1.2	23.8	22.1	25.6	0.7
<i>1350</i>	30.2	28.5	33.1	0.9	25.8	24.4	26.7	0.5
<i>1100</i>	26.4	25.0	27.3	0.5	26.6	25.6	27.3	0.4
<i>900</i>	25.6	24.4	26.2	0.4	25.7	25.0	26.7	0.4
<i>600</i>	26.4	25.6	27.3	0.4	24.1	23.3	25.0	0.4
<i>300</i>	26.9	25.6	27.9	0.4	24.2	23.3	25.0	0.4
<i>Floor</i>	52.6	51.7	53.4	0.3	23.5	22.7	24.4	0.4

Table A.24 Run 6 Temperatures for Field Tree 5 (Doorway)

TC height (mm)	Tree 5 Temperatures (°C)			
	<i>Ave</i>	<i>Min</i>	<i>Max</i>	<i>SD</i>
<i>1900</i>	230.2	222.9	237.5	3.1
<i>1750</i>	220.0	213.5	228.7	2.7
<i>1600</i>	213.3	206.5	221.1	2.8
<i>1450</i>	200.3	188.9	210.6	3.6
<i>1300</i>	145.1	126.0	168.3	8.7
<i>1150</i>	86.1	76.7	93.7	3.3
<i>1000</i>	48.1	40.6	59.2	3.5
<i>850</i>	27.9	26.7	30.8	0.7
<i>700</i>	32.0	30.2	34.3	0.5
<i>550</i>	26.2	25.0	27.3	0.5
<i>400</i>	24.7	22.7	26.2	0.7
<i>250</i>	24.8	22.1	26.7	0.8
<i>100</i>	35.2	32.5	38.3	1.2
<i>Floor</i>	107.0	105.4	108.3	0.5

Run 7: 110 kW Corner Fire

Tables A.25 – A.28 below lists the average, minimum, maximum, and standard deviations of the temperatures recorded by the field trees for run number 7 (110 kW corner fire) during the 10 minute period starting from the 45th minute (results from this experiment were analysed in this report). Ambient temperature at the start of the experiment was 20.5°C.

Table A.25 Run 7 Temperatures for Field Trees 1, 2, and 3

TC height (mm)	Tree 1 Temperatures (°C)				Tree 2 Temperatures (°C)				Tree 3 Temperatures (°C)			
	<i>Ave</i>	<i>Min</i>	<i>Max</i>	<i>SD</i>	<i>Ave</i>	<i>Min</i>	<i>Max</i>	<i>SD</i>	<i>Ave</i>	<i>Min</i>	<i>Max</i>	<i>SD</i>
<i>Ceiling</i>	289.1	287.5	291.0	0.7	271.6	270.1	273.0	0.6	256.1	255.0	257.9	0.6
<i>2375</i>	336.2	308.8	361.5	9.5	324.8	313.5	340.4	6.3	310.3	295.6	324.4	4.6
<i>2350</i>	333.8	311.7	355.8	9.3	321.3	310.6	334.7	5.0	308.5	293.8	319.8	4.3
<i>2300</i>	327.8	305.4	347.3	9.1	318.0	308.3	333.0	5.1	308.0	297.3	317.5	3.8
<i>2250</i>	313.6	291.0	341.6	8.7	313.0	301.9	326.7	5.0	302.1	293.8	309.4	3.0
<i>2200</i>	302.7	284.6	320.4	7.1	302.1	295.0	312.3	3.7	300.5	293.3	307.7	3.1
<i>2150</i>	289.1	275.3	304.2	5.4	294.7	288.6	302.5	3.2	295.3	289.2	303.7	2.8
<i>2100</i>	278.8	266.6	289.8	4.7	283.7	277.6	289.2	2.4	287.9	282.9	296.7	2.4
<i>1850</i>	235.2	213.5	246.2	6.0	242.5	236.3	246.8	2.1	236.6	229.9	242.2	2.5
<i>1600</i>	146.9	135.4	163.0	5.5	170.3	157.7	178.9	3.1	161.6	156.5	167.7	2.1
<i>1350</i>	110.5	103.7	119.5	3.0	140.3	124.8	153.0	4.7	146.6	141.2	152.4	2.5
<i>1100</i>	83.2	79.1	89.0	1.9	103.0	95.5	116.6	4.0	144.2	137.7	153.0	2.7
<i>900</i>	77.7	75.0	82.6	1.5	106.1	101.9	110.1	1.7	123.7	117.2	132.4	2.6
<i>600</i>	82.5	79.1	86.7	1.5	93.6	89.0	99.0	2.2	106.0	102.5	110.7	1.5
<i>300</i>	82.7	77.9	87.8	2.0	72.6	65.1	82.0	4.2	67.8	64.5	73.8	1.7
<i>Floor</i>	207.4	205.3	208.8	0.9	174.5	172.4	175.9	0.9	0.0	0.0	0.0	0.0

Table A.26 Run 7 Temperatures for Field Trees 4, 6, and 7

TC height (mm)	Tree 4 Temperatures (°C)				Tree 6 Temperatures (°C)				Tree 7 Temperatures (°C)			
	<i>Ave</i>	<i>Min</i>	<i>Max</i>	<i>SD</i>	<i>Ave</i>	<i>Min</i>	<i>Max</i>	<i>SD</i>	<i>Ave</i>	<i>Min</i>	<i>Max</i>	<i>SD</i>
<i>Ceiling</i>	229.9	228.1	231.1	0.7	180.7	180.0	181.8	0.4	149.5	148.3	151.8	0.6
<i>2375</i>	280.9	275.3	288.6	2.3	226.1	219.9	233.4	3.0	191.8	185.3	198.3	2.6
<i>2350</i>	288.8	281.7	296.7	2.8	224.3	215.3	235.1	4.3	184.5	176.5	191.2	2.6
<i>2300</i>	289.0	283.4	295.0	2.4	187.5	170.6	204.1	6.3	127.0	115.4	138.3	4.3
<i>2250</i>	290.0	283.4	296.7	2.5	128.6	120.1	142.4	4.1	77.1	72.1	83.2	2.5
<i>2200</i>	285.8	280.5	291.0	2.1	101.3	97.2	104.8	1.7	64.4	60.4	69.1	1.8
<i>2150</i>	283.0	277.6	288.1	2.1	87.6	83.8	92.5	2.0	63.2	59.2	67.4	1.6
<i>2100</i>	280.3	275.9	284.6	2.0	74.6	71.5	79.1	1.6	58.9	55.2	62.7	1.6
<i>1850</i>	238.8	230.5	247.4	3.4	53.2	51.1	56.3	1.0	40.7	36.6	45.9	1.8
<i>1600</i>	145.3	140.7	149.5	1.9	41.4	37.7	43.5	1.0	36.7	34.3	39.5	1.1
<i>1350</i>	123.4	120.7	126.6	1.3	41.8	38.9	44.7	1.2	39.1	37.2	41.2	1.0
<i>1100</i>	102.0	99.0	106.6	1.4	38.1	35.4	41.8	1.4	36.0	34.3	38.9	1.1
<i>900</i>	82.5	79.7	85.5	1.4	34.1	32.5	36.6	0.8	31.6	29.6	33.7	0.7
<i>600</i>	83.5	79.7	89.0	1.9	31.6	30.8	32.5	0.5	31.2	30.2	32.5	0.4
<i>300</i>	61.4	56.3	66.8	2.0	31.4	30.2	32.5	0.5	26.9	26.2	27.9	0.4
<i>Floor</i>	146.3	144.8	147.7	0.6	77.0	75.6	77.9	0.5	62.6	61.6	63.3	0.5

Table A.27 Run 7 Temperatures for Field Trees 8 and 9

TC height (mm)	Tree 8 Temperatures (°C)				Tree 9 Temperatures (°C)			
	<i>Ave</i>	<i>Min</i>	<i>Max</i>	<i>SD</i>	<i>Ave</i>	<i>Min</i>	<i>Max</i>	<i>SD</i>
<i>Ceiling</i>	128.1	127.1	129.5	0.6	0.0	0.0	0.0	0.0
<i>2375</i>	171.6	166.5	177.7	2.0	148.8	143.6	152.4	1.9
<i>2350</i>	164.9	158.9	170.1	2.4	130.9	125.4	134.8	2.1
<i>2300</i>	119.4	111.9	127.1	3.3	110.7	104.8	116.0	2.2
<i>2250</i>	96.7	91.4	103.7	2.6	99.0	94.3	103.7	2.1
<i>2200</i>	83.2	77.3	92.5	3.0	82.3	79.1	84.9	1.4
<i>2150</i>	75.7	72.1	81.4	2.1	72.3	69.1	75.6	1.2
<i>2100</i>	70.0	66.8	73.8	1.4	64.5	60.4	66.8	1.2
<i>1850</i>	40.4	36.6	47.0	2.0	29.5	27.3	30.8	0.6
<i>1600</i>	35.8	33.7	38.9	0.9	31.7	30.2	33.7	0.9
<i>1350</i>	37.5	34.8	40.1	1.2	32.4	31.4	33.7	0.4
<i>1100</i>	33.6	32.0	35.4	0.8	32.9	32.0	33.7	0.4
<i>900</i>	32.1	30.8	33.7	0.5	31.9	30.8	32.5	0.4
<i>600</i>	31.9	30.2	33.1	0.5	29.9	29.1	30.8	0.4
<i>300</i>	30.8	29.6	32.0	0.4	28.1	27.3	29.1	0.5
<i>Floor</i>	52.3	51.7	53.4	0.5	26.3	25.6	26.7	0.3

Table A.28 Run 7 Temperatures for Field Tree 5 (Doorway)

TC height (mm)	Tree 5 Temperatures (°C)			
	<i>Ave</i>	<i>Min</i>	<i>Max</i>	<i>SD</i>
<i>1900</i>	270.3	264.9	273.6	1.8
<i>1750</i>	189.4	171.2	208.2	7.1
<i>1600</i>	121.7	118.3	126.0	1.5
<i>1450</i>	101.1	98.4	103.7	1.2
<i>1300</i>	81.5	79.7	83.8	0.7
<i>1150</i>	68.8	66.2	70.9	0.9
<i>1000</i>	48.0	40.1	55.7	3.6
<i>850</i>	34.1	32.5	36.0	0.6
<i>700</i>	37.4	36.6	39.5	0.5
<i>550</i>	31.8	30.8	33.1	0.5
<i>400</i>	30.4	29.1	31.4	0.5
<i>250</i>	29.9	28.5	31.4	0.6
<i>100</i>	39.5	37.7	42.4	1.0
<i>Floor</i>	101.1	99.6	102.5	0.8

Appendix 2: Tabulated Surface Temperatures

Tables A.29 and A.30 below list the temperatures recorded by the surface thermocouples which were located on the floor and ceiling of the two-compartment structure. Temperature entries with N/A indicate that no surface thermocouple was positioned in line with that particular field tree.

Table A.29 Tabulated Floor Temperatures

Fire Size	Thermocouple Position (Tree Number)								
	<i>1</i>	<i>2</i>	<i>3</i>	<i>4</i>	<i>5</i>	<i>6</i>	<i>7</i>	<i>8</i>	<i>9</i>
<i>55 kW</i>	78.0	89.7	N/A	98.9	55.1	41.1	36.7	39.8	23.0
<i>110 kW</i>	125.8	140.5	N/A	150.6	77.6	52.9	45.3	44.4	22.6
<i>160 kW</i>	161.7	181.7	N/A	199.5	102.1	68.4	56.4	54.0	22.9
<i>110 kW_c</i>	207.4	174.5	N/A	146.3	101.1	77.0	62.6	52.3	26.3

Table A.30 Tabulated Ceiling Temperatures

Fire Size	Thermocouple Position (Tree Number)								
	<i>1</i>	<i>2</i>	<i>3</i>	<i>4</i>	<i>5</i>	<i>6</i>	<i>7</i>	<i>8</i>	<i>9</i>
<i>55 kW</i>	115.4	121.9	130.0	121.2	N/A	89.3	74.8	68.7	N/A
<i>110 kW</i>	176.7	187.2	198.7	184.6	N/A	131.6	109.7	100.3	N/A
<i>160 kW</i>	220.0	235.4	249.9	232.4	N/A	164.4	138.5	124.2	N/A
<i>110 kW_c</i>	289.1	271.6	256.1	229.9	N/A	180.7	149.5	128.1	N/A

Appendix 3: Reproducibility

From 26 November to 1 December 1999, 7 experiments were conducted at McLeans Island. All LPG fires were 55 kW, 110 kW, or 160 kW in size. Of the 7 experiments conducted there were: two 55 kW fires, two 110 kW fires (one in the corner), and three 160 kW fires. Initially, the experiments were conducted with sand as the dispersing agent in the burner. A small quantity of the sand was blown out of the burner at the beginning of the experiments when the main supply of LPG was turned on. This was caused by the sand being too fine to allow the LPG to filter through evenly. To solve this problem, the sand was replaced by coarse gravel. Also, for the first four experiments the doors to the large shed that housed the two-compartment structure were open. The doors to the shed were closed for the 3 later runs to prevent wind from influencing further experiments.

Table A.31 below lists the conditions of each experiment regarding what was used as a dispersing agent in the burner, and whether or not the doors to the shed were open or closed.

Table A.31 Conditions for Each Run

Experiment (Run #, Fire size)	Burner Disperser	Doors Closed? (yes/no)
<i>Run 1 110 kW*</i>	sand	no
<i>Run 2 160 kW</i>	sand	no
<i>Run 3 160 kW*</i>	gravel	no
<i>Run 4 55 kW</i>	gravel	no
<i>Run 5 55 kW*</i>	gravel	yes
<i>Run 6 160 kW</i>	gravel	yes
<i>Run 7 110 kW* (corner)</i>	gravel	yes

* Asterisk indicates these runs were analysed in the main section of this report.

As can be seen from the above table, the 55 kW, 110 kW, 160 kW, and 110 kW corner fires that were analysed in this report were not conducted under the same conditions. Therefore, to justify making comparisons between each fire, it was necessary to determine if the additional variables of changing the disperser type and closing the doors had any influence on the results.

The following comparisons between experiments were made to determine if changing the disperser and closing the doors influenced results:

1. **Run 5 vs. Run 4.** This determined if closing the doors affected the 55 kW fire.
2. **Run 3 vs. Run 2.** This determined if changing the disperser affected the 160 kW fire.
3. **Run 3 vs. Run 6.** This determined if closing the doors affected the 160 kW fire.

Comparisons were made between each thermocouple on each tree. The difference between thermocouples was determined, and expressed as a percentage:

$$Difference(\%) = \frac{E - R}{E} \times 100$$

Where E is the temperature for either Run 3 or Run 5 (Kelvin), and R is the temperature for Runs 2, 4, and 6 (Kelvin).

Runs 2, 4, and 6 were analysed in a manner identical to Runs 3 and 5, i.e. temperatures were determined by averaging results between the 45th and 55th minute, which were then compared with Runs 3 and 5. Results of the comparisons are listed in Tables A.32 – A.38 below, with a table allocated to each field tree.

Table A.32 Results for Tree 1 Comparisons

Thermocouple Height (mm)	Run 5 vs. Run 4	Run 3 vs. Run 2	Run 3 vs. Run 6
<i>Ceiling</i>	0.33%	-1.49%	-0.69%
2375	0.32%	-1.95%	-0.92%
2350	0.30%	-1.83%	-0.95%
2300	0.31%	-1.90%	-0.99%
2250	0.31%	-1.97%	-1.00%
2200	0.28%	-1.98%	-1.01%
2150	0.28%	-2.05%	-1.02%
2100	0.27%	-1.98%	-1.04%
1850	0.28%	-1.82%	-1.08%
1600	0.41%	-1.54%	-1.09%
1350	0.51%	0.38%	-0.14%
1100	1.20%	0.01%	-0.85%
900	1.30%	-0.03%	-1.01%
600	1.27%	-0.48%	-0.89%
300	1.19%	-0.64%	-1.07%
<i>Floor</i>	1.11%	0.20%	-0.74%

Table A.33 Results for Tree 2 Comparisons

Thermocouple Height (mm)	Run 5 vs. Run 4	Run 3 vs. Run 2	Run 3 vs. Run 6
<i>Ceiling</i>	0.26%	-1.40%	-0.46%
2375	0.22%	-1.97%	-0.99%
2350	0.25%	-2.04%	-1.12%
2300	0.32%	-2.18%	-1.17%
2250	0.32%	-2.23%	-0.96%
2200	0.29%	-2.16%	-1.12%
2150	0.31%	-2.13%	-1.18%
2100	0.26%	-1.95%	-1.14%
1850	0.29%	-1.78%	-1.08%
1600	0.42%	-1.41%	-1.15%
1350	2.47%	1.20%	-1.82%
1100	0.20%	-0.67%	-0.59%
900	0.99%	-1.09%	-1.33%
600	1.49%	0.95%	-1.68%
300	1.21%	-1.18%	-2.47%
<i>Floor</i>	0.39%	1.76%	-0.13%

Table A.34 Results for Tree 3 Comparisons

Thermocouple Height (mm)	Run 5 vs. Run 4	Run 3 vs. Run 2	Run 3 vs. Run 6
<i>Ceiling</i>	0.02%	-2.02%	-1.11%
2375	0.07%	-2.56%	-1.22%
2350	0.10%	-2.33%	-1.28%
2300	0.06%	-2.28%	-1.33%
2250	0.08%	-2.20%	-1.43%
2200	0.09%	-2.43%	-1.53%
2150	0.07%	-2.52%	-1.57%
2100	0.09%	-2.54%	-1.69%
1850	-0.01%	-2.86%	-1.76%
1600	-0.14%	-2.99%	-1.83%
1350	-0.84%	0.54%	-0.79%
1100	-0.72%	1.76%	-0.17%
900	-0.98%	1.77%	0.76%
600	-0.19%	2.46%	4.07%
300	-7.41%	-35.39%	-1.45%
<i>Floor</i>			

Table A.35 Results for Tree 4 Comparisons

Thermocouple Height (mm)	Run 5 vs. Run 4	Run 3 vs. Run 2	Run 3 vs. Run 6
<i>Ceiling</i>	0.32%	-2.18%	-0.91%
2375	0.36%	-3.13%	-1.64%
2350	0.42%	-3.18%	-1.66%
2300	0.41%	-3.09%	-1.52%
2250	0.47%	-3.04%	-1.77%
2200	0.43%	-2.84%	-1.68%
2150	0.42%	-2.73%	-1.65%
2100	0.40%	-2.70%	-1.59%
1850	0.38%	-2.00%	-1.66%
1600	0.53%	-1.03%	-1.79%
1350	1.86%	0.88%	-1.97%
1100	2.18%	1.79%	-2.35%
900	1.79%	0.03%	-1.98%
600	1.52%	-1.21%	-2.06%
300	0.96%	-0.94%	-4.20%
<i>Floor</i>	1.09%	1.40%	-0.46%

Table A.36 Results for Tree 5 (Doorway) Comparisons

Thermocouple Height (mm)	Run 5 vs. Run 4	Run 3 vs. Run 2	Run 3 vs. Run 6
<i>Ceiling</i>	N/A	N/A	N/A
1900	0.46%	-2.66%	-1.01%
1750	0.64%	-2.35%	-0.76%
1600	0.83%	-1.79%	-0.75%
1450	1.94%	-0.97%	-1.03%
1300	3.33%	0.30%	-2.23%
1150	2.87%	-2.43%	-2.98%
1000	1.69%	-3.16%	-2.12%
850	1.86%	-0.21%	-0.87%
700	1.79%	1.54%	-1.04%
550	1.67%	0.03%	-1.11%
400	1.64%	0.17%	-1.19%
250	1.57%	0.41%	-1.19%
100	1.56%	0.53%	-1.22%
<i>Floor</i>	0.66%	-0.11%	-1.31%

Table A.37 Results for Tree 6 Comparisons

Thermocouple Height (mm)	Run 5 vs. Run 4	Run 3 vs. Run 2	Run 3 vs. Run 6
<i>Ceiling</i>	0.47%	-1.40%	-0.88%
2375	0.39%	-2.72%	-0.26%
2350	0.51%	-2.63%	-0.50%
2300	0.73%	-2.36%	-0.66%
2250	0.75%	-2.15%	-0.48%
2200	0.77%	-1.56%	-0.47%
2150	0.81%	-1.11%	-0.41%
2100	1.07%	-0.71%	-0.48%
1850	1.56%	0.14%	-1.56%
1600	1.67%	0.02%	-1.58%
1350	1.72%	-0.50%	-1.50%
1100	1.50%	-0.28%	-0.40%
900	1.72%	0.10%	-0.68%
600	1.69%	0.17%	-1.15%
300	1.53%	0.37%	-1.33%
<i>Floor</i>	1.38%	-0.29%	-1.51%

Table A.38 Results for Tree 7 Comparisons

Thermocouple Height (mm)	Run 5 vs. Run 4	Run 3 vs. Run 2	Run 3 vs. Run 6
<i>Ceiling</i>	1.33%	-1.37%	-1.29%
2375	1.16%	-2.31%	-0.78%
2350	1.25%	-2.28%	-0.80%
2300	1.49%	-1.26%	-1.15%
2250	2.05%	-0.65%	-2.03%
2200	2.30%	-0.36%	-2.52%
2150	2.51%	0.08%	-2.87%
2100	2.69%	0.31%	-3.15%
1850	1.26%	1.05%	-3.53%
1600	2.74%	0.14%	-2.21%
1350	1.60%	-0.07%	-0.93%
1100	1.57%	0.15%	-0.34%
900	1.67%	0.27%	-0.69%
600	1.52%	0.48%	-1.82%
300	1.28%	0.41%	-1.16%
<i>Floor</i>	1.42%	-0.46%	-1.19%

Table A.39 Results for Tree 8 Comparisons

Thermocouple Height (mm)	Run 5 vs. Run 4	Run 3 vs. Run 2	Run 3 vs. Run 6
<i>Ceiling</i>	0.69%	-1.23%	-0.46%
2375	0.56%	-2.04%	-0.17%
2350	0.57%	-1.99%	-0.43%
2300	1.08%	-1.35%	-0.95%
2250	1.29%	-1.00%	-1.12%
2200	1.54%	-0.77%	-1.40%
2150	1.71%	-0.63%	-1.59%
2100	1.94%	-0.56%	-1.83%
1850	1.90%	-0.68%	-0.79%
1600	1.82%	0.06%	-2.01%
1350	1.74%	0.38%	-0.93%
1100	1.71%	0.33%	-0.88%
900	1.69%	0.37%	-0.91%
600	1.49%	0.42%	-0.88%
300	1.04%	0.38%	-0.83%
<i>Floor</i>	1.60%	0.15%	0.42%

Table A.40 Results for Tree 9 Comparisons

Thermocouple Height (mm)	Run 5 vs. Run 4	Run 3 vs. Run 2	Run 3 vs. Run 6
<i>Ceiling</i>	N/A	N/A	N/A
2375	0.63%	-1.66%	-0.43%
2350	0.91%	-1.38%	-0.74%
2300	1.15%	-1.30%	-0.78%
2250	1.32%	-1.08%	-1.07%
2200	1.61%	-0.90%	-1.24%
2150	2.04%	-0.77%	-1.36%
2100	2.36%	-0.69%	-1.95%
1850	1.74%	0.07%	-1.94%
1600	2.06%	0.42%	-1.63%
1350	1.99%	0.47%	-1.26%
1100	1.89%	0.47%	-1.12%
900	1.81%	0.49%	-0.97%
600	1.59%	0.49%	-0.79%
300	1.19%	0.40%	-0.82%
<i>Floor</i>	0.70%	-0.66%	-0.20%

The following conclusions can be drawn from the tables above:

1. Comparisons between the thermocouples vary less than 4 % for most trees, particularly in the fire compartment.
2. For trees in the adjacent compartment, the temperature differences increase further away than those in the fire compartment.
3. For the trees in the adjacent compartment, temperature differences increase for the thermocouples that are not in the ceiling jet.
4. Temperature differences are larger for the 55 kW fire than those of the 160 kW fire.

The first point indicates that changing the disperser or closing the doors made little difference to the results. The second point indicates that variations in ambient temperature affect the trees that are further from the fire. The third point again indicates that variations in ambient temperature affect thermocouples that are not located where the fires hot lighter gases are present. The fourth point once again

indicates that changes in ambient temperature will affect temperatures measured for the 55 kW fire, as it produces lower temperatures than the 160 kW fire.

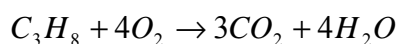
Overall, it appears that changing the disperser and closing the doors made little difference to the results obtained. This analysis has also shown that experiments conducted were reproducible. Ideally, all experiments (different fires, and different fire locations) need to be repeated to authenticate results. However, for the purpose of this report it has been demonstrated that the fire experiments conducted, can be compared justifiably with changes in the gas disperser and closing the doors, as changing these variables does not significantly influence results.

Appendix 4: Gas Analysis – Background Theory

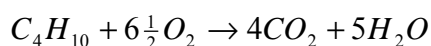
LPG was used to provide the combustible gas for the burner in the compartment experiments. LPG is a mixture of roughly 80% propane (C_3H_8) and 20% butane (C_4H_{10}), to which a small amount of highly pungent ethyl mercaptan (CH_3CH_2SH) has been added so that a leak can be easily smelt.

To determine the ratio of oxygen consumed verses carbon dioxide produced, the combustion reaction for LPG must be known. The complete combustion of LPG in oxygen is as follows (ignoring the small amount of ethyl mercaptan):

For propane:



For butane:



Therefore, for every 4 oxygen molecules used to burn propane, 3 carbon dioxide molecules are produced. Furthermore, for every 6.5 oxygen molecules used to burn butane, 4 carbon dioxide molecules are produced. These chemical reactions illustrate how the ratio of oxygen consumed is directly proportional to the amount of carbon dioxide produced.

The overall consumption of oxygen and production of carbon dioxide for LPG is:

For O_2 consumption:

$$80\%(C_3H_8) \times 4(O_2) + 20\%(C_4H_{10}) \times 6\frac{1}{2}(O_2) = 4.5$$

Therefore 4.5 molecules of O_2 are consumed per molecule of LPG.

For CO_2 consumption:

$$80\%(C_3H_8) \times 3(CO_2) + 20\%(C_4H_{10}) \times 4(CO_2) = 3.2$$

Therefore 3.2 molecules of CO_2 are consumed per molecule of LPG.

Thus the ratio of oxygen consumed verses carbon dioxide produced is 4.5:3.2 or 1.41.